



HAL
open science

Analysis of the foot's internal structures by X-ray image processing and finite element modeling

Nicolas Kroupa

► **To cite this version:**

Nicolas Kroupa. Analysis of the foot's internal structures by X-ray image processing and finite element modeling. Other. Université de Lyon, 2021. English. NNT : 2021LYSEM013 . tel-03367491

HAL Id: tel-03367491

<https://theses.hal.science/tel-03367491>

Submitted on 6 Oct 2021

HAL is a multi-disciplinary open access archive for the deposit and dissemination of scientific research documents, whether they are published or not. The documents may come from teaching and research institutions in France or abroad, or from public or private research centers.

L'archive ouverte pluridisciplinaire **HAL**, est destinée au dépôt et à la diffusion de documents scientifiques de niveau recherche, publiés ou non, émanant des établissements d'enseignement et de recherche français ou étrangers, des laboratoires publics ou privés.



N° d'ordre NNT: 2021LYSEM013

THÈSE de DOCTORAT DE L'UNIVERSITÉ DE LYON
opérée au sein de
École des Mines de Saint-Étienne

École Doctorale N° 488
(Sciences, Ingénierie, Santé)

Spécialité de doctorat: Mécanique et Ingénierie

Soutenue publiquement le 29/03/2021, par:

Nicolas KROUPA

**Analyse des structures internes du pied par traitement d'images
rayons X et modélisation éléments finis**

—

**Analysis of the foot's internal structures by X-ray image processing
and finite element modeling**

Devant le jury composé de:

Gefen, Amit	Professeur	Tel Aviv University, Israel	Rapporteur
Dumas, Raphael	Professeur	IFSTTAR, Lyon	Rapporteur
Payan, Yohan	Directeur de Recherche CNRS	TIMC-IMAG, Grenoble	Examineur
Bouten, Laura	Ingénieur R&D	Decathlon	Examineur
Pansiot, Julien	Ingénieur de recherche	INRIA, Grenoble	Examineur
Molimard, Jérôme	Professeur	Mines Saint-Etienne	Directeur de thèse
Han, Woo-Suck	Professeur	Mines Saint-Etienne	Co-directeur de thèse
Pierrat, Baptiste	Ingénieur de recherche	Mines Saint-Etienne	Encadrant de thèse

Spécialités doctorales

SCIENCES ET GENIE DES MATERIAUX
MECANIQUE ET INGENIERIE
GENIE DES PROCÉDES
SCIENCES DE LA TERRE
SCIENCES ET GENIE DE L'ENVIRONNEMENT

Responsables :

K. Wolski Directeur de recherche
S. Drapier, professeur
F. Gruy, Maître de recherche
B. Guy, Directeur de recherche
D. Graillet, Directeur de recherche

Spécialités doctorales

MATHEMATIQUES APPLIQUEES
INFORMATIQUE
SCIENCES DES IMAGES ET DES FORMES
GENIE INDUSTRIEL
MICROELECTRONIQUE

Responsables

O. Roustant, Maître-assistant
O. Boissier, Professeur
JC. Pinoli, Professeur
N. Absi, Maître de recherche
Ph. Lalevée, Professeur

EMSE : Enseignants-chercheurs et chercheurs autorisés à diriger des thèses de doctorat (titulaires d'un doctorat d'Etat ou d'une HDR)

ABSI	Nabil	MR	Génie industriel	CMP
AUGUSTO	Vincent	CR	Image, Vision, Signal	CIS
AVRIL	Stéphane	PR2	Mécanique et ingénierie	CIS
BADEL	Pierre	MA(MDC)	Mécanique et ingénierie	CIS
BALBO	Flavien	PR2	Informatique	FAYOL
BASSEREAU	Jean-François	PR	Sciences et génie des matériaux	SMS
BATTON-HUBERT	Mireille	PR2	Sciences et génie de l'environnement	FAYOL
BEIGBEDER	Michel	MA(MDC)	Informatique	FAYOL
BLAYAC	Sylvain	MA(MDC)	Microélectronique	CMP
BOISSIER	Olivier	PR1	Informatique	FAYOL
BONNEFOY	Olivier	PR	Génie des Procédés	SPIN
BORBELY	Andras	MR(DR2)	Sciences et génie des matériaux	SMS
BOUCHER	Xavier	PR2	Génie Industriel	FAYOL
BRODHAG	Christian	DR	Sciences et génie de l'environnement	FAYOL
BRUCHON	Julien	MA(MDC)	Mécanique et ingénierie	SMS
CAMEIRAO	Ana	MA(MDC)	Génie des Procédés	SPIN
CHRISTIEN	Frédéric	PR	Science et génie des matériaux	SMS
DAUZERE-PERES	Stéphane	PR1	Génie Industriel	CMP
DEBAYLE	Johan	MR	Sciences des Images et des Formes	SPIN
DEGEORGE	Jean-Michel	MA(MDC)	Génie industriel	Fayol
DELAFOSSE	David	PR0	Sciences et génie des matériaux	SMS
DELORME	Xavier	MA(MDC)	Génie industriel	FAYOL
DESRAYAUD	Christophe	PR1	Mécanique et ingénierie	SMS
DJENIZIAN	Thierry	PR	Science et génie des matériaux	CMP
BERGER-DOUCE	Sandrine	PR1	Sciences de gestion	FAYOL
DRAPIER	Sylvain	PR1	Mécanique et ingénierie	SMS
DUTERTRE	Jean-Max	MA(MDC)		CMP
EL MRABET	Nadia	MA(MDC)		CMP
FAUCHEU	Jenny	MA(MDC)	Sciences et génie des matériaux	SMS
FAVERGEON	Loïc	CR	Génie des Procédés	SPIN
FEILLET	Dominique	PR1	Génie Industriel	CMP
FOREST	Valérie	MA(MDC)	Génie des Procédés	CIS
FRACZKIEWICZ	Anna	DR	Sciences et génie des matériaux	SMS
GARCIA	Daniel	MR(DR2)	Sciences de la Terre	SPIN
GAVET	Yann	MA(MDC)	Sciences des Images et des Formes	SPIN
GERINGER	Jean	MA(MDC)	Sciences et génie des matériaux	CIS
GOEURIOT	Dominique	DR	Sciences et génie des matériaux	SMS
GONDRAN	Natacha	MA(MDC)	Sciences et génie de l'environnement	FAYOL
GONZALEZ FELIU	Jesus	MA(MDC)	Sciences économiques	FAYOL
GRAILLOT	Didier	DR	Sciences et génie de l'environnement	SPIN
GROSSEAU	Philippe	DR	Génie des Procédés	SPIN
GRUY	Frédéric	PR1	Génie des Procédés	SPIN
HAN	Woo-Suck	MR	Mécanique et ingénierie	SMS
HERRI	Jean Michel	PR1	Génie des Procédés	SPIN
KERMOUCHE	Guillaume	PR2	Mécanique et Ingénierie	SMS
KLOCKER	Helmut	DR	Sciences et génie des matériaux	SMS
LAFORST	Valérie	MR(DR2)	Sciences et génie de l'environnement	FAYOL
LERICHE	Rodolphe	CR	Mécanique et ingénierie	FAYOL
MALLIARAS	Georges	PR1	Microélectronique	CMP
MOLIMARD	Jérôme	PR2	Mécanique et ingénierie	CIS
MOUTTE	Jacques	CR	Génie des Procédés	SPIN
NAVARRO	Laurent	CR		CIS
NEUBERT	Gilles			FAYOL
NIKOLOVSKI	Jean-Pierre	Ingénieur de recherche	Mécanique et ingénierie	CMP
NORTIER	Patrice	PR1	Génie des Procédés	SPIN
O CONNOR	Rodney Philip	MA(MDC)	Microélectronique	CMP
PICARD	Gauthier	MA(MDC)	Informatique	FAYOL
PINOLI	Jean Charles	PR0	Sciences des Images et des Formes	SPIN
POURCHEZ	Jérémy	MR	Génie des Procédés	CIS
ROUSSY	Agnès	MA(MDC)	Microélectronique	CMP
ROUSTANT	Olivier	MA(MDC)	Mathématiques appliquées	FAYOL
SANAUR	Sébastien	MA(MDC)	Microélectronique	CMP
SERRIS	Eric	IRD		FAYOL
STOLARZ	Jacques	CR	Sciences et génie des matériaux	SMS
TRIA	Assia	Ingénieur de recherche	Microélectronique	CMP
VALDIVIESO	François	PR2	Sciences et génie des matériaux	SMS
VIRICELLE	Jean Paul	DR	Génie des Procédés	SPIN
WOLSKI	Krzystof	DR	Sciences et génie des matériaux	SMS
XIE	Xiaolan	PR0	Génie industriel	CIS
YUGMA	Gallian	CR	Génie industriel	CMP

Analysis of the foot's internal structures by X-ray image processing
and finite element modeling

Nicolas KROUPA

29/03/2021

Contents

Contents	v
Table of Contents	vi
List of Figures	vii
List of Tables	xi
Introduction générale	1
General introduction	3
I Context	5
I.1 Résumé	6
I.2 Introduction	8
I.3 Foot description	8
I.3.1 Anatomy & Biomechanics	8
I.3.2 Loading & Gait	18
I.4 Footwear devices	21
I.4.1 Shoe description	21
I.5 Experimental and numerical approaches for foot biomechanics	22
I.5.1 Experimental	22
I.5.2 Model	27
I.6 Synthesis and positioning of the study	38
II Automatic extraction of bone position and ligament deformations of the foot from CT images to measure footwear influence on <i>ex-vivo</i> feet under static load	41
II.1 Résumé	42
II.2 Preface	44
II.3 Abstract	44
II.4 Introduction	44
II.5 Materials and Methods	46
II.5.1 Global strategy	46
II.5.2 Experimentation: foot loading	47
II.5.3 Image processing	50
II.5.4 Angle measurement	55
II.5.5 Statistical testing	55
II.6 Result	57
II.6.1 Method results	57
II.6.2 Bare vs Shod analysis	58
II.7 Discussion	60

II.8 Conclusion	61
II.9 Appendix	62
III Calibration of patient-specific foot models on ligament and muscle stiffness for force-driven FE simulations	65
III.1 Résumé	66
III.2 Preface	67
III.3 Abstract	67
III.4 Introduction	67
III.5 Method	69
III.5.1 Experimentations	69
III.5.2 FE model formulation	71
III.5.3 FE model calibration	73
III.5.4 Metrics	77
III.6 Results	78
III.6.1 Connector stiffness	78
III.6.2 Force driven FE simulations outputs evaluation	79
III.6.3 Articulation angle	82
III.7 Discussion	85
III.8 Conclusion	86
III.9 Appendix	87
IV The effect of mid-sole stiffness and drop on foot biomechanics through finite element model	91
IV.1 Résumé	92
IV.2 Preface	92
IV.3 Introduction	93
IV.4 Method	95
IV.4.1 Foot & footwear FE model formulation	95
IV.4.2 Footwear mid-sole variation	97
IV.4.3 Shoe adjustment	98
IV.4.4 Ground contact	99
IV.4.5 Running boundary conditions	99
IV.5 Results	100
IV.5.1 Simulation visualization	100
IV.5.2 Fat pad stress	100
IV.5.3 Plantar skin contact stress	102
IV.5.4 Ligament deformation	105
IV.5.5 Joint angle	109
IV.6 Discussion	113
IV.7 Conclusion	115
Conclusion and future works	117
Conclusion et travaux futurs	121
Bibliography	127

List of Figures

I.1	Anatomical plans & Terms of Relationship	8
I.2	Foot skeleton, dorsal view	9
I.3	Foot bones	10
I.4	Foot articulations Dorsal view	11
I.5	Foot ligaments	12
I.6	Dorsal & Plantar foot muscles	13
I.7	Lower leg muscles description From left to right, anterior, posterior and lateral part with in bold color the muscles affected to the part	14
I.8	Foot sagittal section	15
I.9	Plantar/Dorsal flexion at talocrural joint	16
I.10	Varus/Valgus at subtalar joint	16
I.11	Adduction/Abduction and Supination/Pronation at midtarsal joint	17
I.12	Plantar vault overview	18
I.13	Windlass mechanism by Hicks [Hic54]	19
I.14	Transverse Tarsal Arch by Venkadesan [Ven+20] in (a) the human foot arches represented with the Medial Longitudinal Arch (MLA) and the Transverse Tarsal arch (TTA) in (b)) a thin and floppy sheet of paper becomes considerably stiffer because of transversal curvature. The TTA may have a similar role in feet. Scale bars, 5 cm.	19
I.15	Adelaar 1986	20
I.16	a Evolution of vertical ground reaction force in function of body displacement speed [Kel+96]; b Rear and forefoot strike pattern with their vGRF associated [Lie+10]	20
I.17	Shoe components	21
I.18	Example of video motion capture study	22
I.19	biplanar X-ray fluoroscopy work from Ito et al. [Ito+17]	23
I.20	Typical centre of pressure distribution [Bul+18]	24
I.21	Ground reaction force [CL80]	24
I.22	Inversion test setup [BRK15]	25
I.23	Heel indentation set-up [Erd+06]	25
I.24	Ligament cross-section of 5 <i>ex-vivo</i> subjects [SL10] short plantar ligament (SPL), inferior calcaneo-navicular (ICN) ligament, interosseous second cuneiform-third cuneiform (IC2C3) ligament, and interosseous fourth metatarsal-fifth metatarsal (IM4M5) ligament	26
II.1	graphic summary of the protocol	46
II.2	Test bench for loading the foot, while simultaneously measuring the applied force using a load cell	48
II.3	Test bench positioned in the CT scan	48
II.4	Neutral bare foot acquisition sequence	49

II.5	Foot segment minimization The foot segment is represented with the red point clouds, the loaded <i>skeleton</i> is the black dot clouds	52
II.6	Final minimization on Metatars 5 The bone is represented with the red point clouds, the loaded <i>skeleton</i> is the black point clouds The initial situation displayed in II.6a comes from minimizing the previous segment, in blue ellipsoids the non-aligned area are highlighted.	52
II.7	Deformation protocol Distance between the morphing steps and the <i>target</i> is evaluated with the Hausdorff Root Mean Square distance (HRMSd). The patient's <i>target</i> mesh is displayed in grey and the <i>source</i> bone at different stages of the protocol is displayed in black wireframe. The ligament attachment points of the <i>source</i> are displayed in red and those of the patient calculated with the presented protocol are displayed in blue.	55
II.8	Angle measurement	56
II.9	Foot ref. 2279 Loading Sequence on Neutral position	57
II.10	Ligaments positions calculated by the morphing technique	58
II.11	Foot 2279, Wilcoxon signed-rank test on bone translation amplitudes	62
II.12	Foot 2277, Wilcoxon signed-rank test on bone translation amplitudes	62
II.13	Foot 2275, Wilcoxon signed-rank test on bone translation amplitudes	63
II.14	Legend for upper graphs displayed in Figures II.11, II.12 and II.13	63
III.1	Test bench positioned in the CT scan	70
III.2	Neutral (N) bare foot acquisition sequence	70
III.3	Patient specific foot model	72
III.4	Neutral foot orientation displacement driven simulation outputs (reaction forces and moments) and processed experimental data (bones positions and connectors)	74
III.5	Neutral foot orientation in the loading step 3 The cones represent the reaction moments (\vec{m}_{ib}), the arrows the reaction forces (\vec{f}_{ib}), the coloured lines the deformed connectors (s_{il}) (whose rigidity values are sought to obtain a minimum when resolving the static mechanical equilibrium), in black the links between the connectors' attachment points and the center of mass of the bones on which they intervene (\vec{w}_{ibl} and \vec{t}_{ibl}).	75
III.6	Ligament stiffness classified as increasing result variability The ligaments are named PL for plantar, DO for dorsal, DE for deep, IN for interosseus, AN for anterior, PO for posterior, ME for medial and after the underscore the connected bones are filled in, e.g. C1 for medial cuneiform bone, M1 for metatarsal 1. The names of the ligament clusters are in parentheses e.g. (PLF) for plantar fascia. Muscles are directly referred to by their names. . .	78
III.7	150 % of BW applied in neutral position to the foot referenced 2279, red point is the force-driven simulation results and the black point the experimental bone position. The average difference between bone position simulated and experimental is equal in this situation to $5.80 \text{ mm} \pm 1.37 \text{ mm}$	80
III.8	Difference between simulated and experimental bone position, load by load .	81
III.9	Difference between simulated and experimental bone position, bone by bone	82
III.10	Difference between simulated and experimental results of deformed ligament lengths.	83
III.11	Max shearing at 150% BW in neutral orientation	84

III.12	Pressure at 150% BW in neutral orientation	84
III.13	FE model calibration protocol summary	88
III.14	Angle measurement	89
III.15	Force & displacement driven stress comparison	90
IV.1	Segmentation - Medial view	95
IV.2	Patient specific foot & footwear models - Medial view	97
IV.3	Mid-sole top layer variations for mid-soles generation	97
IV.4	Foot dressing stages - medial view	98
IV.5	Ground contact stages - medial view	99
IV.6	Boundary conditions	99
IV.7	Simulation visualization over time - medial view	100
IV.8	Maximum shearing visualization at 0.05 s	101
IV.9	Maximum shearing of fat pads over time	101
IV.10	Average maximum shearing of fat pads	101
IV.11	Contact pressure & frictional force of fat pads - left anterolateral view	102
IV.12	Contact pressure of fat pads	103
IV.13	Contact pressure of fat pads - Dorsal view	104
IV.14	Ligament strain	105
IV.15	Arch ligaments measures	106
IV.16	Deep transverse ligaments measures	107
IV.17	Medial ligaments & muscles measures	107
IV.18	Chopart joint ligaments measures	107
IV.19	Lateral ligaments & muscles measures	108
IV.20	Lisfranc joint ligaments measures	108
IV.21	Arch sagging Calcaneus Talus Metatarsal1 (CalTalM1) sagittal angle	109
IV.22	Medial arch sagging Calcaneus Talus Metatarsal1 (CalTalM1) transverse angle	110
IV.23	Inversion/Eversion Tibia Talus Calcaneus (TibTalCal) coronal angle	111
IV.24	Plantar/Dorsal flexion Tibia Talus Calcaneus (TibTalCal) sagittal angle	112

List of Tables

I.1	Some ligament stiffness according to the literature	27
I.2	Siegler et al. [SBS88] ligament Young moduli anterior fibulotalar (ATFL), fibulocalcaneal (FCL), posterior fibulotalar (PFTL), tibionavicular (TNL), tibiospring (TSL), posterior tibiotalar (PTTL)	34
II.1	Bodies description	47
II.2	Tested configuration description	49
II.3	Foot segments description	51
II.4	Angles description	56
II.5	Articulation angle nonparametric tests	59
III.1	finite element model components details	71
III.2	Tested configuration description	73
III.3	Difference with experimental measurements displayed foot by foot	79
III.4	Comparison with two other sources of information on stiffness	79
III.5	Angle comparison	82
III.6	Articular angle description	87
IV.1	finite element model components details	96
IV.2	Cluster ligament Drop and Stiffness influence	106

Introduction générale

Le pied est une structure anatomique complexe composée de nombreux os enchevêtrés dans une panoplie de muscles, ligaments, fascias et autres tissus. Son rôle dans le maintien et le déplacement du corps l'expose à une diversité de sollicitations mécaniques qui vont déformer sa structure. Un grand nombre de paramètres vont alors influencer cette déformation de la structure du pied; ils peuvent être spécifiques au patient et à ses pathologies, liés aux caractéristiques de la sollicitation mécanique appliquée au membre, mais aussi dépendre des différents exemplaires de volume chaussant portés comme les chaussures ou les dispositifs médicaux.

Face à cette diversité et à cette complexité, il est devenu nécessaire d'obtenir des mesures de plus en plus précises décrivant l'intérieur du pied afin de progresser dans la caractérisation des comportements qui le régissent. Ces progrès à faire dans la compréhension des comportements du pied face aux sollicitations mécaniques permettront de perfectionner la conception des chaussures, des dispositifs médicaux et de la planification chirurgicale.

C'est dans ce contexte que s'inscrit le projet Capture et Modélisation du Pied Chaussé en Mouvement (CaMoPi) financé par l'Agence Nationale de la Recherche (ANR).

Trois acteurs sont mobilisés sur le sujet pour aborder une série d'obstacles scientifiques et méthodologiques. L'INRIA se concentre sur la capture du mouvement en travaillant sur une plateforme hybride vidéo / rayons X pour suivre en dynamique et directement le déplacement des os du patient pendant une foulée. Le partenaire industriel CTC se concentre sur le transfert industriel des travaux de recherche. L'école des Mines de Saint-Etienne, à travers son Centre Ingénierie et Santé et l'unité de recherche INSERM Sainbiose, se concentre sur la modélisation de la mécanique du pied nu et chaussé dont font l'objet les travaux de cette thèse.

Afin de présenter le contexte scientifique du sujet, le premier chapitre parcourra l'état de l'art avec une description de l'anatomie du pied puis une revue non exhaustive des différentes études menées. Les méthodes de modélisation, en particulier par éléments finis, qui ressortent de ces études seront mises en évidence. Cela nous amènera à nous concentrer sur trois étapes de la modélisation éléments finis correspondant chacune à un chapitre de ce document. Elles seront présentées sous forme d'article avec l'objectif d'être publiées dans des revues avec comité de lecture (1 publiée, 1 en cours de révision, 1 en attente de soumission).

Le deuxième chapitre se consacrera à la modélisation de la géométrie du patient et l'observation de ses comportements internes, en particulier le mouvement des os, lors de différents cas de chargement. Les premiers verrous méthodologiques du temps de construction du modèle ainsi que du suivi précis et individuel de chaque os du pied sont abordés ici avec la mise en place de méthodes de recalage rigides et non rigides. Grâce à ces méthodes, la possibilité d'observer l'intérieur du pied avec et sans la chaussure dans différents cas de chargement est utilisée ici pour étudier l'influence d'une chaussure de sport sur le mouvement des os, la déformation des ligaments et les angles des articulations.

Le deuxième verrou identifié est le manque de connaissance des propriétés mécaniques

du pied d'un patient, ce qui peut rendre sa modélisation irréaliste. Le troisième chapitre abordera ce problème avec une calibration du modèle en assignant des caractéristiques aux matériaux correspondant aux différents composants anatomiques du pied. Ici on se concentrera sur les rigidités passives des ligaments & muscles.

Le quatrième chapitre correspond à la troisième et dernière étape de la modélisation avec le déroulement et l'analyse des simulations. Un modèle construit et calibré avec le protocole mis en œuvre dans cette thèse sera habillé de différents exemplaires de chaussures pour mesurer l'influence de leurs paramètres de conception sur le comportement du pied.

La fin de la thèse synthétisera les résultats obtenus avec leurs applications directes, puis se terminera par les limites et les perspectives de l'étude.

General introduction

The foot is a complex anatomical structure composed of many bones entangled in a variety of muscles, ligaments, fascias and other tissues. Its role in maintaining and moving the body exposes it to a variety of mechanical solicitations that will deform its structure. A large number of parameters will then influence this deformation of the foot structure; they can be specific to the patient and his pathologies, linked to the characteristics of the mechanical load applied to the limb, but also depend on the different types of footwear worn such as shoes or medical devices.

Faced with this diversity and complexity, it has become necessary to obtain increasingly precise measures describing the inside of the foot in order to progress in the characterization of the behaviors that govern it. These advances in the understanding of the foot's behavior under mechanical loading will lead to improvements in the design of footwear, medical devices and surgical planning.

It is in this context that the project Capture and Modeling of the Moving shod Foot (CaMoPi), funded by the Agence Nationale de la Recherche (ANR), is taking place. Three actors are mobilized on the subject to address a series of scientific and methodological barriers.

INRIA is focusing on motion capture by working on a hybrid video/X-ray platform to follow dynamically and directly the movement of the patient's bones during a stride. The industrial partner CTC focuses on the industrial transfer of research work. The Ecole des Mines de Saint-Etienne, through its Centre Ingénierie et Santé and the INSERM Sainbiose research unit, focuses on the modeling of the bare and shod foot mechanics, which is the subject of this thesis.

In order to present the scientific context of the subject, the first chapter will go through the state-of-the-art with a description of the foot's anatomy, followed by a non-exhaustive review of the various studies carried out. The modeling methods, in particular by finite elements, that emerge from these studies will be highlighted. This will lead us to focus on three stages of modeling, each corresponding to a chapter of this document; they will be presented in the form of an article with the objective of being published in peer-reviewed journals (1 published, 1 under review, 1 awaiting submission).

The second chapter will be dedicated to the modeling of the patient's geometry and the observation of his internal behaviors, in particular bone movement, during different loading cases. The first methodological barriers of the model construction time and the precise and individual monitoring of each foot bone are addressed here with the implementation of rigid and non-rigid registration methods. Thanks to these methods, the possibility of observing the inside of the foot with and without the shoe in different loading cases is used here to start studying the influence of a sports shoe on bone movement, ligament strain and joint angles.

The second barrier identified is the lack of knowledge about the mechanical properties of a patient's foot, which can make its modeling unrealistic. The third chapter will address this problem with a calibration of the model by assigning characteristics to the materials

corresponding to the different anatomical components of the foot. Here we will focus on the passive stiffness of the ligaments & muscles.

The fourth chapter corresponds to the third and last step of the modeling with the running and analysis of the simulations. A model built and calibrated with the protocol implemented in this thesis will be dressed with different exemplars of shoes to measure the influence of their design parameters on the behavior of the foot.

The closing part of the thesis will synthesize the results obtained with their direct applications, and will end with the limits and perspectives of the study.

Chapter I

Context

Contents of the chapter

I.1	Résumé	6
I.2	Introduction	8
I.3	Foot description	8
I.3.1	Anatomy & Biomechanics	8
I.3.1.1	Terms of location and direction	8
I.3.1.2	Bones & Principal articulations	9
I.3.1.3	Ligaments	11
I.3.1.4	Muscles and tendons	13
I.3.1.5	Other tissues	15
I.3.1.6	Joint motions	16
I.3.2	Loading & Gait	18
I.4	Footwear devices	21
I.4.1	Shoe description	21
I.4.1.1	Upper	21
I.4.1.2	Shoe-last	21
I.4.1.3	Sole	21
I.5	Experimental and numerical approaches for foot biomechanics	22
I.5.1	Experimental	22
I.5.1.1	Kinematics & Kinetics.	22
I.5.1.2	Mechanical test	24
I.5.2	Model	27
I.5.2.1	Patient/Subject specific model construction workflow for FE analysis	28
I.5.2.2	Finite element foot model applications	36
I.6	Synthesis and positioning of the study	38

I.1 Résumé

La description non exhaustive de l'anatomie et de la biomécanique du pied a mis en évidence qu'il s'agit d'une structure complexe. Elle englobe de nombreux os et tissus et présente une grande diversité de comportements influencés par une multitude de paramètres.

Pour étudier le pied et ainsi mieux comprendre ses mécanismes, la mesure des comportements internes du pied est une source d'information essentielle. L'état de l'art a montré que des verrous scientifiques empêchent la généralisation de l'observation du comportement interne du pied. En premier (1) le temps de création du modèle, puis (2) la difficulté de suivre les os de manière précise et individuelle et (3) le manque de connaissance des caractéristiques matériaux propres au patient.

L'objectif de ce travail est de mieux observer le comportement du pied. Pour cela, une série de travaux expérimentaux et numériques proposera des implémentations pour répondre à ces verrous. Il en résultera une approche permettant d'observer et de mesurer le comportement interne du pied lors de la course avec des chaussures (4).

(1) temps de création du modèle

Dans leur revue de modèles éléments finis de pieds diabétiques, Telfer et al. [Tel+14] soulignent que les modèles complexes qui choisissent d'inclure de nombreux composants anatomiques possèdent des processus de développement et de résolution plus complexes et plus longs, plusieurs jours selon leur expérience. Cette longue intégration a le désavantage de limiter l'application clinique de ce type de modèle mais elle permet d'intégrer les différentes complexités du pied pour essayer de fournir une simulation plus juste.

Ce temps long de développement du modèle est particulièrement problématique car il limite le nombre de sujets/patients sur lesquels les simulations seront effectuées. Cela réduit la représentativité de l'effet mesuré en empêchant la différenciation entre une réponse liée à un individu ou une réponse globale, qui a un effet sur une population entière.

Des méthodes de recalage avec une grande variété de mises en œuvre ont été conçues dans ce contexte, leur application pour la réduction du temps de développement du modèle du pied semble possible car cela a déjà été implémenté pour d'autres structures anatomiques.

(2) difficulté de suivre les os de manière précise et individuelle

Pour suivre les mouvements du pied, la principale technique de l'état de l'art est la capture vidéo. Elle permet de suivre le mouvement de quelques segments du pied, ce qui donne une vue incomplète du comportement interne.

Afin de progresser dans l'observation du comportement interne du pied, le développement de méthodes pour le suivi individuel et précis de chaque os est une source d'information essentielle car les contraintes mécaniques appliquées aux composants du pied en résultent en partie. Un avantage supplémentaire des méthodes de recalage vues précédemment est que lorsqu'une série d'acquisitions est réalisée sur le même patient/sujet, elles permettent de suivre la cinématique de certains composants anatomiques et ainsi d'obtenir des conditions limites précises, faciles à utiliser et spécifiques au patient. Dans le contexte de l'étude du pied, l'exploitation de ces méthodes de recalage est donc particulièrement intéressant pour suivre la position de chaque os sous l'effet du chargement du pied au lieu de suivre de façon classique des segments du pied.

(3) manque de connaissance des caractéristiques matériaux propres au patient

L'état de l'art a montré que dans les modèles du pied, l'attribution de modèles de comportement et paramètres constitutifs associés, qui sont censés décrire un comportement spécifique au patient, sont issus de quelques travaux de caractérisation. La validation du modèle est également limitée, elle se fait principalement en comparant uniquement la distribution des pressions plantaires entre les mesures simulées et les mesures expérimentales.

Comme il existe une grande variabilité en termes de rigidité des tissus, une progression serait l'application de techniques de calibration pour adapter le matériau au patient dans le but d'augmenter la justesse des résultats du modèle. Les mesures pouvant être utilisées pour la validation du modèle peuvent être étendues à des métriques autres que la pression plantaire afin d'axer les études sur d'autres comportements du pied.

(4) comportement interne du pied lors de la course avec des chaussures

Les études sur le port de chaussures lors d'une course à pied sont limitées : l'état de l'art a montré que l'utilisation de la simulation par éléments finis est pratiquement inexistante sur ce sujet et que la mesure expérimentale du comportement interne du pied est presque impossible avec les dispositifs actuels. Par conséquent, il existe très peu d'études paramétriques permettant de mesurer l'influence des paramètres de conception des chaussures de course sur le comportement interne du pied pendant la course.

I.2 Introduction

In order to position the studies carried out on the foot and to highlight their limitations, a presentation of the foot will first be given in this chapter. This presentation will be composed of anatomical descriptions, then the biomechanical aspects will be discussed. A filtering is applied to avoid rewriting the much more detailed and complete information present in the anatomy books and most of all to focus the reading on the essential information used in the modeling phases.

In a second step, a basic shoe design will be presented.

In a third step, the state-of-the-art of the different works carried out on the biomechanics of the foot will be presented. Two axes will be brought, experimentation and modeling.

I.3 Foot description

Most of the artworks in this section come from the book General and Musculoskeletal System, THIEME Atlas of General Anatomy [Sch+10]. This material is used with a license permission issued by Thieme group.

I.3.1 Anatomy & Biomechanics

I.3.1.1 Terms of location and direction

Applied to the foot, the fundamental reference planes and localization terminology are shown in Figure I.1. It contains the terminology that will be used throughout this thesis.

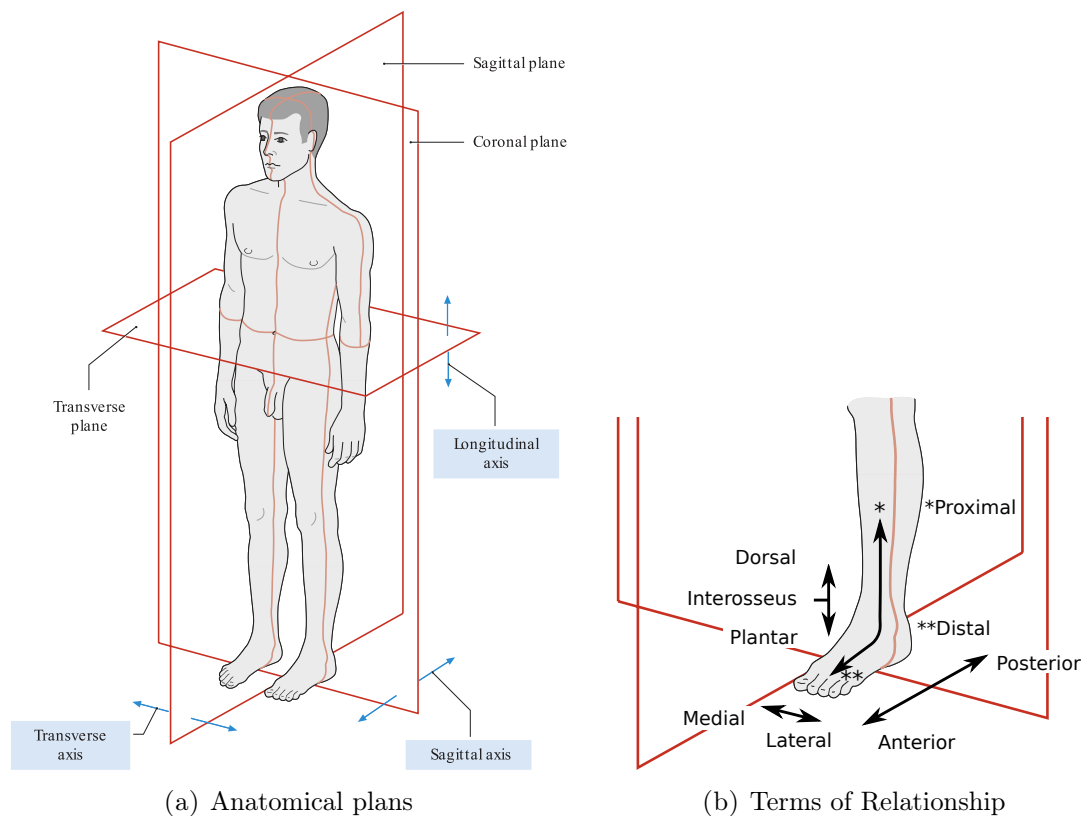


FIGURE I.1: Anatomical plans & Terms of Relationship

I.3.1.2 Bones & Principal articulations

The foot is usually composed of 30 bones, taking into account the tibia and fibula. Bone variants exist in the population, with the presence of more or less accessory bones, for example the presence of lateral sesamoid bones, trigonum and other bones. The main bones are shown in the figure I.2, with the different compartments assigned to them to describe the different areas of the foot.

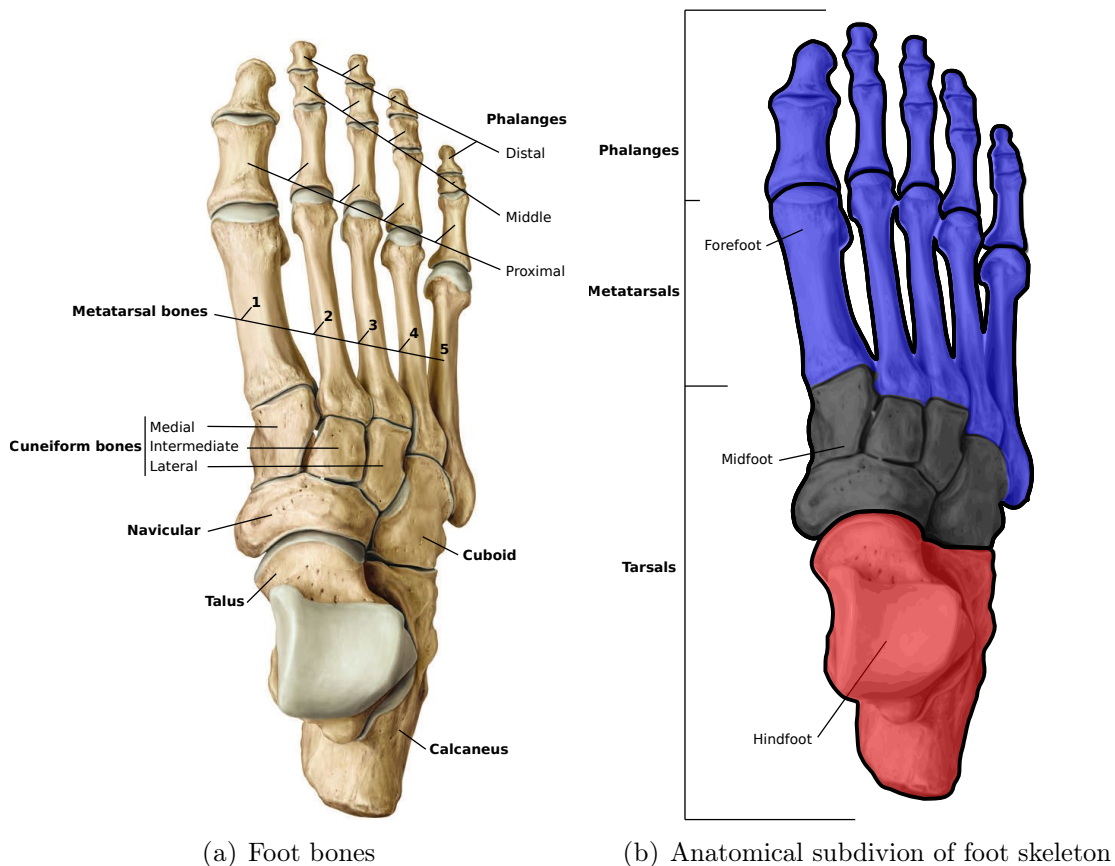
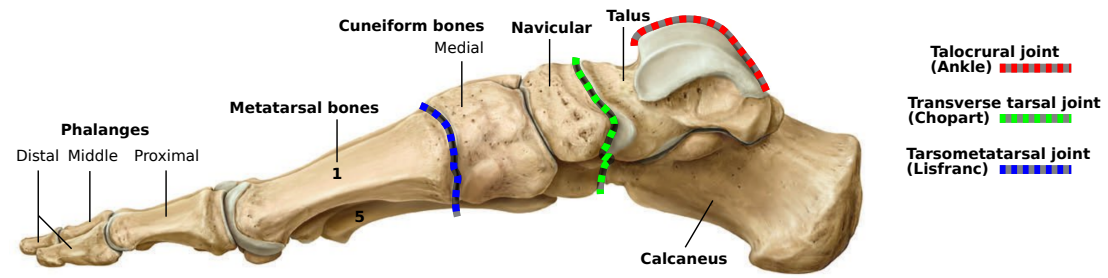


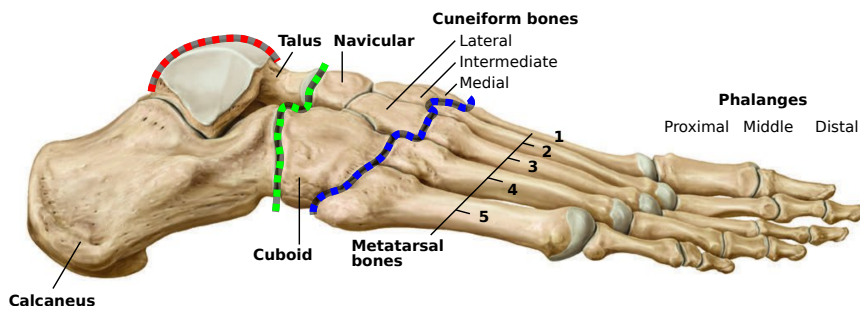
FIGURE I.2: Foot skeleton, dorsal view

The bone aspect is presented in more details with the main joints in figure I.3. We will retain as main articulations:

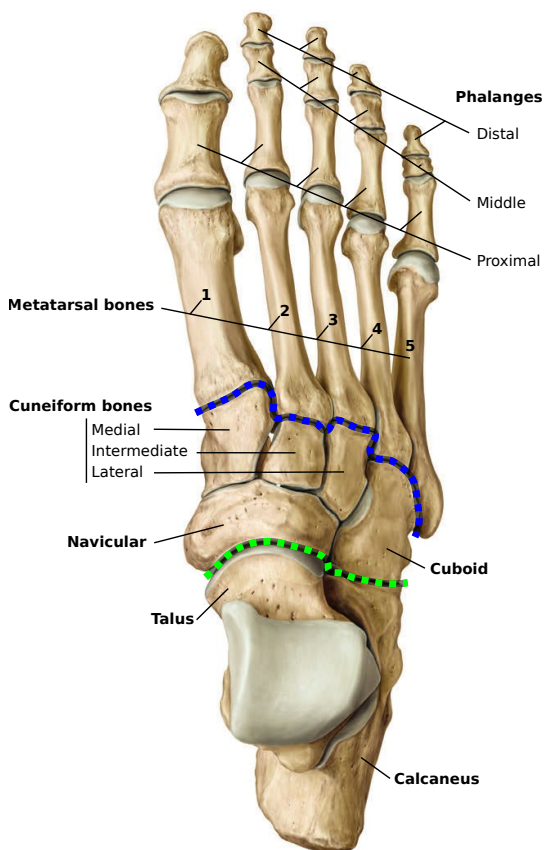
- the ankle joint or talocrural, composed of the talus, tibia and fibula which makes the junction between the lower leg and the foot.
- the transverse tarsal joint, also called the Chopart joint. It makes the junction between the first row of tarsal bones, namely the calcaneus and the talus, and the second row composed of the navicular and the cuboid.
- the tarsometatarsal joint that connect the four bones of the tarsal arch, composed of the cuboid and the three cuneiform bones, with the proximal head of the five metatarsal bones that form the metatarsal arch.



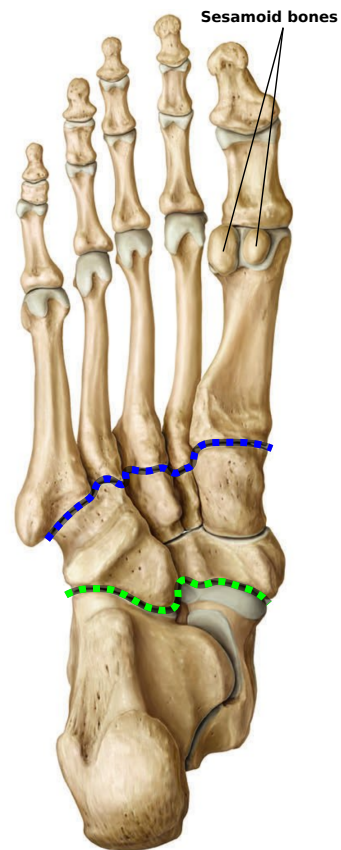
(a) Medial view



(b) Lateral view



(c) Dorsal view



(d) Plantar view

FIGURE I.3: Foot bones

I.3.1.3 Ligaments

The foot is composed of about a hundred ligaments. These bind the bones together to maintain the stability of the foot. They are shown in detail in the figure I.5. Going through the joints in a proximal to distal order, the following logic is present and displayed in figure I.4:

- at the ankle joint or talocrural, 4 groupings of ligaments each in one direction, posterior, anterior, medial and lateral.
- at the articulation of the talus with the calcaneus, the talocalcaneal joint or subtalar, four ligaments, with a first interosseous placement then in the lateral, medial and posterior positions
- at the transverse tarsal joint, also known as the Chopart joint. Numerous ligaments connecting the calcaneus, tibia and talus to the first midfoot bones, composed of the navicular and cuboid, are mainly present in the dorsal region but also in the plantar region.
- at the cuboideonavicular, cuneonavicular, intercuneiform and cuneocuboid joints, dorsal, plantar and interosseous ligaments are present.
- between the midfoot and forefoot, the tarsometatarsal joint also called Lisfranc, dorsal, plantar, and interosseous ligaments are present.
- between the bones of the metatarsals, dorsal, plantar and interosseous ligaments connect the proximal heads together. The distal heads are connected by the deep transverse metatarsal ligaments.
- between the metatarsals and phalanges with the metatarsophalangeal joints (MTP) and then the phalanges between them with the proximal and distal interphalangeal joints (PIP & DIP), there are ligaments and capsules.

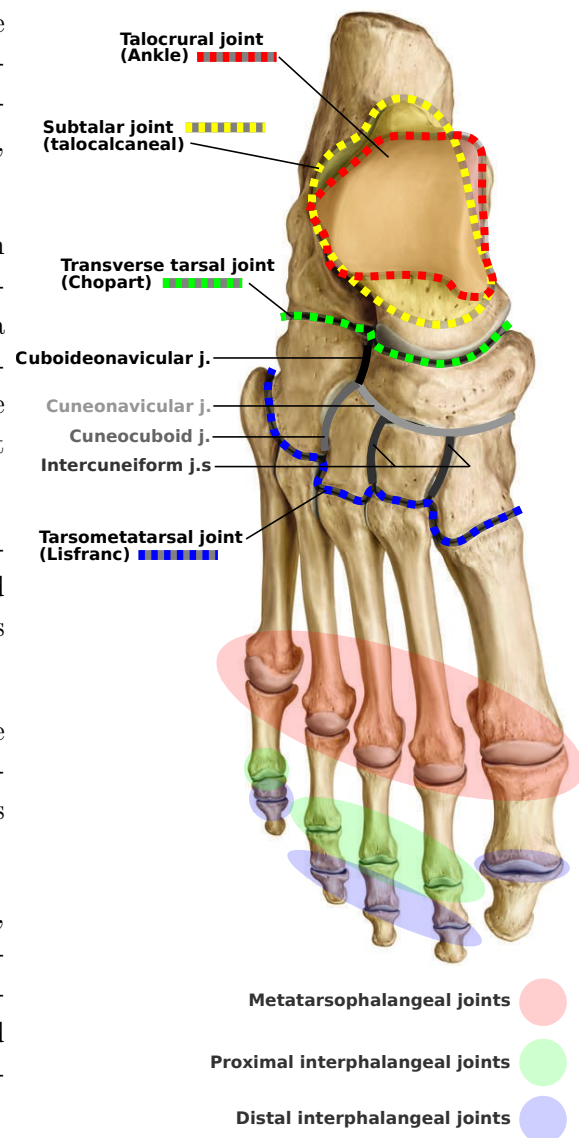


FIGURE I.4: Foot articulations
Dorsal view

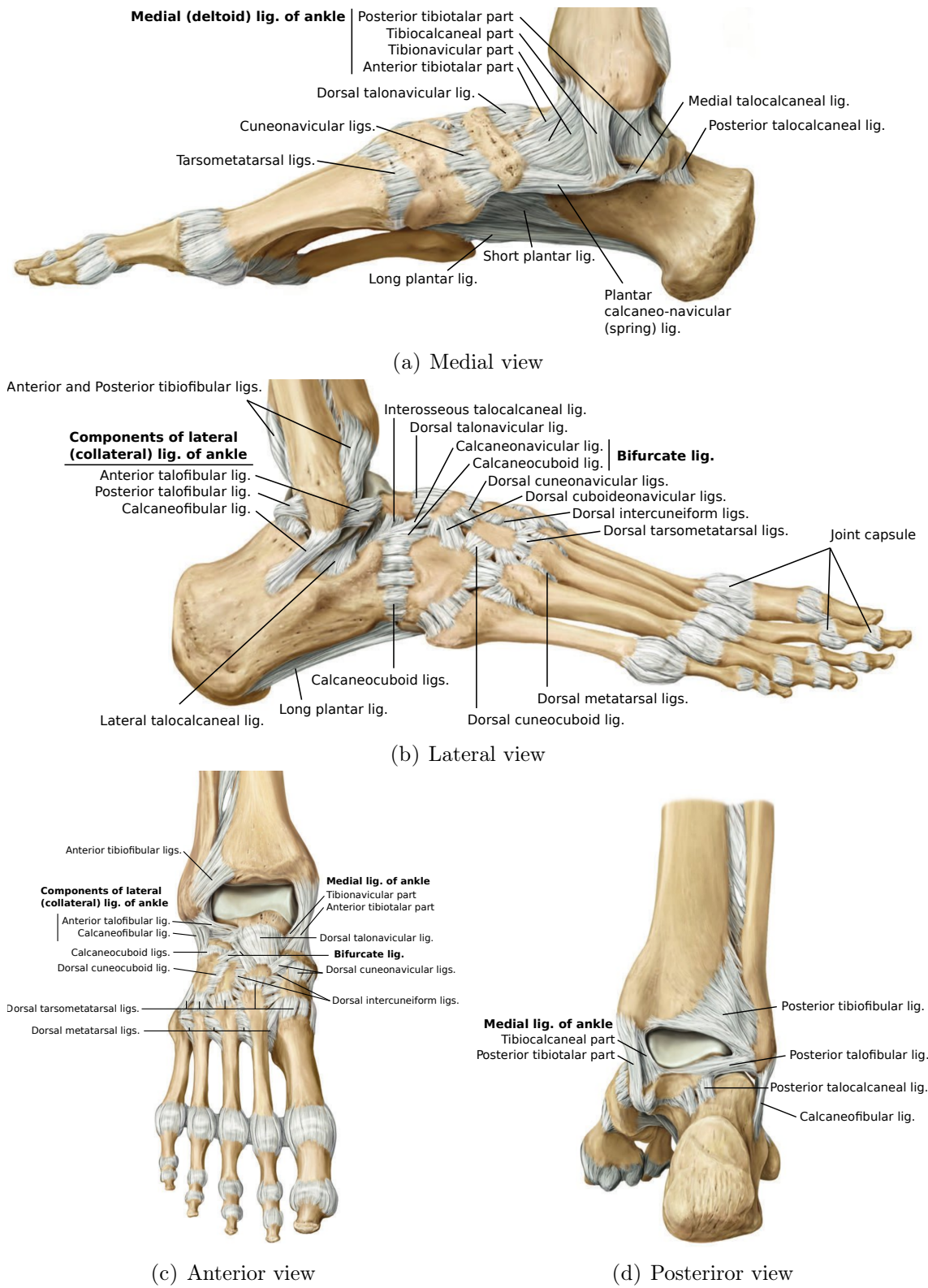


FIGURE I.5: Foot ligaments

I.3.1.4 Muscles and tendons

The activation of the muscles generates the movements of the foot, the positioning of the muscles is done at two levels.

The first corresponds to the extrinsic muscles, it is located at the lower leg, attached to the distal heads of the femur, the fibula and the tibia. It is divided into three parts which are listed below and shown in the figure I.7:

- posterior, mainly for plantar flexion of the foot and toes (flexors).
- anterior, mainly for dorsal flexion of the foot and toes (extensors), but it can actuate partial inversion and more discreetly eversion.
- lateral, mainly for eversion of the foot and to a lesser extent for plantar flexion.

The second corresponds to the intrinsic muscles, it is located at foot level and is divided into two main parts:

- dorsal, to extend the toes (extensors)
- plantar, organized in different layers. From the plantar level to the dorsal one, there are 4 layers:
 - first layer, for flexion and adduction of the hallux and little toe 1 as well as for flexion of the remaining toes 2,3 and 4.
 - second and third layer, without being exhaustive, play a role in assisting the long muscles coming from the lower leg (extrinsic), maintaining the transverse arch of the foot and flexing the toes at the proximal phalanges.
 - fourth layer, for adduction, abduction and flexion of the metatarsal bones.

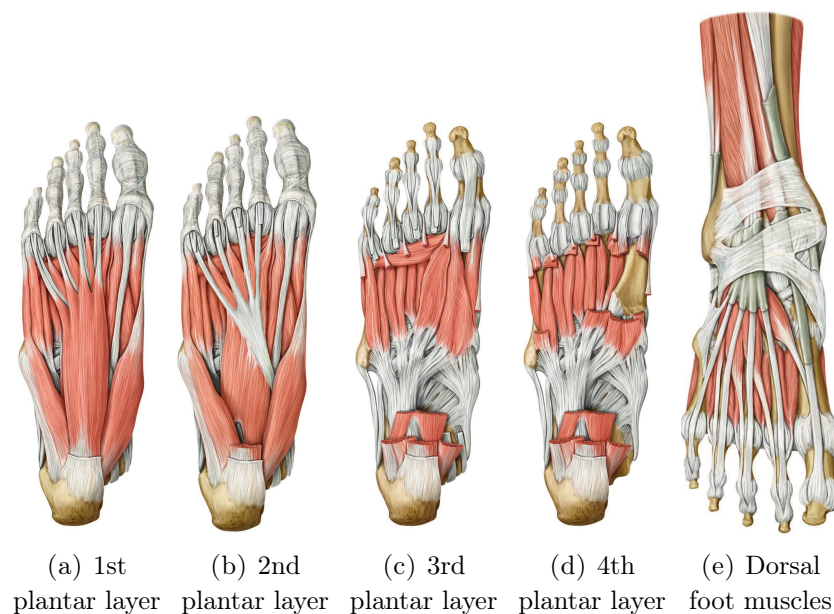


FIGURE I.6: Dorsal & Plantar foot muscles

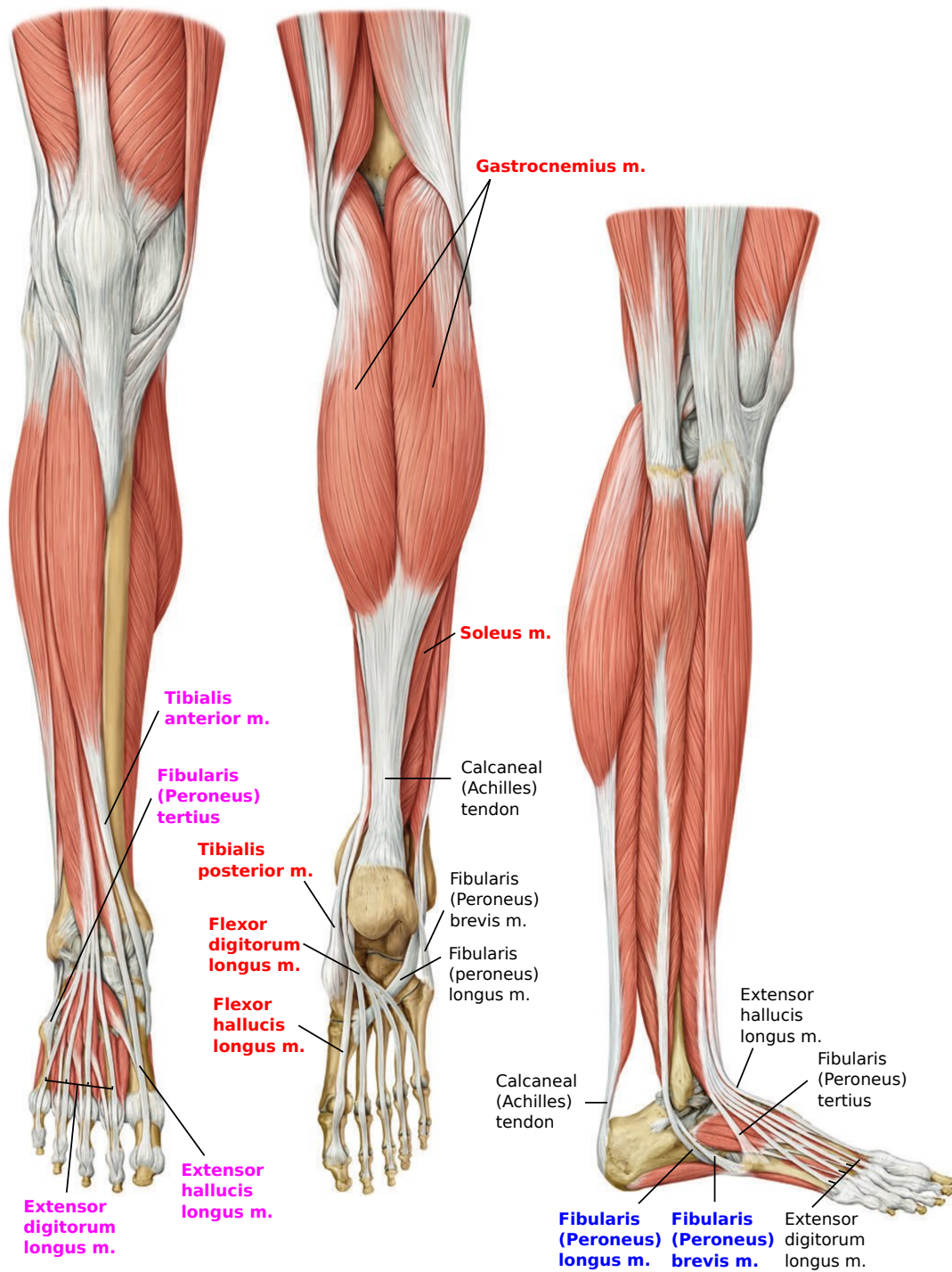


FIGURE I.7: Lower leg muscles description

From left to right, anterior, posterior and lateral part with in bold color the muscles affected to the part

I.3.1.5 Other tissues

Other tissues are also present in the foot. Three are of particular note: the skin, adipose tissue and fascia.

Two areas of skin are commonly distinguished, the dorsal area which is thinner and the plantar area which is thicker.

Adipose tissue in two areas of the foot acts as a cushion. In the heel area under the calcaneus bone it is called the heel fat pad and in the metatarsal head area it is named the metatarsal head fat pad.

A particularly thick connective tissue is the plantar fascia, also called plantar aponeurosis, which plays a strategic role in both maintaining the arch of the foot and protecting its sole. It is located under the 1st layer of the plantar muscles.

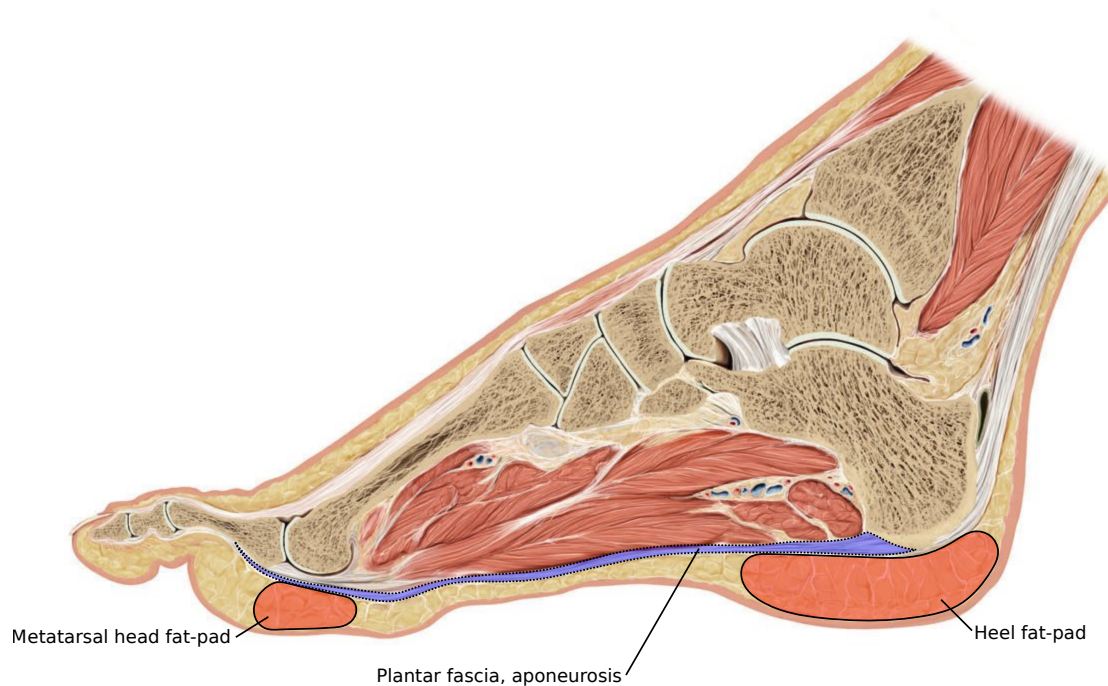


FIGURE I.8: Foot sagittal section

I.3.1.6 Joint motions

The foot motions are present at different joints.

At the ankle, the dorsal and plantar flexion movements are axed, moving the distal segment of the foot respectively upward or downward.

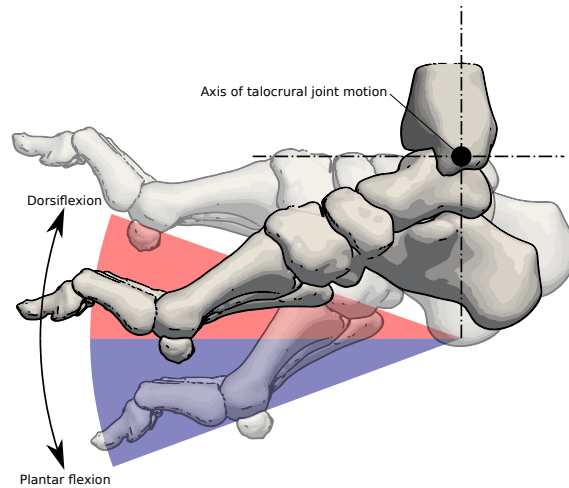


FIGURE I.9: Plantar/Dorsal flexion at talocrural joint

At the subtalar joint is located the varus and valgus movements. In varus, the calcaneus is turned towards the medial side of the talus and in valgus the calcaneus is turned towards the lateral side of the talus.

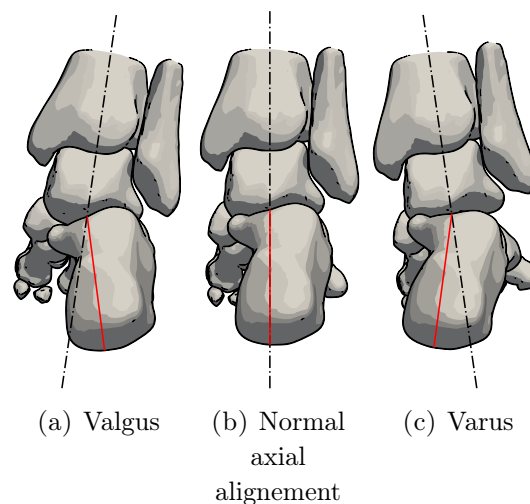


FIGURE I.10: Varus/Valgus at subtalar joint

At the Chopart joint (midtarsal or transverse tarsal joint) two movements take place. The abduction and adduction that move the forefoot laterally or medially relative to the back of the foot. The pronation and supination that rotate, in relation to the back of the foot, the forefoot in one direction or the other. In pronation, the big toe is moved down when the little toe is moved up; in supination, the big toe is moved up and the little toe is moved down.

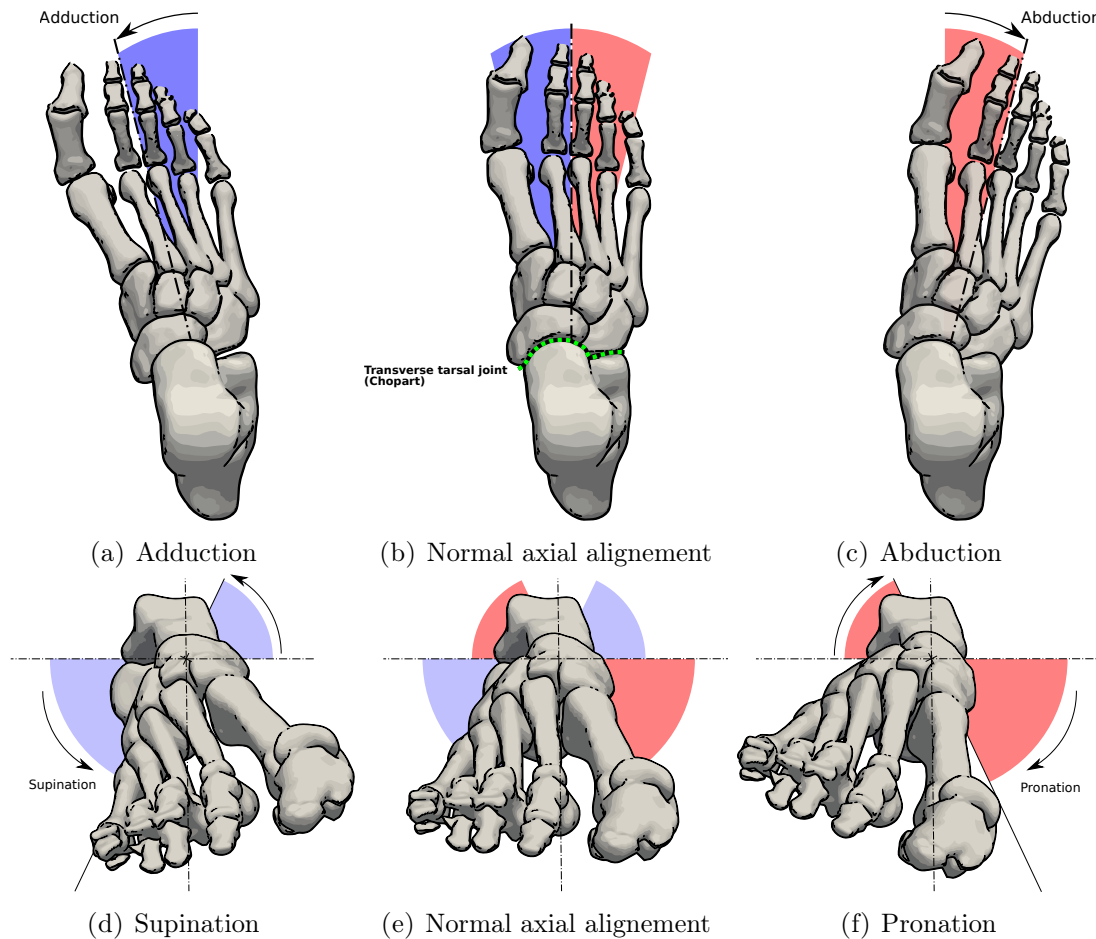


FIGURE I.11: Adduction/Abduction and Supination/Pronation at midtarsal joint

The inversion and eversion movements of the foot are composed of the basic movements at the subtalar and Chopart joints. When the foot is in inversion there is a varus at the subtalar joint and at the Chopart joint adduction plus supination. When the foot is in eversion there is a valgus at the subtalar joint and at the Chopart joint abduction plus pronation.

I.3.2 Loading & Gait

The foot is exposed to different mechanical constraints depending on the movement and placement of the body. When the body is in a perfectly stationary standing position, the load applied to one foot is then static and of a magnitude corresponding to 0.5 times the weight of the body. The load is applied from the tibia to be distributed over the entire foot by arches forming the arch of the foot also named plantar vault. The description and function of the foot arch is actively studied in the research fields of anthropology, paleanthology and biomechanics. A consensus is emerging regarding the specialization of the human foot in endurance walking and running as opposed to the great apes which have a specialization in arboreal locomotion. This consensus is put forward by observing that the arch of the human foot, being curved, is more rigid compared to those of the great apes, being flat, which allows it to restitute with a better efficiency the force used for the propulsion of the foot [HL18].

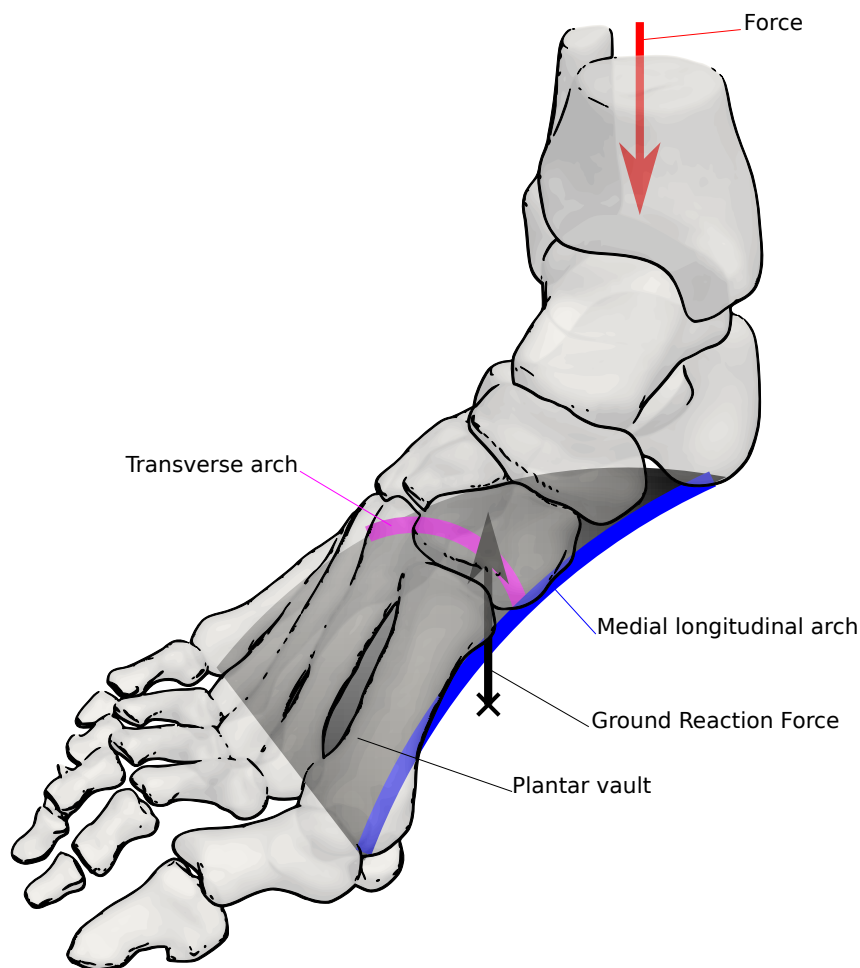


FIGURE I.12: Plantar vault overview

Different mechanical descriptions of the arch behavior exist. Most descriptions focus on the median longitudinal arch, the most commonly accepted mechanical interpretation is the bow coupled with windlass behavior where the plantar fascia plays a major role, as described by Hicks [Hic54] in Figure I.13. The plantar fascia acts on the one hand as a spring connecting the base of the calcaneus and the head of the metatarsals maintaining the structure of the longitudinal arch like a chord maintaining the curvature of the bow branches. But mostly when the toes extend, the tension in the plantar fascia is increased

leading to shortening the distance between the calcaneus and the head of the metatarsals by constraining the increase of the longitudinal arch curvature.

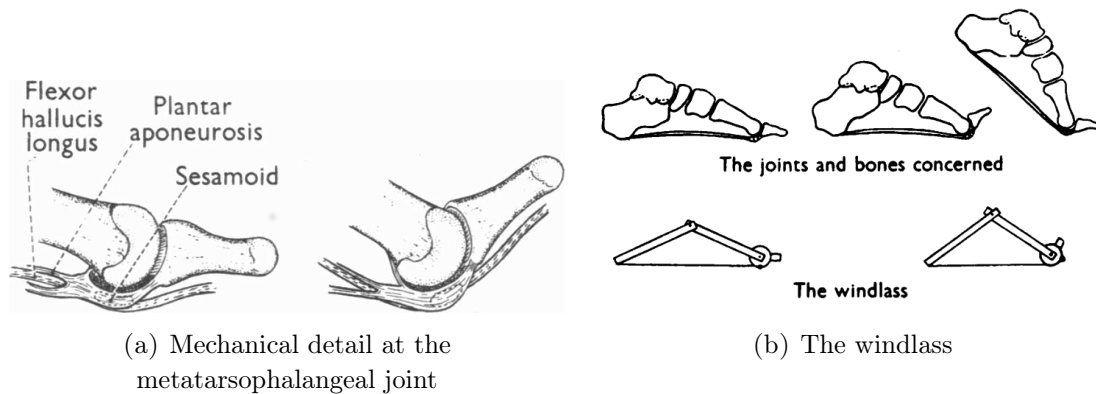


FIGURE I.13: Windlass mechanism by Hicks [Hic54]

Concerning the transverse arch, studies are rarer, the most recent one on the subject has investigated the effect of the curvature of the transverse arch on the overall rigidity of the foot. It proposes an analogy of the sheet of paper, displayed in the figure I.14, to explain the behavior of the transverse arch

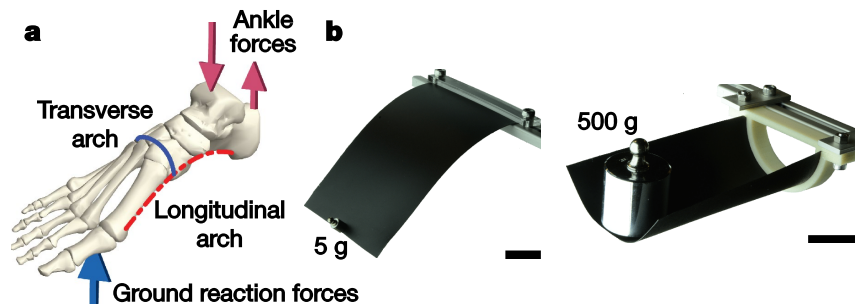


FIGURE I.14: Transverse Tarsal Arch by Venkadesan [Ven+20]

in (a) the human foot arches represented with the Medial Longitudinal Arch (MLA) and the Transverse Tarsal arch (TTA)

in (b) a thin and floppy sheet of paper becomes considerably stiffer because of transversal curvature. The TTA may have a similar role in feet. Scale bars, 5 cm.

Different measures are used to describe the situation encountered by the foot. There is the positioning of the foot according to the progression of the step with spatio-temporal parameters. They can globally describe the gait cycle as in the picture I.15, illustrated by [Ade86], or more precisely by following measurements of foot segment angles. The gait cycle applied to a foot is broken down into two main stages: a phase of contact with the ground called the stance phase and a non-contact phase called the swing phase. In a gait cycle, a permanent contact is ensured by one foot and then the other with a moment when both feet touch the ground. Whereas during a running cycle, a float phase where none of the feet touch the ground is present between the respective stance phases of each foot. Most studies focus on the stance phase of the foot where the foot is exposed to loading.

A second measure used to describe the behavior of the foot is the force applied by the ground on the body in reaction to the subject's weight and dynamic effects. It is most often expressed in terms of its vertical component, but all three components are relevant. In a gait cycle, a "M" shaped vertical loading curve is commonly found, the faster the

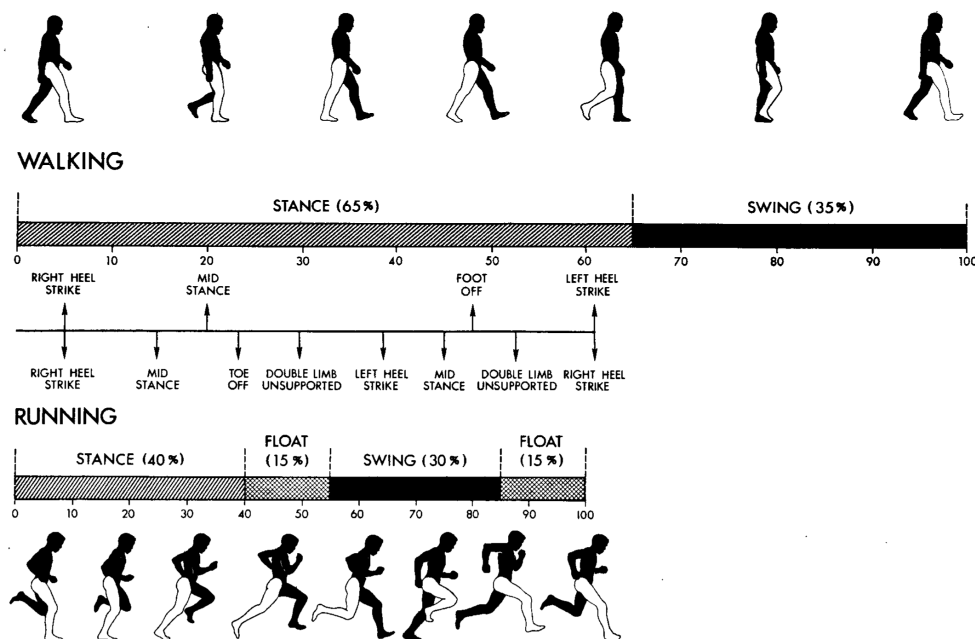


FIGURE I.15: Adelaar 1986

speed, the closer the vertical loading curve gets to a running cycle curve as displayed in figure I.16a by Keller [Kel+96]. For a running cycle there are different types of attacks commonly described, they are associated with different patterns of vertical ground reaction force as displayed in figure I.16b by Lieberman [Lie+10]. The main one on the subjects trained with shoes is the heel attack, then for barefoot trained runners it is an attack from the front of the foot and more rarely from the midfoot [Lie+10].

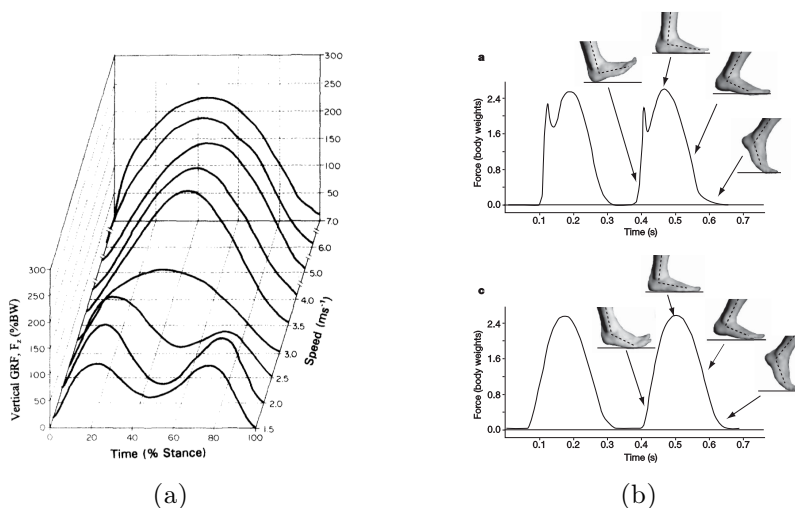


FIGURE I.16: (a) Evolution of vertical ground reaction force in function of body displacement speed [Kel+96]; (b) Rear and forefoot strike pattern with their vGRF associated [Lie+10]

Finally, the third measure will focus on plantar pressure.

We will come back to the acquisition of these different measures in section I.5.1, we use here only their values to introduce the foot movement.

I.4 Footwear devices

Wearing a shoe is intrinsically linked to the foot. It is an object that is the subject of many designs, as illustrated by the presence of many patents on various components of the shoe. Some of its components can be studied to achieve a medical function, for example, the insole thickness and stiffness to reduce peak plantar pressure for diabetic patients.

In the clothing field, footwear are mainly in the prêt-à-porter industry. Different applications are attributed to them, which gives different examples: casual shoes, safety shoes, sport shoes (with variants depending on the sport practiced) etc ...

In this paragraph we will focus on the components and application of the shoe, without considering the fashion accessory aspect that it can have. The contents comes from the CTC's books and informations [CTC08].

I.4.1 Shoe description

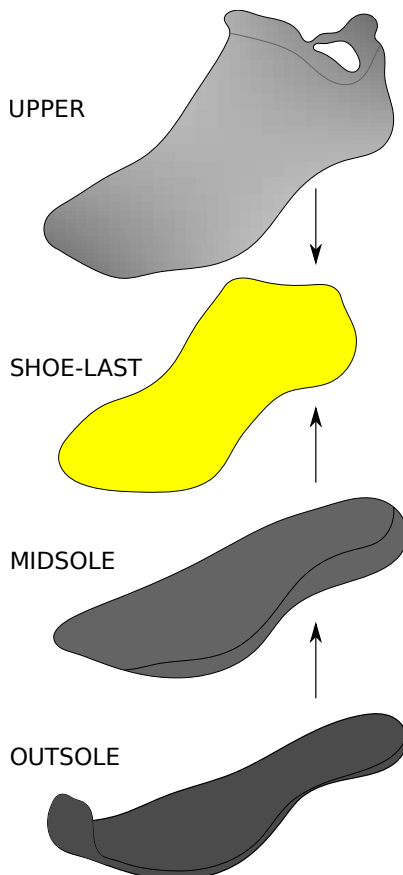


FIGURE I.17: Shoe components

I.4.1.1 Upper

The upper integrates the parts dressing the top of the foot. It is composed of the top for the visible parts, the lining for the parts in contact with the foot and the reinforcements that are placed between the top and the lining to keep the volume of the upper, or to add rigidity.

I.4.1.2 Shoe-last

The shoe-last is not a component in itself of the final product but is an integral part of its manufacture. The volume of the shoe-last represents the volume of the foot adjusted to the design of the shoe; it is designed to ensure the assembly of the finished product's components.

I.4.1.3 Sole

The sole integrates the parts under the foot. It is composed of a first strategic part for the assembly of the final product: la première de montage (the first assembly part). This part is temporarily attached to the shoe-last, upon which the upper and the rest of the sole will be fixed.

We then find different elements with variants depending on the manufacturing process retained. For their mechanical effect, we will retain the midsole and the outsole.

I.5 Experimental and numerical approaches for foot biomechanics

Foot experimentation and modeling are two approaches to study the complex biomechanical behavior of the foot. In this section, the main concept and different variants of these two approaches will be presented without attempting to be exhaustive, as this is a vast subject of active research.

For the experimental part, the synthesis of the methods will be done following the logic that there is a basic method to obtain a first description of the foot behavior and, step by step, more complex methods have been added to enrich this description and provide data to model this behavior.

The model part will focus on construction methods and modeling choices made to study a specific biomechanical behavior of the foot.

I.5.1 Experimental

I.5.1.1 Kinematics & Kinetics

The measurements of basic spatio-temporal parameters, such as the speed of movement, step length, frequency, etc . . . , are the first batch of quantitative measurements to study the gait of the foot. Their acquisition is based on the chronology of events in motion [BM88; Bak07].

Compared to basic spatio-temporal parameters, the kinematics measurements obtained with motion capture provide more detailed and accurate information on the behavior of the foot. It is a progression towards a better understanding of the foot biomechanics leading to a better assessment of foot pathologies and their clinical treatment. The most prevalent approach is based on video capture of the movement of physical markers using visible or infrared light and much more rarely approaches based on X-rays or markerless are used. The capture itself is associated with biomechanical models composed of more or less rigid segments of the foot to record selected joint angles [Ran+08], for example with the flexion of the talocrural joint representing the plantar or dorsal flexion of the foot [Sim+06].

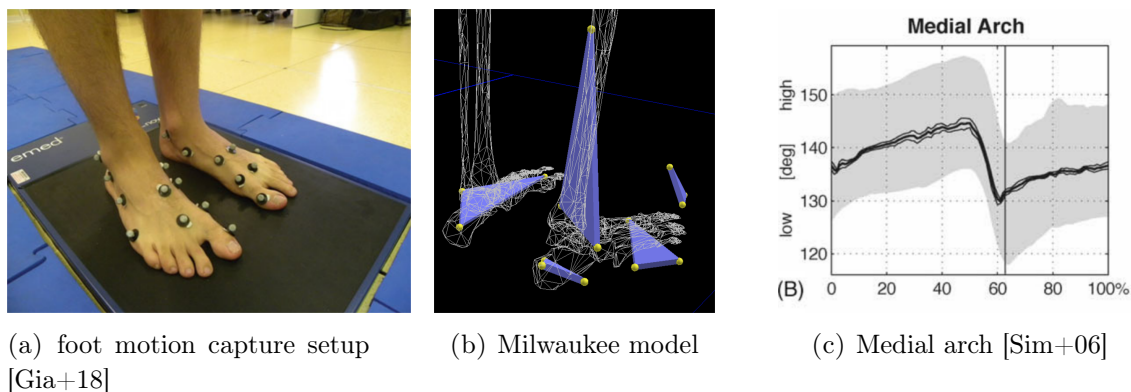


FIGURE I.18: Example of video motion capture study

Various limitations are inherent to the video motion capture method. First of all there is the so-called soft tissue artifact (STA), where the movement of the skin, as it moves the markers, interferes with the estimate of bone movement. The question of whether or not this parasitic movement influences the conclusion of the studies remains an open

topic of discussion. There is a tendency that, despite the development of techniques to correct this effect, the goal of a robust evaluation of the skeletal system's three-dimensional kinematics using skin markers has not yet been achieved [Lea+05]; another study concluded that there were no conclusive solutions to the issue of STA in the analysis of human movement [Pet+10]. Secondly, the technique was designed to capture barefoot movements, the addition of a shoe significantly reduces the number of segments tracked and thus degrades the ability to extract joint angles. And above all, thirdly, despite the models with the most segments tracked, there is no measurement of each foot bone and therefore no exhaustive view of the relative movement between them.

In response to these limitations, other capture methods using medical X-ray and, more rarely, magnetic resonance images, have emerged and composed an active research topic. In fact, to obtain a reliable view of the internal behavior of the foot, computed-tomography (CT) and weight-bearing cone beam CT scanners provide images on which computer processing can be applied to extract information such as the position of individual bones. But it is at the price of an exposure to X-rays, therefore, when working with *in-vivo* subjects, it is limited to a few shots, which must be taken on static configurations because the acquisition requires an immobile anatomical part over a non-instantaneous period of time. Fluoroscopic image processing is then a solution to observe dynamic movement, but it is not yet possible to completely track every bone of the foot because the acquisition volume is limited and requires more sophisticated digital processing to automatise the tracking.

Biplanar X-ray fluoroscopy, is the privileged approach and can be coupled with other type of acquisition to help the digital processing such as classic video motion capture or the tracking of outer skin [PB19].

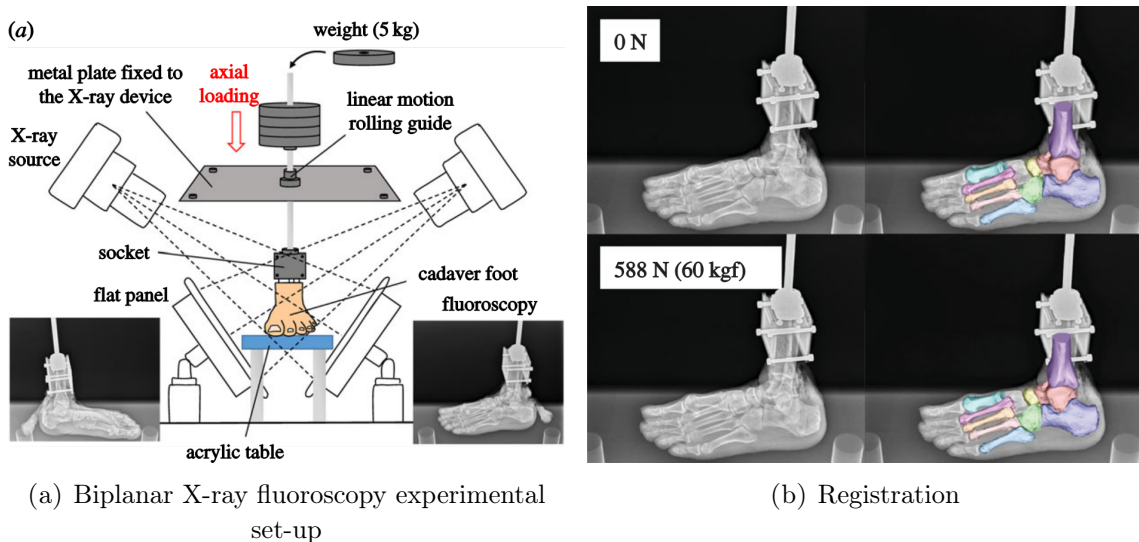


FIGURE I.19: biplanar X-ray fluoroscopy work from Ito et al. [Ito+17]

The use of fluoroscopy adds other valuable internal measurements, which coupled with other types of measurements refine the understanding of the foot's behavior and make an efficient information base for foot modeling. For example, Gefen et al. simultaneously measured heel fat pad tissue deformation and heel-ground contact stresses during the stance phase of gait [GMI01].

Then other types of measurements can be evaluated. Kinetic measurements add information about forces and moments due to displacements. The first measure of kinetics is

the pressure exerted under the foot, the analysis of which began in 1930 using ink. An acceleration of plantar foot pressure studies is made in the years 1985 with the use of modern means of acquisition often of two types, the platform of pressure as well as the embarked system in the shoes. The first modern analyses focus on the influence of displacement speed on the pressure map. Then the diabetic foot is a common application comparing healthy and pathological subjects: diabetic subjects have stiffer tissues resulting in areas of excess pressure compared to a healthy subject, which can promote the development of ulcers [ZL20].

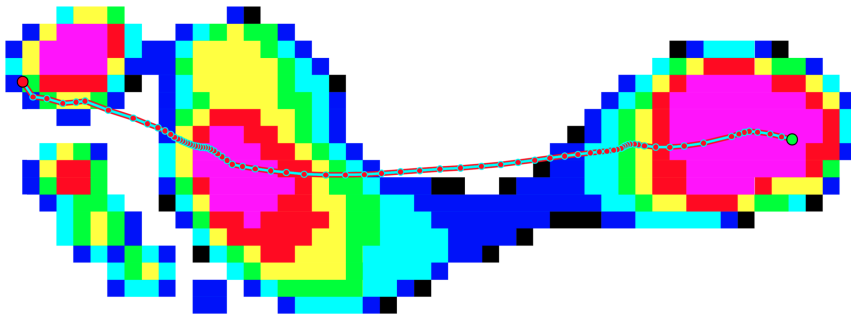


FIGURE I.20: Typical centre of pressure distribution [Bul+18]

The second measure of kinetics is the force exerted on the foot by the ground, it is obtained with force platforms. The analysis of the components of the force, in particular the vertical one, is widely used to quantitatively characterize the gait [MI78].

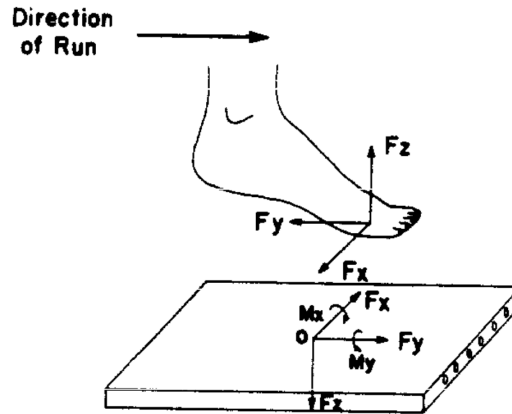


FIGURE I.21: Ground reaction force [CL80]

Joining kinetic measurements, but not directly measuring a mechanical variable, electromyographic measurements capture the physiological contraction activity of muscles with electrodes placed on the surface or, more rarely, at depth. Associated with kinematics, rigid body models and inverse methods, these electromyographic data are essential for finding muscles forces. They are rarely performed on the foot [Zha+17; RJB11] because it has many redundant muscles that are placed deep in the body.

I.5.1.2 Mechanical test

In order to characterize the mechanical behavior of the entire foot, then of its constituents, leading to the determination of the constitutive behavior of the different tissues in the foot,

mechanical tests at different levels of invasiveness are necessary.

From the least to the most invasive the following methods are used:

External mechanical tests are performed either with device (goniometer, arthometer), either without device (manual stress testing). With the device, the inversion of the foot generated by the application of a medial load to the ankle, as shown in Figure I.22 of Brown et al [BRK15], evaluates the laxity of the ankle.



FIGURE I.22: Inversion test setup [BRK15]

Without device there is the anterior drawer test, the talar tilt and many others. They are used to assess joint laxity and help estimate the stiffness of the ligaments involved in the joint, but because they are manual, they do not provide recorded measurements and are only used in clinical applications.

Next, the indentation test, where the plantar tissue is compressed between the indenting head and the bone surface. It is a classic method to determine the stiffness of the plantar soft tissues, in particular the adipose tissues under the heel and the metatarsal heads (fat-pads) [Cha+14; CZC11; Hsu+05; Hsu+07; TLG03; Zhe+12; Erd+06].

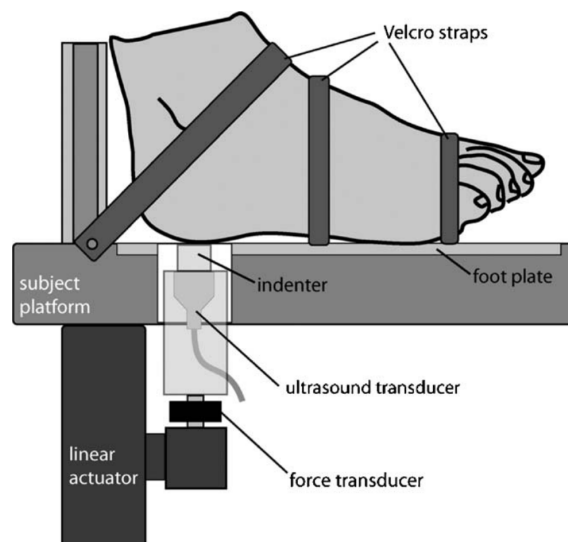


FIGURE I.23: Heel indentation set-up [Erd+06]

Interestingly Erdemir et al. [Erd+06] used the measurement coupled with finite element modeling to characterized the hyperelastic behavior of the heel fat pad.

Non-invasive techniques using ultrasound with shear wave elastography have been performed, especially on the Achilles tendon [Hae+17; Pay+18] considered as the strongest

tendon in the body.

And finally, the most invasive one, therefore practiced on *ex-vivo* feet, the tensile test of the foot's anatomical components. They can be performed directly on the tissue sample, or by isolating the articulation and pulling on the extremity bones.

Schmidt and Ledoux [SL10] efficiently summarized the experimental challenge of ligament testing: to characterize elasticity from mechanical tests, for example with Young's modulus, the length, cross-section and tensile measurements of the object are at least necessary; these two first values are considerably more complex to record on soft tissue than on metal rods. For ligaments, the standard for determining the length is using a caliper, whereas for obtaining the cross-section, there is no standard. Because ligaments can be short and are placed between bones, their cross-section is often difficult to measure and different techniques can be used. Schmidt and Ledoux used casting techniques to study 4 different ligaments and showed strong variability in ligament cross-section between subjects, as shown in Figure I.24. A large study, this time using a fracture-freezing protocol to establish the morphology of the ligament, also measured significant cross section variability [Mka+05].

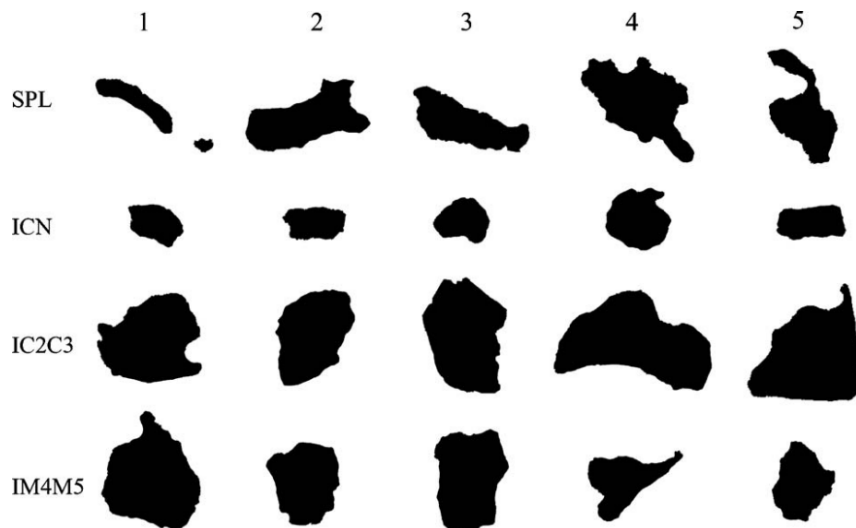


FIGURE I.24: Ligament cross-section of 5 *ex-vivo* subjects [SL10] short plantar ligament (SPL), inferior calcaneo-navicular (ICN) ligament, interosseous second cuneiform-third cuneiform (IC2C3) ligament, and interosseous fourth metatarsal-fifth metatarsal (IM4M5) ligament

To construct a simplified view of the ligament's mechanical behavior, the linear modulus of elasticity in [N/mm], which can also be called stiffness, can be characterized without measuring the poorly observable cross-section and the precise initial length of the ligament. In this case, a tensile test is sufficient and most studies do this by applying tensile forces to the tissue through the bones. Most of them focus on the ankle, as this is an area that is prone to sprain.

Attarian et al. [Att+85] used this approach by mechanically testing isolated ankle bones with the involved ligaments intact. Although the linear modulus of elasticity was calculated, they also pointed out that all ligaments exhibited non-linearity and strain-rate dependence.

With the same approach, and concerning the same articulation, Siegler et al. have worked on collateral ligaments of the ankle [SBS88].

In addition, Beumer et al. have worked on the stiffness assessment of anterior & posterior tibiofibular ligaments and posterior tibiotalar ligaments [Beu+03].

More rarely, the plantar aponeurosis [Kit+94] and the Lisfranc & dorsal cuneometatarsal ligaments [Kur+01] have been analyzed using this approach.

The stiffnesses of the ligaments obtained by these different authors present large variability as shown in the table I.1.

Reference	Ligament	Avg. Stiffness (N/mm)	Std. (N/mm)
Attarian et al. [Att+85]	Anterior talofibular	39.99	8.54
	Calcaneofibular	70.51	6.90
	Posterior talofibular	39.75	13.79
	Tibiotalar	128.82	25.04
Siegler et al. [SBS88]	Lateral collateral ligaments include posterior fibulotalar lig. (PFTL)	164.3	55.5
	fibulocalcaneal (FCL)	126.6	42.9
	anterior fibulotalar (AFTL)	141.8	79.3
	tibiospring (TSL)	122.6	66.9
	posterior tibiotalar (PTTL)	234.3	77.6
	tibionavicular (TNL)	39.1	16.6
Beumer et al. [Beu+03]	Anterior tibiofibular	78	12 ^a
	Posterior tibiofibular	101	16 ^a
	Posterior tibiotalar component of the deltoid ligament	115	15 ^a
Kitaoka et al. ^b [Kit+94]	plantar fascia lateral zone	182.5	37.5
	plantar fascia middle zone	232.5	53.1
	plantar fascia medial zone	203.2	56.6
Kura et al. [Kur+01]	Dorsal cuneometatarsal	66.3	18.3
	Lisfranc	189.7	57.2

^astandard error of mean (SEM), n = 10

^bloading rate of 111.2 N/sec

TABLE I.1: Some ligament stiffness according to the literature

I.5.2 Model

To model biomechanics, there are two main types of models, the multi-body model also named rigid-body or musculoskeletal, and the finite element model.

They are somehow related, as they rely on mechanical equilibrium to compute forces and displacements, but they differ widely in their mathematical and numerical implementation and thus in their application.

Multi-body models are mainly used to calculate the movement of articular chains, taking into account the contact in a simplified way and not calculating the deformation of the objects. Whereas finite element models essentially consist in this case in calculating

the deformation of the objects, the contact and the associated mechanical values (stress, temperature, ...).

Both can be used in a coupled manner, the multibody part to calculate bone motion and the finite element part to calculate soft tissue strain and stress and to include contact.

We will now go through the different methods to build these models, starting with the geometrical aspects, then the material aspects and the boundary conditions, to then define which method is used for a given study. In the work of this thesis, it is a finite element model with some aspects of a multibody model that is exploited so that the soft tissue deformation and stress can be simulated.

I.5.2.1 Patient/Subject specific model construction workflow for FE analysis

I.5.2.1.a Geometry

Modeling the anatomical components of the foot begins with the geometry.

With the methods covered in this thesis, the geometric description finally exploited is mainly discrete geometry and is done in a mesh format that describes points and connectivity.

The geometrical description is mainly done at the macro level with the continuity assumption, which means that the components of the anatomical part, e.g. the collagen fibers of the ligaments, the alveoli of the adipose tissue, etc... are rarely represented geometrically. This will add too much complexity to an already complex case and will make it more difficult to solve the problem while increasing computation time. If the anatomical components need to be studied at a micro level, this is done with a local model.

At the macro level, two aspects must be taken into account: is it a detailed geometry from a patient or is it a simplified representation?

In the case of a simplified representation, it can be taken directly from a sketch or from medical images of patients which can be simplified. In the case of the detailed representation, it starts from the medical image processing.

In practice, simplified and detailed geometries are often mixed in the model. Some components are easily describable from medical images and thus represented in detail, such as bone and homogenized soft tissue, and others are more difficult to process, in which case a simplified version is then used.

Most studies have used detailed bone geometries, then simplified geometries for connective tissue with 1D elements representing tendons, ligaments, then the other soft tissues are often homogenized in a few parts [Gef+00; CTJ01; Gef02; Che+05; Che+10; Isv+12; Gui+14]. A common variant is to represent the plantar fascia with volumetric elements [Wu07; Che+08; Gu+10; Akr+18] or to represent the ligaments with line bundles [Gar+09; Bae+15]. For muscles, the same decomposition with representations in volume, by lines or bundles of lines exists. For macro models, the representation of cartilage is simplified with either a volumetric representation between bones [Gef+00], or by adding an extension to the bone [Isv+12; And+06], or by integrating them into the bone geometry and defining the cartilage behavior into the finite element solver's contact declaration [Won+20a].

The geometric modelling is done by following a classic workflow from image processing and meshing. Each of these themes is vast, so the following descriptions are not exhaustive and focus on applications in macro models.

Processing of medical images

The image processing can be performed on three different medical image sources to generate 2D or 3D geometric descriptions.

Images from the Visible Human Project, where slices of bodies were photographed, is a valuable source of color information used as a standard in biomechanical fields. Magnetic Resonance Imaging (MRI) provide images which offers the ability to segment the patient's tissues in detail. More commonly, X-ray medical images are used, from Computed Tomography (CT scan) to obtain 3D images and fluoroscopy to obtain 2D images.

On these images, regardless of the source, numerical processing is performed to segment the different components. There are attempts to semi-automatize or automatize the process of segmenting the anatomical components of the foot using image segmentation algorithms through four different historical approaches, which are not exhaustive.

The first approach is based on the gray intensity values of the images. It consists in separating the different phases of the image by focusing on the histogram of the image's gray values. Threshold & multi-thresholding techniques such as k-means thresholding and multi-otsu [Ots79] are algorithms that are part of this approach, whose documented limitation is their lack of exploitation of the spatial information.

The second approach is based on the boundary by detecting the phase contour. It is performed by filtering the image with gradient operators and/or using various methods ; these are often active contour models with the snake [KWT88] as the first implementation of energy-based active contour principles, then by geodesic active contour [CKS95] and level set methods.

The third approach is region-based and consists in iteratively encompassing neighboring pixels that have a similar value to the growing region; e.g "split and merge" technique, seeded region growing (SRG) algorithm [AB94] and other statistical region-based segmentation.

And the fourth approach is called hybrid by combining the previous approaches, one well known is the watershed algorithm introduced by Digabel, Beucher and Lantuéjoul [DL78; BL79; BM93], where an analogy is made between the gray intensity of the pixel composing the image and the height/altitude in a topographic representation of this same image. It is used to partition the image by flooding it from its minimum altitude.

For foot segmentation, few automatic or semi-automatic workflows using these approaches exist and only work properly in special cases, therefore the segmentation operation still relies mainly on manual processing by redrawing the contour of the component with curves and then interpolating. An additional difficulty is that, in some cases, the anatomical components to be modeled are simply not clearly segmentable on medical images, so anatomical atlases are used to represent them.

Meshing

To obtain an discrete geometry, the most common approach is to mesh using the curves describing the contour of the anatomical component. To go from an image format description to a mesh format description, algorithms that calculate a mesh from an image are used, such as the Marching Cube or Volumetric Marching Cube algorithm implemented in different software often found in biomechanics (Mimics, ScanIp, 3D slicer, ...).

Registration

To speed up model construction, it is possible to reduce manual processing using methods exploited in Static Shape Analysis (SSA), Computer Graphics and Computer-Aided Design (CAD). It consists to build a detailed initial/generic model that will be registered with rigid and then non-rigid transformations to match the geometry of a new patient. Instead of manually processing each new patient acquisition, the generic model is registered to the new patient acquisition.

Rigid registration commonly goes through 3 transformations.

- Translation, to align the means of the studied geometries with the origin. It is performed by subtracting the mean of the studied geometry from the coordinates of the nodes.
- Rotation, often set by the minimization of a cost function evaluating the alignment.
- Scale (Uniform/isotropic scaling), to work on the same scale between the studied shapes.

Reflection, as an additional treatment, can be added in the rotation treatment. This is particularly useful for transforming a left bone into a right bone.

The dominant method for aligning geometries after initial estimation/pre-alignment is the Iterative Closest Point (ICP) algorithm [CM91; BM92] which uses these transformations, translation and rotation in its initial version, to align geometries. In essence, the following logic is applied iteratively to minimize the distance/error between two geometries, but there are many variations:

1. Selection of pairs of corresponding points between the two geometries
2. Compute and apply transformations
3. Calculate the distance/error between geometries

Rusinkiewicz and Levoy [RL01] listed many of the variants occurring at each step of the algorithm; from point selection (all, uniform or random sampling . . .), the point matching (closest, normal shooting . . .), the weighting and rejection or not of pairs, the error metric even if is often the sum of squared distances between corresponding points, to finally the computation of the transformations and the minimization strategy.

For non-rigid registration a panel of transfer function is then available on top of affine transformation. Two main approaches are the free-form deformation (FFD) [SP86] and the radial basis function [dBvdSB07; SMB14; Bia17] but many others exist using various method such as energy minimization [SHW08], finite element solver, . . .

Non-rigid registration consists of deforming one geometry to fit another, it is also referred to as mesh-morphing.

RBF function has a strong history in point interpolation [Car+01]. Its use has evolved with RBF-based morphing for finite element simulation to avoid remeshing, particularly for fluid simulation [JA07; Mic11; GCB19], and has also been extended to medical applications such as bone morphing [Gra+11]. In summary, its concept is based on few landmark displacements (boundary nodes) to compute the new node positions corresponding to a new patient, a new product design or an updated geometry over time. An entry-level implementation, performed for the first time on foot bones, is explained in Chapter II.

It is not as commonly used in the foot model because it is usually developed on a single bone or organ, so its versatility needs to be tested to treat different bone geometries.

When registration is used, these methods have the advantage of keeping the same topology and nodes to describe the anatomical components, such as bones and organs, of a series of patients. This is the first requirement to then exploit Statistical Shape Analysis (SSA) with Principal Component Analysis (PCA) related to Singular Value Decomposition (SVD) in order to access the mean shape and modes of variation of a geometry.

I.5.2.1.b Constitutive equations

The equation formulation of this section are issued from the Abaqus theory manual [HKS11].

At the macro level, the foot is composed of the soft tissues that surround the bones with their cartilage. Soft tissues are muscles, ligaments, fascias and adipose tissue; they are subject to large strains and follow a non-linear mechanical behavior.

In finite element models, to express the mechanical behavior of soft tissues, the following constitutive equations are exploited :

In the first place, a linear elastic behavior can be used. For springs, the Hooke's Law equation I.1 is used in vector form, with some variants to make the object work only in traction or compression. It is notably used for ligaments & tendons when they are represented by a 1D connector element. For continuous material, the general equation of Hooke's Law, equation I.2, takes into account the change in thickness. It is rarely used as the tissue undergoes large strain and has a non-linear stress-strain relationship, it is therefore recommended to use a hyperelastic material.

$$f = k \cdot u \quad (\text{I.1})$$

With f the force, k the stiffness and u the displacement.

$$\vec{\sigma} = \mathbf{D}^{el} \vec{\epsilon}^{el} \quad (\text{I.2})$$

With $\vec{\sigma}$ the total stress, \mathbf{D}^{el} the elasticity and $\vec{\epsilon}^{el}$ the total elastic strain.

The non-linear elastic aspect can be taken into account with hyperelastic materials based on a strain energy function. Starting from the isotropic, incompressible or almost incompressible behavior and independent of the deformation rate, the simplest hyperelastic model, the Neo-hookean form, equation I.3, is commonly used, followed by Ogden, equation I.4 and others. The Neo-Hookean form is a special case of the polynomial form.

$$U = C_{10}(\bar{I}_1 - 3) + \frac{1}{D_1}(J^{el} - 1)^2 \quad (\text{I.3})$$

With U the strain energy, C_{10} a material parameter (representing the initial shear modulus at low strain), \bar{I}_1 the first strain invariant, D_1 a material parameters (determining the compressibility of the material) and J^{el} the elastic volume ratio.

$$U = \sum_{i=1}^N \frac{2\mu_i}{\alpha_i^2} (\sigma_1^{-\alpha_i} + \sigma_2^{-\alpha_i} + \sigma_3^{-\alpha_i} - 3) + \sum_{i=1}^N \frac{1}{D_i} (J^{el} - 1)^2 \quad (\text{I.4})$$

With μ_i and α_i material parameters.

μ_i refers to the initial shear modulus with $\mu_0 = \sum_{i=1}^N \mu_i$

λ_1, λ_2 et λ_3 are the principal stretches.

Then a time-dependent strain can be added with the viscoelasticity. It is mainly done with Prony series defining relaxation parameters at certain times which, for hyperelastic material, modify the hyperelastic constant or directly the energy function. The hyperelastic constant modified by viscoelasticity is given for the Neo-hookean model in equation I.5 and for Ogden in equation I.6.

$$C_{10}^R(t) = C_{10}^0 \left(1 - \sum_{k=1}^N \bar{g}_k^P (1 - e^{-t/\tau_k}) \right) \quad (\text{I.5})$$

$$\mu_i^R(t) = \mu_i^0 \left(1 - \sum_{k=1}^N \bar{g}_k^P (1 - e^{-t/\tau_k}) \right) \quad (\text{I.6})$$

With $C_{10}^R(t)$ and $\mu_i^R(t)$ the updated material parameters from C_{10}^0 and μ_i^0 the initial parameters, \bar{g}_k^P the shear relaxation modulus and τ_k the relaxation time, both part of the Prony series terms.

The contact between objects can also be defined with different properties. Regarding the tangential behavior of the contact, the Coulomb model is often used with a penalty formulation. This formulation avoids convergence problems by allowing a small displacement between objects until the critical shear stress is reached and the displacement is fully allowed. Coulomb model is displayed in equation I.7

$$\tau_{crit} = \mu p \quad (\text{I.7})$$

With τ_{crit} the critical stress, μ the friction coefficient and p contact pressure,

Regarding the contact behavior in the normal direction, there are different formulations of pressure-overclosure, from hard contact where no overclosure is possible to different definitions of overclosure (linear, exponential ...).

The parametric aspect is important because it defines the output of the simulation, it must therefore be carefully adjusted to obtain a simulation result that is representative of the field reality.

I.5.2.1.c Materials: Parameters of the constitutive equations and geometrical representation

Of the 22 finite element foot model papers screened, which were published from 2000 to 2020, the material parameters were set according to a few works: for bone material 1 article, for cartilage 6 articles, for ligament 4 articles, for plantar aponeurosis 2 articles and for soft tissue 2 articles. Different choices of geometric representation for each foot component are also made. These material and representation aspects will now be examined in a detailed but non-exhaustive manner in order to extract the main model construction methods.

Bone

For bone parameters, the work of Nakamura et al. [NCC81] is mainly used. This is one of the first finite element foot models with an isotropic linear elastic material for bone containing a Young's modulus $E = 7500$ [MPa] and a Poisson's ratio $\nu = 0.3$, justified since these are values frequently used in biomechanical models.

Bones can also be considered rigid, given the important difference between soft tissue and bone rigidity plus the fact that they are only slightly deformed compared to other tissues.

In macro models, their representation is mainly done with tetrahedral elements (3D) and considering that the bone is a completely solid piece. This representation does not take into account that only the trabecular part is very rigid in relation to the surrounding soft tissues and bone marrow, which fills the interior of the bone. The main purpose of this simplification is to avoid complex meshing by separating the fine trabecular volume from the bone marrow, while considering that the bone is so rigid in relation to the soft tissues that this detailed separation will not influence the result of the simulation. The advantage of assigning a high rigidity compared to considering bones as a rigid bodies is to avoid mechanical stress peaks that can reduce the stability of the simulation, whereas considering them as a rigid body simplifies the resolution by decreasing the number of degree of freedom in the simulation.

Cartilage

For cartilage, 6 main articles appear to define the parameters of the material:

Two experimental studies are mainly exploited; they are standard biphasic creep indentation works with similar values, the first by Liu et al. [Liu+97] on 7 pairs of second metatarsal intermediate cuneiform cartilage and the other one by Athanasiou et al. [Ath+98] on the metatarsophalangeal joint. The authors who created foot models from this information assigned to the cartilage a homogeneous linear isotropic material with a Young's modulus of 1 [MPa] and a Poisson's coefficient of 0.1 or 0.4 [Gef+00; Che+05; Che+10; Gu+10; Gui+14]. One author has integrated this information by defining a non-linear normal contact and a frictionless tangential contact without detailing the parameters [Won+20a].

Three numerical works were also used as a source of material parameters. These are the studies by Patil & Jacob et al. [PBH96; Jac+96; JP99] where the values are fixed on the basis of two articles on the femur: one not available for consultation and the other a parametric study for a finite element tibio-femoral model [SSH90]. The authors who created foot models from this information assigned to the cartilage a homogeneous linear isotropic material with a Young's modulus of 10 [MPa] and a Poisson's coefficient of 0.4 [CTJ01; Gef02; Gar+09].

Another finite element model, realized on the shoulder [Büc+02], is used as a source; it takes data from two documents [Kem80; Ben98] to establish a neo-hookean model which is reused by Wu et al [Wu07].

Other works consider cartilage to be rigid [Isv+12] or use rarer, non-detailed sources of information.

Three geometric representations of cartilage are used in macro model. The first with a unique volume between the bones; it has the advantage of being easier to mesh because the volume of the piece is larger than considering several volumes of cartilage each assigned to a bone. In case of large amplitude of bone movement because this representation shifts the point of contact of the bone it can lead to a non-physiological displacement. The second is to represent the fine volume of cartilage specific to each bone, in this case the meshing is complex in addition to the fact that on the main image source used, X-ray imaging, the cartilage is difficult if not impossible to segment. The third is like the second, considering each cartilage specific to the bone but instead of coupling it to the bone it is directly integrated into the bone volume. It is then through the definition of the contact

that the behavior of the cartilage is fully taken into account. This method simplifies the meshing protocol while still having the defect of representing a volume that is often not segmentable.

Ligament

For ligaments, 4 main articles emerge to define the material parameters [RA94; CRP95; SBS88; Cor+03].

The principal one is the work of Siegler et al. [SBS88] who experimentally studied the tensile mechanical properties of ankle joint collateral ligaments in 20 subjects. The authors who created foot models from this information assigned a linear elastic material for all modeled ligaments with a Young's modulus equal to 260 [MPa], a Poisson's coefficient equal to 0.4 and a cross-section equal to 18.4 [mm²] [Che+05; Che+08; Gar+09; Che+10; Gui+14; Won+20a]. The Young's modulus is set by taking the average elastic modulus of the six ligaments obtained by Siegler et al. on which a large variability was also measured, as shown in Table I.2.

	ATFL	FCL	PFTL	TNL	TSL	PTTL
Mean elastic modulus (MPa)	255	512	216.5	320.7	184.5	99.54
Std elastic modulus (MPa)	181.3	333.5	169.5	268.5	133.4	79.32

TABLE I.2: Siegler et al. [SBS88] ligament Young moduli anterior fibulotalar (ATFL), fibulocalcaneal (FCL), posterior fibulotalar (PFTL), tibion-avicular (TNL), tibiospring (TSL), posterior tibiotalar (PTTL)

Then, the finite element work of Chu et al. [CRP95] which used a Young's modulus of 11.5 [MPa] for ligaments is rarely used.

Gefen et al. [Gef+00; Gef02] were the only ones to fit a non-linear behavior from the experimental test of Race et al. [RA94].

A more recent work by Bae et al. [Bae+15] establishes different values for ligament stiffness based again on the work of Siegler et al. [SBS88] but adds some information from Corazza et al. [Cor+03] for the physiological cross-sectional area (PCSA).

In macro models, three geometric representations of ligament are used: 1D, 2D and 3D. 1D is the most common because it simplifies the process of representing anatomical components that are difficult to segment on the most common image source used (X-ray). The more dimensions are added to the representation, the longer the construction and calculation will take as the degree of complexity increases in order to gain greater accuracy in the simulation output.

Plantar fascia

For the plantar fascia, two documents are used to define the material parameters [WR64; Kit+94]. The most cited is the work of Wright et al. [WR64] who carried out tensile tests on the plantar fascia, the studies using this work set a linear stiffness with a Young's modulus equal to 350 [MPa], a Poisson's coefficient equal to 0.4 and a section of 290.7 mm². More recent work by Kitaoka et al. [Kit+94] who also performed tensile tests and extracted stiffness values for different areas of the plantar fascia. The works using this source of information often define a non-linear behavior of the material or directly use the value found by Kitaoka et al.

The same representation method as the ligament is used for the plantar fascia, with 1D, 2D and 3D geometries.

Soft tissue

Regarding soft tissue, the paper from the work of Lemon et al. is often used [Lem+97a]. This is a finite element study of the sole effect in therapeutic footwear which, for the plantar tissue, defined parameters for a hyperelastic formulation from uniaxial stress-strain data obtained in heel testing of 5 subjects *in-vivo*. The location of the test and the variability of the measurements are not presented in the document. The studies citing this article use directly the hyperelastic model [Che+05; Che+10; Gui+14; Won+20a] or a linearized version [Isv+12].

The work of Nakamura et al. [NCC81] is used as a major source of information on the bone parameter but also used to define the soft tissue parameter. This time, the plantar tissue sample is taken from an *ex-vivo* subject and then compressed. This information was used by Gefen et al. in determining a non-linear behavior.

More rarely, the finite element work of Chu et al. [CRP95] fixing a linear material with a Young's modulus of 1.15 [MPa] and a Poisson's ratio of 0.49 is reused, as is the numerical-experimental work of Erdermir et al. [EVC03] which focused on fat pads to establish the parameters of a hyperelastic Ogden form.

Summary of principal limitations on soft tissues properties

In summary, in looking at the material parameters defined for patient-specific finite element models, it is highlighted that it is actually the geometrical aspect of the model that is mainly patient-specific and rarely the material aspect that reuses some publications that can be considered as standard. The parameters of these works used as standards have been calculated on samples of small sizes and their values show large variability. Cartilage, ligament & muscle behaviors are non-linear, but when they are applied in macro-models it is a linearized version that is mainly used to simplify the protocol. Same logic on their graphical representation, it is often simplified to obtain an accessible model development time.

I.5.2.1.d Boundary conditions

3 different boundary conditions are mostly used by the different authors to simulate different foot situations. During the simulation of a complete gait or its stages, extrinsic muscle forces are used in several studies based either on data from the literature [Gef+00; Isv+12]. More recently, it is calculated directly from the kinematics of the subject's foot studied with the OpenSim software [Del+07; Akr+18; Won+20a]. More simply, only the activation of the Achilles tendon is used [Gef02; Che+05; Gar+09; Che+10; Gui+14]. The muscles activity are not necessarily included, the orientation of the foot with e.g. only the displacement of the tibia can be used [Bae+15]. The previous boundary conditions are coupled with an application of the Ground Reaction Force (GRF) through the tibia, or by the ground on which the foot is in contact.

I.5.2.1.e Evaluation

The results of the simulation are compared to the observed value to confirm its representativeness on the studied subject. It can range from the comparison of the plantar

pressure and the peak pressure of dedicated regions, up to the reaction force of the ground and rarely the position of the foot.

I.5.2.2 Finite element foot model applications

The foot is exposed to strong loadings and, compared to the knee or hip, it absorbs them with a structure composed of many smaller bones connected to each other by numerous and redundant connective tissues. Thus, this complex mechanical structure, that faces a variety of loads in addition to being coupled with its active role in the movement of the body, will behave through a multitude of postures. These postures are difficult to observe with experimental measurements; this is why foot models are used to overcome this difficulty or even inability to directly observe them. In addition to the fact that the foot has a complex and difficult to observe behavior, it is also subject to many disorders and pathologies that are treated by a variety of surgeries and treatments.

Finite element simulations have therefore been used to study the foot in different situations. We will now go through the 22 papers in the period 2000 to 2020 that have been screened, to highlight the different applications of this type of simulation. It will go from the study of the bare foot, the foot with shoe, briefly on shoe studies to focus then on the implications of the simulation of the foot with shoe.

Bare foot studies

Without being exhaustive in the disorders, the deformations of the forefoot can be classified according to two differentiated areas of deformity, the big toe and the little toes. They account for 28% and 46% of forefoot operations in Sweden and Australia [Sar+08; MGL08]. At the level of the little toes the typical deformations in the sagittal plane are: claw toes, hammer toes, mallet toes; and in the transverse plane curly toes [Shi+11; Cou84; MDS16]. At the level of the big toe, one deformity is the hallux valgus, where the big toe bends in a lateral direction towards the little toes. Hallux limitus or rigidus with limitation of joint movement, especially in the dorsal direction, and accompanied with pain is also present [Dan86; SB98], as is the deformity of clawed hallux [Ols+03; Kad+05]. These deformations are a common source of forefoot pain and are often associated with footwear, trauma, genetics, inflammatory arthritis, neuromuscular and metabolic diseases [Fre+93]. Two natural causes stand out, the degenerative process with the progression of osteoarthritis and the imbalance of muscle strength.

In this field, finite element foot models have been used in studies to measure the impact of surgical decision or to examine the source of the disorder. Wong et al. [Won+20a] studied the relationship between ligament laxity and hallux valgus disorder by examining metatarsal shaft stress, angulations, joint forces and moments of the first ray when ligament stiffness is decreased. The same concept, by decreasing the rigidity of the deep ligaments, was developed to study the hypermobility of the foot's first ray and its impact on joint resultant force [Won+14]. Isvilanonda et al. [Isv+12] evaluated the source and surgical treatment of clawed hallux deformation by comparing changes in articulation angle and plantar pressure in 7 situations of muscle overpull and two surgical procedures. Budhabhatti et al. [Bud+07] simulated bare 1st ray, hallux limitus, arthrodesis and with therapeutic footwear to compare the simulated configurations in terms of plantar hallux pressure.

A more general use of the finite element model has been made; Gefen et al. [Gef+00] used this finite element approach to look at tissue stress with the perspective of anticipating

the surgical outcome. This effect study is done in another publication [Gef02] where the plantar fascia release surgery is evaluated by decreasing the thickness of the plantar fascia and looking in particular at long plantar ligament stresses and arch deformation. Numerous studies have been conducted on the pathology affected by this surgical procedure to release the plantar fascia, an inflammatory reaction called plantar fasciitis [Che+15; Lia+11, dots].

Diabetes is particularly studied using finite element foot models. The pathology has a stiffening effect on the tissue which generates a greater concentration of stress that can produce tears in the tissue which can turn into ulcers and lead to amputation. Therefore the simulation of plantar tissue stiffening and its impact on the distribution of stress in plantar tissues is one of the most studied subjects in finite element foot models [Gef03a; Che+05; Che+10; Gui+14].

Other pathologies or injuries are studied, such as the work of Wong et al. on ankle fracture [Won+16], posterior tibial tendinopathy [Won+18], subtalar joint arthrodesis [Won+20b]. The syndesmosis lesions has been studied through the work of Liu et al. with a model of the ankle [Liu+13; Liu+16]. There is also the studies of Wang et al. on ankle arthroplasty [Wan+18] or on the surgical treatment by fusion of the tarsometatarsal joint [WLZ14] and many others.

Shod foot and footwear studies

Given the amount of foot research using finite element modeling, it appears likely that this type of model has been adopted as a proven foot analysis tool. An additional degree of complexity has been added by taking into account the interaction with footwear, but studies that do so are much rarer because the complexity of the model is increased.

Nevertheless the question of the interaction of the foot with the shoes is present from the first models of the foot. For example, one publication, that we have seen used as a standard in material properties, is the work of Lemon et al. [Lem+97b]. They studied with a 2D finite element sagittal and local model the effect of the therapeutic insole, which is prescribed for the prevention of the neuropathic foot ulcer recurrence and is placed between the plantar tissue and the midsole. In this work the influence of the insole thickness on the plantar distribution in the forefoot region is examined.

This measure of plantar pressure continued to be used to study the relationship between the foot and the shoe with complete finite element models. Early studies of the screened papers focused on the relief of plantar pressure/stress with the work of Chen et al. [CJT03] and Cheung et al. [CZ08] both of whom coupled a foot model with a sole model. Then, more precisely in the heel region, Gu et al. [Gu+11] studied the effect of the Under the Calcaneus (UCA) midsole plug on the pressure distribution for pressure relief.

Returning to the local model, particular attention is given to the heel area of the foot. Fontanella et al. [Fon+13] examined the impact of sole material choice in the heel area during heel strike. Even-Tzur et al. [Eve+06] studied, at the same phase of the gait, the impact of sole degradation by reducing the sole rigidity and measuring the effect on the plantar tissue stress.

Works using complete models of feet coupled with complete models of shoes appear in 2009, in the screened publications. With a unique loading boundary condition, Cho et al. [Cho+09] focus on the impact phase of running with a simplified foot model coupled with a detailed model of a shoe with its essential components (outsole, midsole, insole, upper) to explore the viability of the modeling process. Also to test the viability of the process,

Qiu et al. [Qiu+11] proposed a more detailed foot model incorporating more bone and connective tissue with a boot-type shoe. In this work, the reaction force on the ground and the applied force by the Achilles tendon are used as boundary conditions to simulate a balance phase of the foot in standing position. To validate the accuracy of the model, the simulated plantar pressure distribution is compared with experimental data and finite element models in the literature.

This has evolved into a complete simulation of walking associated with wearing a shoe with only one publication found: Yu et al. [Yu+13] worked on the construction of a finite element simulation of wearing and walking with a high-heeled shoe.

If the shoe is the main object of the finite element study, the foot is not integrated and a pressure map is used as boundary conditions. This is the approach used in the work of Nishiwaki et al. [Nis08] and Drougkas et al. [Dro+18] in which foot behavior is not calculated and measured.

Coupled foot-shoe macro simulation

The interaction of shoes with the foot are not yet studied in the literature with coupled foot-shoe finite element models integrating the entire step sequence and the complete geometry; even though considerable injury, disturbance and discomfort may be partly due to this interaction which is measurable with this approach.

For example, in distance running, even if it is difficult to prove that the practice of this sport is a source of injury because there are no epidemiological studies given the complexity of such a survey, an opinion based on the observation of endemic injuries to distance runners is that repetition of heavy loads with abnormal alignment is a source of injury. A first proposed etiology is (1) training error, (2) anatomical factors, and (3) footwear and surface, leading to the following common problems: knee pain, posterior tibial syndrome (shin splints), achilles tendinitis, plantar fasciitis, stress fractures, illiotibial tibial tract tendinitis [JBO78; CL80]. Over time and with the evolution of footwear, it has been reported that knee injuries have increased while achilles tendinitis has decreased. One advanced explanation is the change in the shoe sole design with a heel higher than 10 [mm] giving increased stability of the hindfoot [MCT85]. But many discussions pointed out that the studies involved different populations, such as specialized runners and recreational runners, with different definitions of injuries, small sample sizes, and other question marks that lead to the inability to clearly conclude on the link between injury and shoe wear [Nig+15]. That is why understanding the functioning of the foot in this practice and looking for optimized footwear through a multitude of aspects such as patient-specific design, the use of specific materials and many other aspects is an open subject in which the finite element model can give insights. This approach can be extended to other sports, especially those that involve rapid changes of direction placing high stress on the foot, such as many ball games, and it is also viable to study other pathologies as it has been done with barefoot simulations. To this notion of injury can also be added the notion of performance and comfort of the shoe.

I.6 Synthesis and positioning of the study

The non-exhaustive description of the anatomy and biomechanics of the foot has shown that it is a complex structure. It encompasses many bones & tissues as well as a wide variety of behaviors influenced by a multitude of parameters. The state-of-the-art has

shown that scientific barriers prevent the generalization of the foot's internal behavior observation:

1. the time required to create the model
2. the difficulty to follow the bones in a precise and individual way
3. the lack of knowledge of the patient's specific material characteristics.

The objective of this work is to better observe the behavior of the foot. For this purpose, a series of experimental and numerical works will propose implementations to address these barriers. The result will be an approach to observe and measure the internal behavior of the foot during running with shoes.

We will now go through the synthesis of the barriers and the positioning of the study to address them, and finally, we will end with a proposal for application.

Development time

In their review of finite element models of diabetic feet, Telfer et al. [Tel+14] point out that complex models that choose to include many anatomical components have more complex and longer development and resolution processes, several days depending on their experience. This long integration has the disadvantage of limiting the clinical application of this type of model, but it allows to integrate the different complexities of the foot to try providing a more accurate simulation.

This model development time is particularly problematic because it limits the number of subjects/patients on which the simulations will be carried out. This reduces the trueness of the measured effect by preventing the differentiation between a response related to an individual or a global response, which has an effect on an entire population.

Accelerating the development time of a complex model, especially on the geometric aspect, allows to build a database that opens perspectives. The first is the possibility to perform parametric studies not on a single patient/subject but on a series of individuals and thus measure the influence of shoe design parameters on a population. Secondly, once a large number of patient geometries are modeled, the generation of a new geometric model that represents a group no longer requires new acquisition because the mean and the main modes of the geometry are established. This extends even further the ability to study large and numerous populations and to consider, on the one hand, the use of model reduction techniques to speed up the calculation time of the mechanical simulation and, on the other hand, to facilitate the segmentation of new acquisitions.

Registration methods with a wide variety of implementations have been designed in this context, their application for the reduction of the foot geometry model development time seems possible as this has already been done for other anatomical structures.

An additional advantage of this method is that when a series of acquisitions is performed on the same patient/subject it opens up the ability to follow the kinematics of certain anatomical components. This will enable to obtain precise, easy-to-use and patient-specific boundary conditions. In the case of the foot model, it is particularly interesting to follow the position of each bone under the effect of limb loading instead to follow foot segments, giving an incomplete view on the internal behavior. Therefore, an implementation of these methods will be developed in chapter II.

Internal foot observations and comparison

The implementation of registration methods, to accelerate development time and to track the position of each bone, provides more accurate information on the internal behavior of the foot than the state-of-the-art main technique, the video capture that follows the movement of only a few foot segments.

This progression is used, still in chapter II, on *ex-vivo* feet tested in many static loading configurations with and without shoes. Precise quantitative measurements, usually not acquired, are analyzed, so that a comparison of the bare foot vs. shod foot behavior is possible and gives an additional insight into the influence of shoes on the foot.

Patient/subject specific material parameters and validation

The state-of-the-art has shown that the material parameters are the result of limited characterization works and that the validation of the models is mainly done by comparison of the plantar distribution.

Since there is a great variability in terms of tissue stiffness, a progression would be the application of calibration techniques to customize the material onto the patient in order to increase the representativeness of the model output. The measures that can be used for model validation can be extended to metrics other than foot pressure to focus studies on other foot behaviors. Model calibration and more detailed validation implementations will be therefore tested in the chapter III.

Running shod model

In order to study a running stride with a shoe, the state-of-the-art has shown that the use of finite element simulation is practically non-existent and that experimental measurement of the foot's internal behavior is almost impossible. Therefore, there are no parametric studies to measure the influence of running shoe design parameter on the internal behavior of the foot during running.

As a demonstration of the possible application from the protocol developed in this thesis, the running foot will be simulated with different shoes in the chapter IV. It will give the first detailed metric measurements of the running foot with shoes.

Summary

In summary, the proposed methodology would help first by reducing the development time of the foot macro model and observing the movement of each bone. This will allow detailed observations of the foot's internal behavior that will be used to propose in-depth comparisons and provide data to calibrate the foot model leading to parametric studies. It opens interesting perspectives in the field of shoe design for sport or medical applications.

Chapter II

Automatic extraction of bone position and ligament deformations of the foot from CT images to measure footwear influence on *ex-vivo* feet under static load

Contents of the chapter

II.1	Résumé	42
II.2	Preface	44
II.3	Abstract	44
II.4	Introduction	44
II.5	Materials and Methods	46
II.5.1	Global strategy	46
II.5.2	Experimentation: foot loading	47
II.5.2.1	Specimen	47
II.5.2.2	Mechanical bench	47
II.5.2.3	Experimental procedure	49
II.5.3	Image processing	50
II.5.3.1	Unconstrained optimization: Bone registration on global foot skeleton	50
II.5.3.2	Mesh-Morphing: Registration of ligament attachments points	53
II.5.4	Angle measurement	55
II.5.5	Statistical testing	55
II.6	Result.	57
II.6.1	Method results	57
II.6.1.1	Experimentation: feet loading.	57
II.6.1.2	Image Processing: Bone registration on global foot skeleton	57
II.6.1.3	Mesh-Morphing of bones and registration of ligament attachments points	57
II.6.2	Bare vs Shod analysis.	58
II.6.2.1	Bone motion amplitude	58
II.6.2.2	Articulation angle	58
II.6.2.3	Ligament deformation	59

II.7 Discussion	60
II.8 Conclusion	61
II.9 Appendix	62

II.1 Résumé

Le comportement mécanique du pied est le plus souvent étudié expérimentalement, avec le suivi du mouvement de segments qui le composent. La principale limitation de cette approche est qu'elle empêche une étude précise et sans ambiguïté des postures et déformations de ce membre.

Pour décrire plus précisément le comportement interne du pied sous différents charge-ments statiques, une méthodologie originale en deux parties est présentée ici. La première partie est expérimentale, elle consiste à scanner le pied dans différentes configurations. La seconde est numérique, elle est développée pour suivre la position de chacun des os qui composent le pied et pour observer les déformations des ligaments. La technique de suivi des os est basée sur une minimisation hiérarchique des distances, elle a permis de suivre la position des 28 os du pied pour chaque sujet et configuration testés. La mise en place d'une technique de mesh-morphing a permis de cartographier les ligaments afin de suivre leurs déformations.

Le flux de travail numérique développé ici nécessite le traitement manuel d'un scanner par patient. Ce flux est donc simplifié par rapport au traitement classique de l'état de l'art grâce au placement automatique des ligaments (recalage non rigide) et à la possibilité de trouver automatiquement la position de tous les os du pied sur les scanners (recalage rigide). La correspondance des géométries avec le recalage non-rigide est évaluée en moyenne à 0.06 [mm] avec un écart type de 0.09 [mm]. La position des os avec le recalage rigide est évaluée en moyenne à 0.28 [mm] avec un écart type de 0.09 [mm]. Ce sont des résultats satisfaisants compte tenu de la résolution de l'acquisition. Avec cette approche, le temps de modélisation et d'analyse du patient est ramené à un jour, ce qui est bien moins que le temps de modélisation traditionnel de plusieurs jours.

Cette méthodologie a été évaluée dans le cadre d'une étude clinique limitée basée sur trois pieds cadavériques exposés à différents cas de chargement statique. Le protocole a été d'abord réalisé pied nu, puis avec une chaussure de sport afin de mesurer l'influence de la chaussure sur le comportement du pied dans différentes configurations. Sur les cas testés, il a été observé que les os du pied, lorsqu'ils sont considérés comme un groupe, se déplacent davantage lorsque la chaussure est portée en particulier dans une configuration de flexion dorsale. Néanmoins lorsque l'on regarde les déplacements os par os, les mouvements relatifs entre les os sont plus importants sur un pied nu.

Une interprétation de ces résultats consiste à considérer que la chaussure provoque un mouvement plus important du segment du pied tout en limitant le mouvement relatif entre ces os. Une flexion dorsale accrue peut expliquer le mouvement plus important du segment pied. La diminution du mouvement relatif entre les os s'observe en partie par un affaissement moins prononcé de la voûte plantaire et un déplacement médial réduit de l'avant-pied lorsque la chaussure est portée. Ceci est également confirmé par une moindre déformation des ligaments, en particulier de l'aponévrose plantaire.

Ces résultats doivent être interprétés dans les limites principales de cette étude, c'est-

à-dire des scénarios de chargement statique sur des pieds cadavériques. Toutefois, il s'agit d'une première étape nécessaire pour comprendre l'effet des chaussures en découplant les phénomènes passifs et actifs en cause. Les expériences *in-vivo* impliquent des effets passifs et actifs avec l'activité musculaire et l'adaptation du sujet à la contrainte mécanique, tandis que l'expérimentation sur sujet *ex-vivo* fait ressortir uniquement les aspects passifs. Par conséquent, les résultats obtenus ici montrent les influences de la chaussure sur le comportement passif du pied ; ses effets dans des situations dynamiques et actives devraient être au centre des travaux futurs.

II.2 Preface

This second chapter describes the experimentation made on 3 *ex-vivo* feet and two numerical treatment implementation to firstly calculate ligament geometries and secondly to determine bone position through different loading states. The method is used to observe differences between a bare vs shod foot with detailed metrics. This chapter is derived from an article published in *Frontiers in Bioengineering and Biotechnology* (vol. 8, p.560, June 2019) [Kro+20], co-authored with Baptiste Pierrat, Han Woo-Suck, Sylvain Grange, Florain Bergandi and Jérôme Molimard.

II.3 Abstract

The mechanical behavior of the foot is often studied through the movement of the segments composing it and not through the movement of each individual bone, preventing an accurate and unambiguous study of soft tissue strains and foot posture. In order to describe the internal behavior of the foot under static load, we present here an original methodology that automatically tracks bone positions and ligament deformations through a series of CT acquisitions for a foot under load. This methodology was evaluated in a limited clinical study based on on three cadaveric feet in different static load cases, first performed with bare feet and then with a sports shoe to get first insights on how the shoe influences the foot's behavior in different configurations. A model-based tracking technique using hierarchical distance minimization was implemented to track the position of 28 foot bones for each subject, while a mesh-morphing technique mapped the ligaments from a generic model to the patient-specific model in order to obtain their deformations. Comparison of these measurements between the *ex vivo* loaded bare foot and the shod foot showed evidence that wearing a shoe affects the deformation of specific ligaments, has a significant impact on the relative movement of the bones and alters the posture of the foot skeleton (plantar-dorsal flexion, arch sagging and forefoot abduction-adduction on the midfoot). The developed method may provide new clinical indicators to guide shoe design and valuable data for detailed foot model validation.

II.4 Introduction

In the moving foot, bones interact with soft tissues such as ligaments, muscles and fascias, which may undergo large strains. Reliable measurements describing these internal bio-mechanical effects are necessary but difficult to achieve; for example, individual bone movements and deformation of the ligaments of the foot under load are poorly characterized because they are difficult to observe directly. The effect of the shoe has therefore been studied using different types of measurements, including movements of the foot segments, plantar pressures, the user's oxygen demand, associated injuries and many others [Wol+08; FH16; Mor+09; HH09; ZB07; Ful+15]; but the impact of the shoe on the internal biomechanical behavior is poorly characterized as there is no available methodology to obtain such measurement. It is likely that the effect of footwear is mainly observed in dynamic and active situations, however understanding the passive and static effect of a shoe on internal structures is a first step towards a better comprehension of the different mechanisms involved.

A study of the internal behavior of the foot under load requires tracking the bone and soft tissue motions. Thus, the development of a method to access each bone movement coupled

with accurate ligament positioning allows to describe precisely the internal behavior of the foot and to compare in detail different loading configurations of the foot.

To observe the 3D position of each foot bone, the approaches based on medical images, such as X-rays, are privileged. For dynamic and static cases, 2D images from biplanar fluoroscopy can be used [PB19; Ito+15; Ito+17]. For static case only, images from computed tomography (CT) scanners directly provide 3D information but usually involve a manual processing or interpretation which limits their usage to small sample size [Col+14; Fer+08; Lin+18].

Different algorithms have been developed to segment the bones from CT scans, such as the fuzzy logic approach [Hir+00] and graph-cut method [Liu08]. They do not systematically provide robust results or still require a significant amount of manual work. When a sequence of different images of volumes evolving through time is considered, an initial segmentation can be associated to a tracking technique in order to determine the movement of each bone between an reference and a current situation. These model-based techniques [Udu+98] consist of finding the translation and rotation of a Volume Of Interest (VOI) with minimization of a cost function. For example, in his approach, Liu minimizes an energy function that utilizes both boundaries and region-based informations [Liu+08]. The reference situation can thus be carefully segmented using manual or semi-automatic approaches; then, the processing of successive acquisitions made on the subject will be shorter and more automated.

By combining the tracking of each bone between different situations with a patient-specific representation of connective tissues, an analysis of their deformations can be performed. This patient-specific modeling of ligaments can be done by different approaches. The most manual technique is to interpret the patient's medical images and use anatomical atlases. In multibody models, transfer functions based on interpolating techniques are often used to deform an initial model to fit the patient's anatomy. The transfer function can be of different natures, the simplest being scaling. To deform an initial geometry, also called *source* geometry, into the patient's geometry, called *target* geometry, other more sophisticated methods can be used such as mesh-morphing [SHW08; Gra+11].

In this study, we propose an experimental protocol and an associated post-processing methodology to track bone motion and model ligaments in order to describe the influence of the shoe on the position of the bones and the deformation of the ligaments in a restricted static environment with a limited number of *ex vivo* feet; we observe whether bone movement and ligament strain are influenced by wearing a shoe in a passive state to give a first insight into the impact of the shoe on the foot's internal behavior.

II.5 Materials and Methods

II.5.1 Global strategy

A summary of the entire protocol is given here.

First, a *generic source model* of the foot including the geometry of each bone and ligament attachment points was manually constructed from the Visible Human Project (VHP) images using classic segmentation tools and anatomy books. This model has a high level of details due to the quality of the images from the VHP, which would be inaccessible on X-rays medical images.

Second, a series of CT scans were performed on new patients experimenting different configurations with and without shoes as described in section II.5.2.

Third, image processing was performed, starting with the manual segmentation of each bone on the scanner of the barefoot unloaded configuration. Subsequent CT scans in the series were simply thresholded to coarsely separate bone from tissue, without separating each bone individually, resulting in multiple *skeletal configurations*.

Each bone position was identified on the *skeletal configurations* by minimizing the distance between the *manually segmented bones* and the *skeletal configurations* as described in II.5.3.1.

Each bone of the *generic source model* is deformed to fit the *manually segmented bones* by the morphing technique described in II.5.3.2. The interpolation of the deformation places the patient-specific ligament attachment points.

With this strategy, summarized in the graph shown in the Figure II.1, the study of the foot consists of a classic and unique bone segmentation, then automatic placement of ligaments and automatic registration of bones in different scanned configurations, no matter how complex the biomechanical test may be.

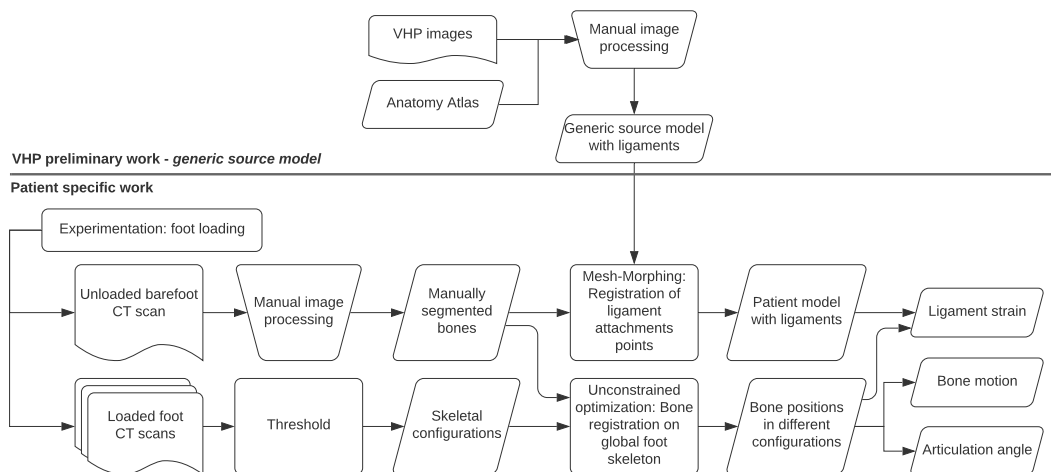


FIGURE II.1: graphic summary of the protocol

II.5.2 Experimentation: foot loading

II.5.2.1 Specimen

The experiments were conducted on a panel of five cadaveric feet coming from different bodies described in Table II.1.

The study was approved by the local Ethics committee (Terre d’Ethique, Saint-Etienne) under the decision IRBN132018/CHUSTE.

Ref.	Sexe	Age (Year)	Weight (kg)
2279	M	86	62
2278	F	85	51
2277	M	94	69
2276	F	91	62
2275	F	74	89

TABLE II.1: Bodies description

When the body arrived, it was directly treated and injected with formaldehyde by the hospital embalmer, then placed in a refrigerator at 4 °C.

On average 11 days after the body arrived, it was removed from the refrigerator to separate the lower leg from the upper leg at the knee level; the soft tissue of the lower leg around its upper end is removed, revealing the tibial plateau. The connection between the lower leg so prepared and the compression bench was made by an intermediate mould made of polyurethane resin (PU) cast in a semi-closed cylinder in Polyvinyl Chloride (PVC). This mould links the tibial plateau on one side and a load cell on the other. External anatomical landmarks on the tibial head and the ankle were used in order to align the axis of loading with the axis of the tibia. Once the PU had solidified and therefore the mold was anchored to the anatomical part, the assembly was placed in a freezer at -25 °C and remained there for an average of 1 month until 48 hours before the tests. 48 hours before the experiments, the foot was placed in a 4 °C refrigerator where it remains for 24 hours, then was placed at room temperature at 17 degrees for 24 hours. Once this defrosting time had elapsed, the foot was attached to the test bench to perform a series of loading tests.

II.5.2.2 Mechanical bench

The mechanical loading of the legs was performed in an X-ray tomographic system. A mechanical test bench was developed, its frame being made of two materials: welded steel profiles for parts not exposed to X-rays and treated wood for the columns to reduce X-ray absorption. The load is applied by forcing the axial displacement of the foot in plantar contact with a plane. The displacement is imposed by the axial movement of a threaded shaft. The applied load is continuously recorded using a load cell (Phidget 500Kg S Type Load Cell). The surface plane on which the foot is compressed is adjustable up to 15° in two directions (medial/lateral, antero-posterior) to simulate different foot orientations. The test bench is displayed alone in Figure II.2 and placed in the CT scan in Figure III.1. The external volume of the bench is 1500 x 400 x 400 mm³.

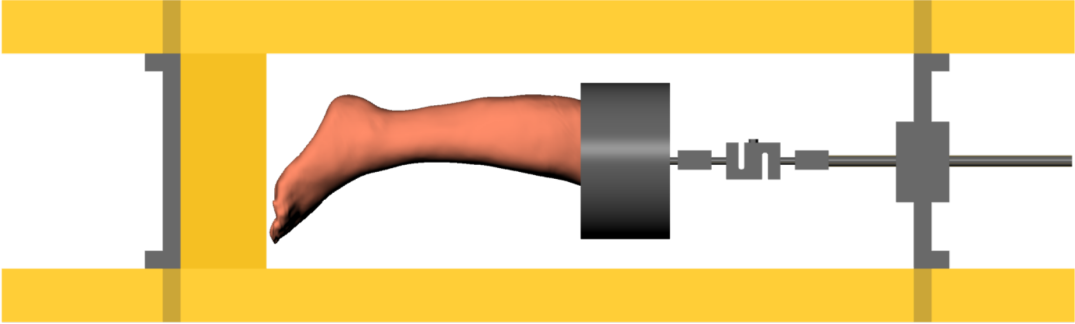


FIGURE II.2: Test bench for loading the foot, while simultaneously measuring the applied force using a load cell

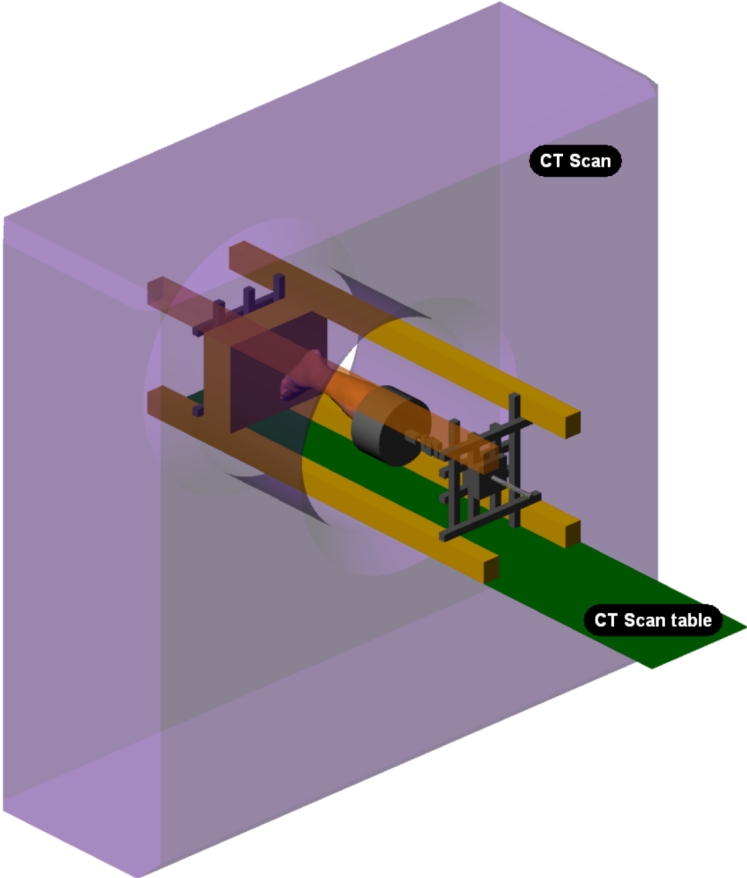


FIGURE II.3: Test bench positioned in the CT scan

II.5.2.3 Experimental procedure

The five cadaveric feet underwent a series of loading. Each foot was first placed in its natural flat position, then two 15° angular variations were applied: plantar/dorsal flexion and inversion/eversion. In each configuration, the applied load was continuously recorded and the situation was CT scanned punctually at different loads, with and without wearing a shoe, as described in Table III.2.

Foot orientation	Body Weight (BW) Loading Ratio			
	Step-0	Step-1	Step-2	Step-3
Neutral (N)	0	0.1	1.0	1.5
Plantar Flexion (PF) Dorsal Flexion (DF)	a	0.1	1	a
Eversion (EV) Inversion (IV)	a	0.1	1 ^b	a

^aLoading not studied because these situations are not encountered by the foot in a classic walking pattern

^bNot possible on bare foot due to sliding

TABLE II.2: Tested configuration description

Three shoes of the same model (Decathlon, Villeneuve-d'Ascq, France) of various sizes were chosen. They are representative of the sports market for occasional runners. The shoes were adapted to each foot size.

A total of 24 scanners, with a resolution of 0.66 x 0.66 x 1.00 mm³, were done for each foot. The data acquired for the bare neutral sequence is displayed in Figure III.2.

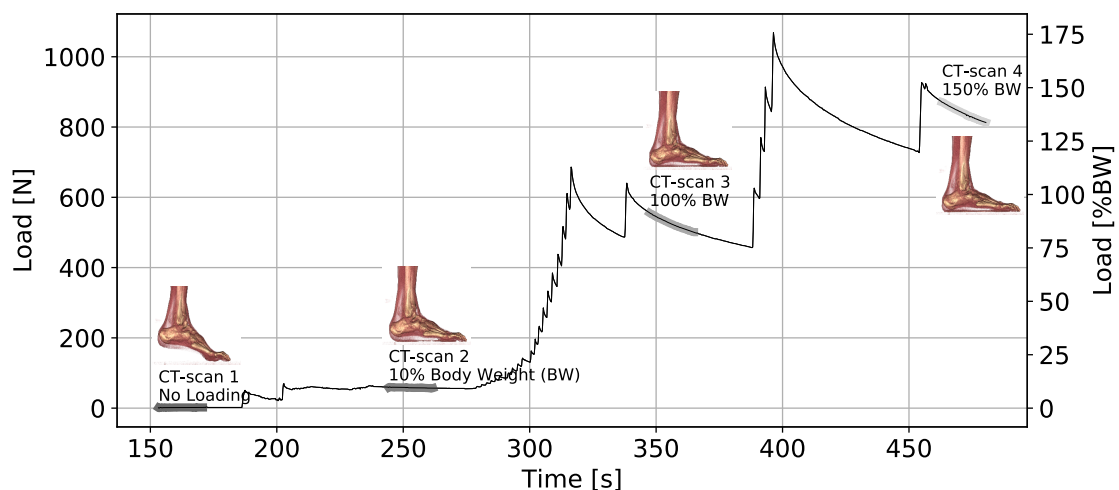


FIGURE II.4: Neutral bare foot acquisition sequence

II.5.3 Image processing

II.5.3.1 Unconstrained optimization: Bone registration on global foot skeleton

The skeleton of the foot, composed of all its bones interconnected, was easily segmented from the 3D images of the CT scan by applying a threshold; it produces a volumetric mask called a *skeleton*.

A classical approach to segment groups of voxels of a threshold, each corresponding to a bone, is to look at their connections and separate the independent groups. Each group can thus be associated to a complete or partial bone part. This simple approach rarely produces good results because the different groups of voxels, each describing a bone, are often interconnected at the joints. Faced with this limitation, the simplest and most manual solution is to remove these voxels creating the interconnections, as no automatic and robust methods are available to our knowledge. Fuzzy logic approaches [Hir+00] have not yielded the expected results in our implementation.

To avoid repeating manual operation on all scanners performed on a subject, we used a method based on an optimization process, minimizing the minimum distance between the manually segmented bones in the *initial* position and the *skeleton* mask.

The minimization consists in looking at a rigid transformation that aligns two point clouds such as the Iterative Closest Point (ICP) method [BM92; RL01]. The unconstrained optimization with Sequential Least Square Programming minimization (SLSQP) [Kra88] provides better results here than the singular value decomposition (SVD) of the corresponding closest point covariance matrix between the two sets as used in ICP. The implementation of SLSQP from the SciPy python package [Vir+19] was used.

The problem is formulated as the following nonlinear unconstrained problem written in the equation II.1.

$$(\mathbf{R}, \vec{T}) = \arg \min \frac{1}{N_p} \sum_{i=1}^{N_p} \|\vec{x}_i - (\mathbf{R} \cdot \vec{p}_i + \vec{T})\|^2 \quad (\text{II.1})$$

With \mathbf{R} the ***Eulerian*** angles rotation matrix and \vec{T} the *Translation* vector, both composing the rigid transformation. \vec{p}_i , each point of the initial set of bone points composed of N_p points. \vec{x}_i the point of the skeleton closest to $(\mathbf{R} \cdot \vec{p}_i + \vec{T})$.

Before individual bone minimization, optimizations of bone segments are performed in a hierarchical fashion in order to obtain acceptable results by avoiding local minima problems. The result of minimization applied to the bone segment defines the initial solution of minimization in the next bone segment. The first treated segment is the entire foot containing all bones except tibia and fibula; its optimization results are presented in Figure II.5. The treated segments are described in Table II.3. The bone minimization of Metatarsal 5 is shown in Figure II.6.

The tracking of the middle and distal phalanges on the foot *skeleton* may be less robust. This can be increased by subtracting the previous bones found in the point cloud describing the entire *skeleton* during bone-by-bone minimizations. Thus, during the bone-by-bone minimization, the distance will no longer be calculated on the complete *skeleton* but on remaining points only. Good results have been obtained with bone-by-bone minimization by passing from proximal bones to distal bones starting with the bones of the lower leg, then the ankle, midfoot, metatarsus, proximal, middle and distal phalanges.

Hierarchy order	Segment name	Bones included
1	Foot ^a	All bones except Tibia and Fibula
2	Upper Ankle	Tibia; Fibula
3	Ankle	Calcaneus; Talus
4	MidFoot	Cuneiform Bones; Cuboid
5	Line1	Metatarsal 1; Medial Sesamoid bones; proximal phalange 1; distal phalange 1
6	Line2	Metatarsal 2; proximal phalange 2; middle phalange 2; distal phalange 2
7	Line3	Metatarsal 3; proximal phalange 3; middle phalange 3; distal phalange 3
8	Line4	Metatarsal 4; proximal phalange 4; middle phalange 4; distal phalange 4
9	Line5	Metatarsal 5; proximal phalange 5; middle phalange 5; distal phalange 5
10	Metatarses	Metatarsal bones; Sesamoid bones
11	Metatarses1+	Metatarsal 1; Medial Sesamoid bones
12	Proximal phalanges	All proximal phalange bones
13	Middle phalanges	All middle phalange bones
14	Distal phalanges	All distal phalange bones
15	Bone ^b	bone-by-bone minimization from the tibia to distal phalanges

^aDisplayed in figure II.5

^bMetatarses 5 displayed in figure II.6

TABLE II.3: Foot segments description

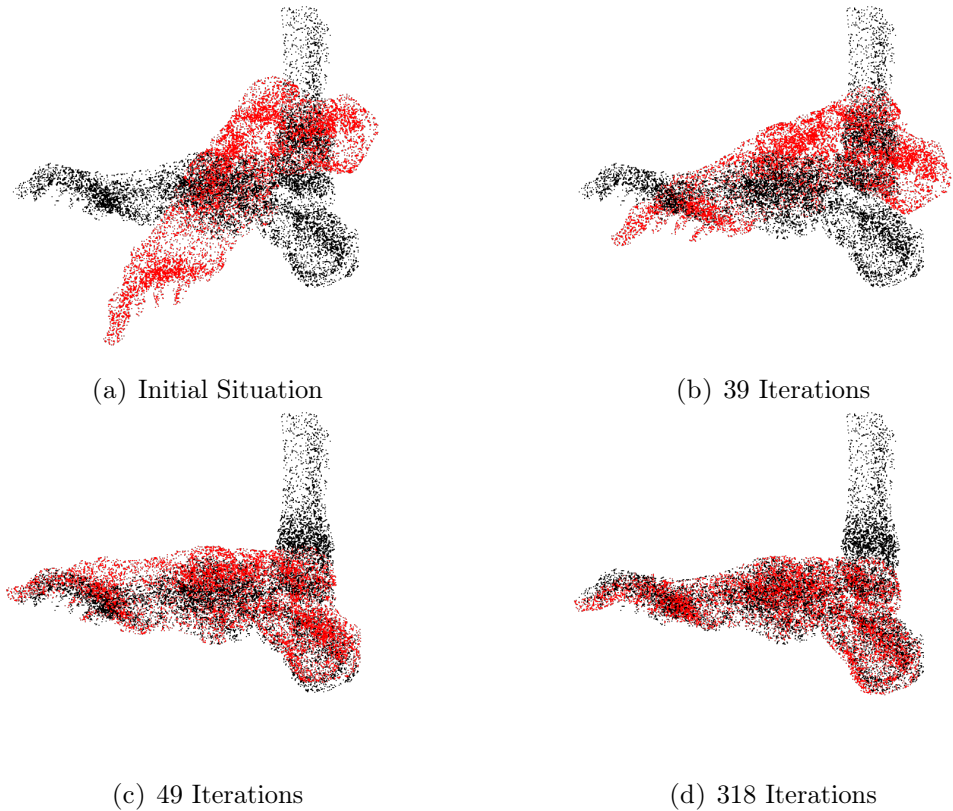


FIGURE II.5: Foot segment minimization
The foot segment is represented with the red point clouds, the loaded *skeleton* is the black dot clouds

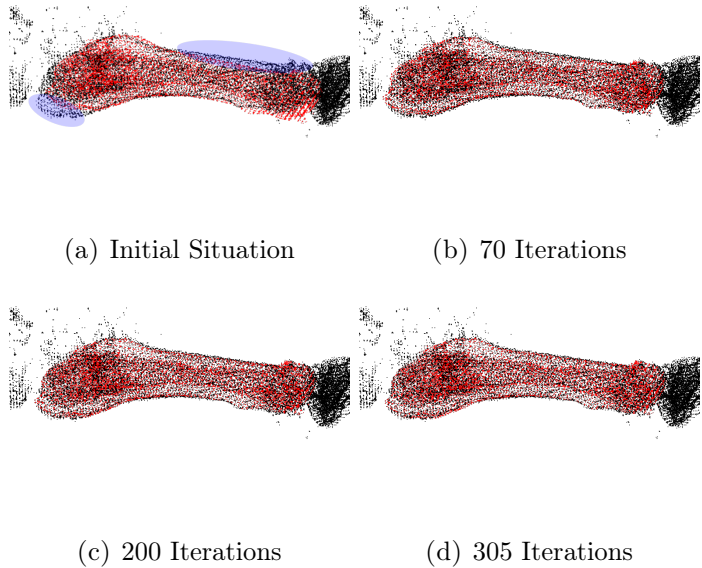


FIGURE II.6: Final minimization on Metatarsal 5
The bone is represented with the red point clouds, the loaded *skeleton* is the black point clouds
The initial situation displayed in II.6a comes from minimizing the previous segment, in blue ellipsoids the non-aligned area are highlighted.

II.5.3.2 Mesh-Morphing: Registration of ligament attachments points

To avoid manual placement of ligaments for each cadaveric foot, the meshes of the *generic source model* bones, whose coordinates of ligament attachment points are known, were deformed towards the geometries of the patients' *target* bones. The *source* model was manually constructed from Visible Human Project (VHP) images and anatomy books.

Aligning the source and target is an essential step to ensure proper morphing progression. A scaling of the *source* to get closer to the *target* was performed to reduce the difference between the two meshes. The result of the calcaneus bone alignment is shown in Figure II.7a.

Once the geometries were aligned, normal projection and smoothing iterations were applied at the *source* to approach the *target*.

Each iteration consisted in the following steps: At time t , compute for each points within the polygonal mesh of the current *source* $\mathbf{X}(t) = [\vec{x}_i(t)]$, the normalized normal vectors $\mathbf{N}(t) = [\vec{N}_i(t)]$ pointing towards the nearest *target* surface. Upstream, the nearest distances $\vec{D}_i = \{d_i\}$ of the *source* nodes with the nearest corresponding point to the *target* were calculated. The index $i = 1, \dots, N_i$ the number of source nodes.

The next positions of the points were calculated with equation II.2

$$\mathbf{X}^*(t+1) = [\vec{x}_i(t) + d_i w(t) \vec{N}_i(t)] \quad (\text{II.2})$$

With $w(t)$ a weight factor that can evolve through iterations. In our case, we have chosen a linear rise of this factor up to a maximum value k_1 as described in equation II.3.

$$w(t) = \begin{cases} a(1+t) & a(1+t) < w_1 \\ w_1 & a(1+t) > w_1 \end{cases} \quad (\text{II.3})$$

Good results were obtained with a parameter a equal to 0.025 and w_1 equal to 1. To avoid the summation of mesh quality degradations on all iterations, we gently smooth with windowed-sinc filter [TZG96], implemented in the Visualization Toolkit (VTK) library [SML06], the deformed mesh to obtain the result of the next iteration $\mathbf{X}(t+1)$. Iterations were stopped when residual distance was below a threshold. The final iteration of the normal calcaneus projection is shown in Figure II.7b.

Once the normal projection is complete, the RBF mesh-morphing can be performed with a variation of the Grassi description [Gra+11].

The first step is to establish $\mathbf{W}(t)$, the weight matrix with only the value of the landmarks positions. The normal distance measurement (ND) [Kim+12], of each target point on the normally projected source, provides us with the initial position of the marks \vec{p}_j , also written \vec{p}_l and the final position \vec{p}_j^* . The index $i = 1, \dots, N_i$ the number of *source* nodes; $j = l = 1, \dots, N_j$ the number of *landmark*.

$$\mathbf{D}_{land.}(t) = \mathbf{K}_{land.}(t) \mathbf{W}(t) \quad (\text{II.4})$$

With $\mathbf{D}_{land.}(t)$ the landmarks displacements matrix as described in equation II.5 and $\mathbf{K}_{land.}(t)$ the landmarks RBF matrix as defined in equation II.6.

$$\mathbf{D}_{land.}(t) = [\vec{p}_j^*(t)] - [\vec{p}_j(t)] \quad (\text{II.5})$$

$$\mathbf{K}_{land.}(t) = [k(\vec{p}_j(t), \vec{p}_l(t))] \quad (\text{II.6})$$

$\mathbf{W}(t)$ is computed with the inversion of $\mathbf{K}_{land.}(t)$ as in equation II.7

$$\mathbf{W}(t) = \mathbf{D}_{land.}(t)\mathbf{K}_{land.}^{-1}(t) \quad (\text{II.7})$$

Once $\mathbf{W}(t)$ was computed, the RBF matrix of the deformed *source* nodes and landmarks was calculated as equation II.8, which is used as an input for the displacement matrix $\mathbf{D}(t)$ as described in equation II.9. $\mathbf{D}(t)$ is added to the *source* nodes of the iteration to calculate next node positions as equation II.10

$$\mathbf{K}(t) = [k(\vec{x}_i(t), \vec{p}_j(t))] \quad (\text{II.8})$$

$$\mathbf{D}(t) = \mathbf{K}(t)\mathbf{W}(t) \quad (\text{II.9})$$

$$\mathbf{X}^*(t+1) = \mathbf{X}(t) + \mathbf{D}(t) \quad (\text{II.10})$$

k is an inverse multiquadratic RBF function defined in II.11.

$$k(\vec{x}, \vec{p}) = \frac{1}{(\|\vec{x} - \vec{p}\|^2 + \|\vec{x} - \vec{p}\|c)^\beta} \quad (\text{II.11})$$

c is the minimum distance of the nearest points between deformed *source* and the *target*. β is described as follows equation II.12

$$\beta = \begin{cases} b * \|\vec{x} - \vec{p}\| & b * \|\vec{x} - \vec{p}\| < k_1 \\ k_1 & b * \|\vec{x} - \vec{p}\| > k_1 \end{cases} \quad (\text{II.12})$$

Good results were obtained with a parameter b equal to 10.0 and k_1 equal to 0.1. To avoid cumulating the mesh degradations of each iteration, a slight smoothing, as described above, can be reused to obtain the result of the iteration $\mathbf{X}(t+1)$.

For robust results, 5 morphing iterations were used, increasing the number of landmarks used at each iteration according to their magnitude. The result of calcaneus RBF morphing is shown in Figure II.7c.

To register ligament attachment points, displacement vectors between the initial *source* and the morphed *source* are interpolated to calculate the position of the attachment points on the patient bone. The attachment points of the ligaments of the calcaneus are shown in the Figure II.7d.

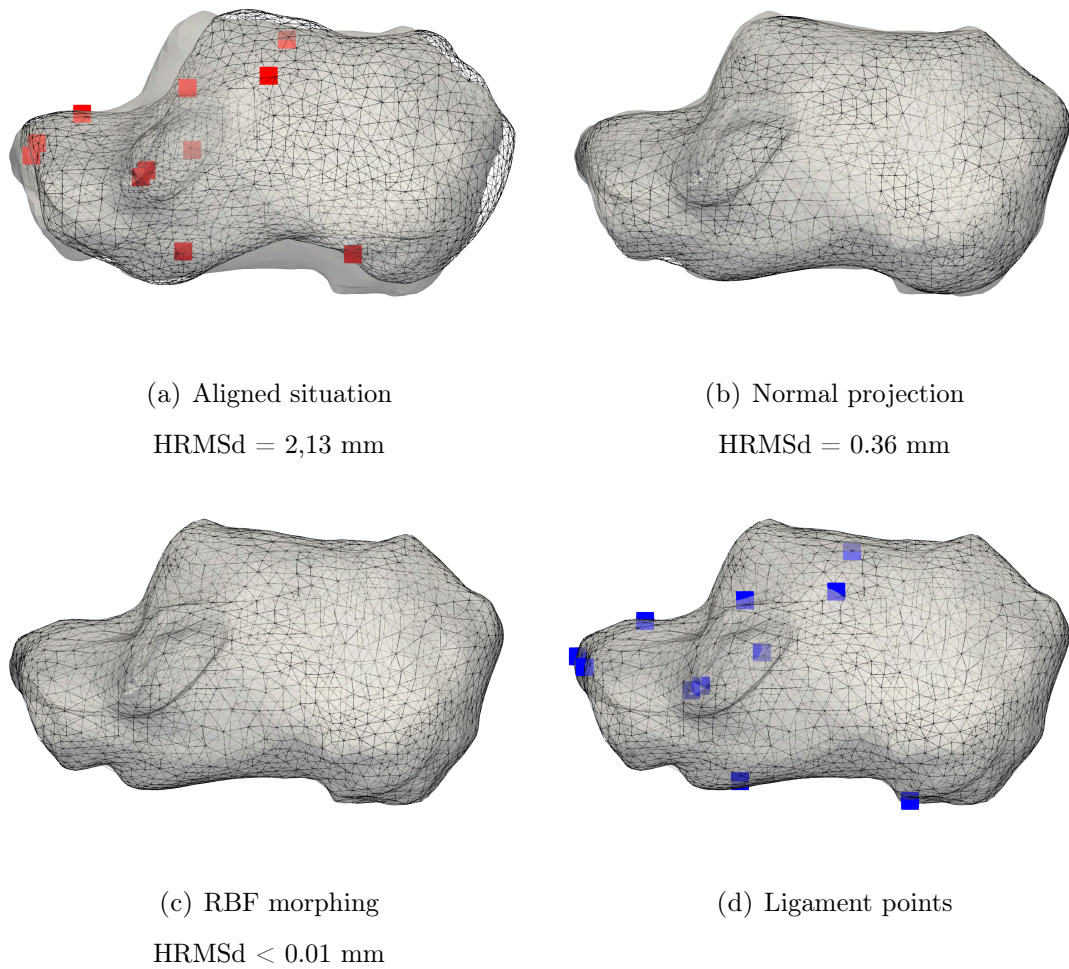


FIGURE II.7: Deformation protocol

Distance between the morphing steps and the *target* is evaluated with the Hausdorff Root Mean Square distance (HRMSd).

The patient's *target* mesh is displayed in grey and the *source* bone at different stages of the protocol is displayed in black wireframe.

The ligament attachment points of the *source* are displayed in red and those of the patient calculated with the presented protocol are displayed in blue.

II.5.4 Angle measurement

To evaluate the joint angles, two angles between the center of mass of the bones are tracked in the three anatomical planes for each configuration tested. Each angle evaluates the foot position as described in the Table II.4 and displayed in Figure III.14.

II.5.5 Statistical testing

Considering the small size of the sample, it is impossible to prove the normality of the distribution. Therefore tests between bare and shod feet will be treated using the Wilcoxon signed-rang test as a non-parametric paired test. The level of signitivity is set at $p = 0.05$. Bone motion amplitudes, joint angles and ligament strain were statistically tested between the shod and bare observations.

Angle Name	Bones	Sagittal	Coronal	Transverse
TibTalCal	Tibia; Talus; Calcaneus	plantar – dorsal flexion (Figure IV.24a)	varus - valgus (Figure IV.23a)	-
CalTalSM	Calcaneus; Talus; Sesamoid Medial	arch sagging (Figure III.14c)	-	abduction – adduction (Figure III.14d)

TABLE II.4: Angles description

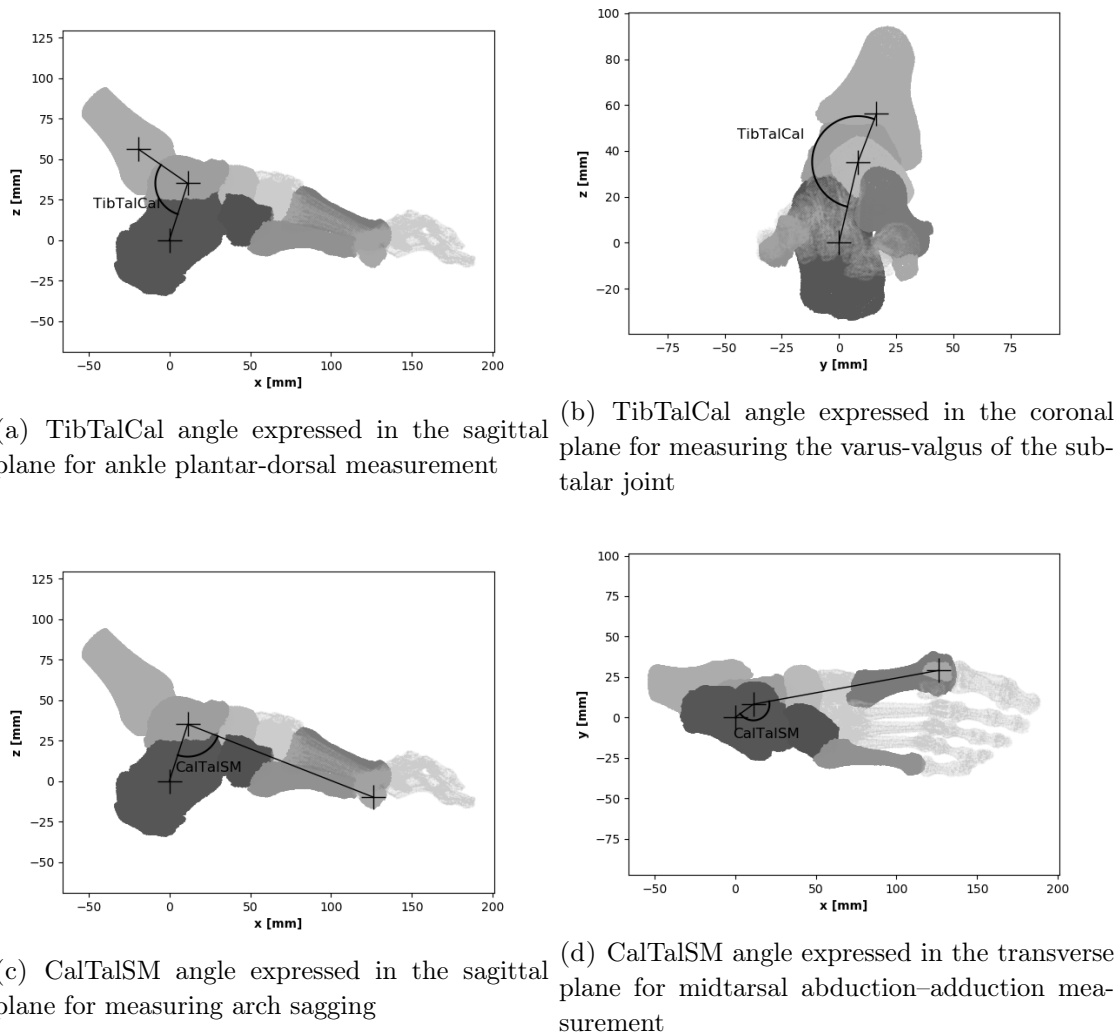


FIGURE II.8: Angle measurement

II.6 Result

II.6.1 Method results

II.6.1.1 Experimentation: feet loading

We kept three feet out of the five feet tested.

Foot 2276 was discarded because of the considerable difference in load between shod experiments and bare experiments.

Foot 2278 was removed due to a high cadaveric rigidity that prevents foot movement.

The initial scan of the foot 2275, done without load, was performed on the foot in a plantar flexion configuration due to the natural position of this foot, while the feet 2277 and 2279 were initially scanned in the neutral position. The 10% load of body weight (BW) on foot 2279 in plantar flexion could not be achieved due to the length of the test bench being too small for this leg size, forcing a load directly above this ratio.

A greater viscoelastic effect is observed on the bare foot than on the same foot in shoes. Figure II.9 shows this difference in viscoelastic effects, especially when the foot is subjected to a load greater than 10% of BW.

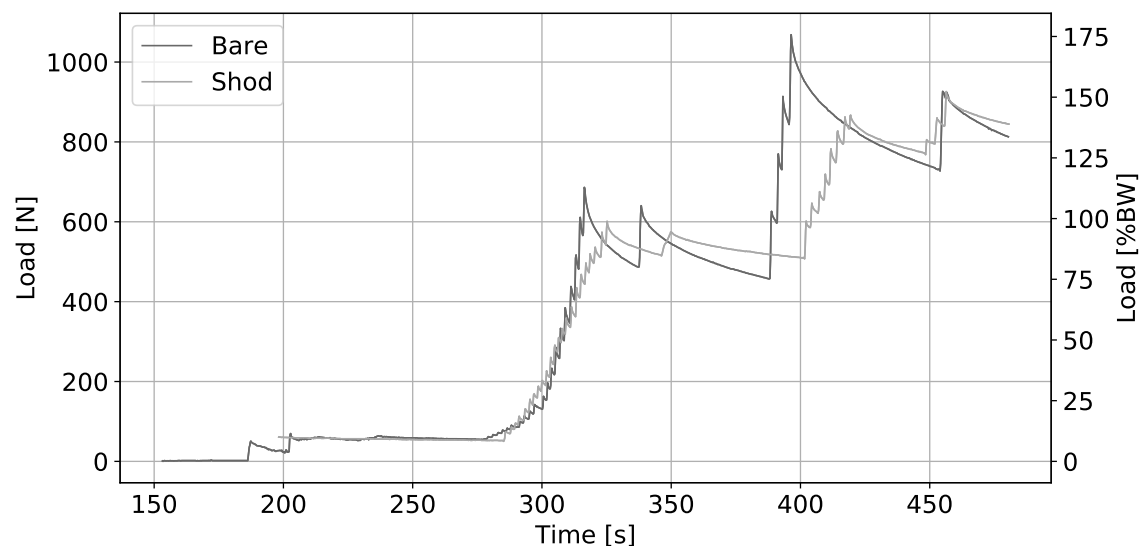


FIGURE II.9: Foot ref. 2279 Loading Sequence on Neutral position

II.6.1.2 Image Processing: Bone registration on global foot skeleton

The results of bone registration was checked visually and yielded satisfactory positioning. The minimum average distance between each registered bone and the skeleton is 0.28 mm with a standard deviation of 0.09 mm.

II.6.1.3 Mesh-Morphing of bones and registration of ligament attachments points

The Hausdorff distance between the mesh-morphed bone and the target bone is on average 0.06 mm with a standard deviation of 0.09 mm.

The calculated ligament positions are shown in Figure II.10, a visual inspection validates the positioning of the ligaments identical to the interpretation of anatomical atlases.

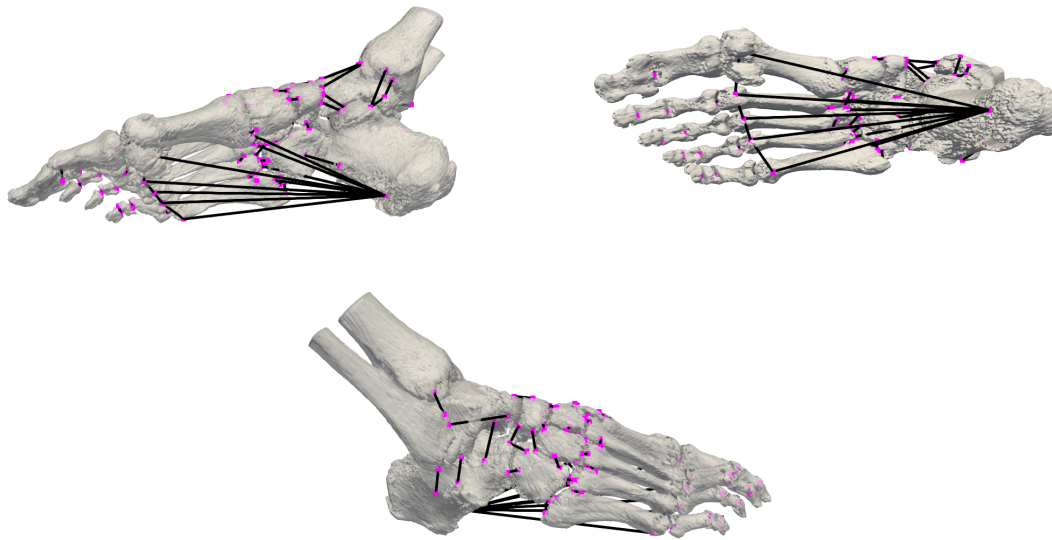


FIGURE II.10: Ligaments positions calculated by the morphing technique

II.6.2 Bare vs Shod analysis

II.6.2.1 Bone motion amplitude

To first test the interaction between bone translation and footwear; Wilcoxon signed-rank tests were performed on the amplitudes of each bone translation between bare foot and shod foot for each configuration. In 81 % of the cases, a significant difference in the amplitude of bone translation was found. The highest differences were observed on dorsal flexion (DF) with a load equal to 0.1 BW. The results are displayed for each foot studied in Figures II.11, II.12 and II.13.

The same test is applied to the amplitudes of bone rotation, in 93% of the cases a significant difference is found, again it is in the dorsal flexion configuration with a load equal to 0.1 BW that the greatest difference is observed.

We observed that the difference in bone displacement between shod feet and bare feet, expressed relative to the tibia, are slightly higher for shod feet (mean = 0.04, sd = 0.13). On the contrary, when expressed relative to the calcaneus, which removes the movement of the foot segment, these differences are reversed; the amplitude of the movements of the shod foot is then smaller than that of the bare foot (mean = -1.64 mm, sd = 2.78 mm).

II.6.2.2 Articulation angle

Non-parametric statistical tests of angle amplitudes were performed to test if wearing the shoe affects the chosen joints. The results are presented in Table II.5.

Even though the variation is not statistically significant, the TibTalCal angle expressed in the sagittal plane for ankle plantar-dorsal measurement tends to be higher when wearing shoes (p-value < 0.10); the median of the angular differences between bare and shod feet is 0.89° resulting from a greater dorsal flexion when wearing the shoe.

No significant difference between shod and barefoot for the TibTalCal angle expressed in the coronal plane measuring the varus-valgus of the subtalar joint was found.

The median difference between the shod and bare CalTalSM angles, expressed in the sagittal plane for measuring arch sagging, is -1.14° , which results in less arch sagging when

Parameter	Test	TibTalCal Sagittal	TibTalCal Coronal	CalTalSM Sagittal	CalTalSM Trans- verse
Bare/Shod	Wilcoxon	0.067 *	0.443	5.37e-05 †	6.29e-05 †

p-value < 0.05

p-value < 0.10

TABLE II.5: Articulation angle nonparametric tests

the footwear is used.

The median of the angle difference between CalTalSM with shoe and bare CalTalSM, expressed in the transverse plane for measuring mid-tarsal abduction-adduction, is -4.46° , resulting in less medial displacement of the forefoot over the midfoot when the shoe is used.

II.6.2.3 Ligament deformation

74 ligaments were modelled and their deformation monitored. The impact of the shoe on ligament deformation was assessed ligament by ligament, 49% had a significant difference in strain between the foot in the shoe and the bare foot.

Certain groups of ligaments see their strain reduced or increased by wearing the shoe; this is the case for the following ligaments:

- plantar aponeurosis ligaments connecting the medial tuberosity of the calcaneus to the heads of the metatarsals and fingers, in which the median difference between the strain with footwear and the strain without footwear is -1%.
- long plantar ligament connecting the calcaneus to the proximal epiphysis of the metatarsals 2 to 5, wherein the median difference between the strain with shoe and the strain without shoe is -0.7%.
- deep transverse metatarsal ligaments connecting adjacent metatarsal heads, median difference between strain with shoe and strain without shoe is equal to -3%
- two of the ligaments composing the deltoid ligament complex, the tibiocalcaneal (+2%) and the anterior tibiotalar (-1%) ligaments while no significant difference is found for the posterior tibiotalar and tibionavicular ligaments.
- one of the ligaments composing the bifurcate ligament complex, the calcaneonavicular ligament (+2%) whereas no significant difference is found for the calcaneocuboid ligament.

No significant differences were found for the following ligaments :

- spring ligament complex
- plantar and interosseous metatarsal ligaments connecting the proximal epiphysis of the adjacent metatarsals 5 to 2
- dorsal cuneonavicular ligaments

II.7 Discussion

The objective of this work was to develop and apply an automated approach to track bone position between different static load cases and provide automated mapping of anatomical components, such as ligaments, to precisely describe the behavior of the foot and use it for overall comparison of the bare foot versus the shod foot. The combination and automation of these two methods allowed us to make new observations with the tracking of the 3D movements and positions of each bone in static cases associated with the calculation of ligament deformations.

The mesh distance between the global skeleton and each registered bone was used to calculate the registration quality, which is satisfactory. Taking into account that this value in itself is not sufficient to confirm a good record, a visual inspection was also carried out to approve the result. Bone registration errors impact ligament deformation, especially for small ligaments. The evaluation of ligament attachment points is difficult to quantify because we did not compare with the manual placement of these nodes by experienced users. The resulting positioning provides a standard view of the patient's ligaments but does not take into account any specificity of the patient such as ligament injury. The result appears logical and respects the hypothesis formulated on the *source* model although the morphing technique has yet to be tested on severely malformed anatomies.

Finite element, spring and multiple body models are often used to calculate the mechanical properties, deformations and stresses of anatomical components as well as to simulate foot behavior [Sop+11; CLL14; Wei+11; Che+05; Gef03b]. Validating such models for a complete foot can be tedious, as there is often a lack of accurate experimental data to compare with simulation results. The measurements obtained with the methods presented here are useful for comparing simulation results with experimental observations and can be used to work on calibrating ligament rigidity in the passive state.

The complete digital workflow requires manual processing of one CT scan per patient, automatic placement of ligament and then allows several configurations to be automatically studied. It was performed on a conventional computer workstation (Intel® Core™ i7-6700 CPU @ 3.40GHz × 8 CPU and 16 Go RAM) and lasts about 1 day per foot. A large number of configurations can be easily tested for a given patient, it will not significantly extend the processing time. Large sample sizes of feet can now be treated more easily, including pathological and deformed feet. With this approach, classical clinical indicators such as the foot posture index (FPI-6), the median angle of the longitudinal arch (MLAA) and many others, can be automatically extracted.

As a proof of concept, a very limited clinical study on three cadaveric feet was conducted. Due to the availability of the mobilized CT scan, experiments were conducted first with bare feet and then with feet wearing sports shoes to reduce protocol time by avoiding dressing/undressing repetitions. The manipulation of the anatomical part may have possibly reduced its rigidity; the latter may be less important during the acquisition of the shod foot than during the bare foot tests which can entailed the observations made. Recommendations for future experiments are to randomize the bare and shod trials, increase the load scale and practice preconditioning to reduce the uncertainty of the observations made.

We observed that the foot segments underwent a greater rigid motion during shod experiments. Similar results were reported on walking by comparing barefoot walking and shod walking, as shown by Morio et al. [Mor+09]. Nevertheless the authors also found that the plantar/dorsal flexion pattern was not affected by the wearing of shoes, whereas

we observed that the amplitude of bone translation is the most influenced by the shoe in dorsal flexion. The type of equipment used, the applied load and the fact that Morio et al. worked with moving feet *in vivo* may explain the difference between their results and our observations.

The relative displacements of the bones in the foot segments are smaller on shod feet than on bare feet.

We interpret these results by considering that the shoe causes rigid movement to the foot segment while restraining the relative movements of these bones. Increased dorsal flexion may be part of the rigid movement of the foot segment when the shoe is worn as shown by the tendency of the TibTalCal angle in the sagittal plane to be higher. The decrease in the relative movement of the bones is also observed by a less pronounced sagging of the plantar arch and a reduced medial displacement of the forefoot when the shoe is worn, it is also confirmed by less deformation of the ligaments, in particular the plantar aponeurosis ligaments.

These results should be interpreted within the main limitation of this study, i.e. passive loading scenarios on cadaveric feet. However, it is a necessary first step in understanding the effect of footwear by decoupling the phenomena involved, as in-vivo experiments involve both passive and active effects. Consequently, these results show indications of a passive role of shoes and that their effect under dynamic and active situations should be the focus of future work.

II.8 Conclusion

This chapter presents a complete workflow for the study of various cases of foot loading acquired in a scanner, obtaining valuable biomechanical indicators on internal structures, which are difficult to capture experimentally. It is automated and could easily be applied to larger foot samples. This method has been successfully evaluated on three cadaveric feet with a range of applied loads, in different positions, with and without shoes. The combination of accurate 3D bone tracking with a ligament model allowed comparison of bone movement and ligament strain under these various conditions, and provided an interesting insight into the effect of wearing a shoe on these internal structures.

To our knowledge, detailed studies on the moving foot under mechanical load are still lacking in the medical field, but also in other fields (fashion, sport, defence). These studies must comply with in-silico clinical requirements, in particular the possibility of treating a representative foot panel and/or developing a patient-specific study. It is therefore necessary to automate the workflow from bone segmentation to mechanical results. The method presented is a step in this direction; it paves the way for the comparison of clinical indicators between different configurations, provides a solid database for the validation of detailed foot models, such as finite element models, which can be exploited for footwear design.

II.9 Appendix

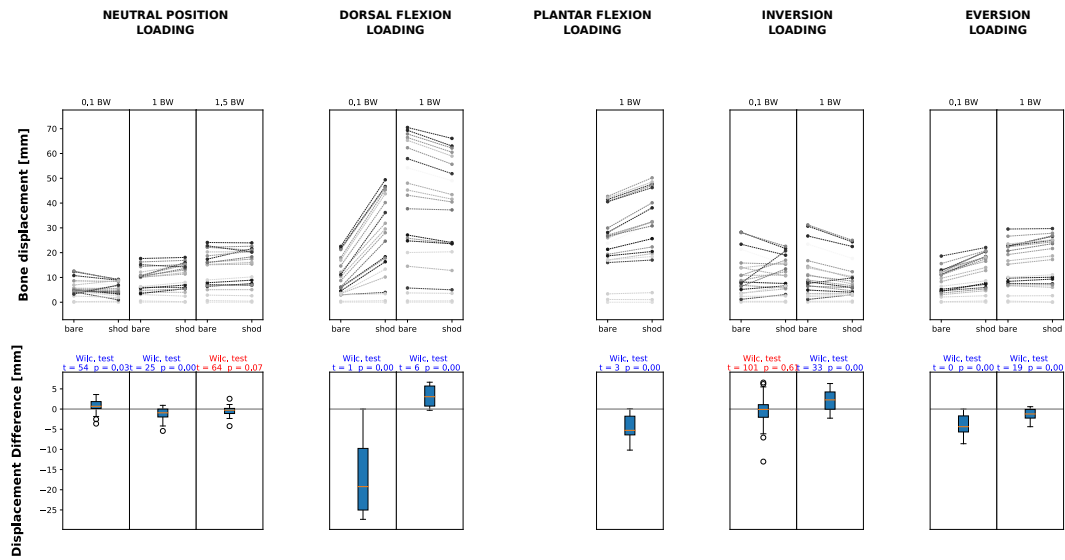


FIGURE II.11: Foot 2279, Wilcoxon signed-rank test on bone translation amplitudes

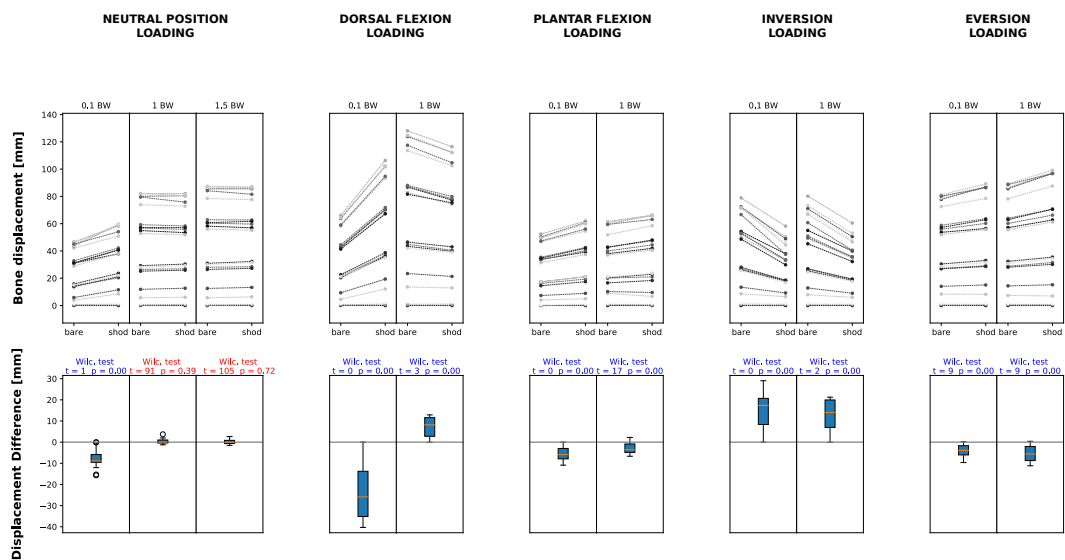


FIGURE II.12: Foot 2277, Wilcoxon signed-rank test on bone translation amplitudes

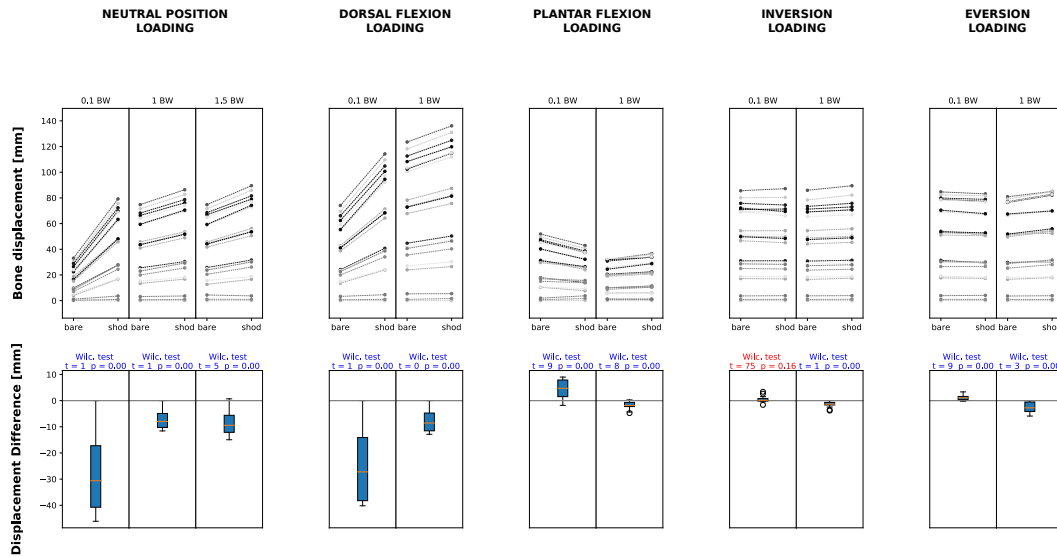


FIGURE II.13: Foot 2275, Wilcoxon signed-rank test on bone translation amplitudes

- Tibia
- Fibula
- Calcaneus
- Talus
- Navicular
- CuneiformMedial
- CuneiformIntermediate
- CuneiformLateral
- Cuboid
- Metatars1
- Metatars2
- Metatars3
- Metatars4
- Metatars5
- SesamoidLateral
- SesamoidMedial
- PhalanxProximal1
- PhalanxProximal2
- PhalanxProximal3
- PhalanxProximal4
- PhalanxProximal5

FIGURE II.14: Legend for upper graphs displayed in Figures II.11, II.12 and II.13

Chapter III

Calibration of patient-specific foot models on ligament and muscle stiffness for force-driven FE simulations

Contents of the chapter

III.1	Résumé	66
III.2	Preface	67
III.3	Abstract	67
III.4	Introduction	67
III.5	Method	69
III.5.1	Experimentations	69
III.5.2	FE model formulation	71
III.5.3	FE model calibration	73
III.5.3.1	Global strategy	73
III.5.3.2	Displacement driven FE simulations	73
III.5.3.3	Static equilibrium	75
III.5.3.4	Force driven FE simulations	76
III.5.4	Metrics	77
III.5.4.1	Bone position	77
III.5.4.2	Articulation angle	77
III.5.4.3	Connectors deformation	77
III.6	Results	78
III.6.1	Connector stiffness	78
III.6.2	Force driven FE simulations outputs evaluation	79
III.6.2.1	Result overview	79
III.6.2.2	Bone position	81
III.6.3	Articulation angle	82
III.6.3.1	Connector deformation	83
III.6.3.2	Fat pad stress	84
III.7	Discussion	85
III.8	Conclusion	86
III.9	Appendix	87

III.1 Résumé

Avec la méthode présentée dans le chapitre précédent II, la position des os et la déformation des ligaments sont suivies dans différentes conditions de chargement statique du pied. Cette méthode a été étendue avec la modélisation des principaux muscles du pied. Les données ainsi obtenues sont utilisées dans ce chapitre pour un protocole de calibration du modèle sur les rigidités des muscles & ligaments, puis pour contrôler les résultats des simulations utilisant ces rigidités.

La grande majorité des modèles éléments finis dédiés au pied sont en fait spécifiques au patient uniquement sur l'aspect géométrique car suffisamment d'outils numériques le permettent, mais sur l'aspect matériau c'est finalement à travers peu de travaux de caractérisation que les propriétés sont affectés au patient. En outre, les évaluations des résultats des modèles sont principalement basées sur la comparaison des distributions de pression plantaire simulées et expérimentales.

Afin de progresser sur l'aspect matériau en le rendant spécifique au patient étudié, une approche par méthode inverse en recherchant l'équilibre mécanique du pied chargé est ici mise en œuvre pour calibrer la rigidité des ligaments & muscles. En vue d'étendre les applications possibles du modèle éléments finis du pied, une évaluation de mesures plus détaillées que les mesures classiques utilisées dans l'état de l'art est effectuée. Dans cette évaluation, les mesures simulées sont comparées aux mesures expérimentales sur la position des os, la déformation des ligaments & muscles, les angles articulaires, ainsi que sur la contrainte mécanique des coussinets adipeux.

Les résultats des simulations sont globalement cohérents avec les données expérimentales en termes de position des os, de déformation des ligaments & muscles et d'angle articulaire, sauf pour les phalanges.

En comparaison de l'utilisation des rigidités disponibles dans la littérature, les résultats obtenus ici sont beaucoup plus proches des résultats expérimentaux, avec une moyenne de $8,29 \text{ [mm]} \pm 4,26 \text{ [mm]}$ pour l'erreur de positionnement des os, une erreur relative moyenne de $14\% \pm 21 \%$ pour la déformation des ligaments, une erreur relative moyenne de $7\% \pm 14 \%$ pour les angles articulaires et, surtout, des simulations qui aboutissent contrairement aux simulations utilisant des données bibliographiques qui peuvent échouer ponctuellement en raison de la simulation d'un comportement anatomiquement impossible. Ainsi, par rapport aux simulations utilisant deux sources de données de la littérature, le protocole de calibration développé ici permet une meilleure représentation de l'expérimental et la possibilité de simuler plus de configurations de chargement. De nombreuses limitations et améliorations vont de pair avec le protocole développé dans ce chapitre, mais il ouvre également de nouvelles perspectives. Ces aspects seront abordés dans la conclusion de ce manuscrit.

III.2 Preface

With the method developed in the previous chapter II, the position of the bones and the deformation of the ligaments were followed through different statically loaded configurations. These data obtained are used in this chapter, with added muscles, (1) in an calibration method based on an inverse method and (2) to control the result of the simulation, thus calibrated. Numerous limitations and improvements come along with the protocol developed here, but also, the use of this approach opens perspectives. These aspects will be discussed more in detail in the conclusion of this manuscript. This chapter is derived from an article submitted in *Journal of biomechanics*, co-authored with Baptiste Pierrat, Han Woo-Suck and Jérôme Molimard. Part of it was presented in the *14th. World Congress on Computational Mechanics & 8th. European Congress on Computational Methods in Applied Sciences and Engineering (WCCM ECCOMAS 2020 - Paris)*.

III.3 Abstract

Patient-specific, force-driven, representative finite element macro-models of the foot can be used to study bone position, ligament strain and tissue stress, which add information to external diagnosis of the foot. The production of such models requires to estimate the parameters of the constitutive equation of ligament and muscle stiffness. To estimate this stiffness distribution of all ligaments and muscles, we present here a methodology based on the static equilibrium of the foot in different load and orientation configurations observed on CT scans performed on 3 *ex-vivo* feet. The force-driven finite element simulation, using the distribution of stiffness calibrated with the method presented in this paper, was evaluated in detail by comparing the simulated positions of bones, ligament strains and joint angles with experimental measurements. It generally shows that they were consistent with experimental data, except for phalanges bones. The errors on bone position, on the strained lengths of the ligaments and muscles and on articulations angles are significantly lower than using data from literature with respectively $8.29 \text{ [mm]} \pm 4.26 \text{ [mm]}$ (mean error), $14 \% \pm 21 \%$ (average relative error) and $7\% \pm 14 \%$ (average relative error). This method can be used to calibrate a patient-specific model in order, firstly, to analyze the foot in different situations with force-driven patient-specific finite element simulations and, secondly, to approximate even more accurately the experimental data, for example, using an iterative method with the stiffness distribution calculated here as a first estimate.

III.4 Introduction

FE foot models are a well established technique used in a variety of applications. They are used for example to evaluate the impact of soft tissue stiffness on plantar foot pressure distribution and bone loading [Che+05], to examine the response of the foot with high-heeled shoe walking [Yu+13], to study ligament strain due to foot rotation [Wei+11], to investigate the impact of joint fusion surgeries [WLZ14] and many other applications.

The direct use of such models for clinical applications is still hindered by several limiting factors, such as time-consuming development of patient-specific geometry and meshing, characterization of the mechanical properties of internal structures such as ligaments and muscles, along with robust validation. FE models are very sensitive to the choice of the numerous material parameters and their calibration technique. Classically, even for a

patient-specific model, soft tissue parameters are selected from characterization and identification works found in the literature. In this case, fat pads [MDB02; Erd+06; Gri+17], plantar aponeurosis [Kit+94; Gef03b] and ankle ligaments [Att+85; SBS88; Beu+03] have been studied to estimate their material parameters. Taking into account the difference in material properties found in the literature, partly due to the difference in experimental protocol, the variability in the choice of constitutive equations by author and the variability between tested subjects, a patient-specific foot model using calibrated materials may offer results that are more representative for a specific individual. The validation of a foot model is a complex subject. It is often a local comparison between simulated and experimental measurements such as the area of plantar pressure maps. Comparisons based on the centre of pressure and the reaction force of the ground are rarely performed. More exhaustive validations should be based on measurements of bone positions and soft tissue deformations [IW10; LW07], but the acquisition of such data is an experimental challenge as it requires precise internal measurements. Nevertheless, a foot model that approximates the position of each bone would be useful in a wide variety of applications, for example, to evaluate changes caused by the design of a sole on the deformation of ligaments and joint angles.

To progress on the aspects of model calibration & validation, the use of internal and precise experimental measurements such as the 3D position of each bone, ligament deformation and others can provide essential information, not only to be exploited with inverse methods for identifying different material parameters and calibrating subject-specific models, but also to evaluate the simulation output with less uncertainty. We have previously proposed a method to obtain bone position and ligament deformation in different orientations of the foot from numerous CT scans performed on 3 *ex vivo* subjects [Kro+20]. We propose here to use this measurement to identify the passive stiffness of each ligament and muscle with an inverse method, in order to obtain a subject specific FE model of the foot that simulates bone positions as a function of foot loading most closely to experimental measurements. Our objective is to provide a model to first investigate the position of the bones, ligament and muscle deformation, then to study soft tissue stresses and strains under a variety of simulated loading conditions.

Our new approach is to identify the passive stiffness of 74 ligaments and 11 muscles to obtain a subject-specific, force-driven FE model that simulates bone positions and soft tissue stresses and strains as a function of load. To identify the passive stiffness of ligaments and muscles we make the hypothesis that ligament and muscle tensions are the main factors contributing to the static equilibrium of the foot structure under static load. According to this hypothesis, the forces and moments of reaction in bones, due to the contact of the foot with the ground and the contact between the bones through the cartilages, are minimized by the contribution of ligaments and muscles; we therefore adjust the distribution of passive ligament and muscle stiffness in the model, by partially solving the system of equations in static equilibrium of the subject's foot exposed to different loads with non-linear least-squares approaches. The force-driven subject-specific FE model thus calibrated, is evaluated by comparing bone position, joint angle and ligament deformation to experimental measurements as well as compared to standard procedures that use bibliographic data. The method was tested on 3 *ex-vivo* bare feet exposed to different statically loaded orientations.

III.5 Method

III.5.1 Experimentations

Ex-vivo human feet from 3 donors have been tested for a series of static loads and orientations in a X-ray computed tomography scan. For each subject an initial unloaded situation was CT scanned; the resulting 3D medical images were used to create subject-specific bone and soft tissue geometric models. For that each bone and soft tissue were segmented; then, ligaments and muscles were added as 1D elements using a mesh morphing technique as a transfer function between a fully-defined generic model with ligaments and muscles and the current subject's model.

Thanks to the test workbench shown in figure III.1, the Neutral (N), Plantar Flexion (PF), Dorsal Flexion (DF), Inversion (IN) and Eversion (EV) orientations of the foot were then tested with different load ranging from 0% to 150% of Body Weight (BW) as described in Table III.2. At each orientation, the load was continuously recorded and punctually, at each chosen load threshold, the situation was CT scanned as shown in figure III.2 in the case of barefoot acquisition sequence with Neutral (N) orientation.

In loaded foot configurations, each bone position was monitored using a hierarchical minimization of the bone mesh distances between the bone-by-bone segmentations of the unloaded foot and the skeleton segmentations of the loaded foot.

Last, the position and deformation of ligaments and muscles were extracted from bone positions. The complete procedure was described in our previous chapter II.

Considering the experimental procedure described above, for each subject, 11 CT scans of the loaded bare foot were acquired and processed.

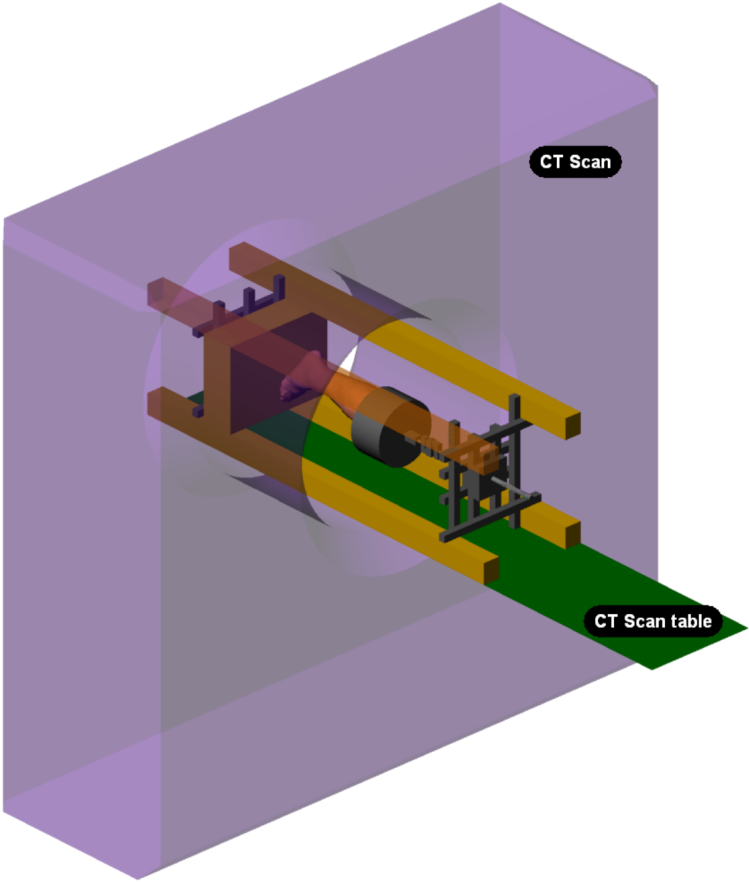


FIGURE III.1: Test bench positioned in the CT scan

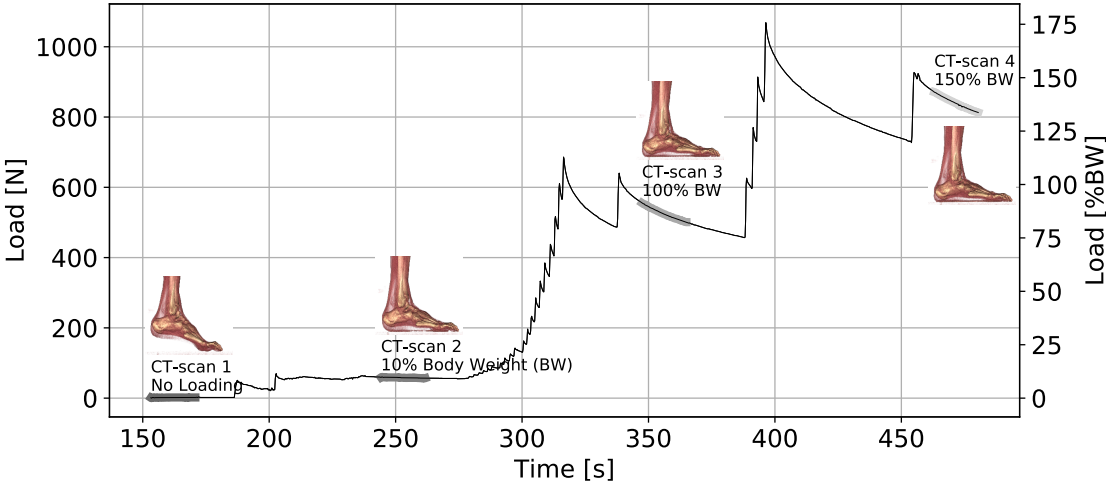


FIGURE III.2: Neutral (N) bare foot acquisition sequence

III.5.2 FE model formulation

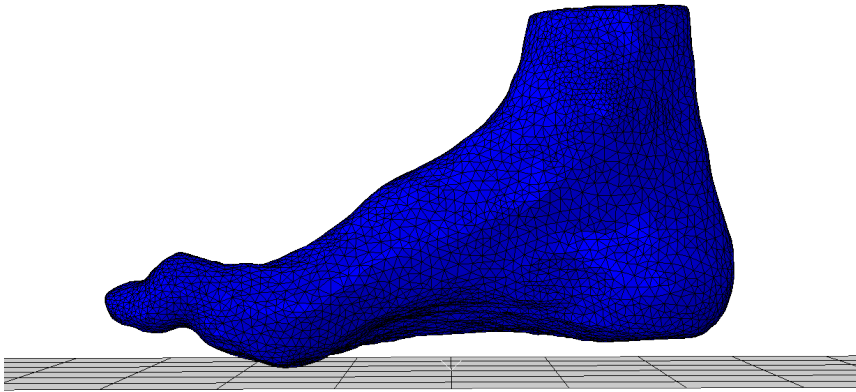
Bone and tissue of the patients were meshed into tetrahedrons with Simpleware[™] (Synopsys, Mountainview, CA, USA) FE module from the Computed Tomography (CT) images of their unloaded foot and then imported into Abaqus Simulia[™] (Dassault Systèmes, Velizy-Villacoublay, France). Bone meshes were considered as rigid bodies; they integrated the simplified geometries of the cartilage generated by dilation of their edge in the articular areas, as the precise geometries of the cartilage were not visible on the CT scans. Two sets of soft tissues were defined: first the fat pad containing the heel and the metatarsal fat pads, then the tissue representing the entire soft tissue matrix minus the fat pads, with the outer skin as an edge. The corresponding nodes between the bone meshes and the tissue meshes were constrained by kinematic coupling. Ligaments and muscles were then added as linear tension spring elements only (stiffness remaining to be calibrated) connecting the meshes of the bones. Two definitions of contact were used, one for contact between the bones and the other for contact of the plantar surface with the ground. The contact between the bones were considered frictionless; the contact between the tissues and the ground has a friction coefficient equal to 0.6, it was set up to avoid a severe distortion of the elements in certain orientations of the foot and taking into account the variability of the coefficients found in the literature [Der+09; Bau+10; Ke+15]. All contacts are implemented numerically using penalty method, following the "hard contact" definition in Abaqus. Abaqus explicit solver was used, and the models were on average composed of 191273 elements.

FE components are described in Table IV.1 and displayed in Figure IV.2

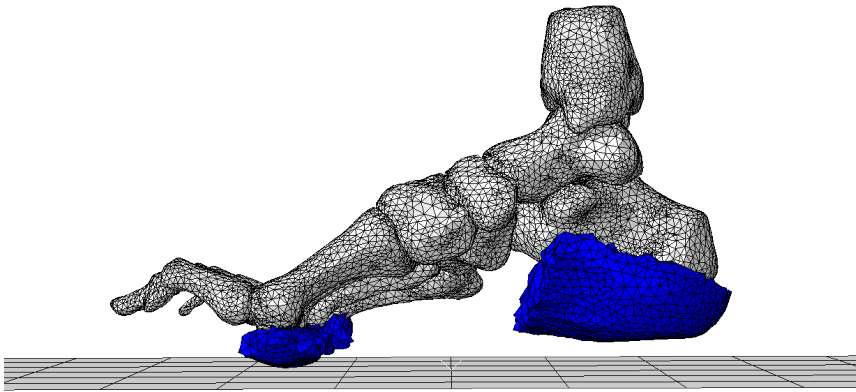
Component	Element type	Material	Constraint	Interaction
Bones	3D-tetrahedra	-	Rigid bodies	Contact between neighbouring bones
Soft Tissue	3D-tetrahedra	Neo-hook C10 = 1.67e-03 [MPa] D1 = 1.2 [MPa ⁻¹]	Kinematic coupling	Plantar surface contact with the ground
Fat-pads	3D-tetrahedra	Ogden $\mu = 1.64e-02$ [MPa] $\alpha = 6.82$ [Erd+06] D1 = 0.24 [MPa ⁻¹]	with corresponding bone nodes	
Ligaments Muscles	Connectors	Linear traction only Calibrated stiffness (III.5.3)		

TABLE III.1: finite element model components details

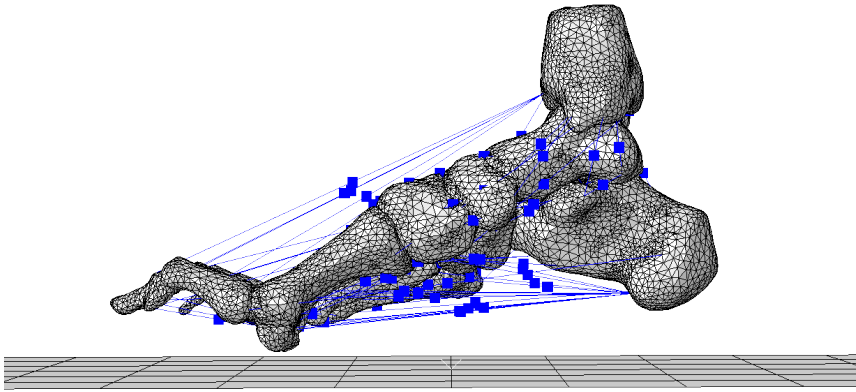
The explicit solver was used with material densities set to 1e-08 [tonnes/mm³] to speed up the calculation compared to the 1e-09 [tonnes/mm³] value usually used. To prevent the effect of bone movement vibrations from distorting soft tissue elements, Rayleigh's alpha damping has been set to 100 through a process of trial and error.



(a) Complete model



(b) Bones and fat-pads displayed



(c) Bones and connectors displayed

FIGURE III.3: Patient specific foot model

III.5.3 FE model calibration

III.5.3.1 Global strategy

To estimate the distribution of 85 connector stiffness (74 ligaments and 11 muscles), we decided to minimize the static equilibrium residuals from all 11 load situations performed on the subject, representing a wide range of possible situations that the foot may encounter, to integrate the maximum number of connectors stressed in traction. Our hypothesis is that ligament and muscle tensions are the main factors contributing to the static equilibrium of the foot structure under static load.

The workflow implemented is then as follows: the first step was to perform FE simulations of the 11 load situations, driven in displacement by the bones (applied as boundary conditions), which were previously determined from the CT acquisitions. This allowed to estimate the reaction forces and moments in the bones due to the contact of the foot with the ground and the contact between the bones. These bone reaction forces and moments were then assembled with internal experimental measurements: position, direction of work and deformation of the connectors (ligaments and muscles) in the static equilibrium equation system, whose residuals were then minimized with non-linear least-squares approaches. The results of the minimization were interpreted as the relative stiffness distribution of the connectors. The stiffness distribution itself was scaled by looking for the minimum difference between the experimental position and the simulated bone position calculated by force-driven FE model, using the relative stiffness distribution as an input. The strategy flowchart is displayed in figure III.13.

III.5.3.2 Displacement driven FE simulations

Displacement driven FE simulations were performed to estimate the reaction forces and moments in the bones due to the contact of the foot with the ground and the contact between the bones. In these simulations, soft tissue and connectors are disabled and bone displacements were used as a boundary condition.

A displacement-driven simulation was carried out for each applied load and each orientation, as described in Table III.2.

Simulation	Foot orientation	Load [%BW]		
		Step-1	Step-2	Step-3
1	Neutral (N)	10	100	150
2	Plantar Flexion (PF)	10	100	
3	Dorsal Flexion (DF)			
4	Eversion (EV)	10	100 ^a	
5	Inversion (IN)			

^aNot possible on bare foot due to sliding, the load was personalized for each patient and corresponding to a beginning of foot sliding

TABLE III.2: Tested configuration description

In the following, reaction forces were designated as \vec{f}_{ib} and reaction moments as \vec{m}_{ib} , with index $i = 1, \dots, N_i$ the number of loading steps tested and index $b = 1, \dots, N_b$ the number of bones.

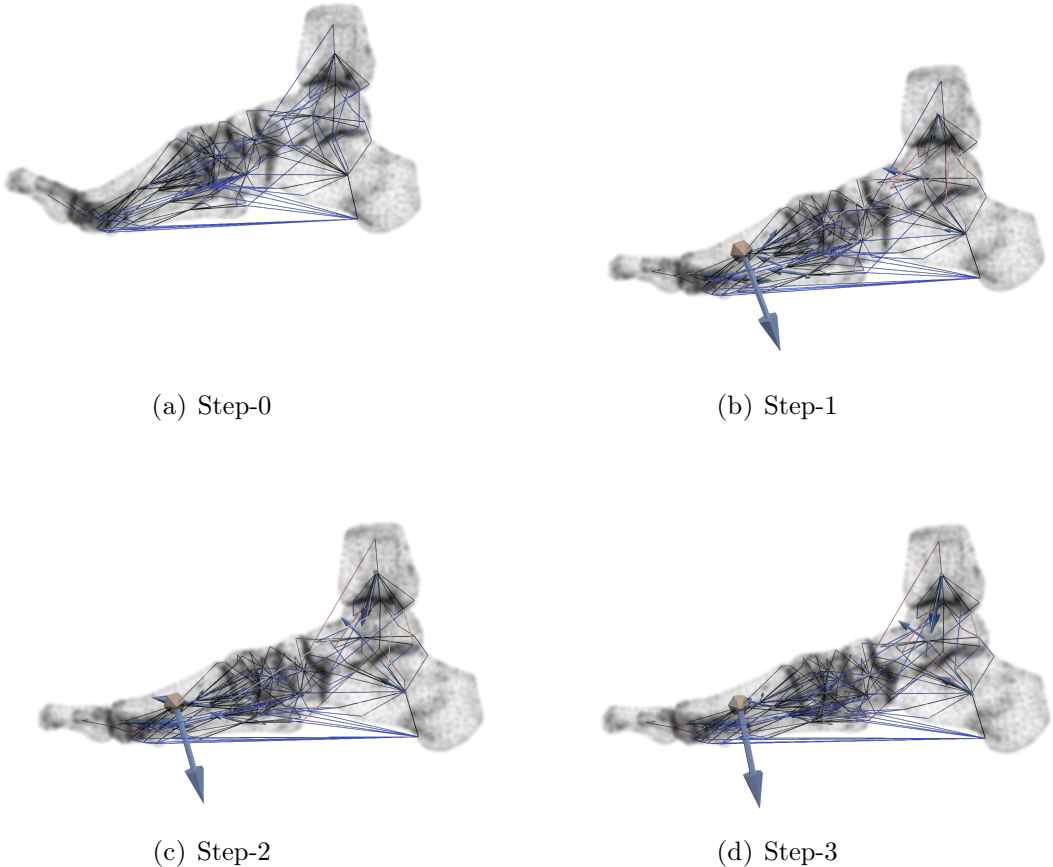


FIGURE III.4: Neutral foot orientation displacement driven simulation outputs (reaction forces and moments) and processed experimental data (bones positions and connectors)

III.5.3.3 Static equilibrium

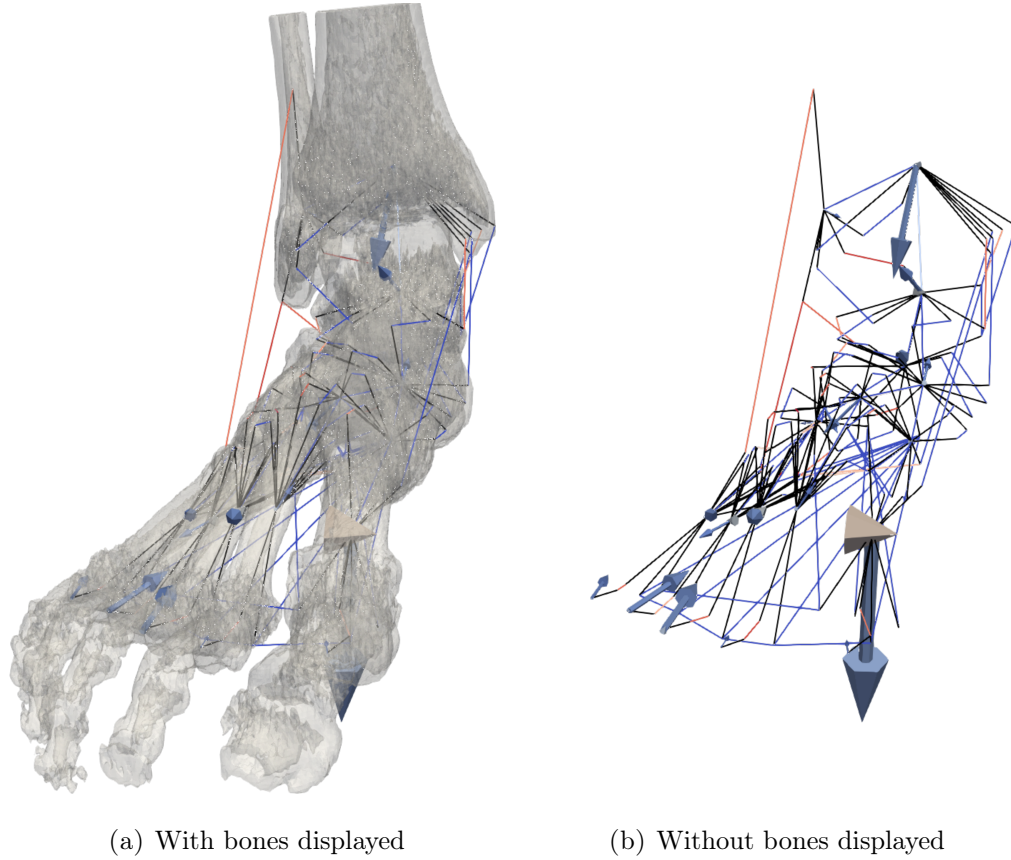


FIGURE III.5: Neutral foot orientation in the loading step 3

The cones represent the reaction moments (\vec{m}_{ib}), the arrows the reaction forces (\vec{f}_{ib}), the coloured lines the deformed connectors (s_{il}) (whose rigidity values are sought to obtain a minimum when resolving the static mechanical equilibrium), in black the links between the connectors' attachment points and the center of mass of the bones on which they intervene (\vec{w}_{ibl} and \vec{t}_{ibl}).

The minimization of the static equilibrium equation system was expressed by:

$$\vec{k} = \arg \min 0.5 \times \|\mathbf{U} \cdot \vec{k} - \vec{F}\|^2 \quad (\text{III.1})$$

With \vec{k} unknown ligament and muscle stiffness written $\vec{k} = \{k_l\}$ with index $l = 1, \dots, N_l$ the number of connectors (ligaments and muscles).

\mathbf{U} integrated the impact of the connectors' contribution on the bones, over 11 loading steps referenced with the index i . It was constructed by assembling the working \vec{w}_{ibl} and torque \vec{t}_{ibl} directions of each connector on bones in \vec{d}_{ibl} and multiplied by their deformations s_{il} . It was expressed as equation III.2.

$$\mathbf{U} = \left[\begin{array}{ccc|c} \left| \begin{array}{c} \vec{w}_{ib_1l_1} \\ \vec{t}_{ib_1l_1} \\ \vdots \\ \vec{d}_{ib_{N_b}l_1} \end{array} \right| & \dots & \left| \begin{array}{c} \vec{d}_{ib_1l_{N_l}} \\ \vdots \\ \vec{d}_{ib_{N_b}l_{N_l}} \end{array} \right| & \left| \begin{array}{c} s_{i1} \\ \vdots \\ s_{iN_l} \end{array} \right| \\ \hline & & & \end{array} \right] \quad (\text{III.2})$$

\vec{F} has assembled all reaction forces \vec{f}_{ib} and reaction moments \vec{m}_{ib} in \vec{r}_{ib} , calculated with displacement-driven FE simulations, of all the loading steps as equation III.3.

$$\vec{F} = \begin{Bmatrix} \left| \vec{f}_{ib_1} \right| \\ \left| \vec{m}_{ib_1} \right| \\ \vdots \\ \left| \vec{r}_{ib_{N_b}} \right| \end{Bmatrix} \quad (\text{III.3})$$

To solve this linear least-squares problem with bounds on the variables because the stiffness must be positive, we used the least-squares solving algorithm combined with the Trust Region Reflective (TRF) algorithm implemented in the SciPy library [Vir+19].

\vec{k} was then normalized to obtain \vec{k}^* corresponding to the distribution of stiffness through the ligaments and muscles .

III.5.3.4 Force driven FE simulations

The scale of stiffness distribution \vec{k}^* was studied here to obtain the stiffness of ligaments and muscles specific to the subject.

Soft tissues, ligaments and muscles were enabled. A simulation was carried out for the Neutral (N), Plantar Flexion (PF), Dorsal Flexion (DF), Inversion (IN) and Eversion (EV) orientations tested on the foot, with the experimental movements and loading applied to the tibia used as boundary conditions: in the vertical direction the experimental force and rotation were applied, in the other directions translation and rotation were applied.

Ligaments and muscle stiffness were determined by iteratively testing the simulation with α and β parameters used in equation III.5 to obtain stiffness simulation input \vec{k}^{**} , until the simulated bone positions were close to the experimental positions using the measurement described in paragraph III.5.4.1. The minimisation was expressed as equation III.4

$$(\alpha, \beta) = \arg \min (\text{SimulatedBonePositions}(\vec{k}^{**}) - \text{ExperimentalBonePosition}) \quad (\text{III.4})$$

with α corresponding to the stiffness scaling factor and β to the minimum stiffness threshold used in equation III.5.

$$\vec{k}^{**} = \left[k_l^{**} = \begin{cases} \beta & \alpha k_l^* < \beta \\ \alpha k_l^* & \alpha k_l^* > \beta \end{cases} \right] \quad (\text{III.5})$$

III.5.4 Metrics

III.5.4.1 Bone position

To determine the difference between the bones position found in the force-driven simulation and the experimental data, the average distance between each bone point of the force-driven simulation and the experimental points was used. Rotation and translation to align the simulated bone components to the experimental bone components were also used to assess the quality of bone positioning. The components were calculated using principal component analysis. The calculation does not take into account sesamoids and phalanges.

III.5.4.2 Articulation angle

To evaluate the joint angles, 12 angles joining the center of mass of the bones were tracked in the three anatomical planes for each configuration and compared to processed experimental measurements. The 12 angles are listed in table III.6.

2 angles in different anatomical planes were particularly monitored to measure relevant foot behaviors. Their graphical representations are displayed in figure III.14.

The differences between the simulated results and the experimental measurements were expressed as absolute values in degree and relative error.

III.5.4.3 Connectors deformation

85 connectors (74 ligaments and 11 muscles) were tracked and their deformed length relative to the experimental data were evaluated by relative error.

III.6 Results

III.6.1 Connector stiffness

Ligament stiffness can be classified in two categories: ligaments with no rigidity found on all subjects, and ligaments with a non-zero rigidity calibrated.

For those ligaments that were found to be stiff, some had significant variability in stiffness between subjects, as the strain between subjects is also variable, and others were quite consistent. In general, when stiffness was higher on average, the variability between subjects was greater, as shown in Figure III.6.

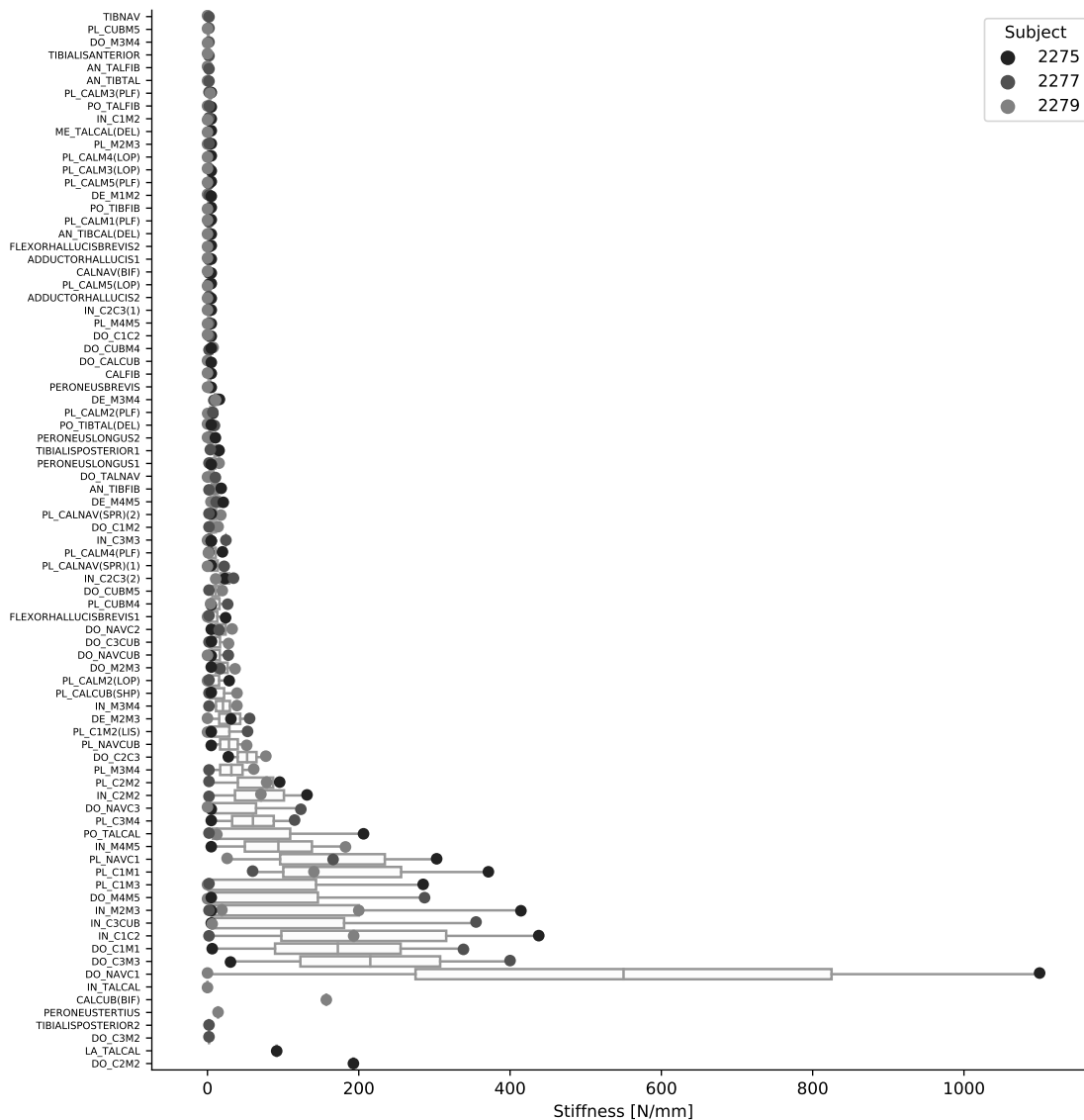


FIGURE III.6: Ligament stiffness classified as increasing result variability

The ligaments are named PL for plantar, DO for dorsal, DE for deep, IN for interosseus, AN for anterior, PO for posterior, ME for medial and after the underscore the connected bones are filled in, e.g. C1 for medial cuneiform bone, M1 for metatarsal 1. The names of the ligament clusters are in parentheses e.g. (PLF) for plantar fascia. Muscles are directly referred to by their names.

Even if we are talking about the stiffness of ligaments and muscles, it must be taken into account that these values, which have a mechanical connotation, are established to calibrate a macro-model in order to obtain simulation results as close as possible to those of the experiment. It is not a search for intrinsic mechanical parameters for each ligament & muscle. The structure being highly redundant, some connectors have no stiffness found because their function can be duplicated with neighboring connectors.

III.6.2 Force driven FE simulations outputs evaluation

III.6.2.1 Result overview

Results with adjusted ligament stiffness distribution, for each individual foot, are displayed in table III.3 and comparison with literature-based stiffness is shown in Table III.4. To facilitate visibility, a loading situation is displayed in the three anatomical planes in Figure III.7.

<i>Foot reference</i>	<i>Bone position (mm)</i>	<i>Rotation (deg)</i>	<i>Translation (mm)</i>	<i>Articulation angle (relative error)</i>	<i>Connector deformation (relative error)</i>
2279	8.31 ± 4.50	5.52 ± 3.39	8.15 ± 4.49	0.06 ± 0.13	0.13 ± 0.14
2277	8.95 ± 5.23	7.02 ± 4.56	8.74 ± 5.29	0.10 ± 0.18	0.12 ± 0.13
2275	7.61 ± 2.58	6.65 ± 4.03	7.35 ± 2.70	0.05 ± 0.07	0.17 ± 0.30

mean \pm standard deviation (sd)

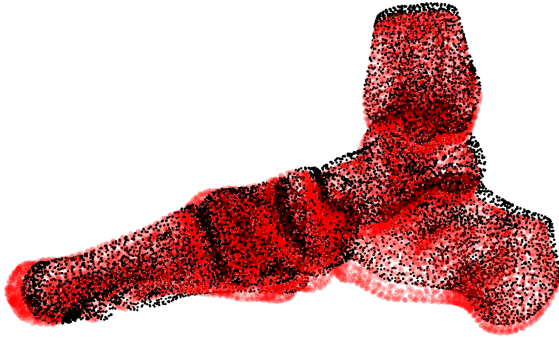
TABLE III.3: Difference with experimental measurements displayed foot by foot

<i>Stiffness information source</i>	<i>Bone position (mm)</i>	<i>Rotation (deg)</i>	<i>Translation (mm)</i>	<i>Articulation angle (relative error)</i>	<i>Connector deformation (relative error)</i>
Adjusted stiffnesses	8.29 ± 4.26	6.40 ± 4.06	8.08 ± 4.33	0.07 ± 0.14	0.14 ± 0.21
[CZ08] ^a	18.31 ± 11.10	13.78 ± 10.20	17.93 ± 11.03	0.10 ± 0.27	0.12 ± 0.13
[Wei+11] ^a	12.23 ± 7.04	13.23 ± 12.62	11.47 ± 6.86	0.14 ± 0.15	0.52 ± 1.11

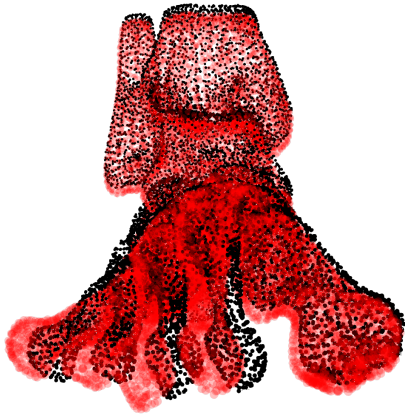
mean \pm sd

^aNo completion of all force-driven FE simulations

TABLE III.4: Comparison with two other sources of information on stiffness



(a) Sagittal plane



(b) Coronal plane



(c) Transverse plane

FIGURE III.7: 150 % of BW applied in neutral position to the foot referenced 2279, red point is the force-driven simulation results and the black point the experimental bone position. The average difference between bone position simulated and experimental is equal in this situation to $5.80 \text{ mm} \pm 1.37 \text{ mm}$

III.6.2.2 Bone position

The bone position difference is displayed in Figure III.8 for each applied load. It is noteworthy that the mean error during the approach phase (corresponding to 10% of the patient body weight applied) had a magnitude corresponding to 111% of the following loading steps mean errors, which corresponded respectively to 100% of the weight of the subject in the dorsal/plantar flexion as neutral orientations and to a weight generating the slipping of the foot in inversion and eversion then 150% of the weight of the body only in neutral position. The bone position error in the 10 % BW loading steps was equal to $8.82 \text{ mm} \pm 4.68 \text{ mm}$ when in the 100 % BW loading steps it was $8.20 \text{ mm} \pm 4.03 \text{ mm}$ and in the 150 % BW loading step it was $6.38 \text{ mm} \pm 2.56 \text{ mm}$.

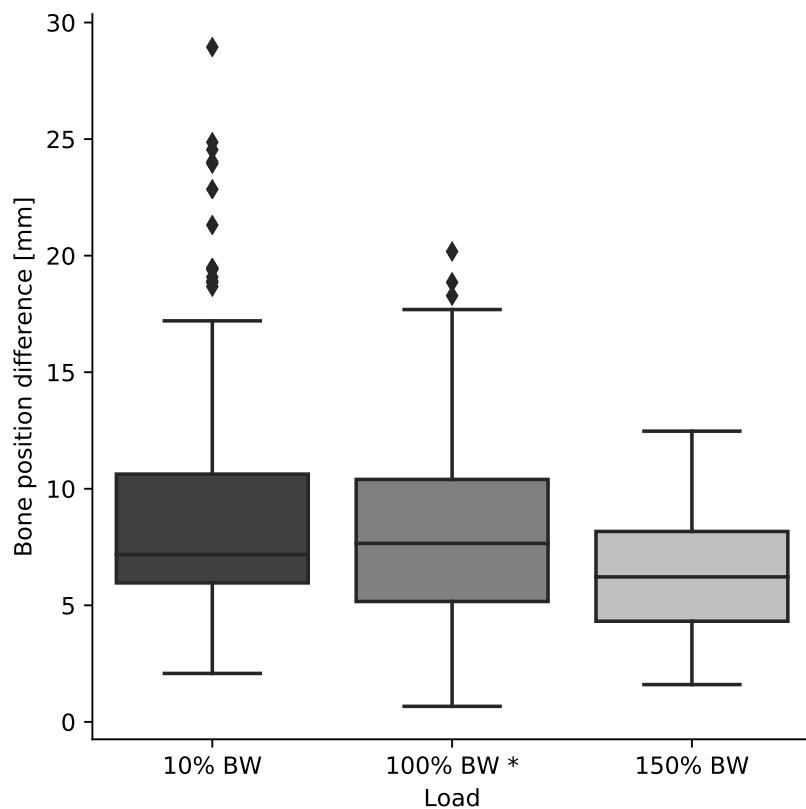


FIGURE III.8: Difference between simulated and experimental bone position, load by load

*Except in the inversion and eversion orientations due to foot slippage. In these orientations, the loading was customized at the beginning of the foot slip.

The force-driven FE simulations were done by applying a load in the vertical direction and movements in the other components to the tibia. The average error on the position of the tibia, all situations combined, was $6.04 \text{ mm} \pm 3.95$. The bone position difference is displayed in Figure III.9 for each bone.

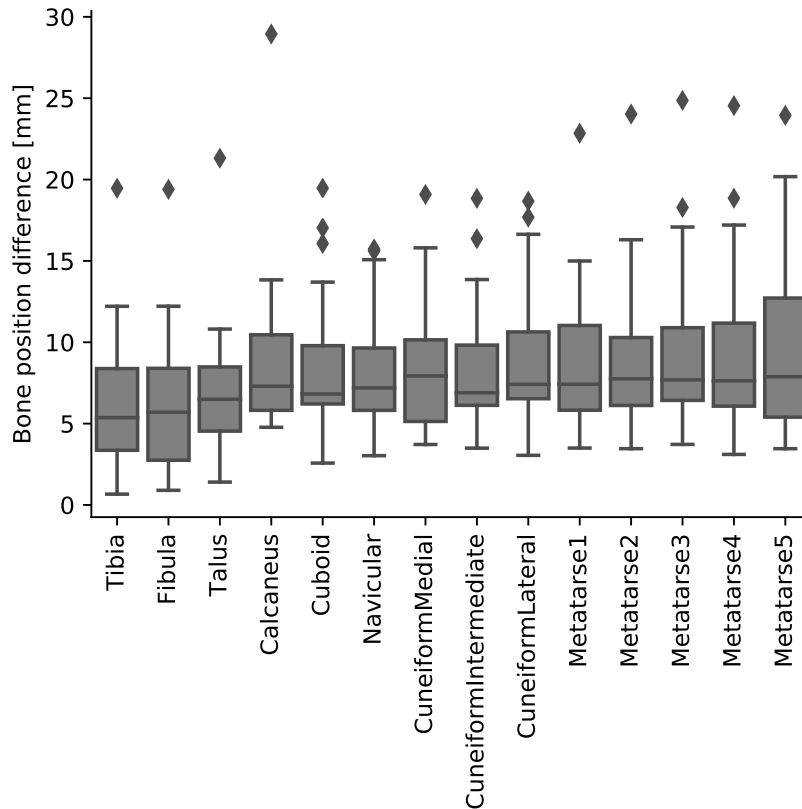


FIGURE III.9: Difference between simulated and experimental bone position, bone by bone

III.6.3 Articulation angle

2 angles were particularly tracked as they gave clear anatomical interpretations. CalTalM1 represents the arch sagging when expressed in the sagittal plane and the abduction-adduction movement in the transverse plane. TibTalCal shows the ankle plantar-dorsal measurement in the sagittal plane and the varus-valgus of the sub-talar joint in the coronal plane - see Figure III.14. Their differences with the experimental data are shown in the table III.5.

Angle	Anatomical plane	Measure	Articulation angle (deg)	Articulation angle (relative error)
CalTalM1	Sagittal	Arch sagging	5.24 ± 4.45	0.05 ± 0.04
	Transverse	Midfoot abduction/adduction	8.00 ± 5.10	0.05 ± 0.03
TibTalCal	Sagittal	Flexion Plantar/Dorsal	5.32 ± 4.81	0.04 ± 0.04
	Coronal	Inversion/Eversion	5.43 ± 4.22	0.03 ± 0.03

mean \pm sd

TABLE III.5: Angle comparison

III.6.3.1 Connector deformation

The differences between the strain obtained experimentally and with the model are shown in Figure III.10. Smaller connectors (defined by an initial length of less than 11 mm) showed a larger difference between simulated and experimental length measurements (0.21 ± 0.26) due to a more sensitive assessment of relative errors on this category of ligament, while longer connectors showed a smaller difference (0.07 ± 0.08). The scanner resolution was $0.66 \times 0.66 \times 1 \text{ mm}^3$.

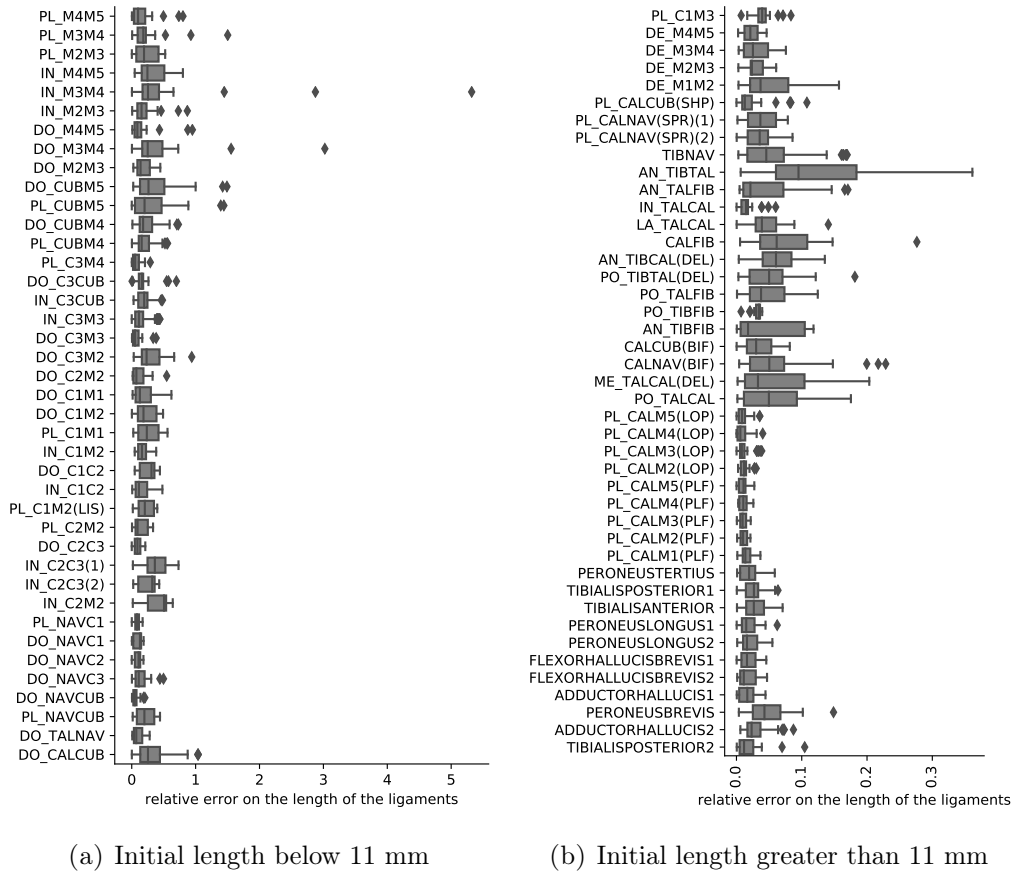


FIGURE III.10: Difference between simulated and experimental results of deformed ligament lengths.

Particular cluster of ligaments were evaluated:

- plantar aponeurosis ligaments (PLF) had an relative error of 0.02 ± 0.015
- long plantar ligaments (LOP) had an relative error of 0.02 ± 0.018
- deep transverse ligaments (DE) had an relative error of 0.07 ± 0.05
- spring ligaments (SPR) had an relative error of 0.07 ± 0.04
- deltoid ligaments (DEL) had an relative error of 0.12 ± 0.10

III.6.3.2 Fat pad stress

The stress results of force-driven simulations tend to be higher than those of displacement-driven simulations, as shown in the graphs in the figure III.15. Two stress components are looked, the maximum shearing measure (τ max) and the pressure.

The maximum shear measure (τ max) is displayed for each fat pad in figure III.11 and the element pressure is displayed in figure III.12. Larger shear and pressure zones appeared at the posterior base of the calcaneus and under the medial sesamoid bones, more discrete stresses were observed under the anterior base of the calcaneus and under the other metatarsal heads.

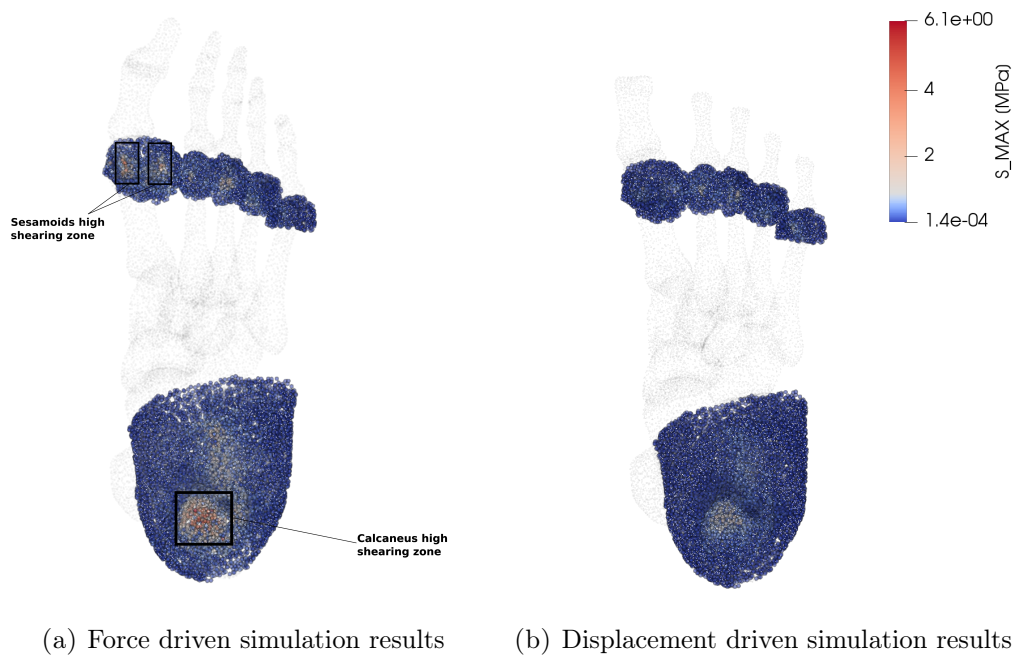


FIGURE III.11: Max shearing at 150% BW in neutral orientation

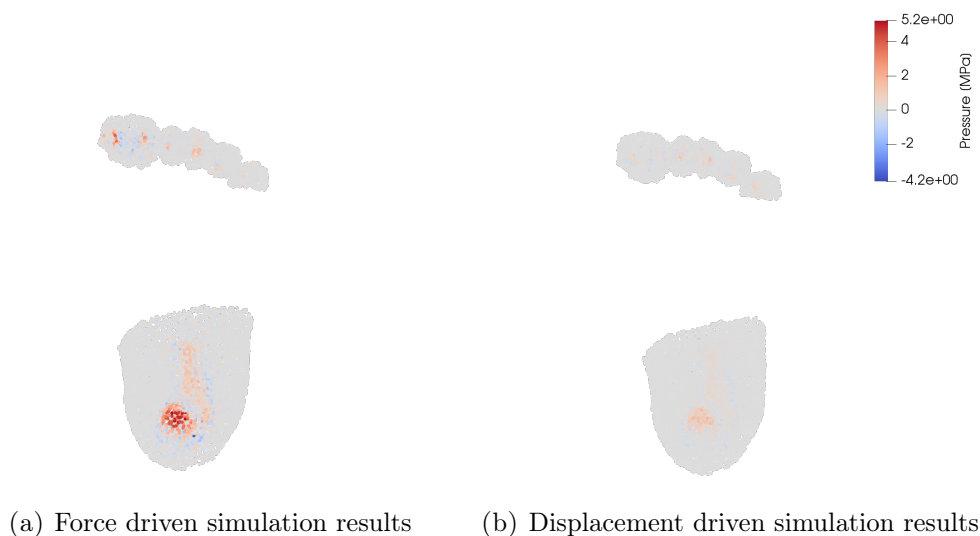


FIGURE III.12: Pressure at 150% BW in neutral orientation

III.7 Discussion

The objective of this work was to implement an inverse method to identify the effective stiffness of all the connectors of the foot (ligaments and muscles) and to compare the results of foot loading simulations, with the effective stiffness distribution integrated in the model, to experimental measurements. These subject-specific finite element models, calibrated with the presented method, are used in force-driven simulations to calculate the position of each bone as a function of a load as well as tissue deformation. They can be used to study joint angles, connector deformation, as well as the strain and stress fields in the fat pads and other tissues for different loading situations.

The limitation of the method is that it calculates a linear tension stiffness only for connectors that have been stretched in the experimental tests and that this calculated stiffness value may vary according to the contact and soft tissue numerical parameters chosen.

To our knowledge, this is the first time that a connector stiffness calibration protocol has been tested and that the results of simulations, exploiting these effective stiffness distribution, have been compared with precise experimental measurements. The results of the force-driven simulations compared to the experimental measurements show overall that they were consistent with the experimental data in terms of bone position, ligament deformation and joint angle except for phalanges bones.

To compare sources of information on stiffness, we have selected two papers, which do not attempt to adjust the position of the bones to the experimental measurements, but report the distribution of their stiffnesses: Cheung and Zhang [CZ08], uses for each ligament a Young's modulus equal to 260 MPa over a cross section of 18.4 mm² and for each connector of the plantar aponeurosis a Young's modulus equal to 350 MPa for a cross section of 58.6 mm²; in a second work, Wei [Wei+11], brings together 20 different ligament stiffnesses from the literature. We performed force-driven finite element simulations with their stiffness distributions to compare their sources of information with the proposed method. The bone positions in the force-based simulation using the effective connector stiffnesses showed better results than when using other sources of stiffness information from the literature. These better results can be explained by the fact that we performed a calibration, which took into account the specificities of the subjects, in order to get as close as possible to experimental measurements, compared to the use of characterization parameters from the literature, which do not cover all the muscles and ligaments of the foot and can have a significant variability.

Two main sources of error have been observed. First, regarding the scaling phase of the stiffness distribution and the use of other sources of stiffness information, both in exploited in force-driven finite element simulation, some element distortion altered the proper completion of the finite element simulations. It seems important to work on the aspect of the quality of the foot mesh to explore a wider range of connector stiffness distribution. Second, we removed the phalanges from the model evaluation because the positions of these bones calculated by the models in relation to the experiments were not consistent. In this area, the hypothesis of a representation of the joint capsule in 1D, working only in traction, did not seem to bring a sufficiently good result. We believe that a 2D, or even 3D, representation of ligaments, capsules and muscles would bring the results of the simulations closer to the experimental measurements.

The calibrated stiffness had different values from the characteristics in the literature. We believe that this difference with the literature characteristics can be explained by the

choice of contact and soft tissue parameters. In fact, we have observed through complementary simulations, that changes in contact and soft tissue material constitutive laws impact the calculated connector stiffness distribution. Complementary simulations were carried out with a linear material whose Young's modulus was modified, only the magnitude of the reaction forces and moments was impacted by a scaling factor, but no changes in orientation were observed, which did not result in any change in the connector stiffness distribution calculated with our method. Slight changes have begun to appear when using hyperelastic materials with the modification of the directions of forces and reaction moments. The same observations were made with the contact parameters. To fully control this limitation, soft tissue and contact characterizations or scientific consensus on contact and soft tissue parameters is required. This difference with the characteristics of the literature is also due to the fact that it is not the intrinsic parameters of the ligaments and muscles that are sought in this work but their calibration to obtain a more accurate macro model.

The approach phase with 10% of the body weight applied as load, with our method brings a higher bone position error than the following simulations with more applied load. This may be due to a choice of linear behavior assigned to the connectors that does not reflect the natural behavior of the ligaments. It can be improved by choosing a non linear material for connectors or by performing a fully tibia driven FE simulation instead of our choice to do a force driven FE simulation in the vertical axis of the tibia plus applying its displacements in the other directions.

It seems encouraging to use this method as a first step to either analyze the foot in different situations with force-driven patient-specific finite element simulations or to better match the experimental data with, for example, an iterative method using the stiffnesses calculated here as a first estimate.

III.8 Conclusion

This paper presents a numerical workflow for identifying ligament and muscle effective stiffness distribution in a patient-specific finite element foot model in order to perform force-driven simulations that yield results close to experimental measurements. The method was implemented on three cadaveric feet on which experiments were carried out with a range of applied loads in different positions. The comparison with the experimental measurements showed overall that the force-driven simulations calibrated with our method are consistent with the experimental data.

Given the number of feet on which the experimental data was acquired, the protocol was performed in a patient-specific manner. If this number of feet is large enough, the protocol can be run in a global manner providing a distribution of the average stiffness of all the feet. The results already obtained can be valuable information for executing iterative minimization algorithms to obtain results closer to experiments, as well as for extending the field of exploitation of finite element models of the foot with the analysis of bone positions, ligament deformities and joint angles.

III.9 Appendix

Angle	Bones
CalTalM1	Calcaneus, Talus, Metatarsel
CalTalNav	Calcaneus, Talus, Navicular
TalNavC1	Talus, Navicular, Cuneiform medial
NavC1M1	Navicular, Cuneiform medial, Metatarsel
CalTalCub	Calcaneus, Talus, Cuboid
TalCubM5	Talus, Cuboid, Metatarsel5
TibTalM1	Tibia, Talus, Metatarsel
TibTalCal	Tibia, Talus, Calcaneus
CalCubM5	Calcaneus, Cuboid, Metatarsel5
CalTalC1	Calcaneus, Cuboid, Cuneiform medial
CalC1M1	Calcaneus, Cuneiform medial, Metatarsel
CalNavM1	Calcaneus, Navicular, Metatarsel

TABLE III.6: Articular angle description

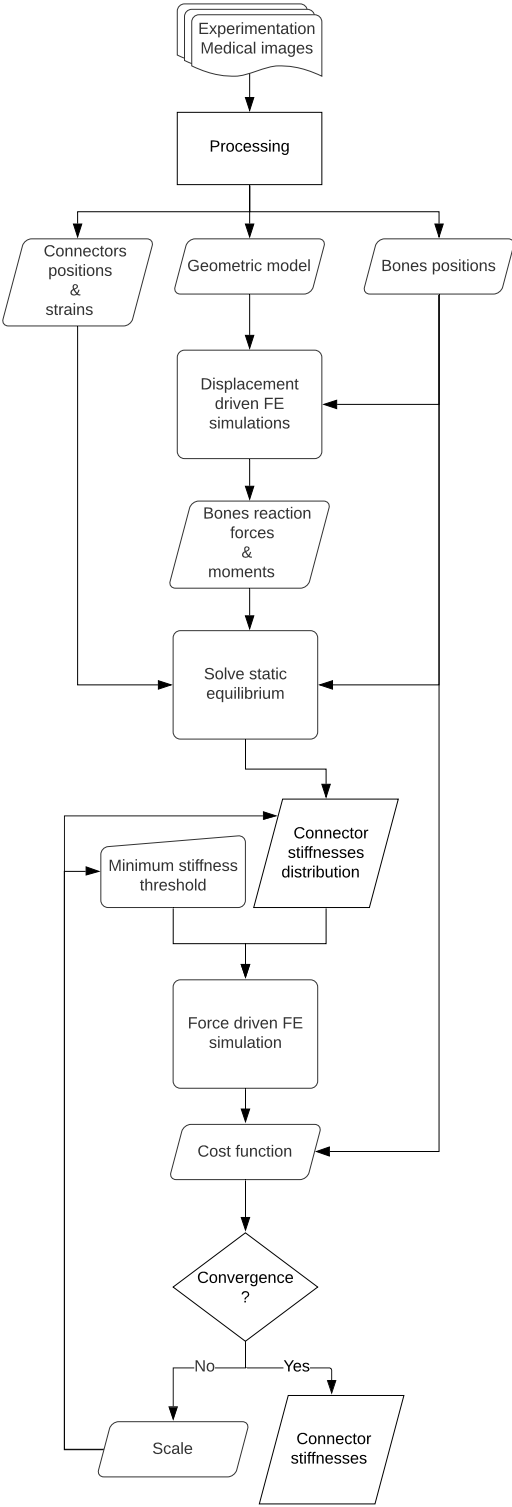
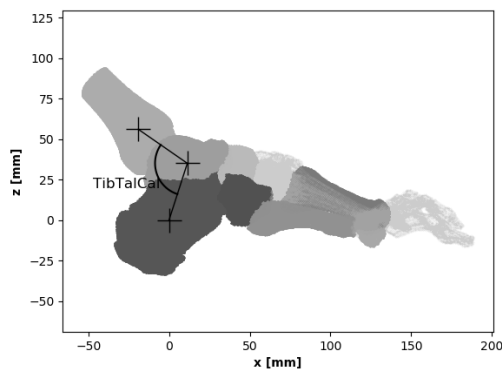
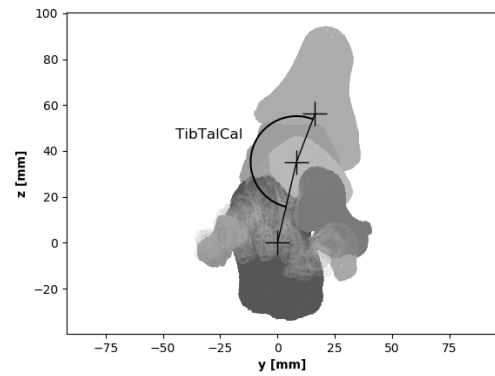


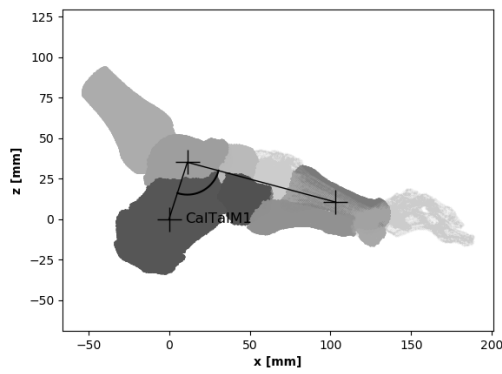
FIGURE III.13: FE model calibration protocol summary



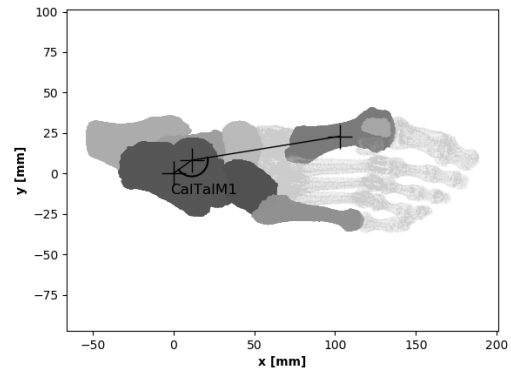
(a) TibTalCal angle expressed in the sagittal plane for ankle plantar-dorsal measurement



(b) TibTalCal angle expressed in the coronal plane for measuring the varus-valgus of the subtalar joint

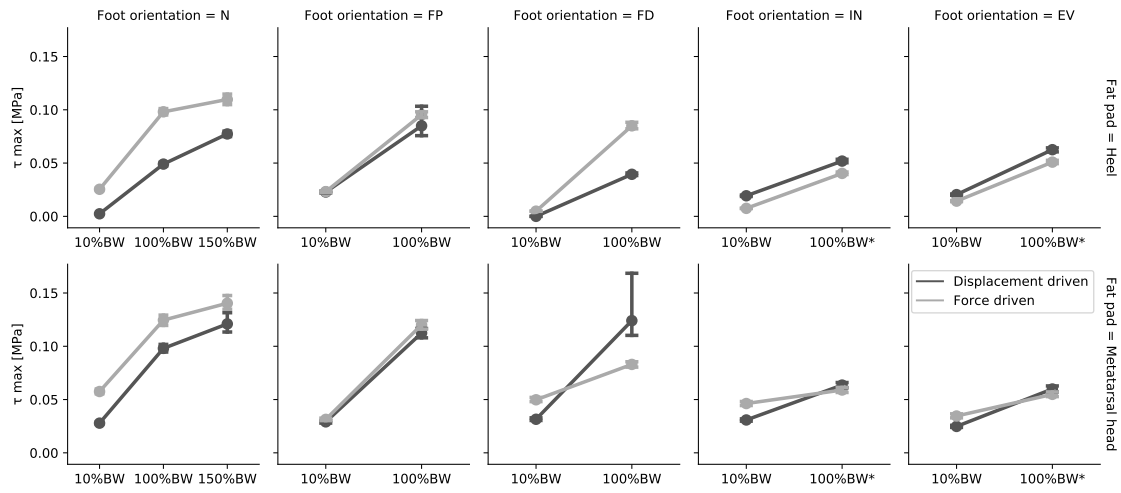


(c) CalTalM1 angle expressed in the sagittal plane for measuring arch sagging

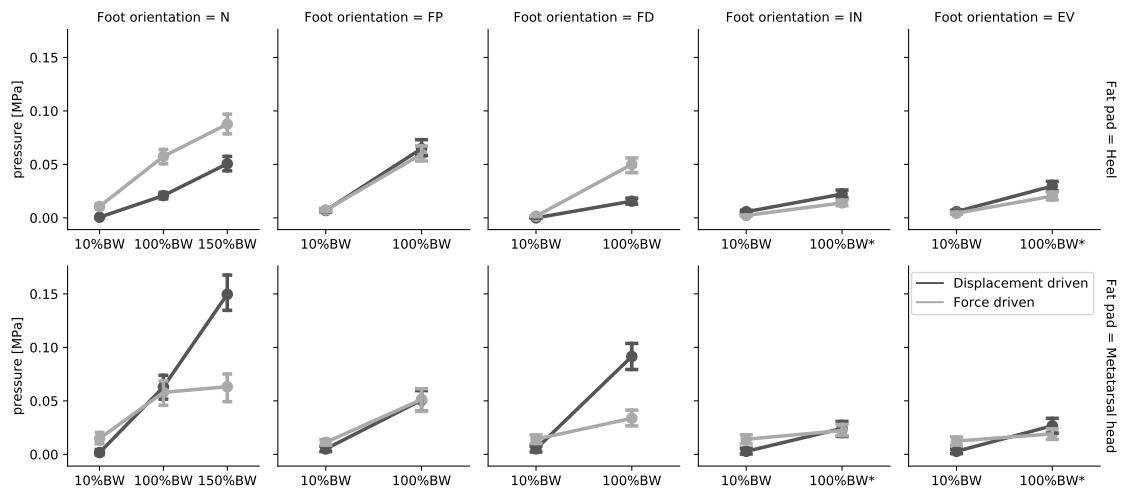


(d) CalTalM1 angle expressed in the transverse plane for midtarsal abduction-adduction measurement

FIGURE III.14: Angle measurement



(a) Maximum shearing comparison



(b) Pressure comparison

FIGURE III.15: Force & displacement driven stress comparison

Chapter IV

The effect of mid-sole stiffness and drop on foot biomechanics through finite element model

Contents of the chapter

IV.1	Résumé	92
IV.2	Preface	92
IV.3	Introduction	93
IV.4	Method	95
IV.4.1	Foot & footwear FE model formulation	95
IV.4.2	Footwear mid-sole variation	97
IV.4.3	Shoe adjustment	98
IV.4.4	Ground contact	99
IV.4.5	Running boundary conditions	99
IV.5	Results	100
IV.5.1	Simulation visualization	100
IV.5.2	Fat pad stress	100
IV.5.3	Plantar skin contact stress	102
IV.5.4	Ligament deformation	105
IV.5.5	Joint angle	109
IV.6	Discussion	113
IV.7	Conclusion	115

IV.1 Résumé

Les méthodes qui ont été développées jusqu'à présent dans ce document ont abordé deux aspects de la modélisation.

Le premier sur l'aspect géométrique avec le mesh-morphing pour représenter les ligaments & muscles d'un patient et la minimisation hiérarchique des distances pour trouver le positionnement des os dans différentes configurations de chargement statique.

Le second sur l'aspect matériau, ré-exploite les données de l'aspect géométrique pour calibrer la rigidité des ligaments/muscles en recherchant l'équilibre mécanique des configurations chargées, puis évalue dans quelle mesure la simulation reproduit les observations expérimentales.

Dans la continuité de ces travaux, un de ces modèles de pieds spécifiques au patient est exploité ici. Différentes chaussures de sport et une foulée de course à pied lui sont appliqués.

De nombreux paramètres de conception de chaussures peuvent être étudiés, l'objectif dans ce travail est d'obtenir une première description de l'effet de paramètre simple de la chaussure en sélectionnant deux paramètres.

- Le premier concerne la différence de hauteur entre l'avant et l'arrière de semelle intermédiaire (drop). Cette mesure est souvent utilisée pour modifier le schéma de frappe du coureur et fait l'objet de recherches en termes d'influence cinématique. L'ajout des mesures de contraintes mécaniques et des observations internes peut donc favoriser une meilleure compression des mécanismes impliqués.
- Le second paramètre est la rigidité de la semelle intermédiaire car elle est séparée de l'aspect géométrique de la chaussure. C'est donc un paramètre que les fabricants peuvent modifier plus simplement.

5 drops et 5 raideurs de semelles intermédiaires ont été testées, soit 25 chaussures simulées avec un pied courant avec une attaque talon. Différentes influences ont été évaluées sur la contrainte de cisaillement maximale des coussinets adipeux, la pression & force de cisaillement au contact entre le sol et la surface de tissu plantaire, la tension ligamentaire et les angles d'articulation.

IV.2 Preface

Chapters II and III addressed two aspects of modeling in response to the barriers identified.

The geometrical aspect of the foot model was addressed in chapter II with the mesh-morphing technique to calculate the positions of the ligaments and muscles specific to the patient, then a hierarchical minimization of the distance to obtain each bone displacement between statically loaded configurations was implemented.

With these data, part of the material aspect has been worked on in the chapter III. The mechanical equilibrium of the loaded configurations was sought by adjusting the stiffnesses of the ligaments and muscles, then the quality of reproduction of the experimental observations that the simulations have shown was evaluated.

Based on these developments, in this chapter we use an improved version of one previously developed patient-specific models, in a running configuration with different shoes, to evaluate the influence of two parameters: mid-sole drop and stiffness.

IV.3 Introduction

The influence of footwear on the foot biomechanics is usually studied by external and experimental measurements, using equipment acquiring pressure maps, Ground Reaction Force (GRF) and bone segment motion capture. With these techniques, it has been shown that the shoe mid-sole thickness influence the striking pattern of the foot, changing the vertical Ground Reaction Force (vGRF) profile [Lie+10; Ham+11]. It has also been shown that mid-sole stiffness has an effect on impact and propulsion during running [CFH83]. Internal measures, using specialized equipment such as X-ray cineradiography, has been used to observe an increased deformation of the heel fat pad when no footwear is worn in a heel strike gait development, [DAK94]. These measurements are less common and performed on smaller samples due to the experimental complexity. Joint angle assessments can also be extracted from X-ray fluoroscopy acquisition, confirming different behavior between bare and shod foot kinematics and temporal spatial parameters of subtalar and talocrural joint [McH+19]. As the foot is a complex structure of about 30 bones, a few hundred ligaments & muscles, and composed of different soft tissues from the fat pad to the skin, it requires internal measures to describe its behavior with as little uncertainty as possible and to add information to the diagnosis [Lin+18]. Instead of repeating these complex acquisitions to analyse various foot situation, the use of numerical models is relevant to access internal mechanical fields. Finite Element (FE) models, can also estimate some quantities impossible to measure experimentally such as stress. It has been widely used to identify material properties [Erd+06; Isv+16], to study the foot in different configurations often in static cases and/or focus on one component of the foot [Wei+11; WLZ14; Che+05; Che+10; Bud+07; Isv+12]. When the models take into account the interaction with the shoe, they focus on plantar pressure and vGRF [CZ05; Sis+13; Yu+13; LLG19], but there is no study investigating internal fields and the influence of shoe design variations on the whole foot when running (parametric study).

Computational modeling of the shod foot is a powerful approach to investigate the influence of various footwear conception parameters on the foot, and thus to support the product design phase. Different objectives can be explored. It can, for example, be focused on the footwear energy restitution profile through time to maximize a movement speed, such as a change of direction in a sport practice, while taking care not to overload specific anatomical components. In the medical field, FE analysis has been used to investigate footwear insoles to avoid peak pressure in diabetic patients to prevent foot ulcers [Lem+97a; Gef03a]. The FE analysis can be extended to other foot pathologies, for example: achilles tendinitis & bursitis, plantar fasciitis, gout, toes deformation as the hallux valgus. It can also accompany reconstruction of the foot after different injury, such as ankle sprain, fractures (ankle, calcaneus, rotational, talar, metatarsal ...) by helping design of footwear or orthosis containing the wounded area at the minimal comfort cost.

The standard workflow of building patient-specific macro FE foot models begins with a detailed segmentation of the 3D medical images of the patient, to then generate the meshes of its different components. Parameters of the constitutive equations chosen to represent the materials must then be determined from the literature or from characterization/identification studies. Once the boundary conditions have been formulated and the simulation performed, experimental validation of the simulation results must be done to check the reliability of the model. Each of these steps brings a dose of simplification related to modeling choices, such as the representation of ligaments (1D, 2D, 3D) or ma-

terial characteristics (linear, non-linear, patient-specific or generic, ...), which can reduce the representativity of the model in addition to the computational complexity. In this study, we use a patient-specific finite element models of the foot to monitor bone position, ligament strain and joint angles. The foot model was developed with the protocol given in chapter III, containing soft tissue with generic parameter from the literature, 30 separated bones, 74 ligaments and 11 muscles connectors with their effective stiffness calibrated in chapter III. The connectors (ligaments & muscles) were calibrated with measurements extracted from a sequence of orientations plus loading applied to the foot while being CT scanned. The results of the calibrated simulation were evaluated by comparing in detail the simulated measurements with the experimental measurements.

To observe the influence of shoe design on the overall and detailed behavior of the foot, we propose here to use an improved version of the previously developed patient-specific FE macro-model in a running situation, wearing a sports shoe with varying design parameters. Many footwear design parameter can be studied. Our first objective in this thesis is to get a first description of the effect of shoe drop and mid-sole stiffness on internal foot behavior by dressing the foot model with the different footwear. The mid-sole drop because it is often used to modify the striking pattern of the runner and is subject to research in terms of kinematic influence; for this, adding the measurements of mechanical stress and internal observations can encourage a better compression of the mechanisms involved. And the stiffness of the mid-sole because it is separated from the geometric aspect of the shoe, therefore it is a parameter that manufacturers can more simply modify.

IV.4 Method

IV.4.1 Foot & footwear FE model formulation

The image acquisition, segmentation and modeling approaches have been presented in a previous chapters II & III. We present here a brief summary of the modeling protocol.

From the scanner of the bare foot in Neutral (N) orientation and without loading, each bone and tissue (fat pads & soft tissue) was segmented. Simplified bone cartilage geometries were generated by dilating the bone edge in the joint area and then joined to the bone geometry, as the precise cartilage geometries were not visible on the CT scans.

From the shod foot, Neutral (N) orientation and unloaded configuration, the different shoe components were segmented. 3 components were isolated, the shoe upper, mid-sole and outer sole.

The different components were meshed into tetrahedrons with Simpleware™ (Synopsys, Mountainview, CA, USA) FE module and then imported into Abaqus Simulia™ (Dassault Systemes, Velizy-Villacoublay, France). The meshing stages are shown in the figure IV.1.

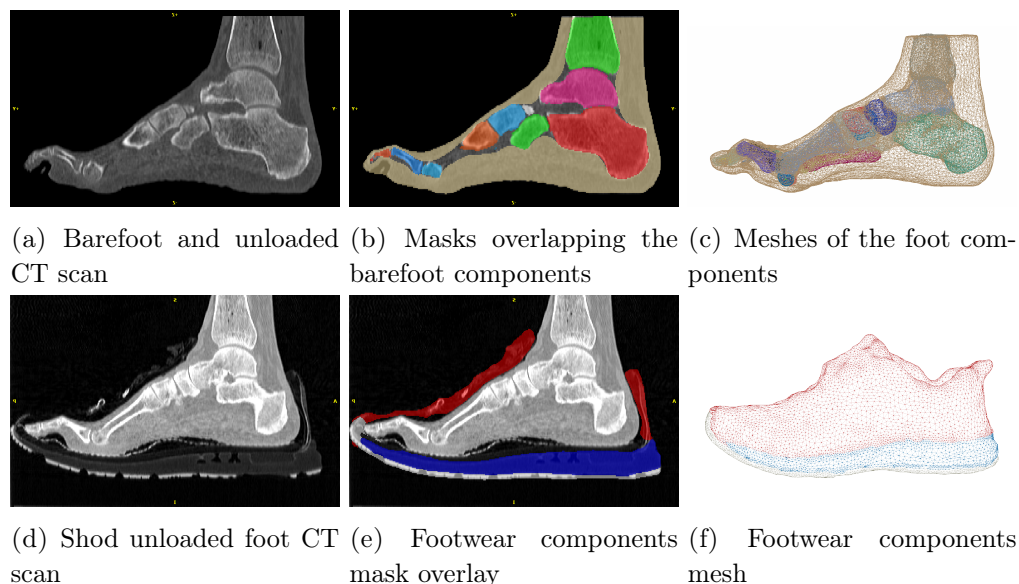


FIGURE IV.1: Segmentation - Medial view

The bone meshes (including their cartilages) were considered as rigid bodies. Three sets of soft tissues were defined, the fat pads with the heel and the metatarsal fat pads, then the soft tissue representing all the other tissues except the fat pads and finally the skin corresponding to the outer surface of the soft and fat pad tissues. The corresponding nodes between the bone meshes and the tissue meshes were constrained by kinematic coupling. Ligaments & muscles connecting the meshes of the bones were added as linear tension elements working only in traction, their geometry and attachment points on the bones were calculated with a transfer function between a detailed generic model and the geometries of the patient's bones. The distribution of their stiffness was estimated by calculating the mechanical equilibrium of the foot system in 11 different configurations tested and scanned. The three components of the shoe were made of different material, Shoe upper and outer sole were considered as linear elastic and mid-sole had parametric Young modulus plus viscoelasticity parameters. The contact between the tissue and the shoe, as the shoe with the ground, follows the Amonton-Coulomb law, with a coefficient of friction equal to 0.3; the contact between neighbouring bones was considered frictionless. All contacts are

implemented numerically using penalty method, following the "hard contact" definition in Abaqus.

FE components are described in Table IV.1 and displayed in Figure IV.2.

Some improvements and exploration have been made compared to the previous modeling protocol of the chapter II. The addition of viscoelasticity eliminated the damping parameters used, bringing the model soft tissues closer to the characterized anatomical components values. The skin was added to test how well it fits into the model protocol and contributes to the stability of the simulation.

Component	Element type	Material	Constraint	Interaction
Bones	3D-tetrahedra	-	Rigid bodies	Contact between neighbouring bones
Soft Tissue	3D-tetrahedra	Neo-hook & visco-elastic ^a C10 = 1.67e-03 [MPa] D1 = 1.2 [MPa ⁻¹]	Kinematic coupling with corresponding bone nodes	Outer surface in contact with the shoe
Fat-pads	3D-tetrahedra	Ogden & visco-elastic ^a $\mu = 1.64e-02$ [MPa] $\alpha = 6.82$ [Erd+06] D1 = 0.24 [MPa ⁻¹]		
Skin	3D-shell	Linear elastic & visco-elastic ^a $E = 2.16$ [MPa] [Gee+11] $\nu = 0.49$ thickness = 0.66 [mm] [CZC11]	-	-
Ligaments Muscles	Connectors	Linear traction only Scaled stiffness distribution	-	-
Shoe upper	3D-tetrahedra	Linear elastic $E = 10$ [MPa] $\nu = 0.49$	-	Inner surface in contact with the foot
Mid-sole	3D-tetrahedra	Linear elastic & visco-elastic ^b $E = 0.25$ to 1.75 [MPa] $\nu = 0.49$	-	
Outer sole	3D-tetrahedra	Linear elastic $E = 10$ [MPa] $\nu = 0.49$	-	ground contact

^aQuasi-linear viscoelasticity, data from [Gri+17]

$g_1 = 0.06, g_2 = 0.77, g_3 = 0, g_4 = 0, g_5 = 0.02$; $\tau_1 = 0.001, \tau_2 = 0.01, \tau_3 = 0.1, \tau_4 = 1, \tau_5 = 10$; $k_i = 0$

^bQuasi-linear viscoelasticity, data from [Dro+18] with ν chosen equal to 0.49

$g_1 = 0.05342237, g_2 = 0.04340568, g_3 = 0.01836394$; $\tau_1 = 1296, \tau_2 = 5184, \tau_3 = 30456$; $k_i = 0$

TABLE IV.1: finite element model components details

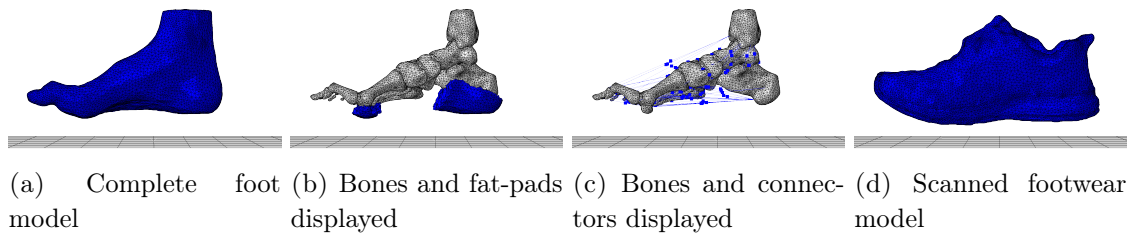


FIGURE IV.2: Patient specific foot & footwear models - Medial view

IV.4.2 Footwear mid-sole variation

4 different mid-soles were generated from the segmented CT scan, with a drop of 25/15 (10) [mm].

2 mid-soles with a reduced drop compared to the original, were generated by removing material at the back of the mid-sole until 20/15 (5) [mm] and 15/15 (0) [mm] drops were reached.

2 mid-soles with an increased drop compared to the original were generated by removing material at the front of the mid-sole until 25/10 (15) [mm] and 25/5 (20) [mm] drops were reached.

The material was removed on the original segmentation by deforming an additive top layer of the mid-sole. The back or front of the top layer was moved vertically to respectively reduce or increase the drop. Mid-sole top layer variations are displayed in figure IV.3.

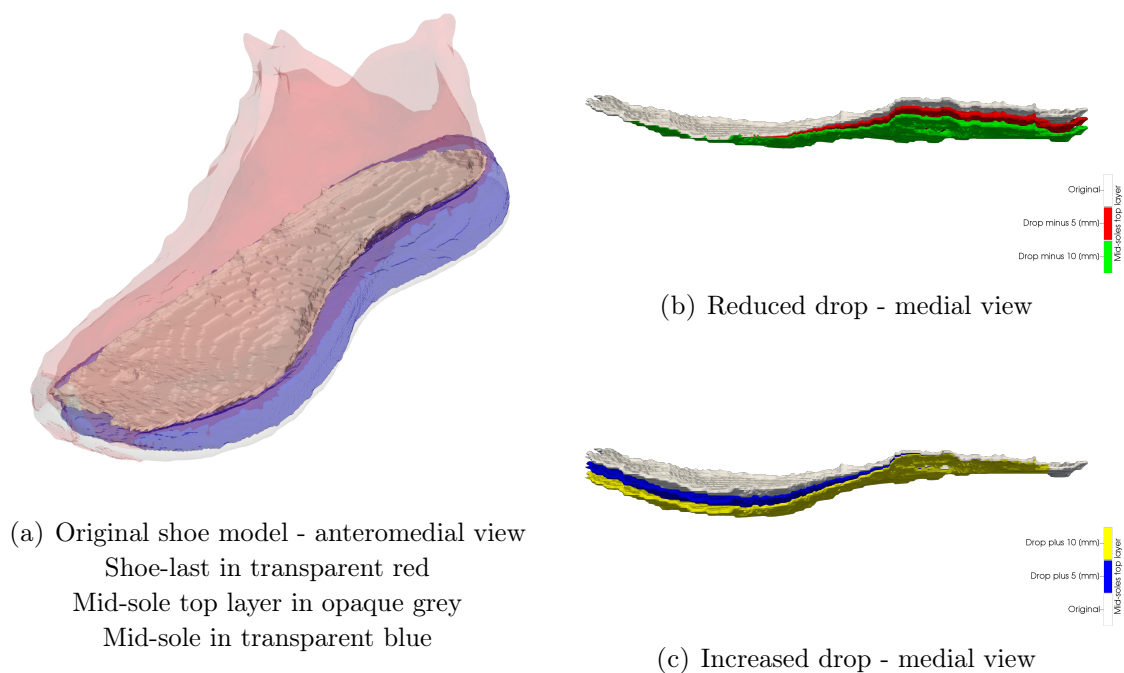


FIGURE IV.3: Mid-sole top layer variations for mid-soles generation

Mid-sole stiffness was parametrized with Young modulus values of 0.75, 1.75, 2.75, 3.75, 4.75 [MPa].

Different simulation results were studied: maximum shear stress, contact pressure & frictional force, ligament strain and articulation angle; their average value was compared and the influence of the mid-sole drop and stiffness parameters were calculated by fitting

second order polynomials with ordinary least squares method as described in equation IV.1.

$$\vec{y} = a_0 + a_1\vec{x}_{drop} + a_2\vec{x}_{stiffness} + a_3\vec{x}_{drop}^2 + a_4\vec{x}_{stiffness}^2 \quad (IV.1)$$

With index $i = 1, \dots, N$ the number of simulation, $N = 5^2$.

$\vec{y} = \{y_i\}$ the response variable for each simulation (averages of maximum shear stress, contact pressure & frictional force, ligament strain and articulation angle).

The drop and stiffness parameters stored in $\vec{x}_{drop} = \{x_{drop_i}\}$ and $\vec{x}_{stiffness} = \{x_{stiffness_i}\}$ containing the normalized values of the parameters (between -1 and 1).

The a values represent the influence of the parameters except for a_0 which prepositions the solution.

IV.4.3 Shoe adjustment

2 steps in Abaqus™ were used to adjust the shoe to the foot model.

The first was to move every bone to its position in the shoe while increasing the scale of the shoe. In the second, the contact between the shoe and the foot is enabled while the shoe nodes return to their initial position (without scaling) corresponding to the observed shod position.

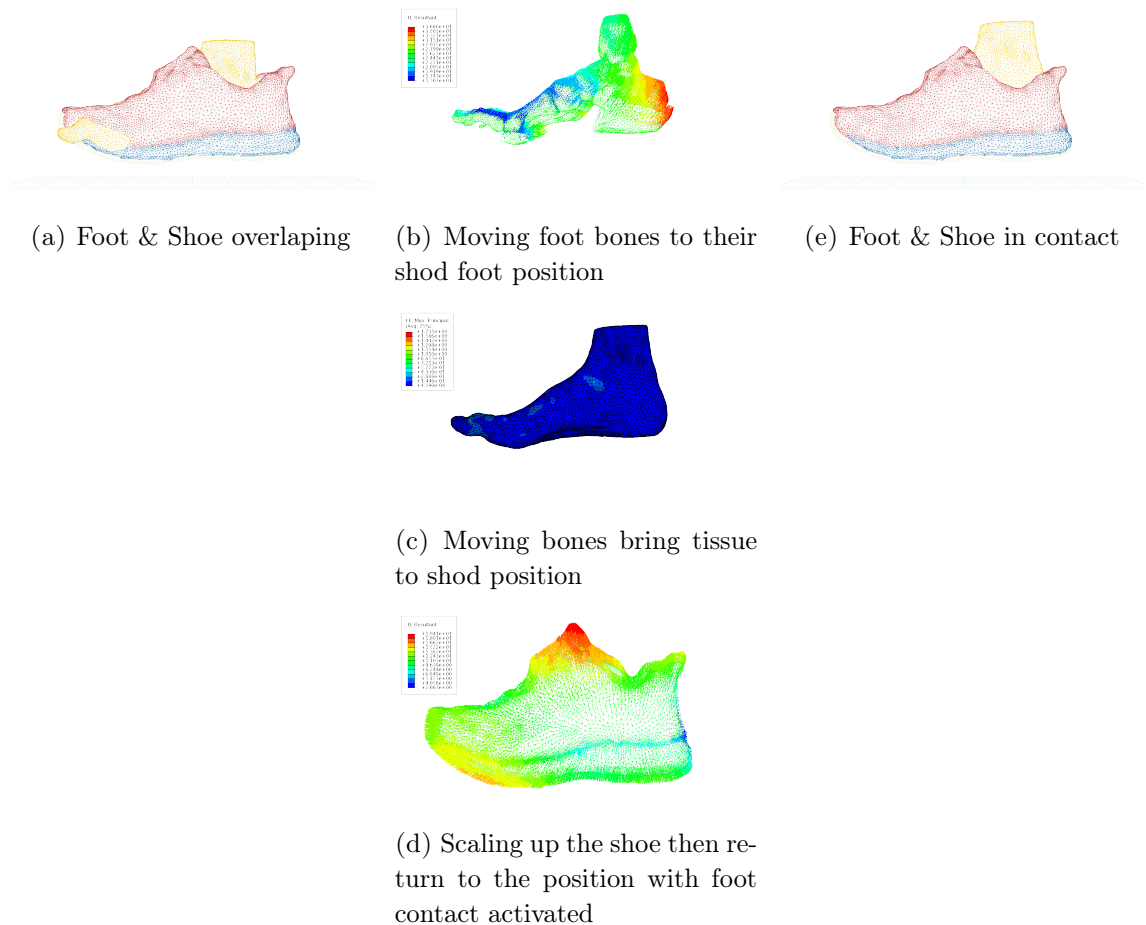


FIGURE IV.4: Foot dressing stages - medial view

IV.4.4 Ground contact

As in our CT scan of the unloaded foot with footwear, the shoe was not in contact with the ground. The tibia was rotated in the sagittal direction by 20 [degrees] while applying a small vertical force to the tibia (10 % of the body weight) and then releasing it to position the foot-shoe assembly in contact with the ground.

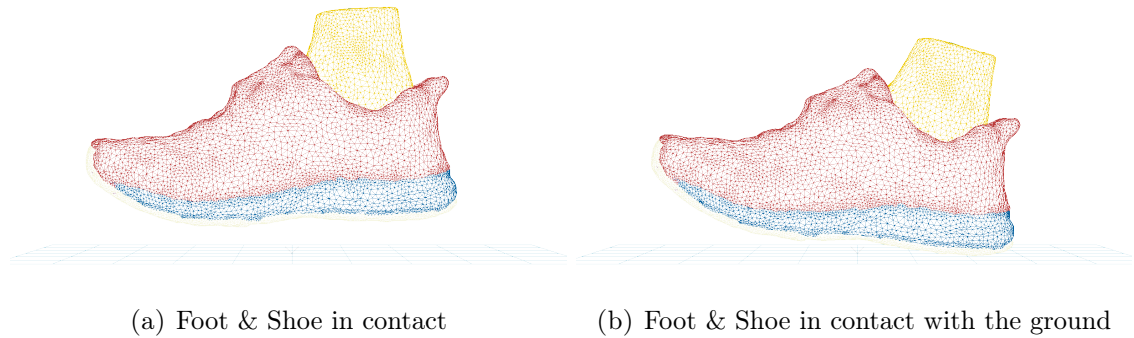


FIGURE IV.5: Ground contact stages - medial view

IV.4.5 Running boundary conditions

Running boundary conditions were applied as displacement and force fields on the tibia.

Rotation of the tibia was set in the sagittal direction from 20 [degrees] of the approach stage to -47 [degrees]. In the coronal plane tibia translation and rotation were set equal to 0.

Tibia vertical force was applied as the mean curve described by Hamil et al [Ham+11]. To get the toe off part of the gait, a force representing the Achilles tendon activity was applied to the Calcaneus following [AWK13]. Force boundary conditions are displayed in figure IV.6a.

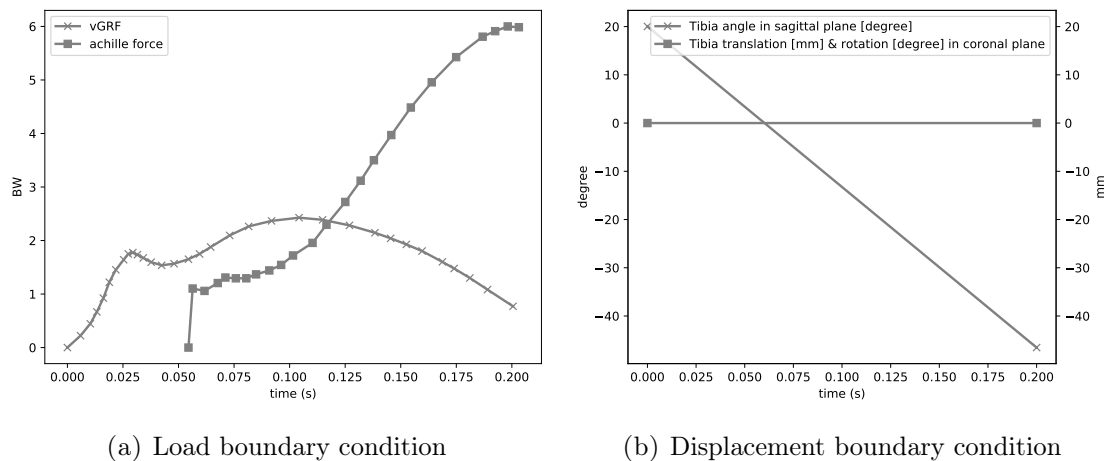


FIGURE IV.6: Boundary conditions

IV.5 Results

IV.5.1 Simulation visualization

An illustrative simulation result is displayed in figure IV.7.

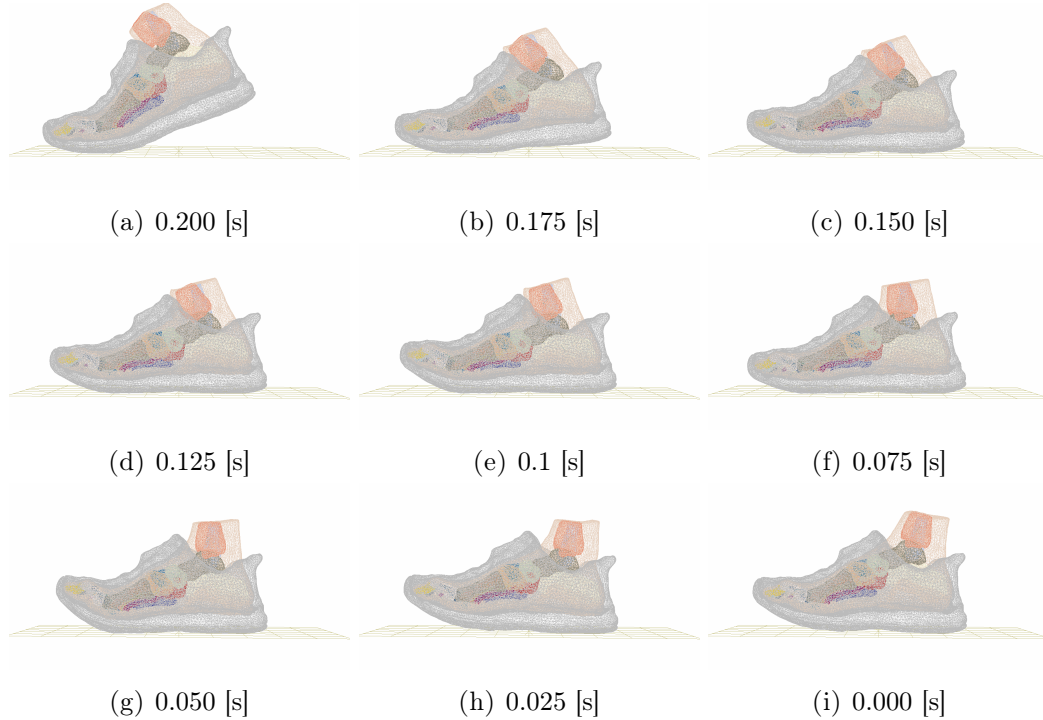


FIGURE IV.7: Simulation visualization over time - medial view

IV.5.2 Fat pad stress

The maximum shear stress in each fat pad (heel and metatarsal head) was tracked in each simulated configuration. The maximum shear stress is displayed for all integration points at a running time of 0.05 [s], for a tested shoe, in figure IV.8.

The maximum shear stress of each fat pad are displayed by averaged value through time in figures IV.9a and IV.9b. The influence of the mid-sole drop as well as the mid-sole stiffness on the distribution of the maximum shear stress was analyzed by comparing the average value of each configuration tested:

- For the metatarsal head fat pad, we observed that in average, the minimum stress converged in a convex manner to the 25/15 drop equal to 10 [mm] and decreased as the mid-sole stiffness increased as displayed in figure IV.10a. The second order polynomial ordinary least square fitting, with a determination coefficient (R^2) of 0.880, calculated that the drop coefficient was equal to -0.0011 (a_1) and that stiffness coefficient was equal to -0.0095 (a_2). Quadratic effects were present on drop ($a_3 = 0.0119$) and stiffness ($a_4 = 0.0060$).
- For the heel fat pad, we observed that the average stress was mainly influenced by the drop, increasing as the drop decreased and that stiffness played a minor role as displayed in figure IV.10b. The second order polynomial ordinary least square fitting, with a determination coefficient (R^2) of 0.917, calculated that the drop coefficient

was equal to -0.0012 (a_1), the quadratic drop coefficient was equal to 0.0092 (a_3) and stiffness coefficients had a p-value superior to 0.05 (a_2 & a_4).

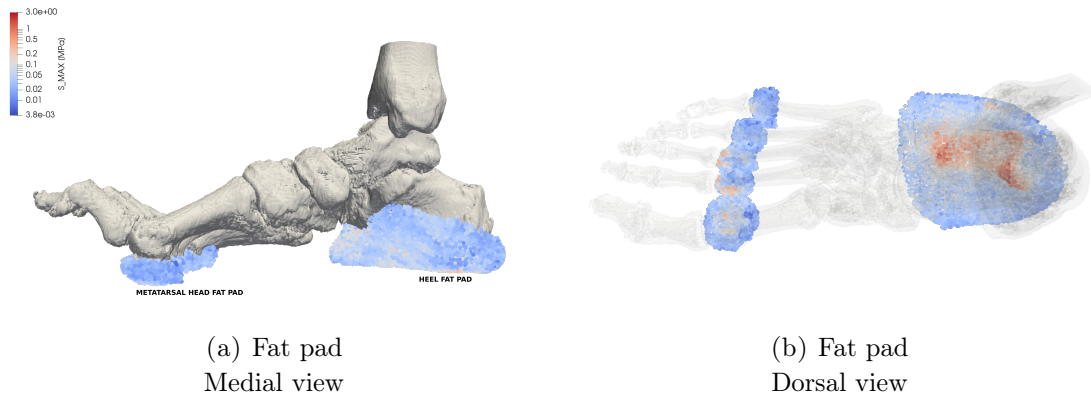


FIGURE IV.8: Maximum shearing visualization at 0.05 s

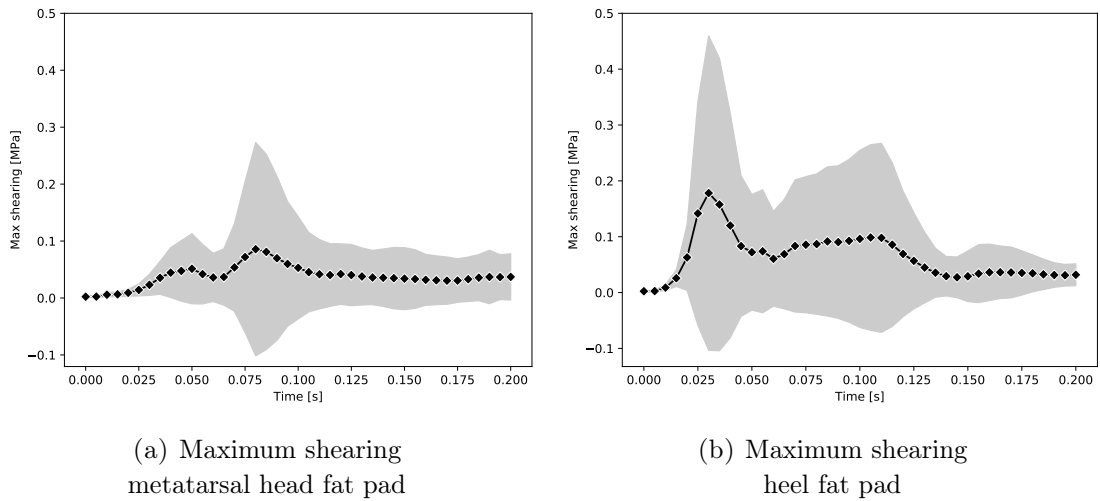


FIGURE IV.9: Maximum shearing of fat pads over time

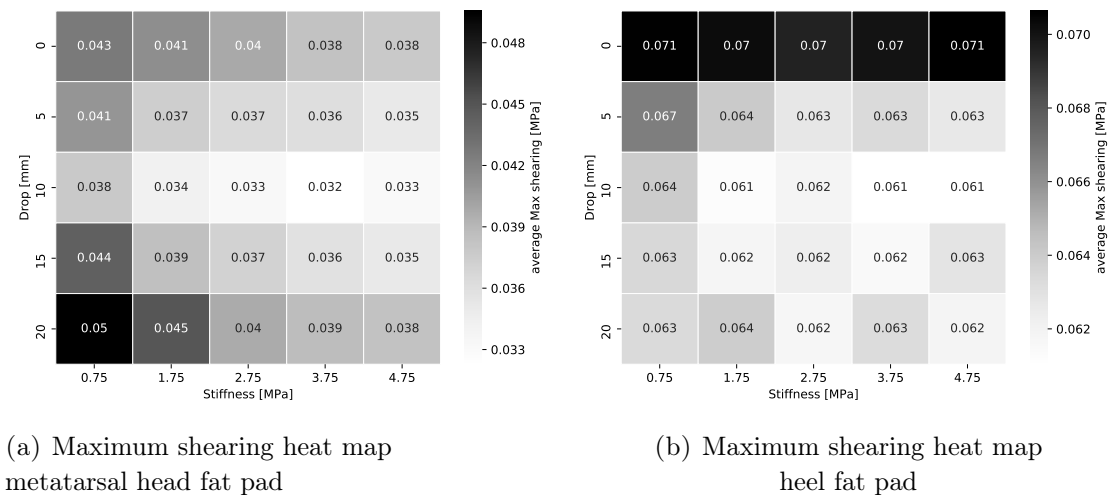
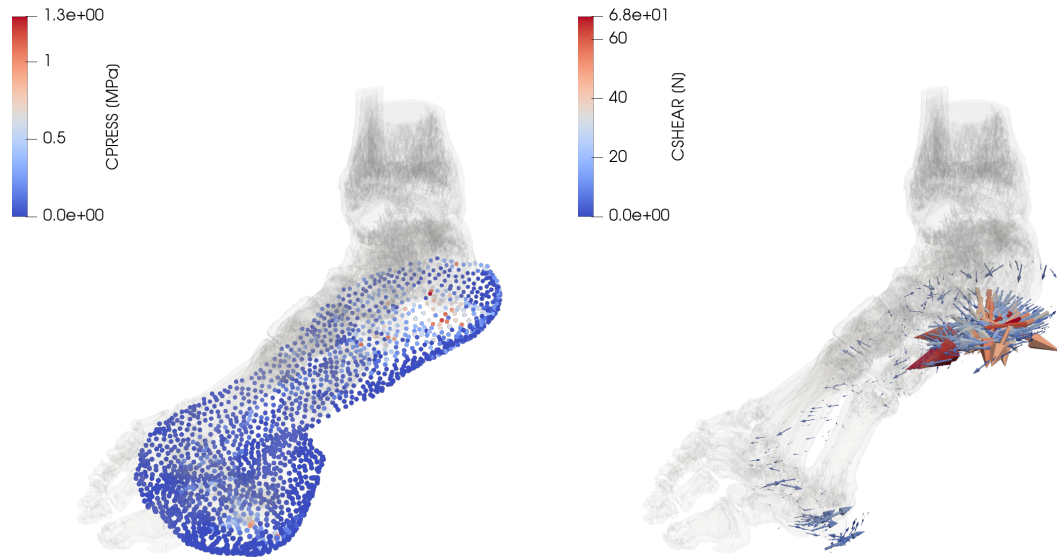


FIGURE IV.10: Average maximum shearing of fat pads

IV.5.3 Plantar skin contact stress

Contact pressure and frictional shear forces were evaluated according to their average value over time and by their average center coordinates.

The contact pressure & frictional force are displayed at a running time of 0.05 [s], for a tested shoe, in figure IV.11.



(a) Contact pressure at time 0.05 [s] (b) Contact frictional force at time 0.05 [s]

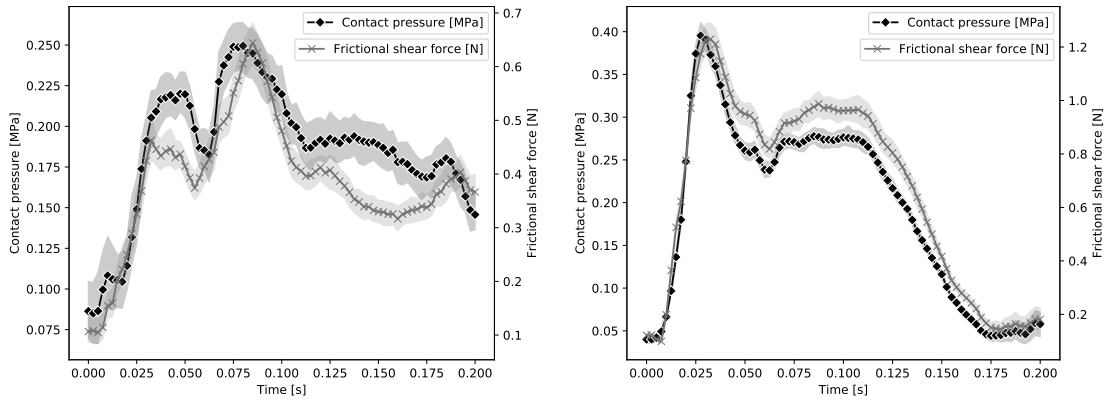
FIGURE IV.11: Contact pressure & frictional force of fat pads - left anterolateral view

The average values over time are displayed for the heel and metatarsal head in figures IV.12a and IV.12b.

The influence of the mid-sole drop as well as the mid-sole stiffness on the distribution of the contact pressure & frictional force were analyzed by comparing the average value of each configuration tested.

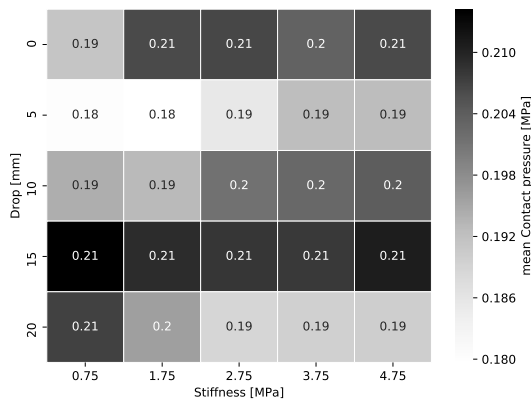
For the heel fat pad, we observed that the average minimum contact pressure converged in a convex manner to the 25/15 drop equal to 10 [mm] and decreased as the mid-sole stiffness decreased as displayed in figure IV.12d. The second order polynomial fitting with ordinary least square shown, with a determination coefficient (R^2) of 0.967, that the drop had a coefficient equal to -0.0040 (a_1) and quadratic drop coefficient was equal to 0.0309 (a_3); stiffness coefficient was equal to 0.0627 (a_2) and quadratic coefficient was equal to -0.0391 (a_4).

For the metatarsal head fat pad the second order polynomial fitting did not provide good results ($R^2 = 0.031$ and p-values > 0.8). We observed that the average minimum contact pressure was distributed disparately even if a minimum converged for the 20/15 drop equal to 5 [mm] as displayed in figure IV.12c. Same observations were made on the frictional shear force displayed in figures IV.12f and IV.12e

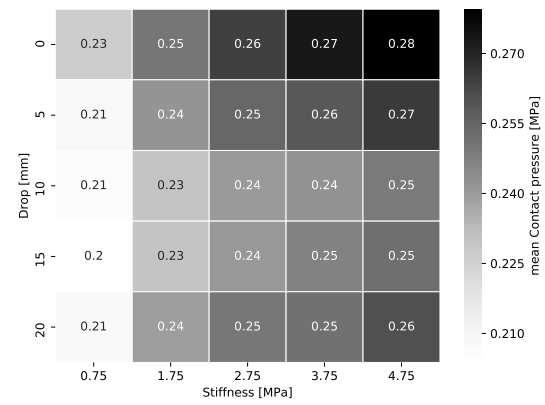


(a) Contact pressure and frictional shear force at the metatarsal head fat pad

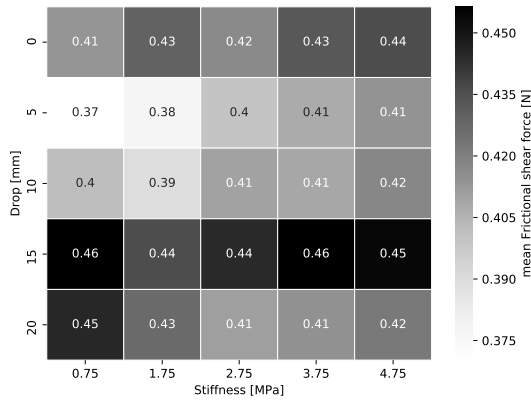
(b) Contact pressure and frictional shear force at the heel fat pad



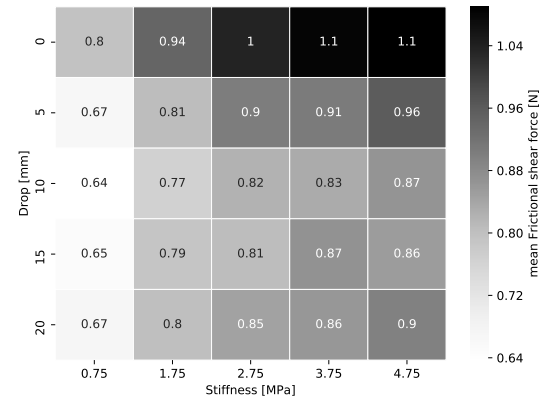
(c) Contact pressure metatarsal head fat pad heat map



(d) Contact pressure heel fat pad heat map



(e) Contact frictional force metatarsal head fat pad heat map

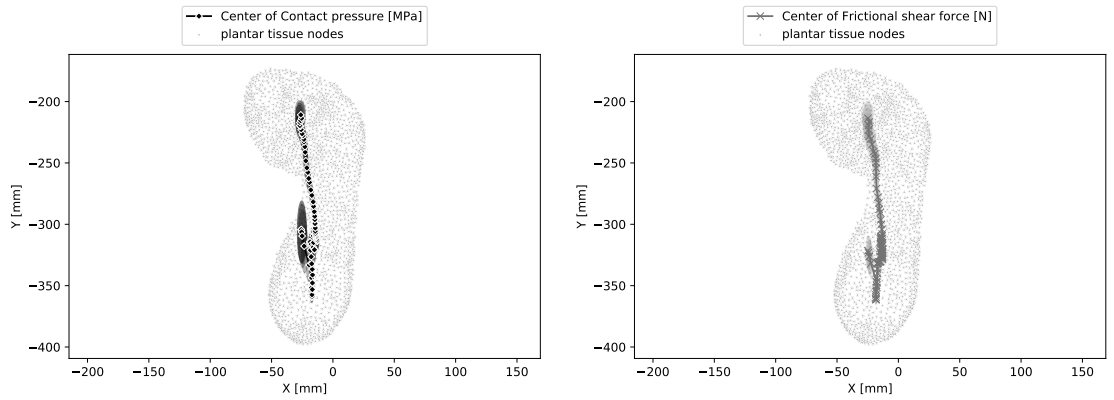


(f) Contact frictional force heel fat pad heat map

FIGURE IV.12: Contact pressure of fat pads

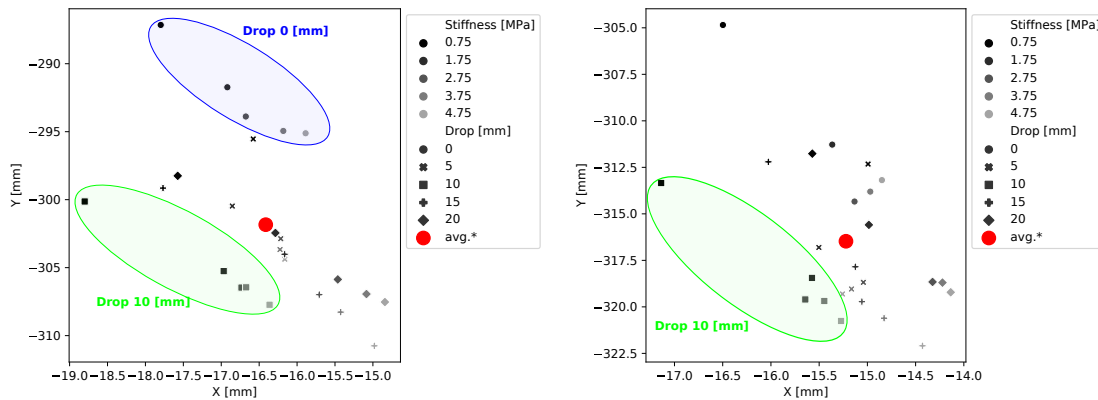
The influence of the mid-sole drop as well as the mid-sole stiffness on the position of the center of pressure & frictional force were analyzed by comparing the average center coordinates of each configuration tested. The center of pressure coordinates over time is displayed in figure IV.13a, and for each configuration tested the mean center coordinates is shown in IV.13c. The center of frictional force coordinates over time is displayed in figure IV.13b, and for each configuration tested the mean center coordinates is shown in IV.13d.

We measured that when the mid-sole stiffness increased the mean center of pressure was displaced to the lateral proximal part of the foot and that as the drop decreased the mean center of pressure was displaced to the medial distal part of the foot. It is confirmed by the second order polynomial fitting with a R^2 of 0.981, with calculated in the y direction a drop coefficient equal to -1.9312 (a_1) and a stiffness coefficient equal to -11.3331 (a_2); quadratic effects were present on drop 13.7651 (a_3) and stiffness 7.0562 (a_4). In the x direction, with only a R^2 of 0.756, only stiffness and quadratic stiffness had a p-value < 0.05, stiffness coefficient was equal to 2.4035 (a_2) and quadratic stiffness equal to -1.4364 (a_4). Same observations were made on the contact frictional force.



(a) Center of contact pressure over time

(b) Center of contact frictional force over time



(c) Center of contact pressure by configuration tested

(d) Center of contact frictional force by configuration tested

* all configurations average

FIGURE IV.13: Contact pressure of fat pads - Dorsal view

IV.5.4 Ligament deformation

All ligament strain of any configuration is displayed in figure IV.14a and comparison between configuration tested in figure IV.14b. For all ligaments, we observed that the average minimum strain was converging to the 25/15 drop equal to 10 [mm] and that when stiffness increased the strain was reduced down to 11% in the best case.

Second order polynomial ordinary least square fitting, with a coefficient of determination (R^2) equal to 0.931, calculated that stiffness coefficient was equal to -0.0202 (a_2) and the drop influence was equal to -0.0019 (a_1). Quadratic effects were present on stiffness ($a_4 = 0.0173$) and drop ($a_3 = 0.0173$).

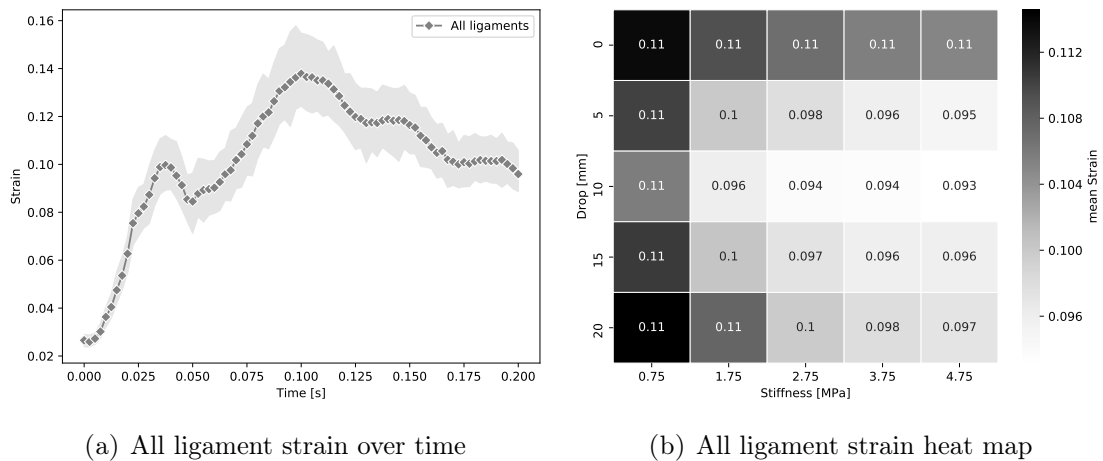


FIGURE IV.14: Ligament strain

Different clusters were set, they are displayed from figure IV.15 to IV.20 and their second order polynomial ordinary least square fitting results in table IV.2:

Cluster	(R^2)	Drop	Stiffness	Square Drop	Square Stiffness
Arch ligaments:					
- Spring (SPR)	0.916	-0.0021	-0.0221	0.0183	0.0149
- Short plantar (SHP)					
- Long plantar (LOP)					
- Plantar fascia (PLF)					
- Adductor Hallucis					
Deep transverse ligaments (DE)	0.758	-0.0017	-0.0302	0.0170	0.0208
Medial ligament:					
- Deltoid (DEL)	0.686	-0.0003	-0.0251	-0.0048	0.0196
Medial ligaments & muscles:					
- Tibionavicular	0.946	0.0020	-0.0127	0.0016	0.0077
- Anterior Tibiotalar					
- Tibialis Posterior 1					
- Tibialis Anterior 1					
Chopart joint ligaments:					
- Bifurcate (BIF)	0.932	1.363e-05	-0.0221	0.0035	0.0156
- Dorsal Calcaneocuboid					
- Dorsal Talonavicular					
Lateral muscle:					
- Peroneus Brevis	0.872	-1.296e-05	0.0380	-0.0017	-0.0268
Lateral muscle:					
- Peroneus Tertius	0.953	0.0021	0.0283	-0.0057	-0.0199
Lateral ligaments:					
- Lateral Talocalcaneal	0.777	0.0004	0.0264	-0.0071	-0.0196
- Interosseous Talocalcaneal					
Lateral ligament:					
- Calcaneofibular	0.909	-0.0009	0.0400	-0.0103	-0.0306
Lateral ligament:					
- Anterior Talofibular	0.957	0.0009	-0.0546	0.0161	0.0397
Lisfranc joint ligaments:					
- Interosseous Tarsometatarsal	0.881	-0.0017	-0.0272	0.0174	0.0187
- Plantar Tarsometatarsal					
- Dorsal Tarsometatarsal					

TABLE IV.2: Cluster ligament Drop and Stiffness influence

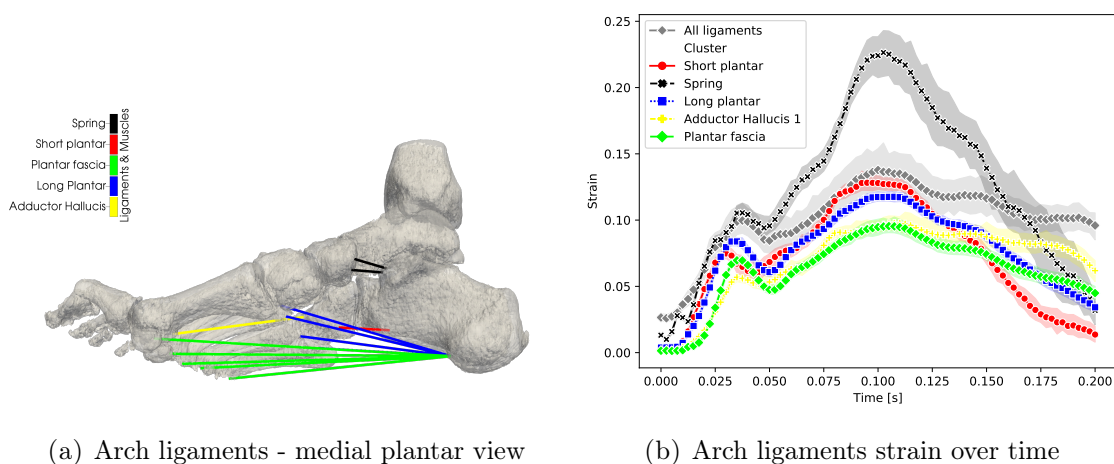


FIGURE IV.15: Arch ligaments measures

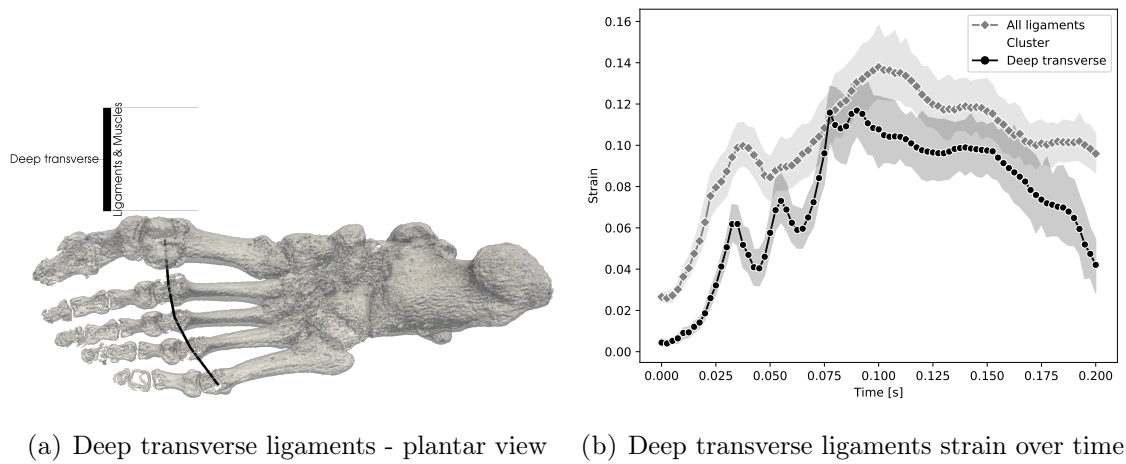


FIGURE IV.16: Deep transverse ligaments measures

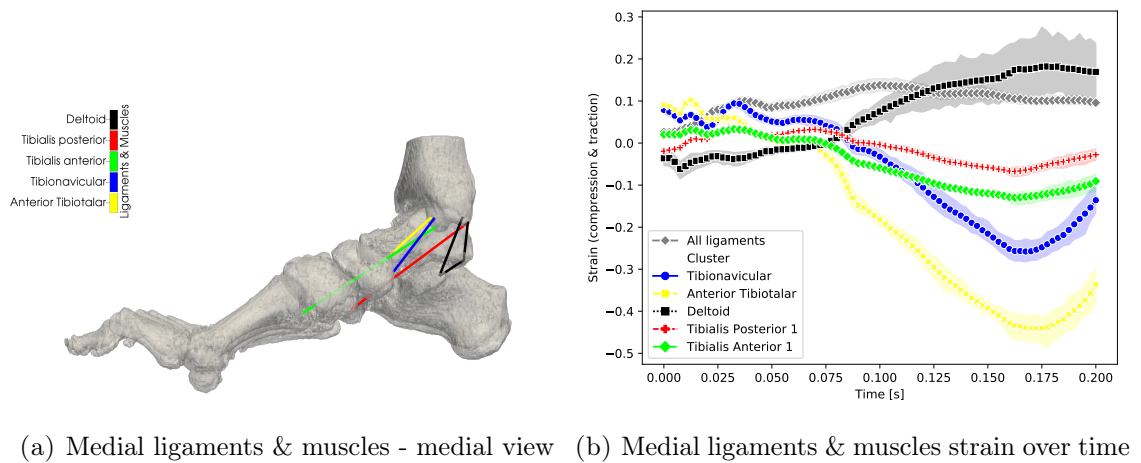


FIGURE IV.17: Medial ligaments & muscles measures

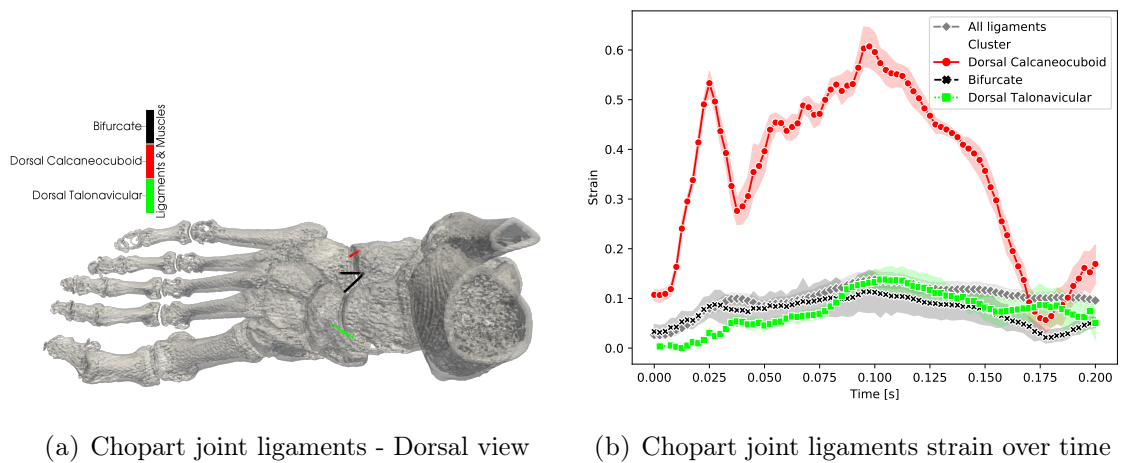
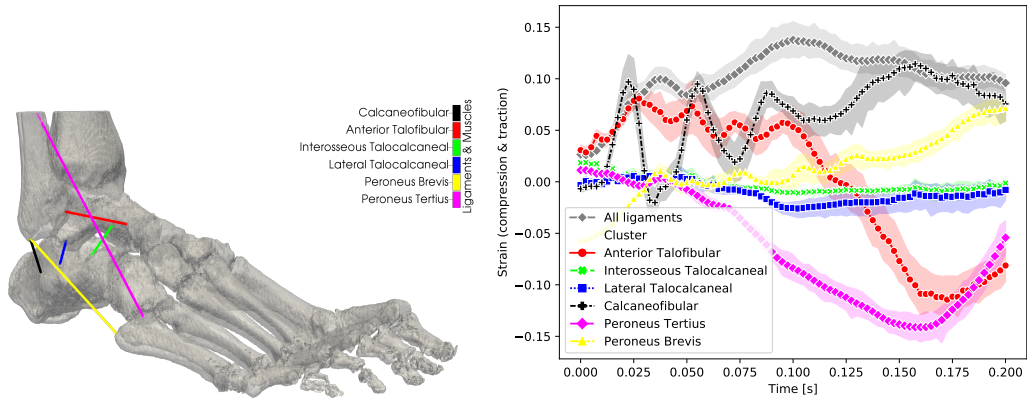
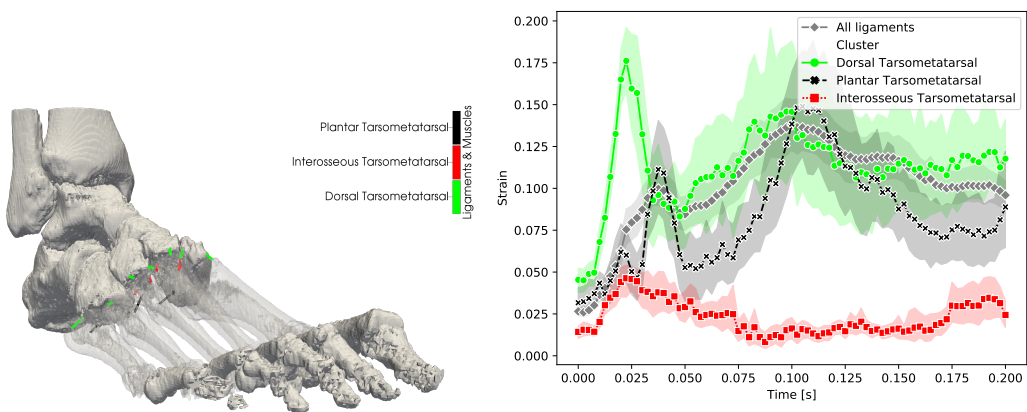


FIGURE IV.18: Chopart joint ligaments measures



(a) Lateral ligaments & muscles - anterolateral view (b) Lateral ligaments & muscles strain over time

FIGURE IV.19: Lateral ligaments & muscles measures



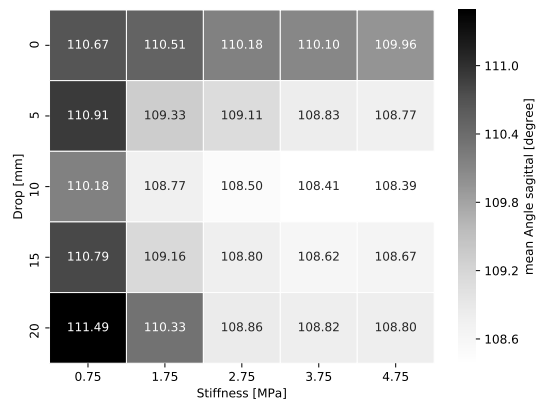
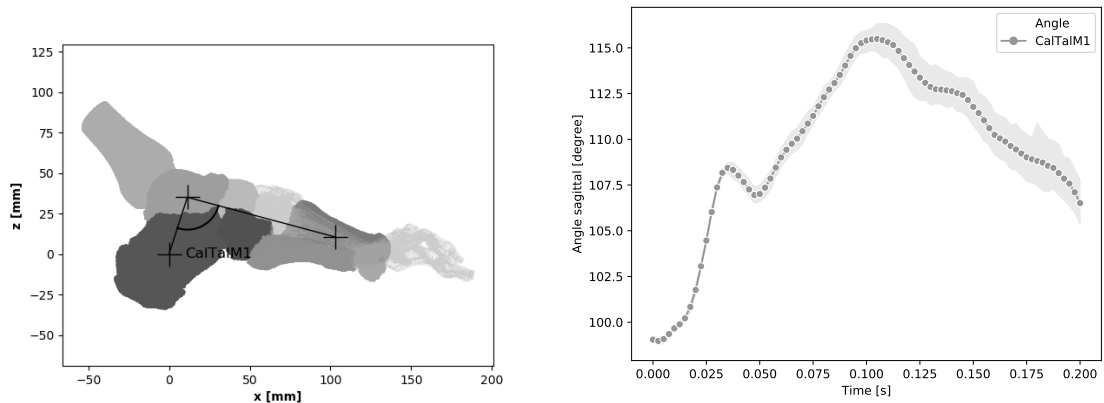
(a) Lisfranc joint ligaments - anterolateral view (b) Lisfranc joint ligaments strain over time

FIGURE IV.20: Lisfranc joint ligaments measures

IV.5.5 Joint angle

The influence of the mid-sole drop as well as the mid-sole stiffness on the distribution of the joint angle was analyzed on four different measures by comparing the average value.

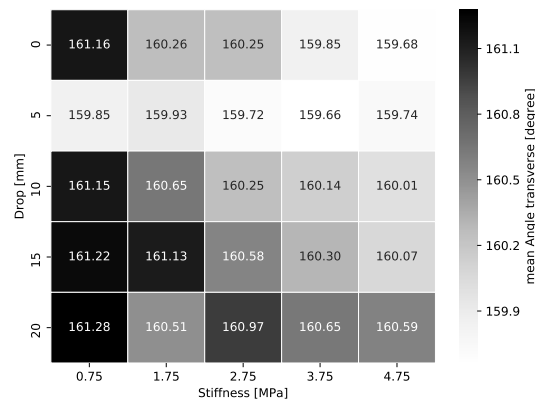
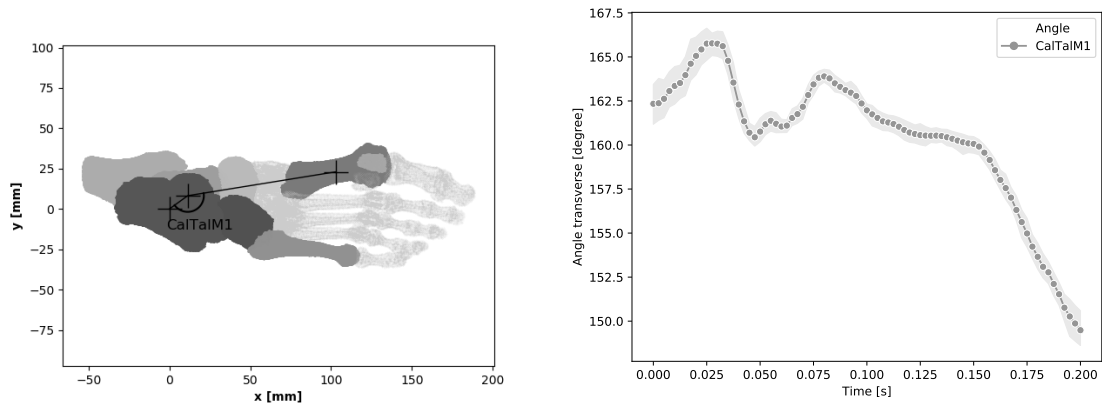
- The arch sagging measures are displayed in Figure IV.21. They showed, that there is a major decreased of arch sagging when the mid-sole stiffness was passing from 0.75 [MPa] to 2.75 [MPa] and that the minimum value converged in a convex manner to the drop 25/15 (10) [mm]. With the drop 15/15 (0) [mm] the stiffness was less influencing the arch sagging compared to the other drop.



(c) CalTalM1 sagittal footwear parameter influence

FIGURE IV.21: Arch sagging
Calcaneus Talus Metatarsal1 (CalTalM1) sagittal angle

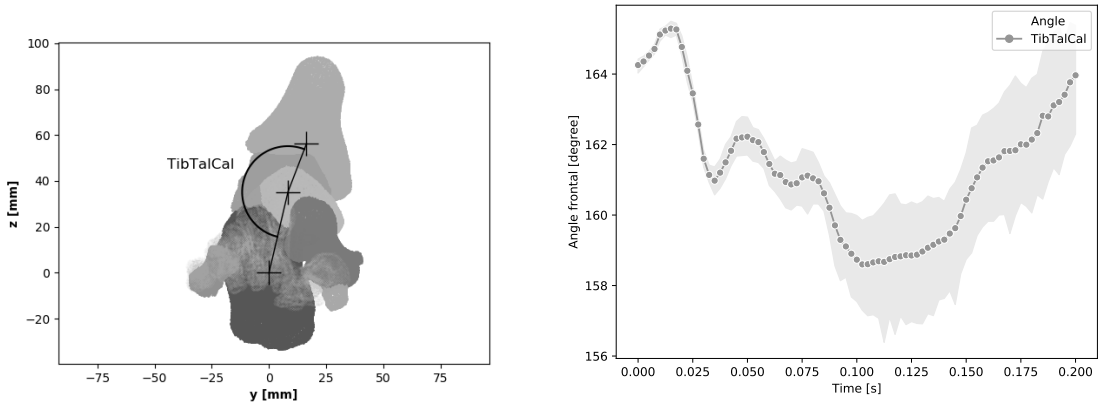
- The medial arch sagging measures are displayed in Figure IV.22. They appeared disparate on the drop parameter and decreased as the stiffness increased.



(c) CalTalM1 transverse footwear parameter influence

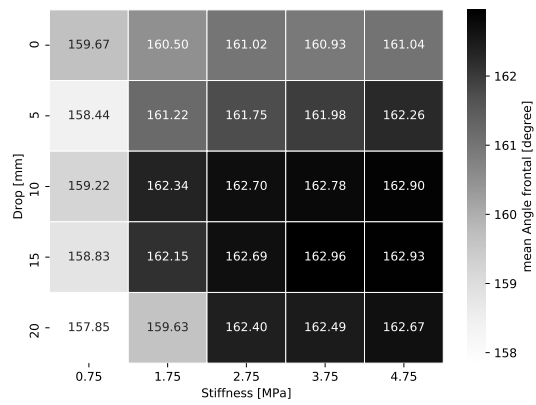
FIGURE IV.22: Medial arch sagging
Calcaneus Talus Metatarsal1 (CalTalM1) transverse angle

- The measures of foot inversion and eversion are displayed in Figure IV.23. As the stiffness increased, the angle increased, corresponding to a larger inversion, it emerged especially between 0.75 [MPa] and 1.75 [MPa]. More eversion was observed at the border of the tested drop interval (0) and (20) [mm].



(a) TibTalCal coronal angle description - Anterior view

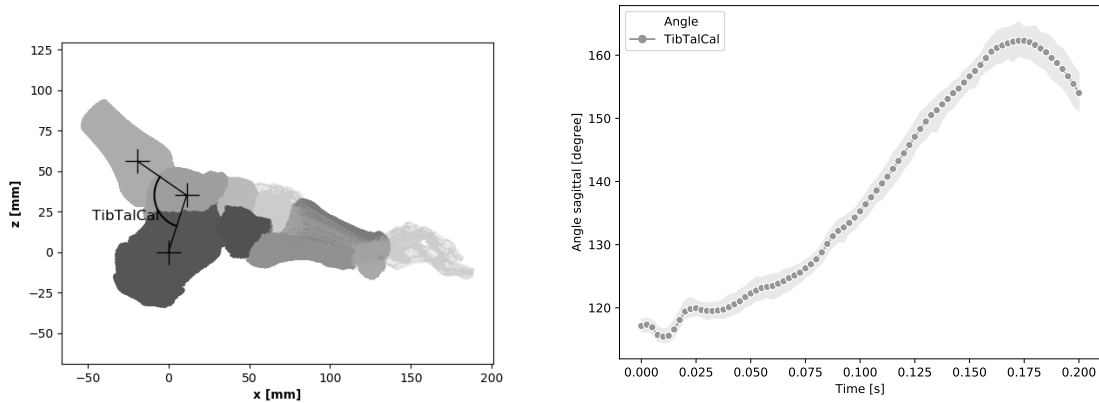
(b) TibTalCal coronal angle over time



(c) TibTalCal coronal footwear parameter influence

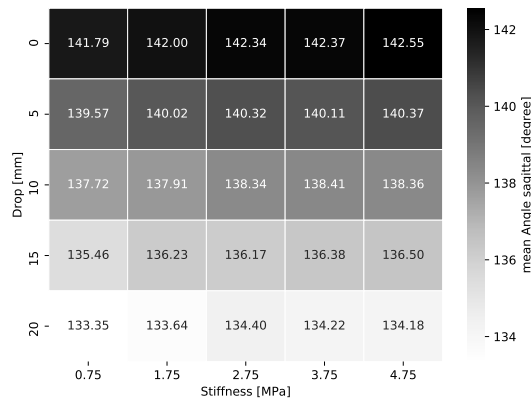
FIGURE IV.23: Inversion/Eversion Tibia Talus Calcaneus (TibTalCal) coronal angle

- The measures of plantar and dorsal flexion are displayed in Figure IV.24. A stiffness impact was found, as stiffness increased the more dorsal flexion was observed, but the magnitude of the effect was limited 0.6 %. The impact of the fall is much more observable as the drop has increased plantar flexion.



(a) TibTalCal sagittal angle description - Lateral view

(b) TibTalCal sagittal over time



(c) TibTalCal sagittal footwear parameter influence

FIGURE IV.24: Plantar/Dorsal flexion Tibia Talus Calcaneus (TibTalCal) sagittal angle

IV.6 Discussion

To get the first indications of the effect of mid-sole drop and stiffness on internal behavior of the running foot, we used an FE assembly of a foot model with different footwear. The patient specific foot model was calibrated by adjusting ligaments & muscles stiffness scale and distribution, using the information of bone position in function of force captured in different scanned configurations. The geometric model of the shoe was also generated from a CT scan and two variations of parameters were studied, the drop and the stiffness of the mid-sole.

Several limitations are associated with the model. (1) First, it is specific of a given patient and therefore does not represent the mean behavior of a population. However, this patient-specificity is easy to adapt to any patient with the mesh-morphing techniques and automation that has been developed within this work. (2) Second, some model choices have been made which inject a dose of simplification and reduce the representativity of the model results to favor an easy building process and limited computation time. For instance ligaments & muscles are composed of 1D linear elements with a linear elastic behavior, and are placed by a transfer function between a detailed generic model and the patient studied. Only three different soft tissue regions were set with constitutive data from the literature. Besides, the meshing process also slightly alters the original geometry. (3) Third, even if the representativity of the model, which was previously evaluated in chapter III, is better compared to the models built from ligament properties available in the literature, differences between simulations and experiments are still notable. Therefore it is more interesting to focus the analysis on the footwear parameter influence on the foot model than focus on the measured value itself. (4) Fourth, muscle activation is only taken into account by the force of the Achilles tendon applied to the Calcaneus, the model therefore only represents the passive behavior of the foot. Our point of view is that it is still relevant to separate the active and passive behavior of the foot, because the influence of one or the other is not yet clear and therefore a better understanding of these behaviors must emerge before coupling them. (5) Fifth, the tibia boundary conditions are similar for the different shoes tested, the model therefore does not take into account how the shoe characteristics affect the overall running kinematics of the subject. (6) Sixth, the shoe-upper is not adjusted according to the variation in the mid-sole drop, therefore the upper analysis of the foot behavior is not analyzed here.

Nevertheless, the FE models provides realistic simulations from the impact until the push up phase of a rear strike running gait; the results obtained lead to a first understanding of the internal behavior of the foot during a running step and give an insight on the influence of the rigidity and the drop of the mid-sole.

The trends for each parameter are as follows:

Concerning the mid-sole drop :

the fat pads of the heel and head of the metatarsals underwent an average maximum shear stress influenced by the mid-sole drop, with the minimum converging convexly to a drop of 10 [mm] in height (25/15). The same logic was observed for the contact pressure & frictional force of the heel fat pad. For the metatarsal fat pad the same behavior was also observed but converging towards a 5 [mm] drop in height (20/15). The mean center of contact pressure was influenced by the drop, moving in a posterior direction as the drop increased. The center of pressure moved posteriorly at impact, where there is the most variation between the simulated centers of pressure. The maximum displacement to the

posterior direction was 4%.

The influence of the mid-sole drop on the strains of all ligaments was converging convexly to a drop of 10 [mm] in height (25/15). The average strain was decreased by 9% between drop 10 [mm] and drop 0 [mm], which generates the greatest average deformation when all ligaments are taken into account.

The variations of the mid-sole drop were made from the scanned shoe with a drop of 10 [mm] in height (25/15) by removing material at the front or rear, so we can also interpret the variation of the maximum shear stress, contact pressure & frictional force, ligament strain converging to a minimum convexly to the scanned drop, due to the reduction of the mid-sole volume.

Joint angles, arch sagging and foot eversion also converged towards the initial drop height of 10 [mm] (25/15). Plantar flexion increased linearly as the drop increased, between the 0 mm drop and the 20 mm drop a 5% greater plantar flexion was measured.

Concerning the mid-sole stiffness :

we observed that when the stiffness was higher, the maximum shear stress of the two fat-pads analyzed was reduced: on average, between the softest and the stiffest mid-sole tested, the mean maximum shear stress was reduced by 5%. But concerning contact pressure & frictional forces, they increased in average of 17% for the mean pressure and 29% for the mean frictional force.

The mean center of pressure & center of frictional force were shifted towards the posterior lateral part of the foot: between the softest and the stiffest mid-sole tested, the mean center of pressure was moved 9 [mm] posteriorly and 2 [mm] laterally.

On the same stiffness interval border, the average strain of all ligaments & muscles decreased by 12%. For the ligaments & muscles that we associated to the support of the longitudinal arch, the decrease in strain was 17% consistent with the observation that the angle of the longitudinal arch was reduced by 2% and that no difference in arch sag in the medial direction was observed. We also observed that the increase in stiffness moves the foot toward a more pronounced inversion of 2% in agreement with the observation that the strain on the ligaments of the lateral compartment increased by 3% while for the opposite compartment, the medial, a decrease of 8% was measured.

It may be tempting to search for an optimal shoe based on the observations made, but various functional or clinical objectives must be defined first. In the medical field, it will require intensive collaboration between the medical staff, the manufacturer and the model maker.

For example, one possible cause of Achilles tendinitis is functional overpronation [CTS84]. In this case, the analysis of the model makes it possible to measure the influence of the shoe parameter on this angle. On our modeled subject, we measured eversion which includes pronation movements: it is more important when the stiffness increases and the angle is smallest with a drop of 20 [mm]. It may then be interesting for this subject to study an optimum around these parameters, taking care that 20 [mm] of drop with less rigidity simulates the highest sagging of the plantar arch and a higher maximum shear stress at the metatarsal head fat pad.

Another objective may be to reduce the contact friction force to prevent blistering. In this case, we observed in our simulations that the 10 [mm] drop with the softer mid-sole material reduced the magnitudes of the frictional forces but generated a higher maximum shear stress in the fat-pad. These parameters could therefore be a starting point for designing a shoe whose objective is to limit the appearance of blisters.

Last, to increase the stability of the ankle, which is one function of the ankle brace medical device often prescribed after a lateral sprain, our observations direct us towards a soft mid-sole because it puts less strain on the lateral ligament.

Therefore, there are many different parameters for footwear, whose optima are linked to the medical and manufacturer's specifications that need to be defined.

Regarding the use of shoes for endurance running, we must be careful not to say that the optimal shoe should aim to generate minimal solicitation on the anatomical components to avoid injury. More in-depth studies to ensure a better understanding of the implications are needed to define the specifications of the shoe.

IV.7 Conclusion

This paper presents a patient-specific finite element foot model, whose ligament & muscle stiffness is calibrated to obtain simulation results close to experimental measurement. It is dressed with different footwear to measure the impact of two shoe parameters: the mid-sole drop and stiffness.

5 drops and 5 stiffnesses were tested, i.e. 25 footwears simulated with the running foot in a heel strike pattern. Different influences were evaluated on fat pad maximum shear stress, contact pressure & frictional force, ligament strain and articulation joint.

This method is a step to use a foot macro-model to evaluate the average response of the population to the shoe with a larger sample of subjects, to further explore design parameters such as viscoelasticity and other geometric parameters, to accompany the design of shoes to generate a set of anatomical behaviors sought on the foot.

Conclusion and future works

Synthesis & Contributions

The biomechanical behavior of the foot and foot-shoe interactions are complex phenomena in which a majority of facets are not yet understood. Despite numerous studies on the subject, both in the experimental and numerical fields, it has been noticed that the methodological aspects by their complexity or their implementation time are limiting. They hamper large studies in terms of sample size, limit observations of internal foot behavior, and reduce the number of numerical macro studies on footwear-foot interaction.

The work of this thesis falls within this context by proposing and testing approaches that facilitate and accelerate the methodological aspects, especially numerical, to obtain measurements describing more precisely the internal behavior of the bare foot and the foot with footwear, to promote a better understanding of the structure involved.

In a first study, which serves as a basis for further work on this thesis, experimental and numerical methods were developed to respond to the main limits of the state-of-the-art classical techniques. The first method was implemented to quickly adjust anatomical components on the acquisition of a new patient, in this case the ligaments, and thus avoid a time-consuming treatment. The second, to automatically find the position of the bones on a series of acquisitions, each of which corresponds to a loading solicitation that the foot may encounter, always with the aim of avoiding tasks requiring considerable mobilization of the user. These two numerical methods were used on acquisitions which constitute our third point of method, this time experimental. This third method consists in exposing the foot to different combinations of loading and orientation, scanning them and then, coupled with the numerical methods developed, obtaining measurements of the foot's internal structure that contrast with the classical state-of-the-art methods that are most often on the outside of the foot.

A second study uses all these data to first calibrate the stiffness of certain anatomical components, ligaments & muscles and thus calibrate patient-specific finite element models. The same data are then used to estimate the extent to which the simulations replicate the experimental data. Compared to the state-of-the-art, this personification of the material, even if it is based on a rather classical inverse method, is a progression that has not been used for foot models in the literature and has shown that the models, thus calibrated, simulated more faithfully the behaviors observed experimentally.

The third study exploited one of the patient-specific finite element models developed in this way, by fitting it to a shoe with two varying design characteristics in order to measure the effect of these parameters on the behavior of the foot during a running stride.

These methods thus made it possible to obtain measurements on the internal behavior of the foot in different situations generated first experimentally and then by simulation in a parametric study. All internal observations of the foot: joint angles, ligament strain, bone position, stress in the tissue and stress at the foot-shoe contact are monitored throughout the running step, providing an accurate view of the foot's behavior.

Synthesis of results

The results of the numerical methods are:

For ligament and muscle registration in a new patient, which consists in deforming a detailed source model to match the patient's geometry, the correspondence between the geometries is evaluated; the result is on average 0.06 [mm] with a standard deviation of 0.09 [mm].

For the positioning of bones in different loading situations, the distance of the deviations is on average 0.28 [mm] with a standard deviation of 0.09 [mm].

These two implementations of registration, one non-rigid and the other rigid, are automated and lead to a patient-specific model creation time of less than one day, which is an improvement over the classical creation time of several days.

To assess the ability of calibrated finite element simulations to reproduce the experimental data, three measures were used comparing the simulated results to the experimental ones. The bone positioning error with a mean error of 8.29 [mm] and a standard deviation of 4.26 [mm]. For ligament strain, a mean relative error of 14% with a standard deviation of 21%. For joint angles, a mean relative error of 7% with a standard deviation of 14%.

These methods allow to access a wide range of indicators based on the internal behavior of the foot. Here is a highlight of such indicators.

For observations from experimental trials where the foot was loaded with and then without the shoe, the effect of the shoe influenced different foot behaviors. In terms of bone displacement, the shoe causes greater translation of the foot segment (mean = 3.79 [mm], sd = 10.92 [mm]), with increased dorsal flexion (mean = 2.80°, sd = 6.81°), while limiting relative translation between bones (mean = -1.64 [mm], sd = 2.78 [mm]). Little difference is measured on average on bone rotation. This effect of the shoe on the decrease in relative bone translation increases with increasing load. The decrease in relative movement between the bones is also observed by a less pronounced sagging of the plantar arch (mean = -1.53°, sd = 1.89°) as well as a significantly reduced medial displacement of the forefoot, relative to the rear of the foot (mean = -3.98°, sd = 4.26°) when the shoe is worn. This is also confirmed by a smaller deformation of the ligaments of the plantar fascia (mean = -1.3%, sd = 1.2%), but above all by the reduction of deformations of the deep transverse ligaments (mean = -3.5%, sd = 3.6%) which reflects a smaller gap between the distal heads of the metatarsals when the foot is loaded with the shoe worn.

For the observations obtained from simulations of the running stride with variations in the stiffness and drop height attributed to the sole of the shoe, some influences emerge.

As the stiffness of the sole increases, different effects are measured. A particularly interesting effect is the reduction of the maximum shear stress at the fat pads (-5%), while the contact stress with the shoe (pressure & friction) increases (+18% and +25% respectively). The influence on ligament strain is significant: taking into account all ligaments, the reduction of the average strain is -12%. Concerning the plantar arch, for the group of ligaments associated with its support, there is a significant reduction in strain (-17%); the angle chosen to express the curvature of the arch is also reduced (-2%). Concerning the ankle joint, a more pronounced inversion is observed (+2%), confirmed by a greater deformation of the ligaments of the lateral compartment (+3%) and reduced for the medial compartment (-8%).

Regarding the drop, a strong quadratic effect is observed with a lower maximum shear stress in the fat pads for the 10 [mm] drop (-12% compared to the 0 [mm] drop generating

the most stress), with however a tendency to relieve the shear stress on the back of the foot as the drop increases: (-10% at the heel fat pad between the maximum and minimum drop tested). There is little impact of the drop on the pressure and shear forces at the foot-shoe contact. The non-linear effect measured on the drop is found on ligament deformation, with -9% between drop 10 [mm] and drop 0 [mm], which generates the greatest average deformation when all ligaments are taken into account. Then, on the aspect of joint angles, the drop mainly influences the dorsal flexion.

Limitations

This work has many limitations. They are at different levels, both experimental and numerical, as working hypotheses are put in place to simplify the treatment of the subject's complexity.

The main limitation is the focus of these studies on the passive behavior of the foot by not considering the activation of the muscles. However, recent studies focus on this aspect by showing that the activity of intrinsic muscles plays a role in the rigidity of the foot structure and could compensate the dorsiflexion moments at the midfoot joints during the push phase [Kel+14; KLC15].

But the role of the active or passive behavior of the foot in the governance of its postures remains an open subject. It therefore seems important to separate the passive part from the active part until a deeper understanding is developed.

Then, the choice to work with cadaveric feet, to simplify their representations and their mechanical behaviors to keep a reasonable processing time, is a limitation that biomechanical modeling in general meets. This limitation pushes biomechanical modeling methods to progress on these aspects. Although simplifying choices were made on modeling, the effort to compare with experiments to assess the accuracy of simulations on internal foot measurements was also made. This accuracy of the model is still limited, but a progression has been initiated and is continuing to push forward on the subject.

The application of displacement boundary conditions to the tibia still does not allow to study the adaptation of its position to the different configurations. In the long term, it is conceivable to use only force boundary conditions to study the response of the upper part of this limb.

The components of the shoe have been greatly simplified, the wearing of the sock and the pressure exerted by the lacing are not taken into account in order to arrive at a first accessible protocol. The association of this type of work with manufacturers and the medical community are essential collaborations to make progress on these aspects but above all, in the long term, to develop industrial and medical applications.

Perspectives

The rigid and non-rigid registration techniques used in this work make it possible to quickly describe the anatomical components of several patients with the same topology. It is on this methodological basis that the statistical shape analysis can be built to elaborate models integrating the bones from an external observation (3D scanner from stereoscopy technique). This should also lead to faster processing of new patient acquisition; the shorter the time, the more likely it is that clinical and/or industrial exploitation will be possible on a large scale. The non-rigid registration of surface or volume representation of ligaments & muscles is possible and can also be extended to other anatomical components such as retinacula, which will allow the construction of increasingly complete models.

The non-rigid registration of clinical measurement points will make it possible to measure clinical indicators commonly used by medical physicians, which will encourage the use of these methods in the medical sector.

The calibration of the ligament & muscle stiffnesses was done here with a fairly basic method that has its limitations, but still shows a clear improvement. This topic now needs to be further investigated by considering, for example, the use of regularization terms in regression with implementations such as Ridge regression (Tikhonov regularization), LASSO ... to explore a multitude of stiffness distributions that can improve the reproducibility score of simulations. Calibration quality can also be enhanced by new mechanical tests. By soliciting the foot to constrain ligaments & muscles that are seldom sollicitated in the tests carried out in this thesis, new information can then be integrated into the digital calibration method. Extension to other anatomical components of the foot is possible with these methods, the objective being to obtain a model of the patient that is specific in as many aspects and as representative as possible.

This detailed foot model can then be coupled to a multitude of shoe models or coupled to a standard model whose variations on a larger number of design parameters are possible such as shoe circumferences (instep, toe, ...), width or manufacturer specific parameters, thus extending the logic of the work done here. Conversely, once the detailed models are sufficiently numerous and analyzed, the construction of reduced models must be considered.

Once this progression on methodological aspects is sufficiently rich, many applications can be envisaged.

For example, by using reduced models, a manufacturer of prêt-à-porter shoes will be able to quickly test the design of its shoes on a variety of foot models and rapidly observe the influence of its design on the behavior of the foot. This information will allow him to quickly adjust his design, thus shortening the duration of the design phase, while having the vision on indicators that are not currently available. Different effects can be sought, from the search for performance to the protection of the user accompanied by the comfort of wearing it.

In the medical sector, the rapid generation of patient-specific models will make it possible to use the digital twin of the patient to test many medical applications that are already the subject of current research (diabetes, surgery, orthotics, etc.). The objective is then to propose a care program designed by measuring its influence on the model.

A relevant medical application to explore is osteochondrosis of the foot with abnormal bone growth in certain areas of the foot that may be associated with mechanical stress and is often observed in young athletes. Testing shoes to attempt finding a design that reduces mechanical stress in areas affected by osteochondrosis could be a treatment proposal. A foot model up to the knee is also relevant because many running injuries are referenced at the knee level.

In the long term, a great challenge lies in the treatment of weakly ionizing acquisitions in static and/or dynamic which are often in 2D from fluoroscopy. The objective is then to find on this type of acquisition the 3D positioning of each bone composing the foot in order to further progress in the observation of the behavior of the foot by having the possibility to carry out a large number of acquisitions. To this end, the use of mechanical models of the foot can be very useful to propose beforehand a positioning of the bones as close as possible to the acquisition. The registration method will then start as close as possible to the final solution and can be constrained by taking into account the mechanical work of the anatomical components of the foot.

Conclusion et travaux futurs

Synthèse & Contributions

Le comportement biomécanique du pied et du couplage pied-chaussure sont des phénomènes complexes dont une majorité de facettes ne sont pas maîtrisées. Malgré de nombreuses études sur le sujet, tant dans le domaine expérimental que numérique, il a été constaté que les aspects méthodologiques par leur complexité ou leur temps de mise en œuvre sont limitant. Ils entravent la réalisation d'études conséquentes en termes de taille d'échantillon, limitent les observations des comportements internes du pied et réduisent le nombre d'études numériques sur l'interaction chaussure-pied.

Les travaux de cette thèse s'inscrivent dans ce contexte en proposant et en testant des approches qui facilitent et accélèrent les aspects méthodologiques, notamment numériques, pour obtenir des mesures décrivant plus précisément le comportement interne du pied et du pied chaussé, afin de permettre une meilleure compréhension des comportements biomécaniques en jeu.

Une première étude, qui sert de socle à la suite des travaux, a mis en place des méthodes dans les domaines expérimental et numérique afin de répondre aux principales limites des techniques classiques de l'état de l'art. La première méthode a été implémentée pour recalibrer rapidement des composants anatomiques lors de l'acquisition d'un nouveau patient, ici les ligaments, et ainsi éviter un long traitement manuel ; la seconde, pour retrouver automatiquement le positionnement des os sur une série d'acquisitions dont chacune correspond à une sollicitation de chargement que le pied peut rencontrer, toujours dans le but d'éviter des tâches nécessitant une mobilisation importante de l'utilisateur. Ces deux méthodes numériques ont été utilisées sur des acquisitions qui constituent notre troisième point de méthode, cette fois-ci expérimentale. Cette troisième méthode consiste à exposer le pied à différentes combinaisons de chargement et d'orientation, à les scanner puis, couplée aux méthodes numériques développées, obtenir des mesures de l'intérieur du pied qui tranchent avec les méthodes classiques de l'état de l'art qui sont le plus souvent sur l'extérieur du pied.

Une deuxième étude utilise l'ensemble de ces données pour d'abord calibrer la rigidité de certains composants anatomiques, les ligaments & muscles et ainsi calibrer des modèles éléments finis spécifiques aux patients. Ces mêmes données sont ensuite utilisées pour estimer dans quelle mesure les simulations reproduisent les données expérimentales. Par rapport à l'état de l'art, cette personnalisation du matériau, même si elle repose sur une méthode inverse assez classique, est une avancée qui n'a pas été utilisée pour les modèles de pieds de la littérature et elle a montré que les modèles, ainsi calibrés, simulaient plus fidèlement les comportements observés expérimentalement.

La troisième étude a exploité un des modèles éléments finis spécifiques aux patients ainsi développé, en le chaussant d'une chaussure dont 2 caractéristiques de conception varient pour mesurer l'effet de ces paramètres sur le comportement du pied lors d'une foulée de course.

Ces méthodes ont ainsi permis d'obtenir des indications sur le comportement interne du pied dans différentes situations générées d'abord expérimentalement puis par simulation dans une étude paramétrique.

Toutes les mesures internes du pied, angles articulaires, déformation des ligaments, position des os, contrainte dans les tissus et contrainte au contact pied-chaussure sont suivies tout au long du pas de course, ce qui fournit une vision précise du comportement du pied.

Synthèse des résultats

Les résultats des méthodes numériques sont :

Pour le recalage des ligaments & muscles chez un nouveau patient, qui consiste à déformer un modèle source détaillé pour épouser la géométrie du patient, la correspondance entre les géométries est évaluée. Le résultat est en moyenne de 0.06 [mm] avec un écart type de 0.09 [mm].

Pour le positionnement des os dans différentes situations de chargement, la distance des déviations est en moyenne de 0.28 [mm] avec un écart type de 0.09 [mm].

Ces deux implémentations de recalage, l'une non-rigide et l'autre rigide, sont automatisées et amènent à un temps de création d'un modèle spécifique au patient en moins d'une journée, ce qui est une amélioration par rapport au temps de création classique de plusieurs jours.

Pour évaluer la capacité des simulations par éléments finis calibrées à reproduire les données expérimentales, trois mesures ont été utilisées comparant les résultats simulés aux résultats expérimentaux. L'erreur de positionnement des os avec une erreur moyenne de 8,29 [mm] et un écart type de 4,26 [mm]. Pour la déformation des ligaments, une erreur relative moyenne de 14% avec un écart type de 21%. Pour les angles articulaires, une erreur relative moyenne de 7% avec un écart type de 14%.

Ces méthodes permettent d'accéder à un large éventail d'indicateurs basés sur le comportement interne du pied. Voici un aperçu de ces indicateurs.

Pour les observations issues d'essais expérimentaux où le pied était chargé avec puis sans la chaussure, l'effet de la chaussure influençait différents comportements du pied. Au niveau du déplacement des os, la chaussure provoque une plus grande translation du segment du pied (moy. = 3.79 [mm], σ = 10.92 [mm]), avec une flexion dorsale accrue (moyenne = 2.80°, σ = 6.81°), tout en réduisant la translation relative entre les os (moy. = -1.64 [mm], σ = 2.78 [mm]). Peu de différence est mesurée en moyenne sur la rotation des os. Cet effet de la chaussure sur la diminution de la translation relative des os augmente avec la montée en charge. La diminution du mouvement relatif entre les os est également observée par un affaissement moins prononcé de la voûte plantaire (moy. = -1.53°, σ = 1.89°) ainsi que par un déplacement médial de l'avant-pied par rapport à l'arrière du pied réduit de manière importante (moy. = -3.98°, σ = 4.26°) lorsque la chaussure est portée. Ceci est également confirmé par une moindre déformation des ligaments de l'aponévrose plantaire (moy. = -1.3%, σ = 1.2%), mais surtout par la réduction des déformations des ligaments transverses profonds (moy. = -3.5%, σ = 3.6%) qui reflète un écartement plus faible entre les têtes distales des métatarses lors du port de la chaussure.

Pour les observations tirées des simulations de la foulée d'une course à pied avec des variations de la rigidité et de la hauteur de drop attribuée à la semelle du chaussant, certaines influences se détachent.

Au fur et à mesure que la rigidité de la semelle augmente, différents effets sont mesurés. Un effet particulièrement intéressant est la réduction de la contrainte de cisaillement maxi-

male au niveau des coussinets adipeux (-5%), alors que les contraintes de contact avec la chaussure (pression & frottement) augmentent (respectivement +18% et +25%). L'influence sur la déformation des ligaments est importante, si l'on tient compte de tous les ligaments la réduction de la déformation moyenne s'élève à -12%. On observe pour le groupe de ligaments associés au maintien de la voûte plantaire une réduction notable de la déformation (-17%), l'angle choisi pour exprimer la courbure de l'arc est également réduit (-2%). Concernant l'articulation de la cheville, on observe une inversion plus prononcée (+2%), confirmée par une déformation plus importante des ligaments du compartiment latéral(+3%) et réduite pour le compartiment médial (-8%).

En ce qui concerne le drop, un fort effet quadratique est observé avec une contrainte de cisaillement maximale plus faible dans les coussinets adipeux pour le drop de 10 [mm] (-12% par rapport au drop 0 [mm] générant le plus de contrainte), avec toutefois une tendance à soulager la contrainte de cisaillement sur l'arrière du pied lorsque le drop augmente: (-10% entre le drop maximal et minimal testé au niveau du coussinet adipeux du talon). On constate peu d'impact du drop sur les pressions et les forces de cisaillement au contact pied-chaussure. L'effet quadratique mesuré sur le drop se retrouve sur la déformation des ligaments, avec -9% entre le drop 10 [mm] par rapport au drop 0 [mm] qui génère la déformation moyenne la plus grande lorsque tous les ligaments sont pris en compte. Ensuite, sur l'aspect angles articulaires, le drop influence principalement la flexion dorsale.

Limitations

De nombreuses limites sont inhérentes à ce travail. Elles se situent à différents niveaux, à la fois expérimentaux et numériques, car des hypothèses de travail sont mises en place pour simplifier le traitement de la complexité du sujet d'étude.

La principale limite est la concentration de ces études sur le comportement passif du pied en ne considérant pas l'activation des muscles. Hors, des études récentes se focalisent sur cet aspect en montrant que l'activité des muscles intrinsèques joue un rôle dans la rigidité de la structure du pied et permettraient de compenser les moments de dorsiflexion au niveau des articulations du milieu du pied pendant la poussée [Kel+14; KLC15]. Mais le rôle du comportement actif ou passif du pied dans la gouvernance de ses postures reste un sujet ouvert. Il semble donc important de séparer la partie passive de la partie active jusqu'à ce qu'une compréhension plus approfondie soit développée.

Ensuite, le fait de travailler sur des pieds cadavériques, de simplifier leurs représentations et leurs comportements mécaniques pour garder un processus accessible, est une limitation que la modélisation biomécanique en général rencontre à chaque instant et pousse à progresser sur ces aspects. Bien que des choix simplificateurs aient été faits, l'effort de comparaison avec les expériences pour évaluer la justesse des simulations sur des mesures internes du pied a également été fait. Cette justesse du modèle est encore limitée, mais une progression a été amorcée et pousse encore à avancer sur le sujet.

L'application de conditions limites de déplacement au niveau du tibia ne permet toujours pas d'étudier l'adaptation de sa position aux différentes configurations. À long terme, il est concevable de n'utiliser que les conditions limites de force pour étudier la réponse de la partie supérieure de ce membre.

Les composants de la chaussure ont été grandement simplifiés, le port de la chaussette et la pression exercée par le laçage ne sont pas pris en compte afin de parvenir à un premier protocole accessible. L'association de ce type de travaux avec des industriels et le corps médical sont des collaborations essentielles pour progresser sur ces aspects mais surtout, à long terme, pour développer des applications industrielles et médicales.

Perpectives

Les techniques de recalage rigides et non rigides utilisées dans ce travail permettent de décrire rapidement et avec la même topologie les composantes anatomiques de plusieurs patients. C'est sur cette base méthodologique que l'analyse statistique des formes peut être construite pour élaborer des modèles intégrant les os à partir d'une observation externe (scanner externe en 3D à partir de technique de stéréoscopie). Cela conduit aussi à un traitement plus rapide de l'acquisition de nouveaux patients, plus le temps est court, plus l'exploitation clinique et/ou industrielle sera possible à grande échelle. Le recalage non rigide de représentation en surface ou en volume des ligaments & muscles est possible et peut également être étendu à d'autres composants anatomiques tels que les rétinacula, ce qui permettra de construire des modèles de plus en plus complets. Le recalage non rigide des points de mesure cliniques donnera accès à des indicateurs cliniques couramment utilisés par les praticiens hospitaliers, ce qui encouragera l'utilisation de ces méthodes dans le secteur médical.

La calibration des rigidités des ligaments & muscles a été faite ici avec une méthode assez basique ayant son lot de limites, mais montrant tout de même une nette amélioration. Le sujet doit maintenant être approfondi en considérant, par exemple, l'utilisation de termes de régularisation dans la régression avec des implémentations telles que Ridge regression (régularisation de Tikhonov), LASSO ... pour explorer une multitude de distributions de rigidité qui peuvent améliorer le score de reproductibilité des simulations. La qualité du calibrage peut également être renforcée grâce à de nouveaux tests mécaniques. En sollicitant le pied pour contraindre des ligaments & muscles travaillant peu dans les tests effectués dans le cadre de cette thèse, de nouvelles informations peuvent alors être intégrées dans la méthode de calibration numérique. L'extension à d'autres composants anatomiques du pied est possible avec ces méthodes, l'objectif étant d'obtenir un modèle de patient spécifique dans le plus grand nombre d'aspects et le plus représentatif possible.

Ce modèle de pied détaillé peut ensuite être couplé à une multitude d'exemplaires de chaussures ou couplé à un modèle standard dont les variations sur un plus grand nombre de paramètres de conception sont possibles tels que les circonférences de la chaussure (au niveau du cou-de-pied, des orteils, ...), la largeur ou des paramètres spécifiques du fabricant, étendant ainsi la logique du travail effectué ici. Inversement, une fois que les modèles détaillés sont suffisamment nombreux et analysés, la construction de modèles réduits doit être envisagée.

Une fois que cette progression sur les aspects méthodologiques sera suffisamment riche, de nombreuses applications pourront être envisagées.

Par exemple, en utilisant des modèles réduits, un fabricant de chaussures de prêt-à-porter pourra rapidement tester le design de ses chaussures sur une variété de modèles de pied et observer rapidement l'influence de son design sur le comportement du pied. Ces informations lui permettront d'ajuster rapidement sa conception, raccourcissant ainsi la durée de sa phase de conception, tout en ayant la vision sur des indicateurs qui ne sont pas disponibles actuellement. Différents effets peuvent être recherchés, de la recherche de performances à la protection de l'utilisateur accompagnées du confort du port.

Dans le secteur médical, la génération rapide de modèles spécifiques aux patients permettra d'utiliser la copie numérique du patient pour tester de nombreuses applications médicales qui font déjà l'objet de recherches actuelles (diabète, chirurgie, orthèses, etc.). L'objectif est alors de proposer un parcours de soins conçu en mesurant son influence grâce au modèle.

Une application médicale pertinente à explorer est l'ostéochondrose du pied avec une

croissance osseuse anormale dans certaines zones du pied qui peut être associée à des sollicitations mécaniques et qui est souvent observée chez les jeunes athlètes. Un modèle de pied allant jusqu'au genou est également pertinent car de nombreuses blessures de course sont référencées au niveau du genou.

A terme, un grand défi réside dans le traitement des acquisitions faiblement ionisantes en statique et/ou dynamique qui sont souvent en 2D issues de la fluoroscopie. L'objectif est alors de retrouver sur ce type d'acquisition le positionnement 3D de chaque os composant le pied afin de progresser encore dans l'observation du comportement du pied. A cette fin, l'utilisation de modèles mécaniques du pied peut être très utile pour proposer au préalable un positionnement des os au plus près de l'acquisition. La méthode de recalage commencera alors au plus près de la solution finale et pourra être contrainte en tenant compte du travail mécanique des composants anatomiques du pied.

Bibliography

- [AB94] R. Adams and L. Bischof. “Seeded Region Growing”. In: *IEEE Transactions on Pattern Analysis and Machine Intelligence* 16.6 (June 1994), pp. 641–647. ISSN: 01628828. DOI: 10.1109/34.295913.
- [Ade86] Robert S. Adelaar. “The Practical Biomechanics of Running”. In: *The American Journal of Sports Medicine* 14.6 (Nov. 1986), pp. 497–500. ISSN: 0363-5465, 1552-3365. DOI: 10.1177/036354658601400613.
- [Akr+18] Mohammad Akrami, Zhihui Qian, Zhemin Zou, David Howard, Chris J Nester, and Lei Ren. “Subject-Specific Finite Element Modelling of the Human Foot Complex during Walking: Sensitivity Analysis of Material Properties, Boundary and Loading Conditions”. In: *Biomechanics and Modeling in Mechanobiology* 17.2 (Apr. 2018), pp. 559–576. ISSN: 1617-7959, 1617-7940. DOI: 10.1007/s10237-017-0978-3.
- [And+06] Donald D. Anderson, Jane K. Goldsworthy, Kiran Shivanna, Nicole M. Grosland, Douglas R. Pedersen, Thaddeus P. Thomas, Yuki Tochigi, J. Lawrence Marsh, and Thomas D. Brown. “Intra-Articular Contact Stress Distributions at the Ankle Throughout Stance Phase—Patient-Specific Finite Element Analysis as a Metric of Degeneration Propensity”. In: *Biomechanics and Modeling in Mechanobiology* 5.2-3 (June 2006), pp. 82–89. ISSN: 1617-7959, 1617-7940. DOI: 10.1007/s10237-006-0025-2.
- [Ath+98] K. A. Athanasiou, G. T. Liu, L. A. Lavery, D. R. Lanctot, and R. C. Schenck. “Biomechanical Topography of Human Articular Cartilage in the First Metatarsophalangeal Joint”. In: *Clinical Orthopaedics and Related Research* 348 (Mar. 1998), pp. 269–281. ISSN: 0009-921X. pmid: 9553561.
- [Att+85] David E. Attarian, Hugh J. McCrackin, Dennis P. DeVito, James H. McElhaney, and William E. Garrett. “Biomechanical Characteristics of Human Ankle Ligaments”. In: *Foot & Ankle* 6.2 (Oct. 1985), pp. 54–58. ISSN: 0198-0211. DOI: 10.1177/107110078500600202.
- [AWK13] Thomas Almonroeder, John D. Willson, and Thomas W. Kernozek. “The Effect of Foot Strike Pattern on Achilles Tendon Load During Running”. In: *Annals of Biomedical Engineering* 41.8 (Aug. 2013), pp. 1758–1766. ISSN: 0090-6964, 1573-9686. DOI: 10.1007/s10439-013-0819-1.
- [Bae+15] Ji Yong Bae, Kyung Soon Park, Jong Keun Seon, and Insu Jeon. “Analysis of the Effects of Normal Walking on Ankle Joint Contact Characteristics After Acute Inversion Ankle Sprain”. In: *Annals of Biomedical Engineering* 43.12 (Dec. 2015), pp. 3015–3024. ISSN: 0090-6964, 1573-9686. DOI: 10.1007/s10439-015-1360-1.
- [Bak07] Richard Baker. “The History of Gait Analysis before the Advent of Modern Computers”. In: *Gait & Posture* 26.3 (Sept. 2007), pp. 331–342. ISSN: 0966-6362. DOI: 10.1016/j.gaitpost.2006.10.014. pmid: 17306979.

- [Bau+10] E. Baussan, M.-A. Bueno, R.M. Rossi, and S. Derler. “Experiments and Modelling of Skin-Knitted Fabric Friction”. In: *Wear* 268.9-10 (Mar. 2010), pp. 1103–1110. ISSN: 00431648. DOI: 10.1016/j.wear.2010.01.010.
- [Ben98] Juan Francisco Benvenuti Garea. “Modélisation tridimensionnelle du genou humain”. Lausanne: EPFL, 1998.
- [Beu+03] Annechien Beumer, Wouter L.W. van Hemert, Bart A. Swierstra, Louis E. Jasper, and Stephen M. Belkoff. “A Biomechanical Evaluation of the Tibiofibular and Tibiotalar Ligaments of the Ankle”. In: *Foot & Ankle International* 24.5 (May 2003), pp. 426–429. ISSN: 1071-1007, 1944-7876. DOI: 10.1177/107110070302400509.
- [Bia17] Marco Evangelos Biancolini. *Fast Radial Basis Functions for Engineering Applications*. Cham: Springer International Publishing, 2017. ISBN: 978-3-319-75009-5 978-3-319-75011-8. DOI: 10.1007/978-3-319-75011-8.
- [BL79] Serge Beucher and Christian Lantuéjoul. “Use of Watersheds in Contour Detection”. In: International Workshop on Image Processing: Real-Time Edge and Motion Detection/Estimation. Rennes, France, Sept. 17–21, 1979.
- [BM88] P Bowker and N Messenger. “The Measurement of Gait”. In: *Clinical Rehabilitation* 2.2 (May 1988), pp. 89–97. ISSN: 0269-2155, 1477-0873. DOI: 10.1177/026921558800200201.
- [BM92] Paul J. Besl and Neil D. McKay. “Method for Registration of 3-D Shapes”. In: Robotics - DL Tentative. Ed. by Paul S. Schenker. Boston, MA, Apr. 30, 1992, pp. 586–606. DOI: 10.1117/12.57955.
- [BM93] S. Beucher and F. Meyer. “The Morphological Approach to Segmentation: The Watershed Transformation”. In: Edward R. Dougherty. *Mathematical Morphology in Image Processing*. Ed. by Edward R. Dougherty. 1st ed. CRC Press, 1993, pp. 433–481. ISBN: 978-1-315-21461-0. DOI: 10.1201/9781482277234-12.
- [BRK15] Cathleen N. Brown, Adam B. Rosen, and Jupil Ko. “Ankle Ligament Laxity and Stiffness in Chronic Ankle Instability”. In: *Foot & Ankle International* 36.5 (May 2015), pp. 565–572. ISSN: 1944-7876. DOI: 10.1177/1071100714561057. pmid: 25511756.
- [Büc+02] P. Büchler, N.A. Ramaniraka, L.R. Rakotomanana, J.P. Iannotti, and A. Farron. “A Finite Element Model of the Shoulder: Application to the Comparison of Normal and Osteoarthritic Joints”. In: *Clinical Biomechanics* 17.9-10 (Nov. 2002), pp. 630–639. ISSN: 02680033. DOI: 10.1016/S0268-0033(02)00106-7.
- [Bud+07] Sachin P. Budhabhatti, Ahmet Erdemir, Marc Petre, James Sferra, Brian Donley, and Peter R. Cavanagh. “Finite Element Modeling of the First Ray of the Foot: A Tool for the Design of Interventions”. In: *Journal of Biomechanical Engineering* 129.5 (Oct. 1, 2007), pp. 750–756. ISSN: 0148-0731, 1528-8951. DOI: 10.1115/1.2768108.
- [Bul+18] Andrew K. Buldt, Saeed Forghany, Karl B. Landorf, George S. Murley, Pazit Levinger, and Hylton B. Menz. “Centre of Pressure Characteristics in Normal, Planus and Cavus Feet”. In: *Journal of Foot and Ankle Research* 11.1 (Dec. 2018), p. 3. ISSN: 1757-1146. DOI: 10.1186/s13047-018-0245-6.

- [Car+01] J. C. Carr, R. K. Beatson, J. B. Cherrie, T. J. Mitchell, W. R. Fright, B. C. McCallum, and T. R. Evans. “Reconstruction and Representation of 3D Objects with Radial Basis Functions”. In: *Proceedings of the 28th Annual Conference on Computer Graphics and Interactive Techniques - SIGGRAPH '01*. The 28th Annual Conference. Not Known: ACM Press, 2001, pp. 67–76. ISBN: 978-1-58113-374-5. DOI: 10.1145/383259.383266.
- [CFH83] T. E. Clarke, E. C. Frederick, and C. L. Hamill. “The Effects of Shoe Design Parameters on Rearfoot Control in Running”. In: *Medicine and Science in Sports and Exercise* 15.5 (1983), pp. 376–381. ISSN: 0195-9131. pmid: 6645865.
- [Cha+14] Panagiotis E. Chatzistergos, Roozbeh Naemi, Lakshmi Sundar, Ambadi Ramachandran, and Nachiappan Chockalingam. “The Relationship between the Mechanical Properties of Heel-Pad and Common Clinical Measures Associated with Foot Ulcers in Patients with Diabetes”. In: *Journal of Diabetes and its Complications* 28.4 (July 2014), pp. 488–493. ISSN: 10568727. DOI: 10.1016/j.jdiacomp.2014.03.011.
- [Che+05] Jason Tak-Man Cheung, Ming Zhang, Aaron Kam-Lun Leung, and Yu-Bo Fan. “Three-Dimensional Finite Element Analysis of the Foot during Standing—a Material Sensitivity Study”. In: *Journal of Biomechanics* 38.5 (May 2005), pp. 1045–1054. ISSN: 00219290. DOI: 10.1016/j.jbiomech.2004.05.035.
- [Che+08] Hsin-Yi Kathy Cheng, Chun-Li Lin, Hsien-Wen Wang, and Shih-Wei Chou. “Finite Element Analysis of Plantar Fascia under Stretch—The Relative Contribution of Windlass Mechanism and Achilles Tendon Force”. In: *Journal of Biomechanics* 41.9 (Jan. 2008), pp. 1937–1944. ISSN: 00219290. DOI: 10.1016/j.jbiomech.2008.03.028.
- [Che+10] Wen-Ming Chen, Taeyong Lee, Peter Vee-Sin Lee, Jin Woo Lee, and Sung-Jae Lee. “Effects of Internal Stress Concentrations in Plantar Soft-Tissue—A Preliminary Three-Dimensional Finite Element Analysis”. In: *Medical Engineering & Physics* 32.4 (May 2010), pp. 324–331. ISSN: 13504533. DOI: 10.1016/j.medengphy.2010.01.001.
- [Che+15] Yen-Nien Chen, Chih-Wei Chang, Chun-Ting Li, Chih-Han Chang, and Cheng-Feng Lin. “Finite Element Analysis of Plantar Fascia During Walking: A Quasi-Static Simulation”. In: *Foot & Ankle International* 36.1 (Jan. 2015), pp. 90–97. ISSN: 1071-1007, 1944-7876. DOI: 10.1177/1071100714549189.
- [Cho+09] Jin-Rae Cho, Seung-Bum Park, Sung-Hyun Ryu, Sung-Ho Kim, and Shi-Bok Lee. “Landing Impact Analysis of Sports Shoes Using 3-D Coupled Foot-Shoe Finite Element Model”. In: *Journal of Mechanical Science and Technology* 23.10 (Oct. 2009), pp. 2583–2591. ISSN: 1738-494X, 1976-3824. DOI: 10.1007/s12206-009-0801-x.
- [CJT03] Weng-Pin Chen, Chia-Wei Ju, and Fuk-Tan Tang. “Effects of Total Contact Insoles on the Plantar Stress Redistribution: A Finite Element Analysis”. In: *Clinical Biomechanics* 18.6 (July 2003), S17–S24. ISSN: 02680033. DOI: 10.1016/S0268-0033(03)00080-9.

- [CKS95] V. Caselles, R. Kimmel, and G. Sapiro. “Geodesic Active Contours”. In: *Proceedings of IEEE International Conference on Computer Vision*. IEEE International Conference on Computer Vision. Cambridge, MA, USA: IEEE Comput. Soc. Press, 1995, pp. 694–699. ISBN: 978-0-8186-7042-8. DOI: 10.1109/ICCV.1995.466871.
- [CL80] Peter R. Cavanagh and Mario A. Lafortune. “Ground Reaction Forces in Distance Running”. In: *Journal of Biomechanics* 13.5 (Jan. 1980), pp. 397–406. ISSN: 00219290. DOI: 10.1016/0021-9290(80)90033-0.
- [CLL14] Wen-Ming Chen, Sung-Jae Lee, and Peter Vee Sin Lee. “The in Vivo Plantar Soft Tissue Mechanical Property under the Metatarsal Head: Implications of Tissues Joint-Angle Dependent Response in Foot Finite Element Modeling”. In: *Journal of the Mechanical Behavior of Biomedical Materials* 40 (Dec. 2014), pp. 264–274. ISSN: 17516161. DOI: 10.1016/j.jmbbm.2014.09.007.
- [CM91] Y. Chen and G. Medioni. “Object Modeling by Registration of Multiple Range Images”. In: *Proceedings. 1991 IEEE International Conference on Robotics and Automation*. 1991 IEEE International Conference on Robotics and Automation. Sacramento, CA, USA: IEEE Comput. Soc. Press, 1991, pp. 2724–2729. ISBN: 978-0-8186-2163-5. DOI: 10.1109/ROBOT.1991.132043.
- [Col+14] Fabrice Colin, Tamara Horn Lang, Lukas Zwicky, Beat Hintermann, and Markus Knupp. “Subtalar Joint Configuration on Weightbearing CT Scan”. In: *Foot & Ankle International* 35.10 (Oct. 2014), pp. 1057–1062. ISSN: 1071-1007, 1944-7876. DOI: 10.1177/1071100714540890.
- [Cor+03] F. Corazza, J.J. O’Connor, A. Leardini, and V. Parenti Castelli. “Ligament Fibre Recruitment and Forces for the Anterior Drawer Test at the Human Ankle Joint”. In: *Journal of Biomechanics* 36.3 (Mar. 2003), pp. 363–372. ISSN: 00219290. DOI: 10.1016/S0021-9290(02)00425-6.
- [Cou84] Michael J. Coughlin. “Mallet Toes, Hammer Toes, Claw Toes, and Corns: Causes and Treatment of Lesser-Toe Deformities”. In: *Postgraduate Medicine* 75.5 (Apr. 1984), pp. 191–198. ISSN: 0032-5481, 1941-9260. DOI: 10.1080/00325481.1984.11698001.
- [CRP95] T.-M. Chu, N.P. Reddy, and J. Padovan. “Three-Dimensional Finite Element Stress Analysis of the Polypropylene, Ankle-Foot Orthosis: Static Analysis”. In: *Medical Engineering & Physics* 17.5 (July 1995), pp. 372–379. ISSN: 13504533. DOI: 10.1016/1350-4533(95)97317-1.
- [CTC08] CTC. *La chaussure sous toutes ses coutures*. Lyon (4 rue Hermann-Frenkel, 69367 Cedex): CTC, 2008. ISBN: 978-2-9505970-7-6.
- [CTJ01] Weng-Pin Chen, Fuk-Tan Tang, and Chia-Wei Ju. “Stress Distribution of the Foot during Mid-Stance to Push-Off in Barefoot Gait: A 3-D Finite Element Analysis”. In: *Clinical Biomechanics* (2001), p. 7.
- [CTS84] D.B. Clement, J.E. Taunton, and G.W. Smart. “Achilles Tendinitis and Peritendinitis: Etiology and Treatment”. In: *The American Journal of Sports Medicine* 12.3 (May 1984), pp. 179–184. ISSN: 0363-5465, 1552-3365. DOI: 10.1177/036354658401200301.

- [CZ05] Jason Tak-Man Cheung and Ming Zhang. “A 3-Dimensional Finite Element Model of the Human Foot and Ankle for Insole Design”. In: *Archives of Physical Medicine and Rehabilitation* 86.2 (Feb. 2005), pp. 353–358. ISSN: 00039993. DOI: 10.1016/j.apmr.2004.03.031.
- [CZ08] Jason Tak-Man Cheung and Ming Zhang. “Parametric Design of Pressure-Relieving Foot Orthosis Using Statistics-Based Finite Element Method”. In: *Medical Engineering & Physics* 30.3 (Apr. 2008), pp. 269–277. ISSN: 13504533. DOI: 10.1016/j.medengphy.2007.05.002.
- [CZC11] Clare Y.L. Chao, Yong-Ping Zheng, and Gladys L.Y. Cheing. “Epidermal Thickness and Biomechanical Properties of Plantar Tissues in Diabetic Foot”. In: *Ultrasound in Medicine & Biology* 37.7 (July 2011), pp. 1029–1038. ISSN: 03015629. DOI: 10.1016/j.ultrasmedbio.2011.04.004.
- [DAK94] D. De Clercq, P. Aerts, and M. Kunnen. “The Mechanical Characteristics of the Human Heel Pad during Foot Strike in Running: An in Vivo Cineradiographic Study”. In: *Journal of Biomechanics* 27.10 (Oct. 1994), pp. 1213–1222. ISSN: 00219290. DOI: 10.1016/0021-9290(94)90275-5.
- [Dan86] H. J. Dananberg. “Functional Hallux Limitus and Its Relationship to Gait Efficiency”. In: *Journal of the American Podiatric Medical Association* 76.11 (Nov. 1986), pp. 648–652. ISSN: 8750-7315. DOI: 10.7547/87507315-76-11-648. pmid: 3814239.
- [dBvdSB07] A. de Boer, M.S. van der Schoot, and H. Bijl. “Mesh Deformation Based on Radial Basis Function Interpolation”. In: *Computers & Structures* 85.11-14 (June 2007), pp. 784–795. ISSN: 00457949. DOI: 10.1016/j.compstruc.2007.01.013.
- [Del+07] Scott L. Delp, Frank C. Anderson, Allison S. Arnold, Peter Loan, Ayman Habib, Chand T. John, Eran Guendelman, and Darryl G. Thelen. “OpenSim: Open-Source Software to Create and Analyze Dynamic Simulations of Movement”. In: *IEEE Transactions on Biomedical Engineering* 54.11 (Nov. 2007), pp. 1940–1950. ISSN: 0018-9294. DOI: 10.1109/TBME.2007.901024.
- [Der+09] S. Derler, R. Huber, H.-P. Feuz, and M. Hadad. “Influence of Surface Microstructure on the Sliding Friction of Plantar Skin against Hard Substrates”. In: *Wear* 267.5-8 (June 2009), pp. 1281–1288. ISSN: 00431648. DOI: 10.1016/j.wear.2008.12.053.
- [DL78] H. Digabel and C. Lantuéjoul. “Iterative Algorithms”. In: 2nd European Symposium on Quantitative Analysis of Microstructures in Material Science. Stuttgart, 1978, pp. 85–99.
- [Dro+18] Dimitris Drougkas, Evangelos Karatsis, Maria Papagiannaki, Serafeim Chatzimoisiadis, Fotini Arabatzi, Stergios Maropoulos, and Alexander Tsouknidas. “Gait-Specific Optimization of Composite Footwear Midsole Systems, Facilitated through Dynamic Finite Element Modelling”. In: *Applied Bionics and Biomechanics* 2018 (Dec. 23, 2018), pp. 1–9. ISSN: 1176-2322, 1754-2103. DOI: 10.1155/2018/6520314.
- [Erd+06] Ahmet Erdemir, Meredith L. Viveiros, Jan S. Ulbrecht, and Peter R. Cavanagh. “An Inverse Finite-Element Model of Heel-Pad Indentation”. In: *Journal of Biomechanics* 39.7 (Jan. 2006), pp. 1279–1286. ISSN: 00219290. DOI: 10.1016/j.jbiomech.2005.03.007.

- [EVC03] Ahmet Erdemir, Meredith L Viveiros, and Peter R Cavanagh. “A Numerical-Experimental Approach For Characterizing Subject Specific Hyperelastic Properties Of The Heel Pad”. In: (2003), p. 2.
- [Eve+06] Nurit Even-Tzur, Ety Weisz, Yifat Hirsch-Falk, and Amit Gefen. “Role of EVA Viscoelastic Properties in the Protective Performance of a Sport Shoe: Computational Studies”. In: *Bio-Medical Materials and Engineering* 16.5 (2006), pp. 289–299. ISSN: 0959-2989. pmid: 17075164.
- [Fer+08] Melanie Ferri, Angela V. Scharfenberger, Gord Goplen, Timothy R. Daniels, and Dawn Pearce. “Weightbearing CT Scan of Severe Flexible Pes Planus Deformities”. In: *Foot & Ankle International* 29.2 (Feb. 2008), pp. 199–204. ISSN: 1071-1007, 1944-7876. DOI: 10.3113/FAI.2008.0199.
- [FH16] Reed Ferber and Blayne A Hettinga. “A Comparison of Different Over-the-Counter Foot Orthotic Devices on Multi-Segment Foot Biomechanics”. In: *Prosthetics and Orthotics International* 40.6 (July 2016), pp. 675–681. DOI: 10.1177/0309364615584660.
- [Fon+13] C.G. Fontanella, A. Forestiero, E.L. Carniel, and A.N. Natali. “Analysis of Heel Pad Tissues Mechanics at the Heel Strike in Bare and Shod Conditions”. In: *Medical Engineering & Physics* 35.4 (Apr. 2013), pp. 441–447. ISSN: 13504533. DOI: 10.1016/j.medengphy.2012.06.008.
- [Fre+93] Carol Frey, Francesca Thompson, Judith Smith, Melanie Sanders, and Helen Horstman. “American Orthopaedic Foot and Ankle Society Women’s Shoe Survey”. In: *Foot & Ankle* 14.2 (Feb. 1993), pp. 78–81. ISSN: 0198-0211. DOI: 10.1177/107110079301400204.
- [Ful+15] Joel T. Fuller, Clint R. Bellenger, Dominic Thewlis, Margarita D. Tsiros, and Jonathan D. Buckley. “The Effect of Footwear on Running Performance and Running Economy in Distance Runners”. In: *Sports Medicine* 45.3 (Mar. 2015), pp. 411–422. ISSN: 0112-1642, 1179-2035. DOI: 10.1007/s40279-014-0283-6.
- [Gar+09] J. M. García-Aznar, J. Bayod, A. Rosas, R. Larrainzar, R. García-Bógallo, M. Doblaré, and L. F. Llanos. “Load Transfer Mechanism for Different Metatarsal Geometries: A Finite Element Study”. In: *Journal of Biomechanical Engineering* 131.2 (Feb. 1, 2009), p. 021011. ISSN: 0148-0731, 1528-8951. DOI: 10.1115/1.3005174.
- [GCB19] Corrado Groth, Emiliano Costa, and Marco Evangelos Biancolini. “RBF-Based Mesh Morphing Approach to Perform Icing Simulations in the Aviation Sector”. In: *Aircraft Engineering and Aerospace Technology* 91.4 (Apr. 1, 2019), pp. 620–633. ISSN: 1748-8842. DOI: 10.1108/AEAT-07-2018-0178.
- [Gee+11] Marion Geerligs, Lambert van Breemen, Gerrit Peters, Paul Ackermans, Frank Baaijens, and Cees Oomens. “In Vitro Indentation to Determine the Mechanical Properties of Epidermis”. In: *Journal of Biomechanics* 44.6 (Apr. 2011), pp. 1176–1181. ISSN: 00219290. DOI: 10.1016/j.jbiomech.2011.01.015.

- [Gef+00] A. Gefen, M. Megido-Ravid, Y. Itzhak, and M. Arcan. “Biomechanical Analysis of the Three-Dimensional Foot Structure During Gait: A Basic Tool for Clinical Applications”. In: *Journal of Biomechanical Engineering* 122.6 (Dec. 1, 2000), pp. 630–639. ISSN: 0148-0731, 1528-8951. DOI: 10.1115/1.1318904.
- [Gef02] Amit Gefen. “Stress Analysis of the Standing Foot Following Surgical Plantar Fascia Release”. In: *Journal of Biomechanics* 35.5 (May 2002), pp. 629–637. ISSN: 00219290. DOI: 10.1016/S0021-9290(01)00242-1.
- [Gef03a] Amit Gefen. “Plantar Soft Tissue Loading under the Medial Metatarsals in the Standing Diabetic Foot”. In: *Medical Engineering & Physics* 25.6 (July 2003), pp. 491–499. ISSN: 13504533. DOI: 10.1016/S1350-4533(03)00029-8.
- [Gef03b] Amit Gefen. “The in Vivo Elastic Properties of the Plantar Fascia during the Contact Phase of Walking”. In: *Foot & Ankle International* 24.3 (Mar. 2003), pp. 238–244. ISSN: 1071-1007, 1944-7876. DOI: 10.1177/107110070302400307.
- [Gia+18] Claudia Giacomozzi, Paolo Caravaggi, Julie A. Stebbins, and Alberto Lear-dini. “Integration of Foot Pressure and Foot Kinematics Measurements for Medical Applications”. In: *Handbook of Human Motion*. Cham: Springer International Publishing, 2018, pp. 789–810. ISBN: 978-3-319-14417-7 978-3-319-14418-4. DOI: 10.1007/978-3-319-14418-4_186.
- [GMI01] Amit Gefen, Michal Megido-Ravid, and Yacov Itzhak. “In Vivo Biomechanical Behavior of the Human Heel Pad during the Stance Phase of Gait”. In: *Journal of Biomechanics* 34.12 (Dec. 2001), pp. 1661–1665. ISSN: 00219290. DOI: 10.1016/S0021-9290(01)00143-9.
- [Gra+11] Lorenzo Grassi, Najah Hraiech, Enrico Schileo, Mauro Ansaloni, Michel Rochette, and Marco Viceconti. “Evaluation of the Generality and Accuracy of a New Mesh Morphing Procedure for the Human Femur”. In: *Medical Engineering & Physics* 33.1 (Jan. 2011), pp. 112–120. ISSN: 13504533. DOI: 10.1016/j.medengphy.2010.09.014.
- [Gri+17] Grigoris Grigoriadis, Nicolas Newell, Diagarajen Carpanen, Alexandros Christou, Anthony M.J. Bull, and Spyros D. Masouros. “Material Properties of the Heel Fat Pad across Strain Rates”. In: *Journal of the Mechanical Behavior of Biomedical Materials* 65 (Jan. 2017), pp. 398–407. ISSN: 17516161. DOI: 10.1016/j.jmbbm.2016.09.003.
- [Gu+10] Y. D. Gu, X. J. Ren, J. S. Li, M. J. Lake, Q. Y. Zhang, and Y. J. Zeng. “Computer Simulation of Stress Distribution in the Metatarsals at Different Inversion Landing Angles Using the Finite Element Method”. In: *International Orthopaedics* 34.5 (June 2010), pp. 669–676. ISSN: 0341-2695, 1432-5195. DOI: 10.1007/s00264-009-0856-4.
- [Gu+11] Y. D. Gu, J. S. Li, M. J. Lake, Y. J. Zeng, X. J. Ren, and Z. Y. Li. “Image-Based Midsole Insert Design and the Material Effects on Heel Plantar Pressure Distribution during Simulated Walking Loads”. In: *Computer Methods in Biomechanics and Biomedical Engineering* 14.8 (Aug. 2011), pp. 747–753. ISSN: 1025-5842, 1476-8259. DOI: 10.1080/10255842.2010.493886.

- [Gui+14] Annamaria Guiotto, Zimi Sawacha, Gabriella Guarneri, Angelo Avogaro, and Claudio Cobelli. “3D Finite Element Model of the Diabetic Neuropathic Foot: A Gait Analysis Driven Approach”. In: *Journal of Biomechanics* 47.12 (Sept. 2014), pp. 3064–3071. ISSN: 00219290. DOI: 10.1016/j.jbiomech.2014.06.029.
- [Hae+17] T.X. Haen, A. Roux, M. Soubeyrand, and S. Laporte. “Shear Waves Elastography for Assessment of Human Achilles Tendon’s Biomechanical Properties: An Experimental Study”. In: *Journal of the Mechanical Behavior of Biomedical Materials* 69 (May 2017), pp. 178–184. ISSN: 17516161. DOI: 10.1016/j.jmbbm.2017.01.007.
- [Ham+11] Joseph Hamill, Elizabeth M. Russell, Allison H. Gruber, and Ross Miller. “Impact Characteristics in Shod and Barefoot Running”. In: *Footwear Science* 3.1 (Mar. 2011), pp. 33–40. ISSN: 1942-4280, 1942-4299. DOI: 10.1080/19424280.2010.542187.
- [HH09] Marco Hagen and Ewald M. Hennig. “Effects of Different Shoe-Lacing Patterns on the Biomechanics of Running Shoes”. In: *Journal of Sports Sciences* 27.3 (Feb. 2009), pp. 267–275. ISSN: 0264-0414, 1466-447X. DOI: 10.1080/02640410802482425.
- [Hic54] J. H. Hicks. “The Mechanics of the Foot. II. The Plantar Aponeurosis and the Arch”. In: *Journal of Anatomy* 88.1 (Jan. 1954), pp. 25–30. ISSN: 0021-8782. pmid: 13129168.
- [Hir+00] Shoji Hirano, Yutaka Hata, Nobuyuki Matsui, Yoshiro Ando, and Makato Ishikawa. “Segmentation of the Fractured Foot CT Image: A Fuzzy-Rule-Based Approach”. In: ed. by Kenneth M. Hanson. June 6, 2000, pp. 854–862. DOI: 10.1117/12.387749.
- [HKS11] David Hibbitt, Karlsson Karlsson, and Paul Sorensen. *Abaqus Theory Manual*. 2011.
- [HL18] Nicholas B. Holowka and Daniel E. Lieberman. “Rethinking the Evolution of the Human Foot: Insights from Experimental Research”. In: *The Journal of Experimental Biology* 221.17 (Sept. 1, 2018), jeb174425. ISSN: 0022-0949, 1477-9145. DOI: 10.1242/jeb.174425.
- [Hsu+05] Chih-Chin Hsu, Wen-Chung Tsai, Carl Pai-Chu Chen, Yio-Wha Shau, Chung-Li Wang, Max Jin-Lung Chen, and King-Jen Chang. “Effects of Aging on the Plantar Soft Tissue Properties under the Metatarsal Heads at Different Impact Velocities”. In: *Ultrasound in Medicine & Biology* 31.10 (Oct. 2005), pp. 1423–1429. ISSN: 03015629. DOI: 10.1016/j.ultrasmedbio.2005.05.009.
- [Hsu+07] Chih-Chin Hsu, Wen-Chung Tsai, Yio-Wha Shau, Kay-Lun Lee, and Ching-Fang Hu. “Altered Energy Dissipation Ratio of the Plantar Soft Tissues under the Metatarsal Heads in Patients with Type 2 Diabetes Mellitus: A Pilot Study”. In: *Clinical Biomechanics* 22.1 (Jan. 2007), pp. 67–73. ISSN: 02680033. DOI: 10.1016/j.clinbiomech.2006.06.009.

-
- [Isv+12] Vara Isvilanonda, Evan Dengler, Joseph M. Iaquinto, Bruce J. Sangeorzan, and William R. Ledoux. “Finite Element Analysis of the Foot: Model Validation and Comparison between Two Common Treatments of the Clawed Hallux Deformity”. In: *Clinical Biomechanics* 27.8 (Oct. 2012), pp. 837–844. ISSN: 02680033. DOI: 10.1016/j.clinbiomech.2012.05.005.
- [Isv+16] Vara Isvilanonda, Joseph M. Iaquinto, Shruti Pai, Peter Mackenzie-Helnwein, and William R. Ledoux. “Hyperelastic Compressive Mechanical Properties of the Subcalcaneal Soft Tissue: An Inverse Finite Element Analysis”. In: *Journal of Biomechanics* 49.7 (May 2016), pp. 1186–1191. ISSN: 00219290. DOI: 10.1016/j.jbiomech.2016.03.003.
- [Ito+15] Kohta Ito, Koh Hosoda, Masahiro Shimizu, Shuhei Ikemoto, Shinnosuke Kume, Takeo Nagura, Nobuaki Imanishi, Sadakazu Aiso, Masahiro Jinzaki, and Naomichi Ogihara. “Direct Assessment of 3D Foot Bone Kinematics Using Biplanar X-Ray Fluoroscopy and an Automatic Model Registration Method”. In: *Journal of Foot and Ankle Research* 8.1 (Dec. 2015). ISSN: 1757-1146. DOI: 10.1186/s13047-015-0079-4.
- [Ito+17] Kohta Ito, Koh Hosoda, Masahiro Shimizu, Shuhei Ikemoto, Takeo Nagura, Hiroyuki Seki, Masateru Kitashiro, Nobuaki Imanishi, Sadakazu Aiso, Masahiro Jinzaki, and Naomichi Ogihara. “Three-Dimensional Innate Mobility of the Human Foot Bones under Axial Loading Using Biplane X-Ray Fluoroscopy”. In: *Royal Society Open Science* 4.10 (Oct. 2017), p. 171086. ISSN: 2054-5703. DOI: 10.1098/rsos.171086.
- [IW10] Joseph M. Iaquinto and Jennifer S. Wayne. “Computational Model of the Lower Leg and Foot/Ankle Complex: Application to Arch Stability”. In: *Journal of Biomechanical Engineering* 132.2 (2010), p. 021009. ISSN: 01480731. DOI: 10.1115/1.4000939.
- [JA07] S. Jakobsson and O. Amoignon. “Mesh Deformation Using Radial Basis Functions for Gradient-Based Aerodynamic Shape Optimization”. In: *Computers & Fluids* 36.6 (July 2007), pp. 1119–1136. ISSN: 00457930. DOI: 10.1016/j.compfluid.2006.11.002.
- [Jac+96] Shanti Jacob, K.M. Patil, L.H. Braak, and A. Huson. “Stresses in a 3D Two Arch Model of a Normal Human Foot”. In: *Mechanics Research Communications* 23.4 (July 1996), pp. 387–393. ISSN: 00936413. DOI: 10.1016/0093-6413(96)00036-5.
- [JBO78] Stanley L. James, Barry T. Bates, and Louis R. Osternig. “Injuries to Runners”. In: *The American Journal of Sports Medicine* 6.2 (Mar. 1978), pp. 40–50. ISSN: 0363-5465, 1552-3365. DOI: 10.1177/036354657800600202.
- [JP99] S. Jacob and M. K. Patil. “Three-Dimensional Foot Modeling and Analysis of Stresses in Normal and Early Stage Hansen’s Disease with Muscle Paralysis”. In: *Journal of Rehabilitation Research and Development* 36.3 (July 1999), pp. 252–263. ISSN: 0748-7711. pmid: 10659808.
- [Kad+05] Nancy J. Kadel, Emily A. Donaldson-Fletcher, Sigvard T. Hansen, and Bruce J. Sangeorzan. “Alternative to the Modified Jones Procedure: Outcomes of the Flexor Hallucis Longus (FHL) Tendon Transfer Procedure for Correction of Clawed Hallux”. In: *Foot & Ankle International* 26.12
-

- (Dec. 2005), pp. 1021–1026. ISSN: 1071-1007, 1944-7876. DOI: 10.1177/107110070502601204.
- [Ke+15] W. Ke, G.-M. Rotaru, J. Y. Hu, R. M. Rossi, X. Ding, and S. Derler. “In Vivo Measurement of the Friction Between Human Skin and Different Medical Compression Stockings”. In: *Tribology Letters* 60.1 (Oct. 2015). ISSN: 1023-8883, 1573-2711. DOI: 10.1007/s11249-015-0580-8.
- [Kel+14] Luke A. Kelly, Andrew G. Cresswell, Sebastien Racinais, Rodney Whiteley, and Glen Lichtwark. “Intrinsic Foot Muscles Have the Capacity to Control Deformation of the Longitudinal Arch”. In: *Journal of The Royal Society Interface* 11.93 (Apr. 6, 2014), p. 20131188. ISSN: 1742-5689, 1742-5662. DOI: 10.1098/rsif.2013.1188.
- [Kel+96] Ts Keller, Am Weisberger, JI Ray, Ss Hasan, Rg Shiavi, and Dm Spengler. “Relationship between Vertical Ground Reaction Force and Speed during Walking, Slow Jogging, and Running”. In: *Clinical Biomechanics* 11.5 (July 1996), pp. 253–259. ISSN: 02680033. DOI: 10.1016/0268-0033(95)00068-2.
- [Kem80] Geoffrey E. Kempson. “The Mechanical Properties of Articular Cartilage”. In: *The Joints and Synovial Fluid*. Elsevier, 1980, pp. 177–238. ISBN: 978-0-12-655102-0. DOI: 10.1016/B978-0-12-655102-0.50011-4.
- [Kim+12] Hak Soo Kim, Samuel B. Park, Simon S. Lo, James I. Monroe, and Jason W. Sohn. “Bidirectional Local Distance Measure for Comparing Segmentations: Bidirectional Local Distance Measure”. In: *Medical Physics* 39.11 (Oct. 19, 2012), pp. 6779–6790. ISSN: 00942405. DOI: 10.1118/1.4754802.
- [Kit+94] Harold B. Kitaoka, Zong Ping Luo, Eric S. Growney, Lawrence J. Berglund, and Kai-Nan An. “Material Properties of the Plantar Aponeurosis”. In: *Foot & Ankle International* 15.10 (Oct. 1994), pp. 557–560. ISSN: 1071-1007, 1944-7876. DOI: 10.1177/107110079401501007.
- [KLC15] Luke A. Kelly, Glen Lichtwark, and Andrew G. Cresswell. “Active Regulation of Longitudinal Arch Compression and Recoil during Walking and Running”. In: *Journal of The Royal Society Interface* 12.102 (Jan. 2015), p. 20141076. ISSN: 1742-5689, 1742-5662. DOI: 10.1098/rsif.2014.1076.
- [Kra88] D. Kraft. *A Software Package for Sequential Quadratic Programming*. Deutsche Forschungs- Und Versuchsanstalt Für Luft- Und Raumfahrt Köln: Forschungsbericht. Wiss. Berichtswesen d. DFVLR, 1988.
- [Kro+20] Nicolas Kroupa, Baptiste Pierrat, Woo-Suck Han, Sylvain Grange, Florian Bergandi, and Jérôme Molimard. “Bone Position and Ligament Deformations of the Foot From CT Images to Quantify the Influence of Footwear in Ex Vivo Feet”. In: *Frontiers in Bioengineering and Biotechnology* 8 (June 19, 2020), p. 560. ISSN: 2296-4185. DOI: 10.3389/fbioe.2020.00560.
- [Kur+01] Hideji Kura, Zong-Ping Luo, Harold B. Kitaoka, W. Paul Smutz, and Kai-Nan An. “Mechanical Behavior of the Lisfranc and Dorsal Cuneometatarsal Ligaments: In Vitro Biomechanical Study.” in: *Journal of Orthopaedic Trauma* 15.2 (Feb. 2001), pp. 107–110. ISSN: 0890-5339. DOI: 10.1097/00005131-200102000-00006.

- [KWT88] Michael Kass, Andrew Witkin, and Demetri Terzopoulos. “Snakes: Active Contour Models”. In: *International Journal of Computer Vision* 1.4 (Jan. 1988), pp. 321–331. ISSN: 0920-5691, 1573-1405. DOI: 10.1007/BF00133570.
- [Lea+05] Alberto Leardini, Lorenzo Chiari, Ugo Della Croce, and Aurelio Cappozzo. “Human Movement Analysis Using Stereophotogrammetry”. In: *Gait & Posture* 21.2 (Feb. 2005), pp. 212–225. ISSN: 09666362. DOI: 10.1016/j.gaitpost.2004.05.002.
- [Lem+97a] David Lemmon, T.Y. Shiang, Azfar Hashmi, Jan S. Ulbrecht, and Peter R. Cavanagh. “The Effect of Insoles in Therapeutic Footwear—A Finite Element Approach”. In: *Journal of Biomechanics* 30.6 (June 1997), pp. 615–620. ISSN: 00219290. DOI: 10.1016/S0021-9290(97)00006-7.
- [Lem+97b] David Lemmon, T.Y. Shiang, Azfar Hashmi, Jan S. Ulbrecht, and Peter R. Cavanagh. “The Effect of Insoles in Therapeutic Footwear—A Finite Element Approach”. In: *Journal of Biomechanics* 30.6 (June 1997), pp. 615–620. ISSN: 00219290. DOI: 10.1016/S0021-9290(97)00006-7.
- [Lia+11] Jun Liang, YunFeng Yang, GuangRong Yu, WenXin Niu, and YuBin Wang. “Deformation and Stress Distribution of the Human Foot after Plantar Ligaments Release: A Cadaveric Study and Finite Element Analysis”. In: *Science China Life Sciences* 54.3 (Mar. 2011), pp. 267–271. ISSN: 1674-7305, 1869-1889. DOI: 10.1007/s11427-011-4139-0.
- [Lie+10] Daniel E. Lieberman, Madhusudhan Venkadesan, William A. Werbel, Adam I. Daoud, Susan D’Andrea, Irene S. Davis, Robert Ojiambo Mang’Eni, and Yannis Pitsiladis. “Foot Strike Patterns and Collision Forces in Habitually Barefoot versus Shod Runners”. In: *Nature* 463.7280 (Jan. 2010), pp. 531–535. ISSN: 0028-0836, 1476-4687. DOI: 10.1038/nature08723.
- [Lin+18] François Lintz, Cesar de Cesar Netto, Alexej Barg, Arne Burssens, Martinus Richter, and Weight Bearing CT International Stu. “Weight-Bearing Cone Beam CT Scans in the Foot and Ankle”. In: *EFORT Open Reviews* 3.5 (May 2018), pp. 278–286. ISSN: 2396-7544, 2058-5241. DOI: 10.1302/2058-5241.3.170066.
- [Liu+08] Jiamin Liu, Jayaram K. Udupa, Punam K. Saha, Dewey Odhner, Bruce E. Hirsch, Sorin Siegler, Scott Simon, and Beth A. Winkelstein. “Rigid Model-Based 3D Segmentation of the Bones of Joints in MR and CT Images for Motion Analysis: Segmentation of Bones of Joints for Motion Analysis”. In: *Medical Physics* 35.8 (July 17, 2008), pp. 3637–3649. ISSN: 00942405. DOI: 10.1118/1.2953567.
- [Liu+13] Qinghua Liu, Kun Zhang, Yan Zhuang, Zhong Li, Bin Yu, and Guoxian Pei. “Analysis of the Stress and Displacement Distribution of Inferior Tibiofibular Syndesmosis Injuries Repaired with Screw Fixation: A Finite Element Study”. In: *PLoS ONE* 8.12 (Dec. 3, 2013). Ed. by Carlos M. Isales, e80236. ISSN: 1932-6203. DOI: 10.1371/journal.pone.0080236.
- [Liu+16] Qinghua Liu, Guanghui Zhao, Bin Yu, Jianbin Ma, Zhong Li, and Kun Zhang. “Effects of Inferior Tibiofibular Syndesmosis Injury and Screw Stabilization on Motion of the Ankle: A Finite Element Study”. In: *Knee Surgery, Sports Traumatology, Arthroscopy* 24.4 (Apr. 2016), pp. 1228–1235. ISSN: 0942-2056, 1433-7347. DOI: 10.1007/s00167-014-3320-y.

- [Liu+97] George T. Liu, Lawrence A. Lavery, Robert C. Schenck, Dan R. Lanctot, Chong F. Zhu, and Kyriacos A. Athanasiou. “Human Articular Cartilage Biomechanics of the Second Metatarsal Intermediate Cuneiform Joint”. In: *The Journal of Foot and Ankle Surgery* 36.5 (Sept. 1997), pp. 367–374. ISSN: 10672516. DOI: 10.1016/S1067-2516(97)80039-7.
- [Liu08] Lu Liu. “Interactive Separation of Segmented Bones in CT Volumes Using Graph Cut”. In: *Medical Image Computing and Computer-Assisted Intervention – MICCAI 2008*. Vol. 5241. Berlin, Heidelberg: Springer Berlin Heidelberg, 2008, pp. 296–304. ISBN: 978-3-540-85987-1 978-3-540-85988-8. DOI: 10.1007/978-3-540-85988-8_36.
- [LLG19] Yuhua Li, Kf Leong, and Yaodong Gu. “Construction and Finite Element Analysis of a Coupled Finite Element Model of Foot and Barefoot Running Footwear”. In: *Proceedings of the Institution of Mechanical Engineers, Part P: Journal of Sports Engineering and Technology* 233.1 (Mar. 2019), pp. 101–109. ISSN: 1754-3371, 1754-338X. DOI: 10.1177/1754337118803540.
- [LW07] Peter C. Liacouras and Jennifer S. Wayne. “Computational Modeling to Predict Mechanical Function of Joints: Application to the Lower Leg With Simulation of Two Cadaver Studies”. In: *Journal of Biomechanical Engineering* 129.6 (2007), p. 811. ISSN: 01480731. DOI: 10.1115/1.2800763.
- [McH+19] Benjamin D. McHenry, Karen M. Kruger, Emily L. Exten, Sergey Tarima, and Gerald F. Harris. “Sagittal Subtalar and Talocrural Joint Assessment between Barefoot and Shod Walking: A Fluoroscopic Study”. In: *Gait & Posture* 72 (July 2019), pp. 57–61. ISSN: 09666362. DOI: 10.1016/j.gaitpost.2019.05.024.
- [MCT85] D.C. McKenzie, D.B. Clement, and J.E. Taunton. “Running Shoes, Orthotics, and Injuries.” in: *Sports Medicine* 2.5 (1985), pp. 334–347. ISSN: 0112-1642. DOI: 10.2165/00007256-198502050-00003.
- [MDB02] Janice E. Miller-Young, Neil A. Duncan, and Gamal Baroud. “Material Properties of the Human Calcaneal Fat Pad in Compression: Experiment and Theory”. In: *Journal of Biomechanics* 35.12 (Dec. 2002), pp. 1523–1531. ISSN: 00219290. DOI: 10.1016/S0021-9290(02)00090-8.
- [MDS16] Karan Malhotra, Kinner Davda, and Dishan Singh. “The Pathology and Management of Lesser Toe Deformities”. In: *EFORT Open Reviews* 1.11 (Nov. 2016), pp. 409–419. ISSN: 2396-7544, 2058-5241. DOI: 10.1302/2058-5241.1.160017.
- [MGL08] Hylton B Menz, Mark F Gilheany, and Karl B Landorf. “Foot and Ankle Surgery in Australia: A Descriptive Analysis of the Medicare Benefits Schedule Database, 1997–2006”. In: *Journal of Foot and Ankle Research* 1.1 (Dec. 2008), p. 10. ISSN: 1757-1146. DOI: 10.1186/1757-1146-1-10.
- [MI78] S. Miyazaki and H. Iwakura. “Foot-Force Measuring Device for Clinical Assessment of Pathological Gait”. In: *Medical & Biological Engineering & Computing* 16.4 (July 1978), pp. 429–436. ISSN: 0140-0118, 1741-0444. DOI: 10.1007/BF02442661.

-
- [Mic11] Andreas K. Michler. “Aircraft Control Surface Deflection Using RBF-Based Mesh Deformation”. In: *International Journal for Numerical Methods in Engineering* 88.10 (Dec. 9, 2011), pp. 986–1007. ISSN: 00295981. DOI: 10.1002/nme.3208.
- [Mka+05] Chimba Mkandawire, William R. Ledoux, Bruce J. Sangeorzan, and Randal P. Ching. “Foot and Ankle Ligament Morphometry”. In: *The Journal of Rehabilitation Research and Development* 42.6 (2005), p. 809. ISSN: 0748-7711. DOI: 10.1682/JRRD.2004.08.0094.
- [Mor+09] Cédric Morio, Mark J. Lake, Nils Gueguen, Guillaume Rao, and Laurent Baly. “The Influence of Footwear on Foot Motion during Walking and Running”. In: *Journal of Biomechanics* 42.13 (Sept. 2009), pp. 2081–2088. ISSN: 00219290. DOI: 10.1016/j.jbiomech.2009.06.015.
- [NCC81] S. Nakamura, R. D. Crowninshield, and R. R. Cooper. “An Analysis of Soft Tissue Loading in the Foot—a Preliminary Report”. In: *Bulletin of Prosthetics Research* 10-35 (1981), pp. 27–34. ISSN: 0007-506X. pmid: 7332829.
- [Nig+15] Bm Nigg, J Baltich, S Hoerzer, and H Enders. “Running Shoes and Running Injuries: Mythbusting and a Proposal for Two New Paradigms: ‘Preferred Movement Path’ and ‘Comfort Filter’”. In: *British Journal of Sports Medicine* 49.20 (Oct. 2015), pp. 1290–1294. ISSN: 0306-3674, 1473-0480. DOI: 10.1136/bjsports-2015-095054.
- [Nis08] Tsuyoshi Nishiwaki. “Running Shoe Sole Stiffness Evaluation Method Based on Eigen Vibration Analysis”. In: *Sports Technology* 1.1 (Jan. 2008), pp. 76–82. ISSN: 1934-6182, 1934-6190. DOI: 10.1080/19346182.2008.9648453.
- [Ols+03] Soren L. Olson, William R. Ledoux, Randal P. Ching, and Bruce J. Sangeorzan. “Muscular Imbalances Resulting in a Clawed Hallux”. In: *Foot & Ankle International* 24.6 (June 2003), pp. 477–485. ISSN: 1071-1007, 1944-7876. DOI: 10.1177/107110070302400605.
- [Ots79] Nobuyuki Otsu. “A Threshold Selection Method from Gray-Level Histograms”. In: *IEEE Transactions on Systems, Man, and Cybernetics* 9.1 (Jan. 1979), pp. 62–66. ISSN: 0018-9472, 2168-2909. DOI: 10.1109/TSMC.1979.4310076.
- [Pay+18] Catherine Payne, Peter Watt, Mara Cercignani, and Nick Webborn. “Reproducibility of Shear Wave Elastography Measures of the Achilles Tendon”. In: *Skeletal Radiology* 47.6 (June 2018), pp. 779–784. ISSN: 0364-2348, 1432-2161. DOI: 10.1007/s00256-017-2846-8.
- [PB19] Julien Pansiot and Edmond Boyer. “CBCT of a Moving Sample From X-Rays and Multiple Videos”. In: *IEEE Transactions on Medical Imaging* 38.2 (Feb. 2019), pp. 383–393. ISSN: 0278-0062, 1558-254X. DOI: 10.1109/TMI.2018.2865228.
- [PBH96] K. M. Patil, L. H. Braak, and A. Huson. “Analysis of Stresses in Two-Dimensional Models of Normal and Neuropathic Feet”. In: *Medical & Biological Engineering & Computing* 34.4 (July 1996), pp. 280–284. ISSN: 0140-0118, 1741-0444. DOI: 10.1007/BF02511238.
-

- [Pet+10] Alana Peters, Brook Galna, Morgan Sangeux, Meg Morris, and Richard Baker. “Quantification of Soft Tissue Artifact in Lower Limb Human Motion Analysis: A Systematic Review”. In: *Gait & Posture* 31.1 (Jan. 2010), pp. 1–8. ISSN: 1879-2219. DOI: 10.1016/j.gaitpost.2009.09.004. pmid: 19853455.
- [Qiu+11] Tian-Xia Qiu, Ee-Chon Teo, Ya-Bo Yan, and Wei Lei. “Finite Element Modeling of a 3D Coupled Foot–Boot Model”. In: *Medical Engineering & Physics* 33.10 (Dec. 2011), pp. 1228–1233. ISSN: 13504533. DOI: 10.1016/j.medengphy.2011.05.012.
- [RA94] Amos Race and Andrew A. Amis. “The Mechanical Properties of the Two Bundles of the Human Posterior Cruciate Ligament”. In: *Journal of Biomechanics* 27.1 (Jan. 1994), pp. 13–24. ISSN: 00219290. DOI: 10.1016/0021-9290(94)90028-0.
- [Ran+08] Leah Rankine, Jason Long, Karl Canseco, and Gerald F. Harris. “Multi-segmental Foot Modeling: A Review”. In: *Critical Reviews in Biomedical Engineering* 36.2-3 (2008), pp. 127–181. ISSN: 0278-940X. DOI: 10.1615/critrevbiomedeng.v36.i2-3.30. pmid: 19740070.
- [RJB11] Guillaume Rao, André Jacques, and Eric Berton. “A MULTI-DOMAIN EMG-DRIVEN 3D FINITE ELEMENT OF THE FOOT FOR DYNAMIC ACTIVITIES”. In: International Society of Biomechanics. Brussels, July 2011, p. 2.
- [RL01] S. Rusinkiewicz and M. Levoy. “Efficient Variants of the ICP Algorithm”. In: *Proceedings Third International Conference on 3-D Digital Imaging and Modeling*. Third International Conference on 3-D Digital Imaging and Modeling. Quebec City, Que., Canada: IEEE Comput. Soc, 2001, pp. 145–152. ISBN: 978-0-7695-0984-6. DOI: 10.1109/IM.2001.924423.
- [Sar+08] Carlos Saro, Ann-Sophie Bengtsson, Urban Lindgren, Johanna Adami, Paul Blomqvist, and Li Felländer-Tsai. “Surgical Treatment of Hallux Valgus and Forefoot Deformities in Sweden: A Population-Based Study”. In: *Foot & Ankle International* 29.3 (Mar. 2008), pp. 298–304. ISSN: 1071-1007, 1944-7876. DOI: 10.3113/FAI.2008.0298.
- [SB98] M. J. Shereff and J. F. Baumhauer. “Hallux Rigidus and Osteoarthritis of the First Metatarsophalangeal Joint”. In: *The Journal of Bone and Joint Surgery. American Volume* 80.6 (June 1998), pp. 898–908. ISSN: 0021-9355. DOI: 10.2106/00004623-199806000-00015. pmid: 9655109.
- [SBS88] Sorin Siegler, John Block, and Carson D. Schneck. “The Mechanical Characteristics of the Collateral Ligaments of the Human Ankle Joint”. In: *Foot & Ankle* 8.5 (Apr. 1988), pp. 234–242. ISSN: 0198-0211. DOI: 10.1177/107110078800800502.
- [Sch+10] Michael Schuenke, Erik Schulte, Udo Schumacher, Lawrence M Ross, Edward D Lamperti, and Markus Voll. *General Anatomy and Musculoskeletal System (THIEME Atlas of Anatomy)*. Thieme, 2010. ISBN: 1-60406-286-X.
- [Shi+11] Khalid Shirzad, Carter D. Kiesau, James K. DeOrio, and Selene G. Parekh. “Lesser Toe Deformities:” in: *American Academy of Orthopaedic Surgeon* 19.8 (Aug. 2011), pp. 505–514. ISSN: 1067-151X. DOI: 10.5435/00124635-201108000-00006.

-
- [SHW08] Ian A. Sigal, Michael R. Hardisty, and Cari M. Whyne. “Mesh-Morphing Algorithms for Specimen-Specific Finite Element Modeling”. In: *Journal of Biomechanics* 41.7 (Jan. 2008), pp. 1381–1389. ISSN: 00219290. DOI: 10.1016/j.jbiomech.2008.02.019.
- [Sim+06] J. Simon, L. Doederlein, A.S. McIntosh, D. Metaxiotis, H.G. Bock, and S.I. Wolf. “The Heidelberg Foot Measurement Method: Development, Description and Assessment”. In: *Gait & Posture* 23.4 (June 2006), pp. 411–424. ISSN: 09666362. DOI: 10.1016/j.gaitpost.2005.07.003.
- [Sis+13] Lise Sissler, André Jacques, Guillaume Rao, Eric Berton, and Nils Gueguen. “A 3-D Finite Element Model of the Foot-Shoe Structure during a Walking Cycle for Shoe Sole Design”. In: *Footwear Science* 5 (sup1 June 2013), S36–S37. ISSN: 1942-4280, 1942-4299. DOI: 10.1080/19424280.2013.799541.
- [SL10] Kelly H. Schmidt and William R. Ledoux. “Quantifying Ligament Cross-Sectional Area via Molding and Casting”. In: *Journal of Biomechanical Engineering* 132.9 (2010), p. 091012. ISSN: 01480731. DOI: 10.1115/1.4001881.
- [SMB14] Daniel Sieger, Stefan Menzel, and Mario Botsch. “RBF Morphing Techniques for Simulation-Based Design Optimization”. In: *Engineering with Computers* 30.2 (Apr. 2014), pp. 161–174. ISSN: 0177-0667, 1435-5663. DOI: 10.1007/s00366-013-0330-1.
- [SML06] Will Schroeder, Ken Martin, and Bill Lorensen. *The Visualization Toolkit: An Object-Oriented Approach to 3D Graphics ; [Visualize Data in 3D - Medical, Engineering or Scientific ; Build Your Own Applications with C++, Tcl, Java or Python ; Includes Source Code for VTK (Supports Unix, Windows and Mac)*. In collab. with Inc Kitware. 4. ed. Clifton Park, NY: Kitware, Inc, 2006. 512 pp. ISBN: 978-1-930934-19-1.
- [Sop+11] Ran Sopher, Jane Nixon, Elizabeth McGinnis, and Amit Gefen. “The Influence of Foot Posture, Support Stiffness, Heel Pad Loading and Tissue Mechanical Properties on Biomechanical Factors Associated with a Risk of Heel Ulceration”. In: *Journal of the Mechanical Behavior of Biomedical Materials* 4.4 (May 2011), pp. 572–582. ISSN: 17516161. DOI: 10.1016/j.jmbbm.2011.01.004.
- [SP86] Thomas W. Sederberg and Scott R. Parry. “Free-Form Deformation of Solid Geometric Models”. In: *Proceedings of the 13th Annual Conference on Computer Graphics and Interactive Techniques - SIGGRAPH '86*. The 13th Annual Conference. Not Known: ACM Press, 1986, pp. 151–160. ISBN: 978-0-89791-196-2. DOI: 10.1145/15922.15903.
- [SSH90] G J M A Schreppers, A A H J Sauren, and A Huson. “A Numerical Model of the Load Transmission in the Tibio-Femoral Contact Area”. In: *Proceedings of the Institution of Mechanical Engineers, Part H: Journal of Engineering in Medicine* 204.1 (Mar. 1990), pp. 53–59. ISSN: 0954-4119, 2041-3033. DOI: 10.1243/PIME_PROC_1990_204_228_02.
- [Tel+14] Scott Telfer, Ahmet Erdemir, James Woodburn, and Peter R. Cavanagh. “What Has Finite Element Analysis Taught Us about Diabetic Foot Disease and Its Management? A Systematic Review”. In: *PLoS ONE* 9.10 (Oct. 7, 2014). Ed. by Amit Gefen, e109994. ISSN: 1932-6203. DOI: 10.1371/journal.pone.0109994.
-

- [TLG03] J Tong, C.S Lim, and O.L Goh. “Technique to Study the Biomechanical Properties of the Human Calcaneal Heel Pad”. In: *The Foot* 13.2 (June 2003), pp. 83–91. ISSN: 09582592. DOI: 10.1016/S0958-2592(02)00149-9.
- [TZG96] Gabriel Taubin, Tong Zhang, and Gene Golub. “Optimal Surface Smoothing as Filter Design”. In: *Computer Vision — ECCV ’96*. Ed. by Bernard Buxton and Roberto Cipolla. Berlin, Heidelberg: Springer Berlin Heidelberg, 1996, pp. 283–292. ISBN: 978-3-540-49949-7.
- [Udu+98] J.K. Udupa, B.E. Hirsch, H.J. Hillstrom, G.R. Bauer, and J.B. Kneeland. “Analysis of in Vivo 3-D Internal Kinematics of the Joints of the Foot [MRI Analysis]”. In: *IEEE Transactions on Biomedical Engineering* 45.11 (Nov./1998), pp. 1387–1396. ISSN: 00189294. DOI: 10.1109/10.725335.
- [Ven+20] Madhusudhan Venkadesan, Ali Yawar, Carolyn M. Eng, Marcelo A. Dias, Dhiraj K. Singh, Steven M. Tommasini, Andrew H. Haims, Mahesh M. Bandi, and Shreyas Mandre. “Stiffness of the Human Foot and Evolution of the Transverse Arch”. In: *Nature* 579.7797 (Mar. 5, 2020), pp. 97–100. ISSN: 0028-0836, 1476-4687. DOI: 10.1038/s41586-020-2053-y.
- [Vir+19] Pauli Virtanen, Ralf Gommers, Travis E. Oliphant, Matt Haberland, Tyler Reddy, David Cournapeau, Evgeni Burovski, Pearu Peterson, Warren Weckesser, Jonathan Bright, Stéfan J. van der Walt, Matthew Brett, Joshua Wilson, K. Jarrod Millman, Nikolay Mayorov, Andrew R. J. Nelson, Eric Jones, Robert Kern, Eric Larson, C. J. Carey, İlhan Polat, Yu Feng, Eric W. Moore, Jake VanderPlas, Denis Laxalde, Josef Perktold, Robert Cimrman, Ian Henriksen, E. A. Quintero, Charles R. Harris, Anne M. Archibald, Antônio H. Ribeiro, Fabian Pedregosa, Paul van Mulbregt, and SciPy 1.0 Contributors. *SciPy 1.0—Fundamental Algorithms for Scientific Computing in Python*. July 23, 2019. arXiv: 1907.10121 [physics]. URL: <http://arxiv.org/abs/1907.10121> (visited on 11/12/2019).
- [Wan+18] Yan Wang, Zengyong Li, Duo Wai-Chi Wong, Cheng-Kung Cheng, and Ming Zhang. “Finite Element Analysis of Biomechanical Effects of Total Ankle Arthroplasty on the Foot”. In: *Journal of Orthopaedic Translation* 12 (Jan. 2018), pp. 55–65. ISSN: 2214031X. DOI: 10.1016/j.jot.2017.12.003.
- [Wei+11] Feng Wei, Stanley C. Hunley, John W. Powell, and Roger C. Haut. “Development and Validation of a Computational Model to Study the Effect of Foot Constraint on Ankle Injury Due to External Rotation”. In: *Annals of Biomedical Engineering* 39.2 (Feb. 2011), pp. 756–765. ISSN: 0090-6964, 1573-9686. DOI: 10.1007/s10439-010-0234-9.
- [WLZ14] Yan Wang, Zengyong Li, and Ming Zhang. “Biomechanical Study of Tarsometatarsal Joint Fusion Using Finite Element Analysis”. In: *Medical Engineering & Physics* 36.11 (Nov. 2014), pp. 1394–1400. ISSN: 13504533. DOI: 10.1016/j.medengphy.2014.03.014.
- [Wol+08] Sebastian Wolf, Jan Simon, Dimitrios Patikas, Waltraud Schuster, Petra Armbrust, and Leonhard Döderlein. “Foot Motion in Children Shoes—A Comparison of Barefoot Walking with Shod Walking in Conventional and Flexible Shoes”. In: *Gait & Posture* 27.1 (Jan. 2008), pp. 51–59. ISSN: 09666362. DOI: 10.1016/j.gaitpost.2007.01.005.

- [Won+14] Duo Wai-Chi Wong, Ming Zhang, Jia Yu, and Aaron Kam-Lun Leung. “Biomechanics of First Ray Hypermobility: An Investigation on Joint Force during Walking Using Finite Element Analysis”. In: *Medical Engineering & Physics* 36.11 (Nov. 2014), pp. 1388–1393. ISSN: 13504533. DOI: 10.1016/j.medengphy.2014.03.004.
- [Won+16] Duo Wai-Chi Wong, Wenxin Niu, Yan Wang, and Ming Zhang. “Finite Element Analysis of Foot and Ankle Impact Injury: Risk Evaluation of Calcaneus and Talus Fracture”. In: *PLOS ONE* 11.4 (Apr. 27, 2016). Ed. by Lei Ren, e0154435. ISSN: 1932-6203. DOI: 10.1371/journal.pone.0154435.
- [Won+18] Duo Wai-Chi Wong, Yan Wang, Aaron Kam-Lun Leung, Ming Yang, and Ming Zhang. “Finite Element Simulation on Posterior Tibial Tendinopathy: Load Transfer Alteration and Implications to the Onset of Pes Planus”. In: *Clinical Biomechanics* 51 (Jan. 2018), pp. 10–16. ISSN: 02680033. DOI: 10.1016/j.clinbiomech.2017.11.001.
- [Won+20a] Duo Wai-Chi Wong, Yan Wang, Tony Lin-Wei Chen, Fei Yan, Yinghu Peng, Qitao Tan, Ming Ni, Aaron Kam-Lun Leung, and Ming Zhang. “Finite Element Analysis of Generalized Ligament Laxity on the Deterioration of Hallux Valgus Deformity (Bunion)”. In: *Frontiers in Bioengineering and Biotechnology* 8 (Sept. 8, 2020), p. 571192. ISSN: 2296-4185. DOI: 10.3389/fbioe.2020.571192.
- [Won+20b] Duo Wai-Chi Wong, Yan Wang, Wenxin Niu, and Ming Zhang. “Finite Element Analysis of Subtalar Joint Arthroereisis on Adult-Acquired Flexible Flatfoot Deformity Using Customised Sinus Tarsi Implant”. In: *Journal of Orthopaedic Translation* (Mar. 2020), S2214031X20300139. ISSN: 2214031X. DOI: 10.1016/j.jot.2020.02.004.
- [WR64] D. G. Wright and D. C. Rennels. “A Study of the Elastic Properties of Plantar Fascia:” in: *The Journal of Bone & Joint Surgery* 46.3 (Apr. 1964), pp. 482–492. ISSN: 0021-9355. DOI: 10.2106/00004623-196446030-00002.
- [Wu07] Lijun Wu. “Nonlinear Finite Element Analysis for Musculoskeletal Biomechanics of Medial and Lateral Plantar Longitudinal Arch of Virtual Chinese Human after Plantar Ligamentous Structure Failures”. In: *Clinical Biomechanics* 22.2 (Feb. 2007), pp. 221–229. ISSN: 02680033. DOI: 10.1016/j.clinbiomech.2006.09.009.
- [Yu+13] Jia Yu, Jason Tak-Man Cheung, Duo Wai-Chi Wong, Yan Cong, and Ming Zhang. “Biomechanical Simulation of High-Heeled Shoe Donning and Walking”. In: *Journal of Biomechanics* 46.12 (Aug. 2013), pp. 2067–2074. ISSN: 00219290. DOI: 10.1016/j.jbiomech.2013.05.009.
- [ZB07] B. Zipfel and L.R. Berger. “Shod versus Unshod: The Emergence of Forefoot Pathology in Modern Humans?” In: *The Foot* 17.4 (Dec. 2007), pp. 205–213. ISSN: 09582592. DOI: 10.1016/j.foot.2007.06.002.
- [Zha+17] Congsheng Zhang, Qingsong Ai, Wei Meng, and Jiwei Hu. “A Subject-Specific EMG-Driven Musculoskeletal Model for the Estimation of Moments in Ankle Plantar-Dorsiflexion Movement”. In: *Neural Information Processing*. Ed. by Derong Liu, Shengli Xie, Yuanqing Li, Dongbin Zhao, and El-Sayed M. El-Alfy. Vol. 10637. Lecture Notes in Computer Science. Cham: Springer

- International Publishing, 2017, pp. 685–693. ISBN: 978-3-319-70092-2 978-3-319-70093-9. DOI: 10.1007/978-3-319-70093-9_73.
- [Zhe+12] Y.P. Zheng, Y.P. Huang, Y.P. Zhu, M. Wong, J.F. He, and Z.M. Huang. “Development of a Foot Scanner for Assessing the Mechanical Properties of Planar Soft Tissues under Different Bodyweight Loading in Standing”. In: *Medical Engineering & Physics* 34.4 (May 2012), pp. 506–511. ISSN: 13504533. DOI: 10.1016/j.medengphy.2011.11.005.
- [ZL20] Siti Syazni Zulkifli and Wei Ping Loh. “A State-of-the-Art Review of Foot Pressure”. In: *Foot and Ankle Surgery* 26.1 (Jan. 2020), pp. 25–32. ISSN: 12687731. DOI: 10.1016/j.fas.2018.12.005.

NNT: 2021LYSEM013
Author: Nicolas KROUPA
Title: Analysis of the foot's internal structures
by X-ray image processing and finite element modeling
Speciality: Mechanics and Engineering
Keywords: Foot, Biomechanics, X-ray, Rigid & non-rigid registration, Finite element, Patient specific model

Abstract

The foot is a complex anatomical structure consisting of many bones surrounded by a variety of tissues. By its role of supporting and moving the body, it is exposed to a whole series of mechanical loads that will deform its structure. This deformation is influenced by many parameters that may be specific to the patient's anatomy and pathologies, linked to the characteristics of the applied mechanical load, but also depend on the design parameters of the device that is worn. In order to make progress in the characterization of these foot deformations, which are diverse and complex, it has become necessary to obtain increasingly precise measurements describing the inside of the limb. This progression is one of the steps intended to accompany the improvement of footwear design, medical devices and surgical planning by having a better understanding of the foot's response to mechanical constraints.

To study the biomechanics of the foot by accessing internal measurements, two approaches are coupled here, one experimental and the other numerical.

A first study was carried out to : (1) perform mechanical tests on a series of *ex-vivo* feet with and without shoes in an X-ray tomographic scanner and (2) develop and implement numerical treatments applied to these acquisitions to obtain observations of the internal behavior of the foot. The comparison of these behaviors between shod and barefoot configurations allowed a first measurement of the shoe's influence on internal foot measurements.

A second study uses these captured data to propose a calibration of patient specific finite element models of the feet. This calibration, using an inverse method to identify the passive rigidity of the ligaments & muscles, improves the accuracy of the models.

Finally, a third study will exploit a model thus calibrated by exposing it to a running stride while wearing a specimen of a shoe whose design parameters will vary. The influences of these parameters are measured and can constitute a first set of indications to adjust the design of the shoe.

NNT: 2021LYSEM013
Auteur: Nicolas KROUPA
Titre: Analyse des structures internes du pied
par traitement d'images rayons X et modélisation éléments finis
Spécialité: Mécanique et Ingénierie
Mots-Clefs: Pied, Biomécanique, Rayon-X, Recalage rigide & non-rigide, Élément finis, Modèle spécifique au patient

Résumé

Le pied est une structure anatomique complexe constituée de nombreux os entourés d'une variété de tissus. Par son rôle de maintien et de déplacement du corps, il est exposé à toute une série de sollicitations mécaniques qui vont déformer sa structure. Cette déformation est influencée par de nombreux paramètres qui peuvent être spécifiques à l'anatomie du patient et à ses pathologies, liés aux caractéristiques de la sollicitation mécanique appliquée, mais aussi dépendre des paramètres de conception du dispositif qui le chausse. Afin de progresser dans la caractérisation de ces déformations du pied, qui sont diverses et complexes, il est devenu nécessaire d'obtenir des mesures de plus en plus précises décrivant l'intérieur du membre. Cette progression est une des démarches destinées à accompagner l'amélioration de la conception des chaussures, des dispositifs médicaux et de la planification chirurgicale en ayant une meilleure compréhension de la réponse du pied aux sollicitations mécaniques.

Pour étudier la biomécanique du pied en accédant à des mesures internes, deux approches sont ici couplées, l'une expérimentale et l'autre numérique.

Une première étude a été réalisée pour : (1) effectuer des tests mécaniques sur une série de pieds *ex-vivo* avec et sans chaussures dans un scanner tomographique à rayons X et (2) développer et mettre en œuvre de traitements numériques appliqués à ces acquisitions pour obtenir des observations du comportement interne au pied. La comparaison de ces comportements entre les configurations avec chaussures et pieds nus a permis une première mesure de l'influence de la chaussure sur des mesures internes au pied.

Une deuxième étude utilise ces données capturées pour proposer un calibrage de modèles éléments finis spécifiques aux pieds des patients. Cette calibration, en utilisant une méthode inverse pour identifier la rigidité passive des ligaments & muscles, améliore la justesse des modèles.

Finalement, une troisième étude exploitera un modèle ainsi calibré en l'exposant à une foulée de course tout en portant un exemplaire d'une chaussure dont les paramètres de conception varieront. Les influences de ces paramètres sont mesurées et peuvent constituer un premier ensemble d'indications pour ajuster la conception de la chaussure.